



**The Effect of Process  
Parameters and Aging on  
Lime Sludge Density and  
Stability**

**MEND Report 3.42.2b**

**This work was prepared on behalf of the MEND Program and sponsored by  
Rio Algom  
Kidd Creek Division of Falconbridge Ltd.  
Hudson Bay Mining and Smelting and  
CETEM**

**February 1999**

**THE EFFECT OF PROCESS  
PARAMETERS AND AGING  
ON LIME SLUDGE DENSITY  
AND STABILITY**

FEBRUARY 1999

**MINING AND MINERAL SCIENCES LABORATORIES**  
J.M. Zinck, C.M. Hogan, W.F. Griffith, and J.H.G. Laflamme

**Work performed for MEND. Sponsored by:**  
CETEM, RIO ALGOM, FALCONBRIDGE - KIDD DIVISION,  
HUDSON BAY MINING & SMELTING, CANMET

Job No. 51144

MINING AND MINERAL SCIENCES LABORATORIES  
REPORT MMSL 97-085 (CR)

## EXECUTIVE SUMMARY

To better understand sludge production and behaviour a study was completed at CANMET to assess the effect of process parameters during AMD treatment and sludge aging on metal leachability and sludge density.

Several process parameters (recycle rate, agitation rate, flocculant usage and ferric-ferrous iron ratio) were examined through continuous pilot plant testing. The sludge produced was characterized through physical, chemical, mineralogical and metal leaching analyses to ascertain optimal conditions to produce dense, stable, lime treatment sludge. In addition, batch tests were completed to study the effect of sulphate concentration in the AMD stream. The method of neutralization was examined to observe its effect on sludge production.

This study found recycling can affect several treatment related factors and can impact on long term sludge stability, as well as intermediate concerns such as sludge density. Increased recycling, while beneficial in terms of plant efficiency and reagent costs, increased the heavy metal content of the sludge and led to greater metal leachability. As well, sludge recycling in a high hydrodynamic shear environment was found to be detrimental to the formation of large, compact particles as particle abrasion and particle growth processes occurred counterproductively.

Slow, controlled neutralization was shown to increase settling rates by five-fold. This has significant implications with respect to clarification requirements. Through supersaturation control, as with staged-neutralization, settling rates can be further increased by 50%. Furthermore, lime consumption can be reduced through selection of a controlled or staged method of neutralization, reducing reagents costs by 10-15%.

Results suggest that a greater proportion of ferric iron in the raw water enhances sludge density and settleability. However, the amount of zinc leached from the sludge increased with increasing ferric iron concentration in the raw water.

The addition of excess lime to HDS-type treatment sludges resulted in lower metal leachability, however, the physical properties of the sludge were adversely affected by this potential remediation technique.

An investigation into sludge aging found that when the aging time was increased the degree of metal mobility from sludge samples declined, while the proportion of calcite and gypsum increased. This was accomplished through a process of dissolution and recrystallization of the sludge components. This supports the theory presented in Part I of this project (3.42.2a), that the calcite and gypsum are the >final< phases of the aged sludge and in the long term (i.e. millennia), the sludge may transform into a carbonate rock with a minor iron oxide phase (Zinck *et al.* 1997). Oxidation rims of goethite and magnetite which formed around sulphide particles present in the aged sludge suggest that long-term codisposal of sludge and tailings may be beneficial for both waste management and metal leachability.

Further work should focus on:

- § relating these aging tests with controlled field tests;
- § modeling the data contained herein to optimize lime treatment systems;
- § investigating metal leachability and sludge aging for the codisposal environment;  
and
- § examining the long term environmental stability and mechanisms responsible for metal mobility from ettringite and desautelsite compounds.

## SOMMAIRE

Afin de mieux comprendre la production et le comportement des boues, CANMET a procédé à l'évaluation des incidences des paramètres de fonctionnement pendant le traitement du drainage minier acide (DMA) et du vieillissement des boues sur la lixivibilité du métal et la densité des boues.

Plusieurs paramètres de fonctionnement (taux de recyclage, degré d'agitation, utilisation de flocculants et rapport ferric-ferreux) ont été examinés par des essais continus en usine-pilote. La boue produite a été caractérisée par des analyses physiques, chimiques, minéralogiques et liées à la lixiviation du métal en vue d'assurer des conditions optimales pour la production de boues stables et denses suite au traitement de neutralisation à la chaux. De plus, on a mené des essais par lots afin d'étudier les incidences de la teneur en sulfate sur le flux de DMA et examiné la méthode de neutralisation afin d'en observer les effets sur la production de boues.

L'étude a révélé que le recyclage peut affecter plusieurs des éléments liés au traitement, avoir un impact à long terme sur la stabilité des boues et donner lieu à des préoccupations d'ordre intermédiaire, telle la densité des boues. Une augmentation du recyclage bien qu'avantageuse quant à l'efficacité de l'usine et au coût des réactifs, a augmenté la teneur en métaux lourds des boues et entraîné une plus grande lixivibilité du métal. Dans le même ordre d'idées, le recyclage des boues dans une zone de cisaillement hautement hydrodynamique s'est avéré préjudiciable à la formation de particules larges et compactes, les processus d'abrasion et de formation particulaire se produisant de façon contre-productive.

La neutralisation lente et contrôlée des boues a accru de cinq fois leur taux de sédimentation, ce qui a eu des incidences importantes sur les exigences en matière de clarification. Le contrôle de la sursaturation et la neutralisation en étapes ont permis d'augmenter le taux de sédimentation de 50 %. De plus, la consommation de chaux peut être réduite par la sélection d'une méthode de neutralisation contrôlée ou par étapes, ce qui permet de réduire le coût des réactifs de 10 à 15 %.

Les résultats suggèrent qu'une plus grande proportion de fer ferrique dans l'eau brute promeut la densité et la décantabilité des boues. Toutefois, la quantité de zinc lixivié à partir des boues augmente en fonction de l'augmentation de la concentration de fer ferrique dans l'eau brute.

L'addition d'un excédent de chaux aux boues de traitement de type HDS a réduit la lixivibilité du métal, mais les propriétés physiques des boues ont été inversement affectées par cette technique potentielle de réhabilitation.

Une enquête sur le vieillissement des boues a démontré que l'accélération du vieillissement entraînait une diminution du degré de mobilité du métal contenu dans les échantillons de boue et une augmentation de la proportion de calcite et de gypse. Cette étude a été réalisée au moyen des processus de dissolution et de recristallisation des composantes de la boue. Cet essai appuie la théorie présentée dans la Partie I de ce projet (3.42.2a), à savoir que le

calcite et le gypse sont les phases \* finales + de transformation de la boue vieillie et, à long terme, ( p.ex. des millénaires), les boues peuvent se transformer en roche carbonatée et comporter une phase moins importante d'oxyde de fer (Zinck *et al.*1997). Les bords oxydés de goethite et de magnétite qui se sont formés autour des particules sulfurées présentes dans la boue vieillie suggèrent que la co-déposition à long terme de boues et de résidus peut être avantageuse tant dans le cas de la gestion des résidus que sur le plan de la lixivabilité du métal.

Les travaux complémentaires devraient être axés sur :

- § l'établissement de liens entre les essais sur le vieillissement et des essais contrôlés sur le terrain;
- § la modélisation des données ci-incluses afin d'optimiser les systèmes de traitement à la chaux;
- § l'étude de la lixivabilité du métal et du vieillissement des boues en fonction de la zone de co-déposition; et
- § l'examen de la stabilité de l'environnement à long terme et des mécanismes responsables de la mobilité du métal à partir de composés d'ettringite et de desautelsite.

## **ACKNOWLEDGEMENTS**

Funding for this project was provided by CETEM, Rio Algom, Hudson Bay Mining and Smelting, Falconbridge - Kidd Creek Division and CANMET.

The authors wish to acknowledge the contribution of the following CANMET staff: Rene Guillas, Ron Horton and Regina Karwowska for performing the analytical work; and Paul Carrière and Michel Beaulne for performing the X-ray diffraction and mineralogical sample preparation work. Thanks also to Geneviève Béchard of CANMET for technical discussions and editorial review.

In addition, the authors wish to acknowledge the contribution of Alan Moore for his technical guidance and glass blowing skills in the pilot plant construction and the following students from the Technical University of Nova Scotia for their work on this project: Carla MacQuarrie, Sonja Crnogorac and Mark Mason.

# TABLE OF CONTENTS

EXECUTIVE SUMMARY .....	i
SOMMAIRE .....	iii
ACKNOWLEDGEMENTS .....	v
LIST OF TABLES .....	ix
LIST OF FIGURES .....	x
1.0 INTRODUCTION.....	1
1.1 Lime Neutralization Treatment Methods .....	1
1.2 This Study .....	1
2.0 MATERIALS AND ANALYTICAL PROCEDURES .....	3
2.1 Reagents .....	3
Synthetic Acid Mine Drainage .....	3
Slaked Lime and Flocculant .....	3
2.2 Handling and Storage .....	3
Sample Storage.....	3
Lyophilization .....	3
2.3 Physical Characterization .....	3
Percent Solids.....	4
Bulk Density.....	4
Particle Size Determination.....	4
Settling Rate .....	4
Viscosity.....	4
2.4 Chemical Analyses .....	5
Chemical Composition.....	5
Neutralization Potential.....	5
Sulphate Determination by Barium Sulphate Precipitation .....	5
Ferrous Iron Determination by Dichromate Titration .....	5
Solids Content of AMD Generated by Lime Neutralization .....	6
2.5 Mineralogy .....	6
2.6 Leachability .....	6



3.0	HIGH DENSITY SLUDGE PILOT PLANT .....	7
3.1	Design and Construction .....	7
3.2	Pilot Plant Configuration for the HDS Study.....	8
3.3	Test Conditions .....	9
3.4.	The Chemical Process .....	10
3.5	Future Design Modifications.....	11
4.0	PILOT PLANT SCALE TESTS .....	13
4.1	Agitation Rate .....	13
	Introduction .....	13
	Methods.....	13
	Results13	
4.2	Flocculant Addition.....	18
	Introduction .....	18
	Results18	
	Discussion .....	22
4.3	Recycle Rate.....	24
	Introduction .....	24
	Methods.....	24
	Results24	
	Discussion .....	28
4.4	Ferric-Ferrous Ratio .....	30
	Introduction .....	30
	Methods.....	30
	Results30	
	Discussion .....	35
5.0	BATCH TESTS.....	37
5.1	Batch Test Procedure.....	37
5.2	Sulphate Concentration .....	37
	Introduction .....	37
	Methods.....	37
	Results37	
	Discussion .....	40
5.3	Rate of Neutralization .....	42
	Methods.....	42
	Results43	
	Discussion .....	43
6.0	EFFECT OF EXCESS BUFFERING ON SLUDGE STABILITY.....	44
6.1	Introduction .....	44
6.2	Materials and Methods.....	44
6.3	Results and Discussion.....	44

7.0	SLUDGE AGING .....	51
7.1	Materials and Method.....	51
7.2	Metal Leachability.....	52
7.3	Mineralogy .....	56
	X-Ray Diffraction Analysis.....	56
	Detailed Mineralogy - High Density Sludge .....	58
7.4	Field Study .....	59
7.5	Discussion .....	61
8.0	CONCLUSIONS .....	63
8.1	Process Parameters.....	63
8.2	Raw Water Composition .....	63
8.3	Excess Alkalinity.....	65
8.4	Sludge Aging.....	65
9.0	RECOMMENDATIONS .....	66
9.1	Plant Practice.....	66
9.2	Further Work.....	66
10.0	REFERENCES.....	67

APPENDIX A: X-Ray Diffraction Patterns for the Low Density (S-6) and Synthetic Sludges . A-1

APPENDIX B: Detailed Mineralogy Report for the High Density Sludge (W-8)..... B-1

## LIST OF TABLES

3.3.1	A summary of the pilot plant flowrates and retention times .....	10
3.4.1	Chemical analyses of effluents sampled from each reactor .....	11
4.1.1:	Metal and sulphate composition of AMD and effluent produced under different agitation rates .....	16
4.1.2:	Effect of agitation rate on leachability of sludge discharge using the Ontario LEP.....	16
4.2.1:	Comparison of Percol 338 and 727 flocculants. ....	19
4.2.2:	Comparison of Percol E10 and 338 flocculants. ....	19
4.2.3:	Effect of flocculant concentration on particle size distribution. ....	23
4.2.4:	Composition of AMD and effluent produced under different flocculant concentrations .	23
4.4.1:	Properties of sludge produced by treating AMD with various ferric-ferrous ratios.....	30
4.4.2:	Metal leachability from sludges produced from AMD with varying ferric-ferrous ratios (Ontario LEP). ....	35
5.2.1:	Metal leachability as af function of raw water sulphate concentration .....	40
5.3.1:	Time and pH parameters for staged neutralization process.....	42
5.3.2:	Effect of rate of neutralization on solids generation, lime consumption, settling rates and NP .....	43
6.1:	Physical characteristics and chemical composition of J7 and synthetic sludges.....	45
6.2:	Effect of excess lime on chemical and physical characteristics of sludge .....	46
6.3:	Effect of excess lime on sludge leachability .....	49
6.4:	Particle size distribution for industrial and synthetic sludges treated with excess lime ...	50
7.1:	Physical characteristics and chemical composition of W-8, S-6 and synthetic sludges....	51
7.2:	Summary of sludge aging tests performed on fresh industrial sludges and fresh synthetic sludge .....	52
7.3:	Leachate concentration from Ontario LEP for the high density sludge (W-8).....	53
7.4:	Leachate concentration from Ontario LEP for the low density sludge (S-6) .....	54
7.5:	Leachate concentration from Ontario LEP for the synthetic sludge.....	55
7.6:	Summary of XRD findings after aging low density and synthetic sludge samples.....	57
7.7:	Summary of mineralogical findings after aging high density sludge (W-8) .....	60

## LIST OF FIGURES

3.1.1:	A front view of the High Density Sludge Pilot Plant .....	7
3.2.1:	A schematic of the HDS pilot plant configuration .....	8
4.1.1:	Effect of agitation on particle size distribution .....	14
4.1.2:	Particle size distributions of sludges formed with and without recycle .....	14
4.1.3:	Physical properties of sludges produced under different agitation rates .....	17
4.2.1:	Effect of Percol E10 concentration on settling rate.....	20
4.2.2:	Effect of flocculant concentration on particle size.....	21
4.3.1:	Recycle ratio versus recycle rate .....	25
4.3.2:	Effect of recycling on percent solids .....	25
4.3.3:	Recycling rate versus settling rate of sludge .....	25
4.3.4:	Relationship between lime consumption and percent sludge recycle .....	25
4.3.5:	Relationship between recycling and viscosity.....	26
4.3.6:	Comparison of particle size distribution for recycled and unrecycled sludges .....	27
4.3.7:	Effect of recycle rate on particle size distribution.....	27
4.3.8:	Relationship between metal content of sludge and zinc mobility.....	28
4.4.1:	Percent solids versus ferric-ferrous ratio .....	31
4.4.2:	Settling rate versus ferric-ferrous ratio.....	31
4.4.3:	Lime consumption versus ferric-ferrous ratio .....	32
4.4.4:	Viscosity versus ferric-ferrous ratio .....	32
4.4.5:	Polymer dosage versus ferric-ferrous ratio.....	33
4.4.6:	Settling rate versus polymer dosage .....	33
4.4.7:	Effect of ferric/ferrous iron ratio on particle size distribution .....	33
4.4.8:	Mean particle size versus ferric-ferrous ratio.....	34
4.4.9:	Zinc leachability versus ferric-ferrous ratio .....	34
5.2.1:	Effect of sulphate concentration on percent solids.....	38
5.2.2:	Effect of sulphate concentration on total solids production .....	38
5.2.3:	Effect of sulphate concentration on settling rate .....	38
5.2.4:	Particle size distribution for sludge generated at various sulphate concentrations .....	39
5.2.5:	Effect of sulphate concentration on zinc and aluminum leachability.....	40
6.1:	Effect of excess lime on chemical properties of sludge .....	47
6.3:	Particle size distribution for J7 sludge and synthetic sludge treated with excess lime .....	50
7.1:	Zn leachability versus time at different temperatures for the high density sludge aged under atmospheric conditions .....	56
7.2:	Zn leachability versus time at different temperatures for the high density sludge aged under saturated conditions .....	56

## 1.0 INTRODUCTION

At present, the "best available technology economically achievable" (BATEA) for the treatment of acid mine drainage is lime neutralization (Dinardo *et al.* 1991). Despite recent improvements to the traditional neutralization method (Demopoulos *et al.* 1995; Dinardo *et al.* 1991; Flynn 1990; Kuit 1980; Kuyucak *et al.* 1991; Vachon *et al.* 1987), it is estimated that as much as 6.7 million cubic metres of lime treatment sludge is produced annually in Canada (Zinck *et al.* 1997).

In addition, the Canadian mineral industry is faced with questions related to the long term stability of acid mine drainage (AMD) treatment sludges, and their environmentally acceptable disposal. Recent studies (Ford *et al.* 1998; Zinck *et al.* 1997) have indicated that lime sludge is stable, as defined by waste regulations, if disposed in a pond type environment. However, the majority of the lime treatment sludge produced is voluminous and consists of an amorphous hydroxyl-carbonate-sulphate-hydrate which serves to scavenge metal species.

### 1.1 Lime Neutralization Treatment Methods

There are three main AMD lime neutralization treatment methods used in the industry. These processes are classified as basic, conventional and high density sludge (HDS). These processes produce sludges of varying stability and volume. The denser the sludge generated, the less the volume of sludge produced and the lower the handling and disposal costs. The basic system will densify sludge to 1-5% solids, the conventional system to 3-10% solids and the HDS to 10-30% solids.

The three systems all involve the use of lime as the alkali used to neutralize AMD. The basic system consists of adding lime directly to the raw water stream to neutralize the acid and precipitate the metals. The precipitated metals settle in a sludge pond and the overflow is released to the environment.

The conventional system involves liming and aeration in one or more reactors. Aeration is an important component required to oxidize the ferrous iron to ferric iron. The conventional method uses a polymer to flocculate the sludge to assist with solid-liquid separation.

The HDS process consists of lime addition, aeration and recycling of sludge. It also involves the use of a polymer to flocculate the sludge. Variations on the high density process include the Geco Process (Aubé and Payant 1997) and the Staged-Neutralization Process (Zinck 1993; Demopoulos *et al.* 1995).

### 1.2 This Study

To better understand sludge production and behaviour, a study was completed at CANMET to assess the effect of process parameters during AMD treatment and sludge aging on metal leachability and sludge density. The main criteria used to determine success of a test parameter was whether the thickener overflow and produced sludge met regulations for effluent quality and sludge leachability (Zinck *et al.* 1997). While other studies (Svank and Shumate 1973) have investigated factors affecting sludge density, few (Huck *et al.* 1977) have utilized a

continuous HDS type plant to systematically examine these variables. A modular lime neutralization pilot plant facility (Zinck *et al.* 1997b) was used for this investigation. The configuration used in this study is a scaled-down version of an industrial HDS-type plant currently used in Canada. Details on the plant design and construction are given in Chapter 3.

Results from the pilot tests are presented in Chapter 4. Batch tests were also conducted to study the effect of sulphate concentration and method of neutralization. These results are given in Chapter 5. Two independent studies examining excess buffering and sludge aging were completed and the results are discussed in Chapters 6 and 7 respectively.

## **2.0 MATERIALS AND ANALYTICAL PROCEDURES**

### **2.1 Reagents**

#### 2.1.1 Synthetic Acid Mine Drainage

For routine tests a 400 L batch of synthetic AMD was prepared. Sulphate salts of the following metals were dissolved in tap water to obtain the given concentrations: Cu (10 mg/L); Zn (150 mg/L); Al (200 mg/L); Mn (10 mg/L); Mg (108 mg/L); Fe (II) (400 mg/L); Fe (III) (900 mg/L); Pb (1 mg/L); Cd (2 mg/L); Co (2 mg/L); and As (2 mg/L). Final unadjusted pH was 2.2 - 2.4 and sulphate concentration was 4690 mg/L.

#### 2.1.2 Slaked Lime and Flocculant

A 20 % (w/v) slurry of slaked lime (Anachemia laboratory-grade calcium oxide) was used for all the batch and pilot plant tests. For flocculation tests in the pilot plant Percol E10 (Allied Colloids) was used. A stock solution of 0.5% (w/v) Percol E10 was prepared in distilled water and used within 2-3 days. Working solutions, ranging from 0.005% to 0.05% (w/v) Percol E10, were prepared daily.

### **2.2 Handling and Storage**

#### 2.2.1 Sample Storage

Samples of sludge and effluent collected for analysis were stored in glass bottles that had been washed with hot water and laboratory-grade detergent, rinsed with dilute nitric acid, then rinsed with distilled water. The samples were stored at 4 °C until analysis.

#### 2.2.2 Lyophilization

A Labconco Lyph-Lock<sup>L</sup> 6 Liter freeze drier was used to dry the samples. The samples were flash frozen in liquid nitrogen then freeze-dried for 24-48 h. The freeze-dried samples were vacuum sealed in Kapak polyethylene-lined polyester bags for long term preservation. Lyophilization was performed to maintain the structural integrity of sludge samples sent for mineralogical analyses.

### **2.3 Physical Characterization**

The following physical characterizations were performed in the laboratory.

### 2.3.1 Percent Solids

Percent solids determinations were performed by sample weight loss after oven drying to constant weight at 90°C (16-24 h) (adapted from Zinck, 1993). For pilot plant operations, where a fast determination was needed to set run conditions, the percent solids were determined using a Sartorius moisture balance programmed to run at 120°C for 20 min then at 115°C for 40 min. Values obtained with the moisture balance were typically 5-10% higher than the oven dried method.

### 2.3.2 Bulk Density

Bulk density of the sludges was determined by weighing 10 or 25 cm<sup>3</sup> of the sample in a glass cylinder of set volume on an analytical balance.

### 2.3.3 Particle Size Determination

Particle size determination was completed on samples of fresh sludge using a Microtrac laser scattering particle size distribution analyzer. The particle size range for the analyzer was 0.10 to 700  $\mu\text{m}$ . Methanol was used as the dispersant fluid. The samples were run in duplicate using a run time of 2 minutes.

### 2.3.4 Settling Rate

A 1-L glass cylinder (64 mm x 485 mm (O.D. x H)) was filled with 1-L of test sample. The graduated cylinder was calibrated with distance markings using a ruler. The cylinder was inverted to mix the sample then left to stand for 10 s for surface movement to subside. The height of the solid-liquid interface was recorded at one minute intervals for 10 minutes, at two minutes intervals for the next ten minutes, at 5 minute intervals until 45 minutes had passed, then at 60 minutes. The final volume reading was recorded at 24 h.

### 2.3.5 Viscosity

Viscosity was measured using a modified viscosity cup consisting of a 250 mL plastic separatory funnel fitted with a 4 mm bore plastic stopcock. A 200 mL volume of the sludge slurry was poured into the funnel, the stopcock was immediately opened and the time taken for 100 mL of the sludge to be collected was recorded. Each sample was tested five times and the average calculated. The viscosity apparatus was calibrated with 4 viscosity standards (Cannon7 Certified) ranging from 28.9 cP to 198.6 cP at 25°C and a straight line correlation was used to determine sludge viscosity.



## 2.4 Chemical Analyses

Some chemical characterizations (sulphate, pH, ferrous iron and solids content of AMD generated by lime neutralization) were done in the sludge laboratory. All other tests were done by the Analytical Services Group (ASG), Materials, Processing and Services which is ISO 9002 certified. Methods used by ASG are outlined in the ASG Quality Manual 1996-1997.

### 2.4.1 Chemical Composition

The sludge samples and effluents were analyzed for the following components: Al, As, Ca, Cd, Co, Cu, Fe<sup>2+</sup>, Fe<sub>total</sub>, Mg, Mn, Pb, Zn, S, Si, SO<sub>4</sub>, CO<sub>2</sub> and C<sub>total</sub>. The analyses were carried out using ICP-MS, ICP-IRIS, ICP, AA, LECO Analyzer, ion chromatography and gravimetric techniques. QA/QC protocols followed can be found in the ASG Quality Manual 1996-1997.

### 2.4.2 Neutralization Potential

The neutralization potential was determined by treating an oven-dried sludge sample with excess standardized hydrochloric acid and heating to ensure complete reaction. A fizz test was employed to ensure that the amount of acid added was sufficient to react with all the acid-consuming minerals present. The unconsumed acid was titrated with standardized base to pH 8.3 to allow calculation of calcium carbonate equivalent of the acid consumed (Lawrence and Marchant 1991).

### 2.4.3 Sulphate Determination by Barium Sulphate Precipitation

Vogel's method (Jeffrey *et al.* 1989) was modified, as given below. A 50 mL volume of liquid sample was added to a glass beaker. Concentrated HCl (0.5 mL) was added and the volume made up to 225 mL with distilled water. The solution was heated to boiling, then 12 mL of warm 5% barium chloride solution was added drop-wise with constant stirring. The precipitate was left to settle, then the supernatant was tested for complete precipitation by addition of a few drops of barium chloride solution. If precipitation was incomplete, 1-2 mL barium chloride solution was added. If precipitation was complete the solution was left to stand for 18 h. The solution was rechecked for complete precipitation then vacuum filtered through a preweighed, mixed cellulose acetate and nitrate membrane. The precipitate was dried at 90°C for 18-24 h, cooled in a desiccator then weighed. The weight of the precipitate was multiplied by 0.4116 (% SO<sub>4</sub> in BaSO<sub>4</sub>) to obtain the weight of SO<sub>4</sub>. The weight of SO<sub>4</sub> was divided by the sample volume to obtain concentration of SO<sub>4</sub> in the sample.

### 2.4.4 Ferrous Iron Determination by Dichromate Titration

Vogel's method (Jeffrey *et al.* 1989) was used, as given below. A 10-25 mL aliquot of test solution was added to a 125 mL Erlenmeyer flask. Distilled water was added to obtain a final

volume of 50 mL. Fifteen mL of 15% H<sub>2</sub>SO<sub>4</sub> - 15% H<sub>3</sub>PO<sub>4</sub> and 5 drops of 0.2% diphenylamine sulphate indicator were added. The solution was titrated with 0.1 N K<sub>2</sub>CrO<sub>7</sub> until the end-point was reached (i.e. when first tinge of purple appeared that remained permanent on shaking). Ferrous iron concentration was obtained by multiplying the normality of the potassium dichromate solution times the volume used to reach the end point times 55.847 (MW of iron). This value was divided by the volume of test solution.

#### 2.4.5 Solids Content of AMD Generated by Lime Neutralization

A 15% (w/v) slurry of slaked lime was added to a 500 mL volume of AMD at a flow rate of 0.5 mL/min with continuous magnetic stirring at 400 rpm until the pH reached 10.0. The solution was sparged with compressed air throughout the neutralization. The mixture was left to stir for a total reaction time of 1.0 h. The precipitate was allowed to settle for 1.0 h. The solids were collected by vacuum filtration through #3 Whatman filter paper. The solids were oven dried at 90°C for 16-24 h then weighed.

## **2.5 Mineralogy**

Mineralogical analysis of sludges is complicated by their high water content and amorphous nature. The samples were freeze-dried to remove the water while maintaining their structural integrity. The sludges were examined by X-ray diffractometry (XRD). If additional information was required the sludges were then analyzed by the scanning electron microscope (SEM) equipped with an energy dispersive X-ray analysis (EDX) system.

## **2.6 Leachability**

Sludge samples were subjected to the Ontario Leachate Extraction Procedure 347 (LEP) (Government of Ontario 1994). According to this procedure, if the sample contained distinct liquid and solid phases it was separated into its component phases using pressure filtration. With the sludge samples under investigation this procedure removed only a portion of the liquid, leaving the bulk of the liquid entrapped with the solids in a gel-like mass of unknown homogeneity. This procedure was modified to meet sample requirements. Samples taken from the well-mixed sludge slurry were weighed then extracted, without phase separation. The solids content was used to determine the actual dry weight of the solids for extraction; the volume of liquid present in the sample was subtracted from the volume of water added to provide a final liquid-to-solid ratio of 20:1.

The initial leachant for the Ontario LEP was water. However, once the sample was added the pH of the leaching solution was monitored at set intervals during the course of the extraction and manually adjusted to pH 5.0 with acetic acid if the pH was greater than 5.2. Since there is a specified maximum for acid addition, a pH of 5.0 may not be attained for highly alkaline samples. The leachates were analyzed for the following metals: Cd, Fe, Pb, Zn.

Detailed information on metal leachability from AMD treatment sludges is reported in Part 1 of this research study (Zinck *et al.* 1997).

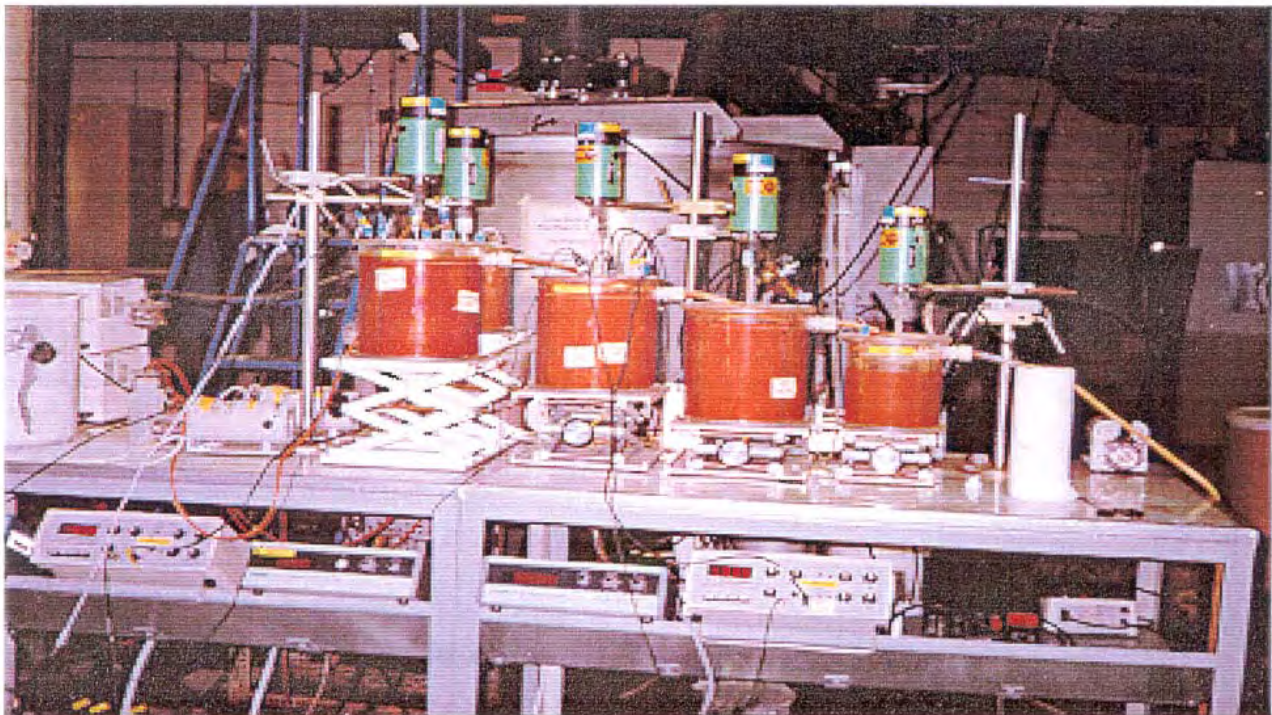
### 3.0 HIGH DENSITY SLUDGE PILOT PLANT

#### 3.1 Design and Construction

The pilot plant was developed and built under the auspices of a MMSL core project in this area. The aim was to construct a modular and transportable unit that could be modified to test different plant processes and effluents of relevance to industrial treatment plants. The unit can be run continuously (with a turnover time of about 12 h at a flow rate of 200 mL/min), semi-continuously or in batch mode.

The HDS process configuration used in this study was based on analysis of other lime neutralization processes. It allows for a thorough monitoring of the treatment system so that chemical reactions and physical changes which occur when the process parameters are altered can be assessed. The basic structure consists of two components; the bench unit and the thickener (Figure 3.1.1). The bench is constructed of two carts, each cart measures 30" x 4'. These carts are equipped with castors for easy transport and "leveling bolts" at the bottom to provide stability. The two carts are bolted together to produce a stable bench. This bench is equipped with shelves underneath the top to house electrical instruments such as pH meters/controllers, pumps, etc. Containers used in the pilot plant include in-house designed 6-L acrylic continuous stir tank reactors (CSTR) and 400mL modified glass beakers. The reactors are placed on lab jacks, which are adjusted in height to create a cascade effect. The thickener used is a 115L hydroclassifier (30" in dia) with a rake. The hydroclassifier was modified to thicken the sludge in the underflow and clarify the water.

Figure 3.1.1: A front view of the High Density Sludge Pilot Plant. Mechanical stirrers, each equipped with six-blade turbine impellers, are provided for all the reactors.



### 3.2 Pilot Plant Configuration for the HDS Study

The pilot plant configuration used for the HDS study consists of a gravity-fed cascade of tanks that use **stepwise** neutralization, aeration, flocculation and sludge recycle processes to produce a high density sludge (Figure 3.2.1). This process was similar to the HDS process used at Mine Doyon. Synthetic AMD is pumped into **the** first reactor (**R1**), and the **pH** is increased to 3.5 with recycled sludge from the thickener underflow. The amount of sludge recycled to **R1** is controlled by the **pH** in **R1**. In **R1** iron (III) and **aluminum** undergo hydrolytic precipitation; gypsum formation and metal **coprecipitation/** adsorption may also occur. **R1** overflows to the second reactor (**R2**), where air is sparged at 0.6 L/min to oxidize any ferrous iron to its ferric state. The **pH** in **R2** is adjusted to **pH** 10.0 with the overflow of recycled sludge and slaked lime from the sludge/lime rapid mix tank. Sludge is added to the sludge/lime tank at a pre-set rate, while the amount of lime added to the sludge/lime tank is controlled by the **pH** in the **R2** tank. Raising the **pH** to 10 ensures complete hydrolytic precipitation of zinc, iron and the other remaining metals. **R2** overflows to the retention tank (**R3**) to complete metal precipitation and iron oxidation, with air sparged at 0.6 L/min. Polymer is added at the **R3** overflow line, and the slurry enters the short retention polymer tank. The slurry from the polymer tank then flows by gravity into the thickener.

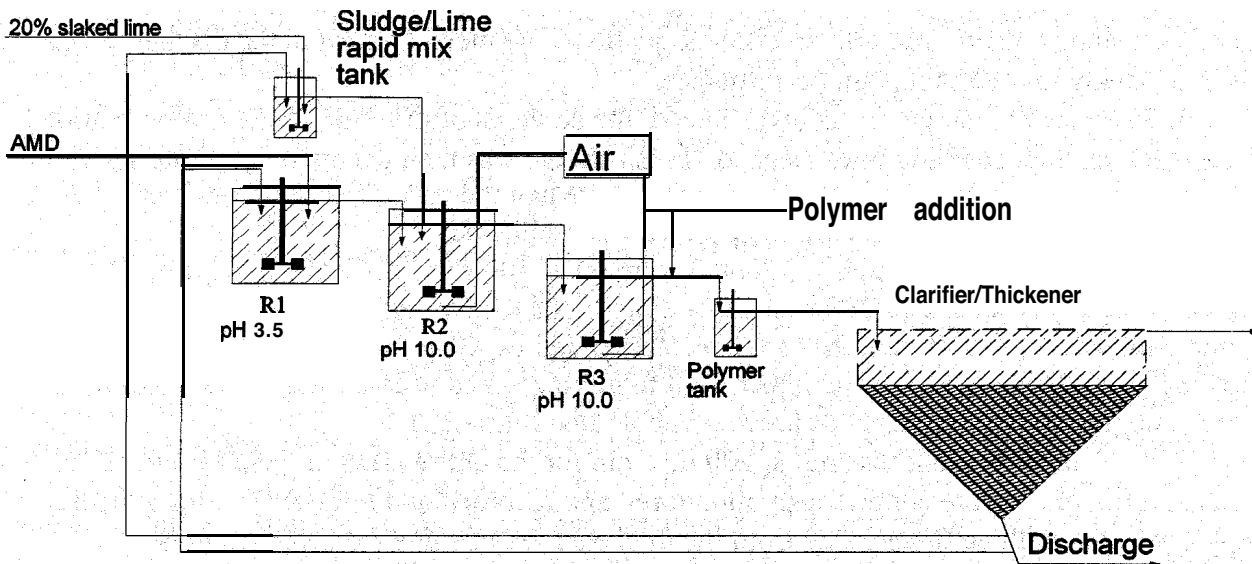


Figure 3.2.1: A schematic of the HDS pilot plant configuration.

Prior to this study several commissioning runs were made to test the system configuration and locate potential problems. Several modifications were made to the plant that are worth noting.

Introduction of a feedwell in the center of the thickener prevented short-circuiting of the sludge particles, and produced better sludge settling and less turbid effluent. This modification also improved the visual determination of the sludge bed height which is used to calculate the sludge bed retention. This information was used to verify whether suitable volumes of sludge were discharged from the system to maintain a constant bed height.

Initially, additional lime was added to R2 if the tank was below pH 10. This was modified so that the pH in R2 was controlled by feedback to the sludge/lime slurry tank. The pH probe in R2 was set at pH 9.8. When the pH fell below this level additional slaked lime was added to the sludge/lime rapid mix tank. The overflow from the rapid mix tank then entered R2. This improved the dissolution of the lime prior to addition to R2 and provided better pH control. The discharge was measured for pH on a weekly basis when samples were collected for metal determination.

A plant kill switch was later introduced as a safeguard when the plant was run under low supervision (i.e. nights, weekends). The kill switch is triggered if the pH in the reactors overshoots the upper set point of 10.8. This may occur as a result of blockage, breakage or equipment malfunction. The kill switch also prevents excessive lime addition which may lead to extensive scaling and plant disruption.

### **3.3 Test Conditions**

The test parameters studied and optimized in the HDS pilot plant were agitation rate, recycle rate, flocculant concentration and sludge discharge rate. The focus of this study was primarily on sludge quality rather than effluent quality. The metal content in the discharge was measured weekly to ascertain plant performance.

Before a new parameter was investigated the contents of the entire system were emptied and the reactors, thickener and lines cleaned. Fresh sludge was then generated until the standard bed height was reached, then recycling was initiated. When the parameter variables were changed the system was run for 12 - 14 h, until the process was stabilized.

Agitation rates for Reactors 1, 2, and 3 were set at 400 rpm, while the rapid mix sludge/lime tank was set at 200-300 rpm depending on the density of the recycle sludge. The polymer tank was set at 250 rpm, the speed recommended by the polymer manufacturer. Zeta-Meter, Inc. (1993) claims there is an upper limit to mixing speed because high shear conditions can break up microflocs and delay or prevent visible floc formation.

The pilot plant was run at 200 mL/min for the entire HDS process (Table 3.3.1). The pH and flowrates were continuously monitored and recorded at 4 h intervals during the day.

Samples were taken three times a day from the thickener recycle line for percent solids determination.

The preferred recycle sludge flowrate was set at 10% of the total flowrate. When the rates were increased, the thickener became very turbid, making it impossible to see the sludge bed height. Sludge discharge was started after plant equilibrium was achieved. The discharge pump was controlled by a programmable timer set to run every four hours for 5 minutes at a flowrate of 100 mL/min. In most cases the time to reach steady state was 12 hours.

Table 3.3.1: A summary of the pilot plant flowrates and retention times.

Tanks	Flowrate mL/min	Active Volume L	Retention Time min
Sludge/lime rapid mix tank	0-60	0.125	0-6
Reactor 1	140-200	6	30-50
Reactor 2	200	6	30
Reactor 3	200	6	30
Polymer tank	200	0.175	1
Thickener	200	115	575

### 3.4. The Chemical Process

The units of the HDS pilot plant were assessed biweekly to ensure that the plant was running at high efficiency. Chemical and physical analyses were performed on samples collected from each reactor, as well as the thickener to ensure that the retention times, mixing rates, aeration, flocculation and neutralization processes were sufficient to obtain complete metal precipitation and sludge densification.

The results for one of the biweekly tests are discussed below. The following test conditions were used: agitation rate of 400 rpm for R1, R2 and R3 and 250 rpm for polymer tank; recycle rate of 20%; iron concentration of 900 mg Fe<sup>3+</sup>/L and 500 mg Fe<sup>2+</sup>/L; polymer concentration of 0.045 mg E10/g solids. The metal composition of the reactor effluents are shown in Table 3.4.1. Synthetic AMD (pH 2.8) was pumped into reactor 1. A small amount of recycled sludge from the thickener was added to raise the pH to 3.5. Under acidic conditions the metals in the sludge were resolubilized, so that the concentration of all the metals in R1 increased, except for iron. AMD consisted of iron in the ferric state (900 mg/L) and the ferrous state (500 mg/L). At pH 3.5, most of the ferric iron had precipitated, leaving mainly ferrous iron (478 mg/L, as determined by titration). The concentration of Mn, Zn, Cd, Co and Mg in R1 effluent doubled, as the pH range for their precipitation is much higher. The metal concentration of Cu and Al in the effluent increased to a lesser extent. Some of the copper likely coprecipitated with the ferric iron, whereas aluminum has a low metal solubility and was expected to partially precipitate at this pH (Vachon *et al.* 1987).

In R2, all the metals have precipitated out to the same levels detected in the polymer overflow tank. Provincial regulations for effluent discharge are met for copper, iron and zinc. No ferrous or ferric iron was present in R2. Compressed air was sparged into R2 at 0.6 SLPM and completely oxidized ferrous iron to ferric iron which precipitated out.

The role of R3 was to ensure that complete ferrous oxidation and metal precipitation had occurred. Reactor 3 does not appear to be required with this AMD source under these run conditions. It was included in the configuration as it may be required when test conditions are more demanding, such as at higher ferrous iron concentrations.

Calcium levels were followed throughout the system. They were originally low, at levels normally present in tap water (20 mg/L). In R1 the Ca concentration increased to 470 mg/L as lime and gypsum present in the lime/sludge mixture dissolved in the acidic AMD solution. Additional lime was fed into R2 and the Ca concentration increased to 683 mg/L. A large portion of the added Ca precipitated out as gypsum ( $\text{CaSO}_4 \cdot 2\text{H}_2\text{O}$ ). Gypsum scaling is extensive in R2 as reflected in the large drop in sulphate concentration from 4966 to 1686 mg/L. No additional lime was added after R2 and the Ca levels declined. The final concentration in the thickener overflow was roughly equimolar to that of  $\text{SO}_4$ , and reflects the solubility of  $\text{CaSO}_4$  in water.

Table 3.4.1 Chemical analyses of effluents sampled from each reactor

Reactor Effluent	pH	Fe <sup>2+</sup> mg/L	SO <sub>4</sub> mg/L	Metal Concentration, mg/L								
				Cu	Fe	Ca	Mn	Zn	Cd*	Co	Mg	Al
AMD	2.40	475.7	4467	9.7	1084	20.7	12.7	158.4	2.5	2	114.3	218.5
Sludge/ Lime		0	1238	<0.1	<0.3	503.4	<0.03	<0.2	<0.1	<0.7	0.1	<2
R1	3.52	477.5	4922	15.7	389	469.6	26.8	318.7	4.8	4.5	231.9	290.8
R2	9.82	0	1686	<0.1	<0.3	683.4	<0.03	<0.2	<0.1	<0.7	2.5	<2
R3	9.80	0	1585	<0.1	<0.3	632	<0.03	<0.2	<0.1	<0.7	5.4	<2
Polymer Tank	9.50	0	1576	<0.1	<0.3	629.5	<0.03	<0.2	<0.1	<0.7	5.6	<2
Thickener		0	2225	<0.1	<0.3	867.6	<0.03	<0.2	<0.1	<0.7	15.5	<2
Most stringent provincial regulations for effluent discharge (Zinck <i>et al</i> , 1997)				0.3	3			0.5	0.05			

\* The ICP method used for analysis was unable to determine Cd concentration at levels below 0.1 mg/L.

### 3.5 Future Design Modifications

CANMET plans to further optimize liquid/solids separation in the HDS pilot plant. Many existing mine drainage plants utilize one of the following types of liquid-solid separators: (1) conventional clarifiers, (2) upflow solids contact or flocculator clarifiers, and (3) thickeners. The high density sludge system requires both clarity of final effluent from the clarifier and sludge densification produced from thickeners. Consequently, most liquid-solid separators employed in



mine drainage plants should be called clarifiers, but because of their large diameter requiring heavy-duty raking mechanisms, they are termed thickeners.

To meet the recommended rise velocity (EPA, 1983), and improve sludge settling and densification, the existing conventional type thickener/clarifier in the HDS configuration will be replaced with a column type thickener/clarifier. A column thickener with a rise velocity of 0.02 m/min has been built and is under investigation as part of a CANMET core project. The optimum bed height of 35-40 cm provides a sludge inventory of 6-7 L.

## 4.0 PILOT PLANT SCALE TESTS

### 4.1 Agitation Rate

#### 4.1.1 Introduction

The effect of agitation rate on sludge properties is an important parameter in sludge production. It was the first parameter examined as it would strongly influence the results of the other tests. Benefits of higher agitation rate include better dispersion of added lime and recycled sludge, improved aeration resulting in faster oxidation rates for ferrous iron, and efficient mixing so larger, solid particles remain suspended. Disadvantages include increased energy requirements and possible particle attrition. In general, the higher the agitation rate and the greater the turbulence, the more efficient the mixing.

#### 4.1.2 Methods

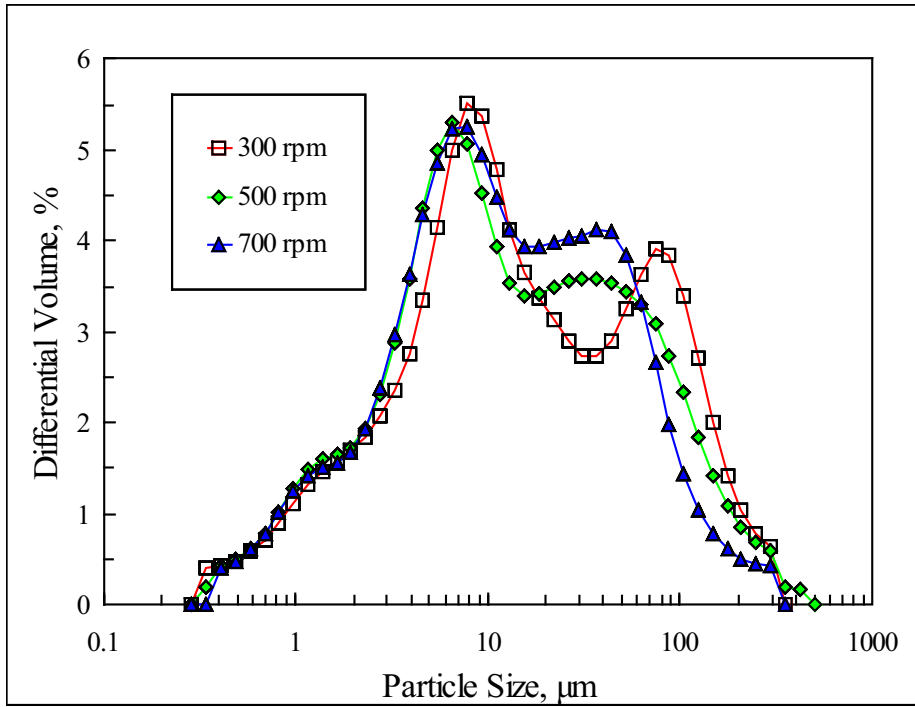
Mixing was done mechanically by means of a rotating 6-bladed turbine impeller. The reactors were designed with 4 equidistant baffles to increase turbulence and to prevent swirling and vortex formation. Agitation rates of 300, 500 and 700 rpm were investigated in the three CSTR reactors to determine the optimal mixing rate for sludge production. The Reynolds number for 200 rpm, 400 rpm and 600 rpm were approximately 5500, 11000 and 16500, respectively. The polymer tank was run at a constant agitation rate of 250 rpm. The raw water flowrate was 200 mL/min with a 20% (v/v) sludge recycle ratio. Percol E10 was added at 0.04 mg/g dry solids. Fractions were collected at the reactor overflow tubes, then chemically and physically characterized.

#### 4.1.3 Results

##### ***Particle Size***

At higher agitation rates the particle size distribution shifted to a lower size fraction (Figure 4.1.1). This could be due to particle shearing or to greater particle compaction during secondary (heterogeneous) nucleation. The average particle size decreased with increase in agitation. The mean particle size (50%) was 12.0  $\mu\text{m}$  at 300 rpm, 11.0  $\mu\text{m}$  at 500 rpm and 10.7  $\mu\text{m}$  at 700 rpm. The 300 rpm system exhibited a pronounced bimodal particle size distribution curve. This bimodal distribution is expected when both freshly-produced sludge and recycled sludge are present (Demopoulos *et al.* 1995). The smaller particles appear to be newly formed gypsum particles and precipitated metals, while the larger particles may be recycled sludge coprecipitated with freshly deposited metal hydroxides. At 500 and 700 rpm the bimodal distribution is less pronounced due to reduction of the larger size particle peak, likely caused by attrition at higher speeds. Examination of sludge produced at 300 rpm, with and without sludge recycle, explains the dual nucleation theory discussed above (Figure 4.1.2). Sludge generated without recycle has a peak maximum at 18.5  $\mu\text{m}$ . Recycle of the sludge results in attrition of this peak, reducing the peak maximum to 7.8  $\mu\text{m}$ . Concurrently, a portion of the recycled material combines with newly formed metal hydroxides and gypsum to form a broad range of larger

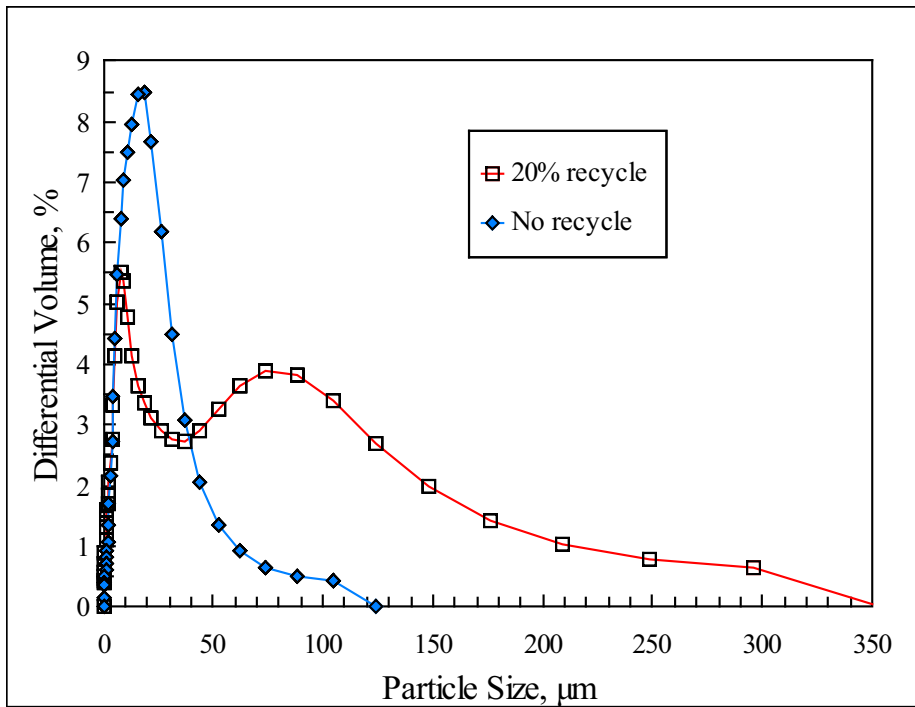
particles (peak maximum of  $74 \mu\text{m}$ ). Further discussion on the effect of sludge recycle on



particle size distribution is given in Section 4.3.

Figure 4.1.1: Effect of agitation on particle size distribution, with 20% sludge recycle

Figure 4.1.2: Sludges formed, with and without recycle, at 300 rpm



### ***Chemical Composition of AMD and Effluent***

Federal and provincial regulations are in place for release of mining effluents into the environment. An effluent is considered unsafe if its metal concentration exceeds the regulatory limits. The metal and sulphate compositions for AMD and the effluents produced at different agitation rates are given in Table 4.1.1. All agitation rates yielded effluents that were well below the most stringent provincial regulations limits for discharge. The metal content of the effluent was similar for all agitation rates. This suggests that agitation rate impacted primarily on the physical mechanisms rather than the chemical mechanisms. The 300 rpm agitation rate had the lowest turbidity value of 97 NTU compared with 136-137 NTU for the 500 and 700 rpm systems. Higher turbidity is likely due to the formation of fines (as a result of shearing) at the higher agitation rates.

### ***Metal Leachability of Sludge Discharge***

The leachability of sludge produced under the different agitation rates was tested using the Ontario Leachate Extraction Procedure. The sludge samples were tested for cadmium, iron, lead and zinc leachability using an acetic acid extraction test. Leachability was comparable for iron and lead at all agitation rates (Table 4.1.2). Metal leaching for cadmium and zinc was lowest for the sludge produced at 500 rpm. All the agitation rates produced sludges that met provincial leachate regulations for discharge.

### ***Physical Properties***

Percent solids was equivalent for all the agitation rates at roughly 31% (Figure 4.1.3). The fastest settling rate was 2.0 m/h at 500 rpm. The 700 rpm system had a significantly lower settling rate of 0.6 m/h, likely due to a higher incidence of particle shearing. A low flocculant concentration (0.04 mg/g solids) was used for these tests; settling rates may be improved with higher flocculant concentrations. Viscosity was low for all systems, ranging from 18 to 25 cP. There was no problem with Adonutting® of the thickener sludge which may be encountered at higher viscosities (Aubé and Payant, 1996).

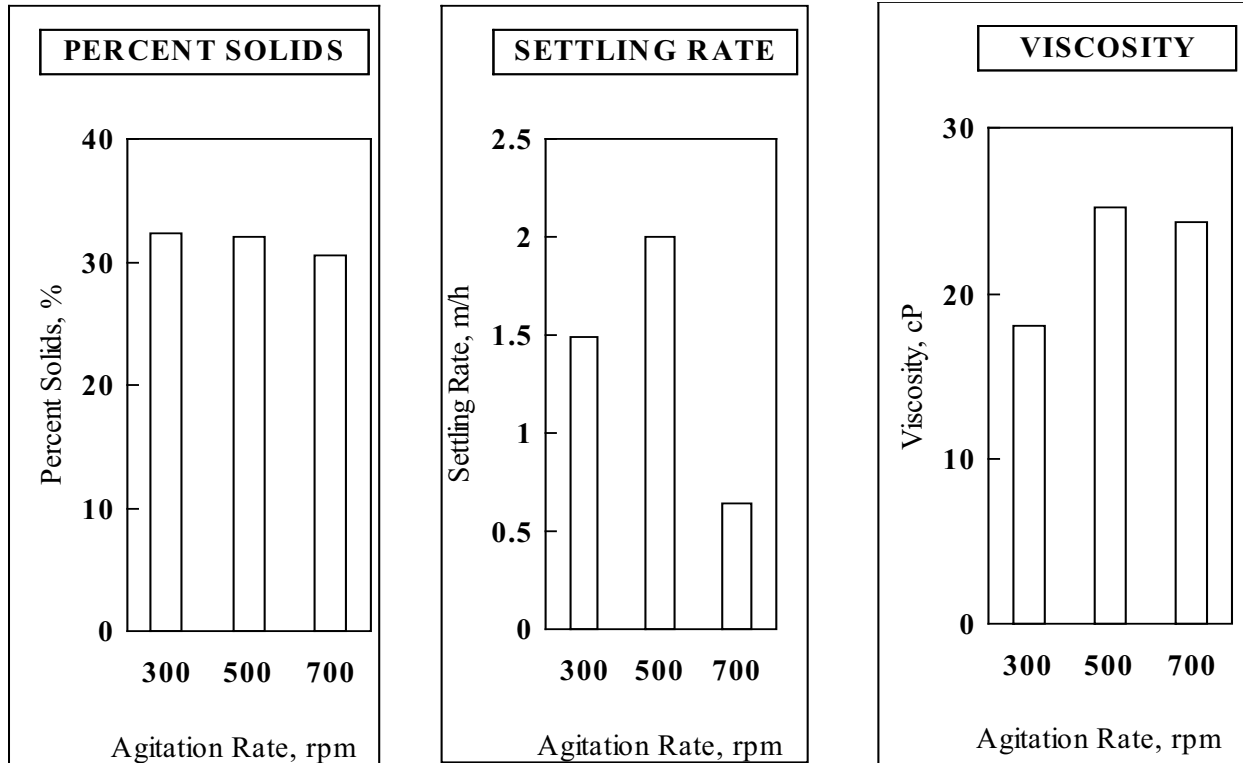
Table 4.1.1: Metal and sulphate composition of AMD and effluent produced under different agitation rates

Source	Agitation rate (rpm)	Turbidity (NTU)	Concentration, mg/L									
			Cu	Fe	Zn	Mg	Mn	Al	Ca	Co	Cd	SO <sub>4</sub>
AMD	-		11.1	919	160.6	114.7	11.66	205	22.97	2.0	2.6	4379
Effluent	300	97	<0.1	<0.3	<0.2	18.1	<0.03	<2	750.2	<0.7	<0.1	1988
Effluent	500	137	<0.1	<0.3	<0.2	12.1	<0.03	<2	833.9	<0.7	<0.1	2099
Effluent	700	136	<0.1	<0.3	<0.2	26.7	<0.03	<2	806.4	<0.7	<0.1	2118
Most stringent provincial regulations for effluent discharge (Zinck <i>et al.</i> 1997)			0.3	3.0	0.5						0.05	

Table 4.1.2: Effect of agitation rate on leachability of sludge discharge using the Ontario LEP

Agitation rates (rpm)	Metals in Sludge Leachate				
	Cd $\mu\text{g/L}$	Fe mg/L	Pb $\mu\text{g/L}$	Zn mg/L	
300	403.4	<0.1	1.7	2.05	
500	63.5	<0.1	2.4	0.26	
700	267.3	<0.1	1.8	1.74	
Most stringent provincial regulations for sludge discharge (Zinck <i>et al.</i> 1997)	500	1000	5000	500	

Figure 4.1.3: Physical properties of sludges produced under different agitation rates



#### 4.1.4 Discussion

The agitation rate to be used for further tests was selected by examining the chemical and physical characteristics of the sludges produced at the different rates. Agitation rate had little effect on either the effluent quality or sludge leachability and all samples met Canadian regulatory limits (Zinck *et al.* 1997). Although effluent discharge requirements were met, the effluent turbidities were somewhat high, ranging from 97-136 NTU. This suggests that improvements should be made to the process to eliminate or reduce these fine particles which are not settling out. The flocculant concentration of 0.040 mg Percol E10/g solids may be too low for proper clarification.

An agitation rate of 400 rpm was selected for further tests as a compromise between 300 rpm which had the lowest turbidity and 500 rpm which had the fastest settling rate. In general, the cost of mechanical stirring increases with agitation rate; and as such would be higher at 500 rpm than 300 rpm. However, proper mixing of the slurry must be ensured; 300 rpm may be too low to keep material suspended if larger particles are formed or faster settling rates are achieved.

It is postulated that at lower agitation rates porous particles with floc-like characteristics form. Increasing the agitation speed reduces the apparent particle size through tighter aggregation. These denser particle/aggregates settle more quickly than the larger, porous particles/flocs formed at 300 rpm. At 700 rpm, the high hydrodynamic shear causes particle collisions and attrition resulting in the formation of fines which hinder sludge settleability and effluent clarity.

## 4.2 Flocculant Addition

### 4.2.1 Introduction

Flocculant type and concentration has a major impact on sludge properties. Flocculation serves three purposes in sludge neutralization processes; it aids in clarification so the effluent can be safely released, it promotes the formation of metal hydroxide-gypsum flocs which settle more rapidly and it produces a denser, higher solids sludge.

A large number of nonionic, anionic and cationic water-soluble polymers of varying ionic charge density and molecular weight are available for use in mineral processing. The ionic types are designed for different applications, with the anionic flocculants suggested for use with suspensions containing minerals, under neutral and alkaline condition. Percol E10, Percol 338 and Percol 727 are all anionic flocculants widely used in the Canadian mining industry. Percol E10 is a high molecular weight, slightly anionic polyacrylamide flocculant, 338 is a moderately high molecular weight polyacrylamide flocculant and 727 is a very high molecular weight polyacrylamide flocculant. These flocculants are used in a wide variety of mineral processing operations, with 338 recommended for thickening of metal hydroxides and 727 suggested for sedimentation of fine sands and clays. Dosage depends on the application but normally lies in the range of 2 g to 200 g per tonne of dry material flocculated (or 0.002 mg - 0.22 mg/g solids) (Allied Colloids Data Sheet). Industries surveyed reported flocculant dosages varying from 0.10mg/g solids to 0.25 mg/g solids (Zinck *et al.* 1997, Aubé and Payant 1996).

Determination of optimal polymer concentration is critical. Excess flocculant is uneconomical and may inhibit flocculation and lower the settling rate (Benefield *et al.* 1982; Zeta-Meter 1993). Another problem with polymer overdosing is sludge Adonutting@. This occurs when the sludge becomes very thick and turns with the rakes in the thickener rather than moving towards the core. A hole forms in the centre and low density sludge is collected and recycled. Aubé and Payant (1996) reported that high concentrations of flocculant contributed to sludge Adonutting@.

Solids content of the mixture must be taken into account for determination of optimal polymer concentration. An inverse relationship exists between solids content and optimal polymer dosage. At low solids content a large excess of polymer is required to enmesh the relatively few particles. At high solids content, as for recycled systems, flocculation will occur at a lower dosage (Benefield *et al.* 1982). Determination of optimal polymer concentration will be for recycled systems.

### 4.2.2 Results

#### ***Batch Tests on Flocculant Type***

Three flocculants, Percol E10, 338 and 727, were evaluated for their effect on sludge settleability. All flocculants were supplied as free flowing granular powders from Allied Colloids. Flocculants were prepared at 0.05% strength (w/v) in distilled water and used within 24 h. Tests were done by collecting 1-L quantities of unflocculated sludge from the outlet pipe of R3 and gently mixing by inversion with the flocculant. Settling tests (See Methods, Section 2.3.4) were then run.

The first part of the test compared Percol 338 and 727 (Table 4.2.1). Percol 338 performed significantly better than 727 at both flocculant concentrations, achieving a settling rate



of 13.7 m/h when added at 2.0 mg/L sludge.

Table 4.2.1: Comparison of Percol 338 and 727 flocculants.

Flocculant	Volume Added, mL/L sludge	Final Concentration, mg flocculant/L sludge	Settling Rate, m/h
Percol 338	1.0	0.5	5.5
Percol 338	4.0	2.0	13.7
Percol 727	1.0	0.5	1.1
Percol 727	4.0	2.0	10.6

In the next stage, Percol E10 was compared with 338 (Table 4.2.2). At low concentrations, both polymers had poor settling rates, ranging from 0.8 to 1.4 m/h. When the flocculant concentration was increased to 2.0 mg/L sludge the settling rate for Percol E10 of 13.3 m/h was superior to Percol 338 at 3.5 m/h.

Different settling rates were obtained from one series to the next for the same flocculant added at the same concentration. The sludge properties for these two tests were different, in particular the solids content which directly impacts on flocculant performance.

Percol E10 was selected for further studies as it had the best performance with this AMD solution, and it is a common industry choice in both its granular form (Percol E10) and as a liquid dispersion (Percol 90L) (Zinck *et al.* 1997)

Table 4.2.2: Comparison of Percol E10 and 338 flocculants.

Flocculant	Volume Added, mL/L sludge	Final Concentration, mg flocculant/L sludge	Settling Rate, m/h
Percol E10	1.0	0.5	1.4
Percol E10	4.0	2.0	13.3
Percol 338	1.0	0.5	0.8
Percol 338	4.0	2.0	3.5

#### **Batch Tests on Flocculant Concentration**

Tests were done by collecting 1-L quantities of unflocculated sludge from the outlet pipe of R3 and gently mixing by inversion with Percol E10 to produce concentrations of 0.01, 0.05,

0.10 and 0.5 mg E10/g solids. Settling tests were done in duplicate.

The settling rates increased with E10 concentration up to 0.1 mg E10/g solids then leveled out (Figure 4.2.1). The settling rates were 0.49 m/h at 0.01 mg; 1.47 m/h at 0.05 mg; 2.21 m/h at 0.1 mg E10 and 2.38 m/h at 0.5 mg/g solids. These settling tests were done in 1-L graduated cylinders and do not reflect what will occur in larger thickeners. In general, batch tests require a lower polymer concentration for optimal settling, but have poorer settling rates than thickeners. However, they provide a good approximation as to the relative efficiency and dosage range of the polymers. Based on the batch tests the optimal flocculant concentration was 0.10 mg/g solids. This will serve as a starting point for further optimization tests in the pilot plant.

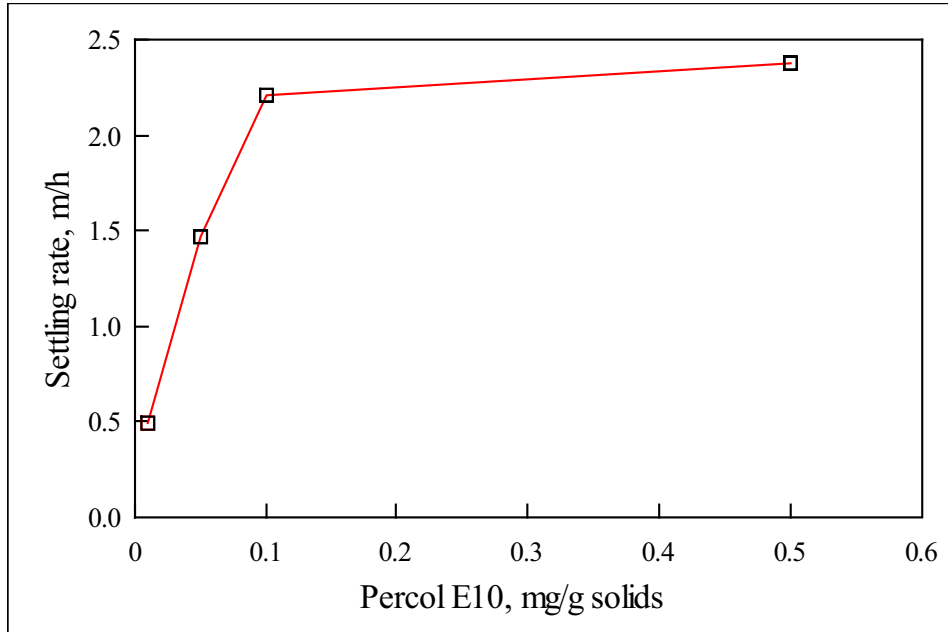


Figure 4.2.1: Effect of Percol E10 concentration on settling rate.

### ***Pilot Plant***

The pilot plant was run at 200 mL/min with a 10% (v/v) sludge recycle rate. Agitation rate of the flocculant tank was set at 250 rpm. This rate was recommended by the manufacturer to prevent shearing, but allows sufficient mixing. Percol E10 was added at concentrations of 0.06 mg/g solids, 0.10 mg/g solids, 0.18 mg/g solids and 0.24 mg/g solids. Chemical and physical characteristics of the recovered sludge and effluent were determined. Settling rates were run on sludge collected from the outlet pipe of the Polymer Mixing Tank.

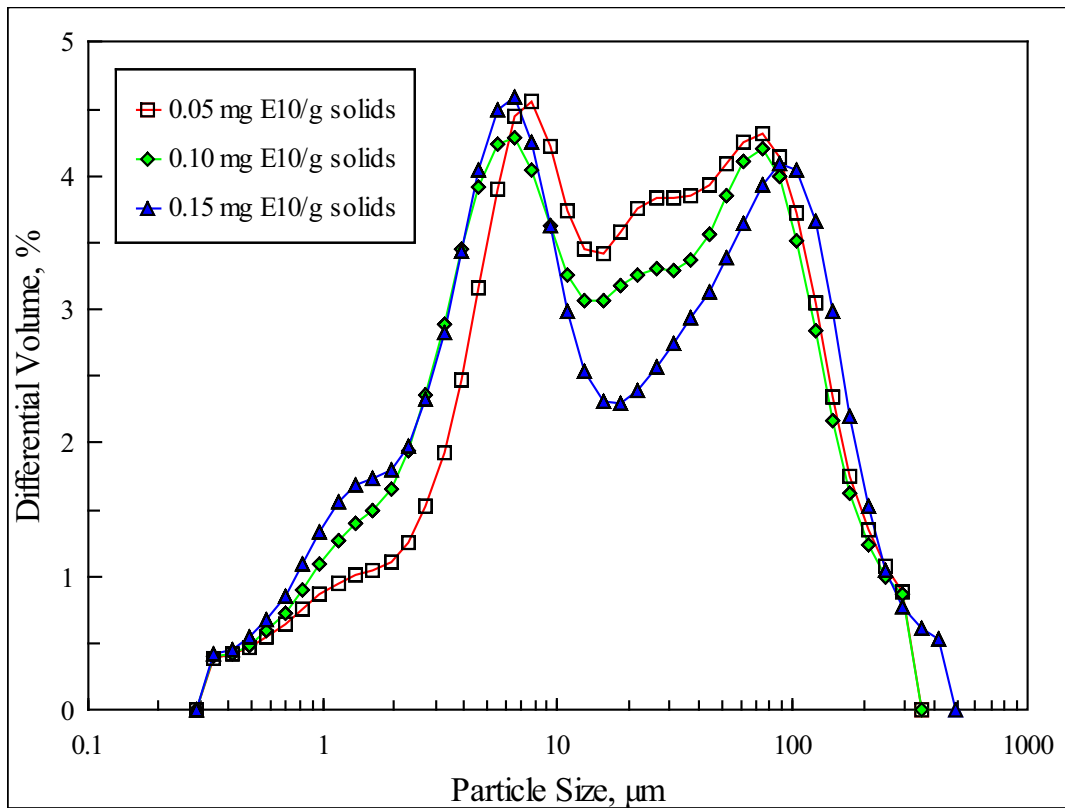
Settling rates of 5.10, 5.94 and 11.33 m/h were obtained when flocculant was added at 0.06 mg/g, 0.10 mg/g and 0.18 mg/g solids, respectively. At the highest concentration tested, 0.24 mg/g solids, donutting was encountered so the run was stopped.

The settling rate increased dramatically when flocculant concentration was increased from 0.10 to 0.18 mg/g solids. This effect was not seen when the settling tests were done in batch reactors. A major difference between tests was the solids content was much higher for the pilot plant/recycled system. At 10% recycle the solids content was about 30-35%, while the batch test used neutralized AMD with a solids content of 7%. A greater number of particles per unit volume provides more opportunity for particles to interact and combine to form floc particles, resulting in a higher settling rate. In addition, skeletal flocs are formed without recycling, whereas denser particles are formed with recycling.

### ***Particle Size***

Particle size distribution showed a pronounced increase in bimodality as flocculant concentration increased (Figure 4.2.2). The recycled peak also became narrower when the flocculant concentration was increased.

Figure 4.2.2: Effect of flocculant concentration on particle size.



Particle size distribution for the different flocculant concentrations showed that the

average particle size (50%) decreased with flocculant addition (Table 4.2.3). This result was not expected, but seems to be due to an abundance of newly-formed small particles which decreased in size when the flocculant concentration was increased.

The beneficial effect of polymer dosage on sludge settleability was examined by eliminating these newly-formed small particles ( $<13\mu\text{m}$ ), from the particle size distribution. The newly-formed sludge particles for the recycled system had peak sizes ranging from 6-8 $\mu\text{m}$ . When these newly-formed small particles, are removed from the calculation, the pattern shifts. The average particle size increased when polymer dosage was increased. This trend suggests that the presence of larger, coarse particles promotes settling. The larger particles would not be slowed down by friction as much as the finer particles and would drag the smaller particles along as they settle.

### ***Chemical Composition of AMD and Effluent***

Turbidities of the effluents were low for all flocculant concentrations examined (Table 4.2.4). Turbidities were measured to assess the performance of the thickener with respect to its ability to handle changes in process parameters. Factors such as insufficient polymer, high fines formation, chemistry of sludge, low sludge density, high recycling rates, high flow rates can all impact on sludge settleability. Turbidity also provides an indication of metal carryover in the effluent. The effluent met Canadian regulations for discharge for copper, iron, zinc, cadmium and lead (Zinck *et al.* 1997). Percol E10 at concentrations  $\geq 0.10$  mg/g solids is efficient at clarifying this AMD solution so that the effluent stream meets discharge requirements.

### ***Physical Properties***

The viscosities of the sludges were low, with values of 23.7, 26.9 and 21.8 cP obtained for 0.06, 0.10 and 0.18 mg Percol E10/g solids. These viscosities were below 50 cP (the viscosity where donutting is expected). Sludge donutting was encountered at the highest flocculant concentration examined, 0.24 mg/g solids. However, the viscosity of this sludge could not be quantified due to poor flowability. Overall, there did not appear to be a correlation between polymer concentration and viscosity.

### **4.2.3 Discussion**

Percol E10 was selected for further studies as it performed the best for this AMD and it is a popular industry choice. However, if other AMD sources were tested the optimal flocculant type should be re-evaluated. The optimal flocculant concentration for fast settling in the pilot plant is less than 0.24 mg/g and is equal to or greater than 0.18 mg/g solids. For future work, under these run conditions, the working range would be 0.15 - 0.20 mg/g solids. A range would allow for fluctuations that occur in the solids content while the system establishes equilibrium. Careful monitoring of the system would allow for more precise adjustments to the polymer concentration.

To give room for further process optimization when testing the other parameters without encountering donutting it was decided to use a sub-optimal flocculant concentration. In particular, recycling studies will be done with up to 40% (v/v) solids recycle. Consequently, further studies were done with Percol E10 at 0.045 - 0.07 mg/g solids.

Table 4.2.3: Effect of flocculant concentration on particle size distribution.

Percol E10 mg/g solids	mg/L (ppm)	Viscosity cP	Solids Content %	Settling Rate m/hr	Particle Size Determinations				
					µm, 10%	µm, 50%	µm, 90%	µm, mV	µm, 50%*
0.06	2.4	23.7	34.06	5.10	2.68	18.7	107.2	40.2	54.0
0.10	4.4	26.9	30.35	5.94	1.86	15.0	103.2	37.7	56.6
0.18	8.0	21.8	32.12	11.33	1.58	13.9	122.4	43.9	69.9
0.24	10.8				S/L separation difficulties				

\* when newly formed sludge particles, < 13.1 µm, are removed from the calculation

Table 4.2.4: Composition of AMD and effluent produced under different flocculant concentrations

Percol E10 conc. % (w/v)	Source	Turbidity (NTU)	Metal Concentration**											
			Cu mg/L	Fe <sup>2+</sup> mg/L	Fe mg/L	Zn mg/L	Mg mg/L	Mn mg/L	Al mg/L	Ca mg/L	Co µg/L	Cd µg/L	Pb µg/L	SO4 mg/L
0.06	AMD		11.2	445.6	1388	154	119	162	244	22.6	2410	2480	1000	4758
0.10	Effluent	9.0	*	*	*	*	*	*	*	*	*	*	*	2151
0.18	Effluent	5.2	<0.010	0.0	<0.07	0.2	12.9	0.012	<1.3	719	2.0	0.7	<1	2282
	Effluent	8.0	<0.010	0.0	<0.07	<0.05	11.9	0.015	<1.3	734	2.2	1.4	<1	2186
Most stringent provincial regulations for effluent discharge (Zinck <i>et al</i> 1997)			0.3		3.0	0.5						50	200	

\* Below detection limit .

\*\* Samples were not filtered prior to analyses and will include dissolved as well as suspended metal concentrations.

## 4.3 Recycle Rate

### 4.3.1 Introduction

The terms recycle ratio and recycle rate are both used to describe recycle proportions. A recycle ratio of 20:1 means that 20 grams of solid are recycled for every gram of solid that is produced in the system. A recycle rate of 20% indicates 20% of the total flow is recycled sludge and 80% is AMD. For this study, tests were performed with no recycle up to a maximum of 40% recycle rate. The AMD flowrate was 200 mL/min. Polymer concentration when recycled sludge was added ranged from 0.034 to 0.062 mg/g solids. The no recycle system had a polymer concentration of 0.088 mg/g solids. Standard plant operating conditions were applied, with R1, R2 and R3 run at 400 rpm and the polymer tank run at 250 rpm.

An important factor in the HDS plant is the recycle ratio. The terms recycle ratio and recycle rate are both used to describe recycle proportions. The recycle rate is the percent of thickener underflow which is recycled. A recycle rate of 20% indicates 20% of the total flow is recycled sludge and 80% is AMD. The solids recycle ratio is the amount of sludge recycled over the amount of sludge produced by the incoming feed, per unit time (Aubé and Payant 1996). A recycle ratio of 20:1 indicates 20 grams of solid are recycled for every gram of solid produced in the system. Plants in industry vary from those running with no recycle up to those with ratios of 40% recycle. For this study, tests were performed at intervals from 0% to 40% recycle rate.

### 4.3.2. Methods

The flowrate was 200 mL/min. Polymer concentration when recycled sludge was added ranged from 0.034 to 0.062 mg/g solids. The no-recycle system had a polymer concentration of 0.088 mg/g solids. Standard plant operating conditions were applied, with R1, R2 and R3 run at 400 rpm and the polymer tank run at 250 rpm.

### 4.3.3 Results

#### ***Recycle rate and ratio***

As expected, a plot of recycle ratio versus recycle rate exhibited a linear relationship (Figure 4.3.1).

#### ***Percent solids***

The percent solids in the sludge increased significantly with recycling (from 7% with no recycle up to 33% with recycle) (Figure 4.3.2). Increasing the amount of sludge that was recycled from 10% to 40% had only a marginal effect on the percent of solids in the sludge. Recycling introduced seed material which facilitated particle growth and increased sludge density.

#### ***Settling rate***

The settling rate of sludge produced at various recycling rates is shown in Figure 4.3.3. There appeared to be a decline in the settling velocity with increased recycling. The settling rate increased slightly with minimal recycling (10%) then decreased as more sludge was recycled. The solids content in the polymer tank was high, especially for the 30% and 40% recycle rates, and likely led to insufficient mixing of the polymer and particles. In addition,

the decline in sludge settleability may result from particle overcrowding and interparticle interactions.

**Lime consumption**

There was a direct relationship between the amount of lime required to treat the AMD solution and the percent of sludge recycled. As the amount of sludge that was recycled was increased, the lime demand to treat the same volume of AMD decreased. This trend reached an asymptotic value around a recycle rate of 50% as the sludge can only neutralize the AMD to a limited pH and additional lime would be required to reach the target pH. This relationship is evident in Figure 4.3.4.

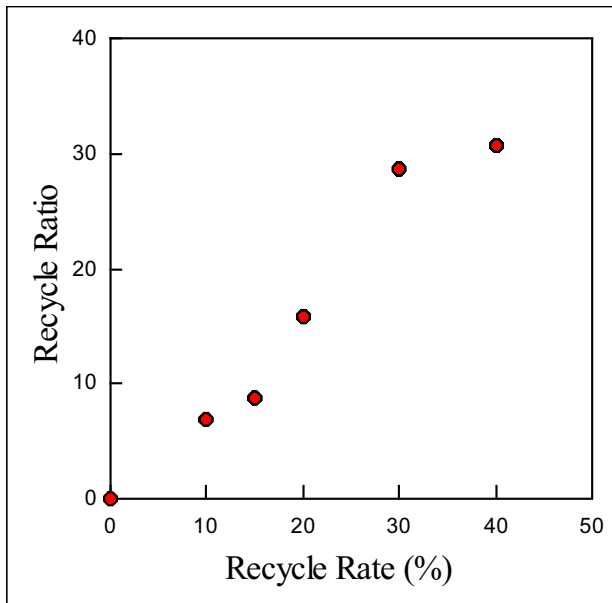


Figure 4.3.1: Recycle rate versus recycle ratio

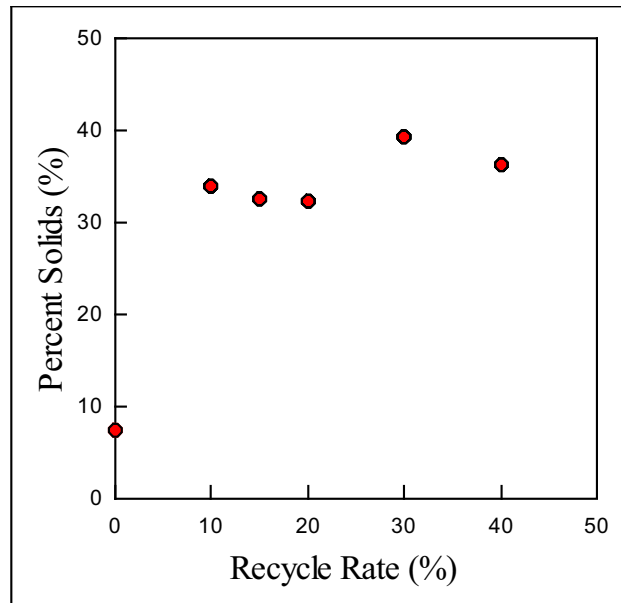


Figure 4.3.2: Effect of recycling on percent solids

Figure 4.3.3: Recycling rate versus settling rate of sludge

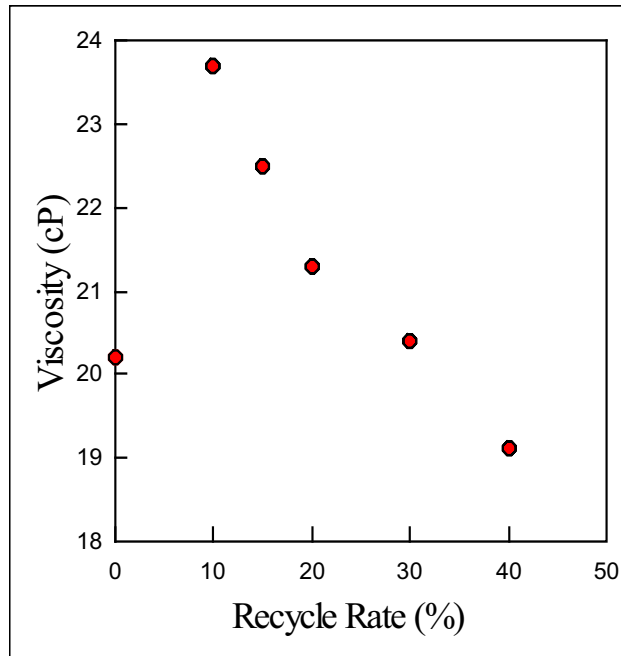
Figure 4.3.4: Relationship between lime consumption and percent sludge recycle



### **Viscosity**

In general, the viscosities of the sludges produced in this study were similar. The lowest viscosity was reported for sludge generated with no recycling. As the recycle rate increased from 10% to 40%, the viscosity of the sludge decreased (Figure 4.3.5). The maximum viscosity encountered was 24 cP, well within the pumpable viscosity range.

Figure 4.3.5:  
between recycling and

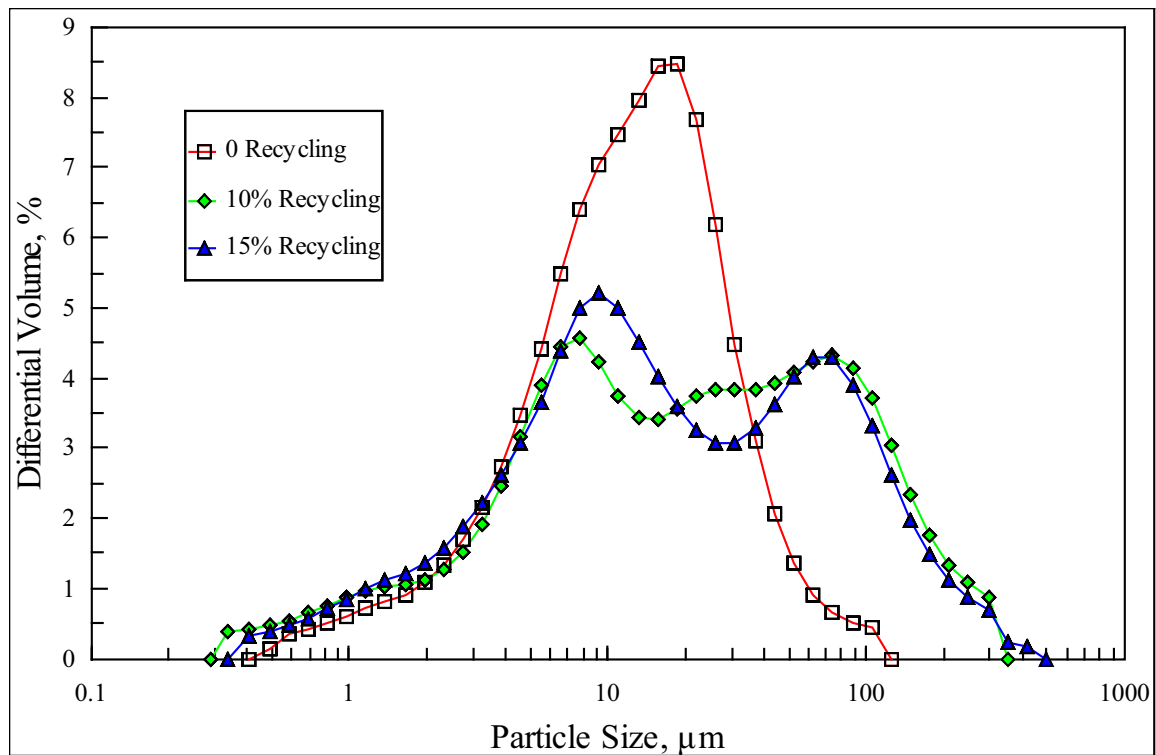


Relationship  
viscosity

### **Bulk density**

Bulk density is a determination of the weight of the sludge in a set volume fraction. The bulk density generally correlates with the solids content in the sludge (Zinck *et al.* 1997).

Therefore, the relationship between bulk density and recycle rate is similar to the relationship observed between percent solids and recycle ratio. Recycling serves to increase the bulk density.



The bulk density of sludge generated without recycling was approximately  $1.05 \text{ g/cm}^3$ , while recycle sludges reported bulk densities of approximately  $1.25 \text{ g/cm}^3$ . As with the percent solids, bulk density appears relatively unaffected by the amount of sludge recycled.

### ***Particle size***

The particle size of sludge produced under varying recycle rates was measured. In the absence of recycling, the sludge displayed a unimodal size distribution with an average particle size of  $\sim 15 \text{ }\mu\text{m}$ . In contrast, recycled sludge displayed a bimodal size distribution (Figure 4.3.6). This behaviour has been observed by others (Demopoulos *et al.* 1995). With increased volume of recycle the mean particle size increased and the particle size distribution shifted to larger size fractions. The volume of particles of a larger size increased with recycle rate (Figure 4.3.7)

Figure 4.3.6: Comparison of particle size distribution for recycled and nonrecycled sludges

Figure 4.3.7: Effect of recycle rate on particle size distribution

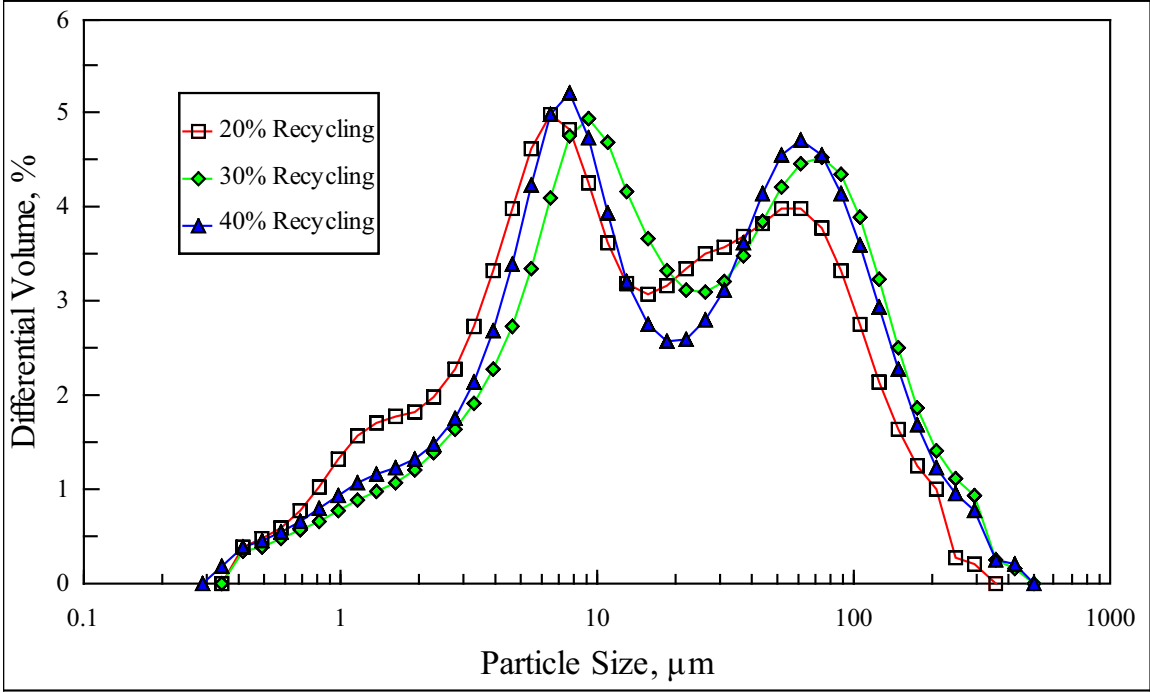
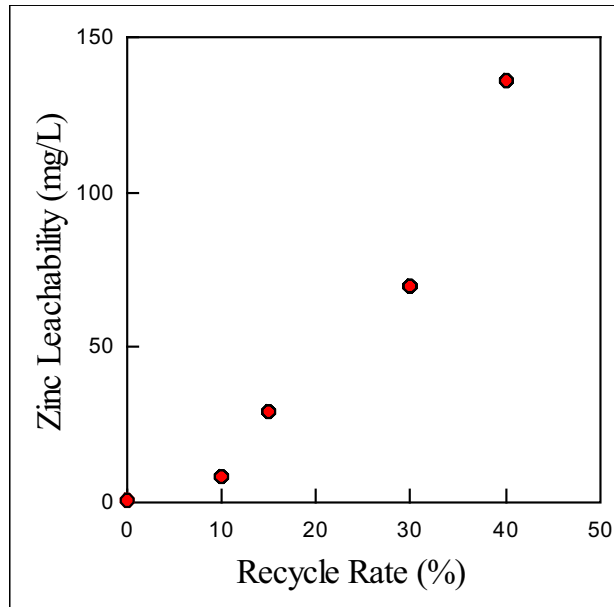


Figure 4.3.8:  
between recycle rate of  
mobility



Relationship  
sludge and zinc

### ***Metal leachability***

The effect of recycle rate on metal leachability from the sludge was studied for Cd, Cu, Fe, Pb and Zn. Marginal metal leachability for Cu, Fe and Pb was noted when sludge recycle was increased. However, in the case of zinc, metal leachability increased significantly with increasing sludge recycle (Figure 4.3.8). Cadmium also showed increase leachability with recycle rate, increasing from 0.01ppb in the absence of recycling to 4.4 ppb at 40% recycle. Zinc and cadmium are particularly sensitive to acid leaching due to their high hydrolytic precipitation pH. When the recycle rate was increased, the metal loading in the sludge was also increased, ultimately impacting metal leachability.

In addition, the decrease in lime consumption (Figure 4.3.4) would reduce the neutralization potential of the sludge thus providing less alkalinity. As result, the leachate pH would decrease and metal leaching would rise. Recycle rate affects both metal loading and lime consumption as thus indirectly affects metal mobility.

#### 4.3.4 Discussion

Recycling is an important component in any high density sludge type treatment process. Recirculated sludge provides seed particles on which particle growth can occur. The recycle ratio or rate determines the amount of sludge recycled back through the system. Some studies suggest that to optimize sludge density for a HDS-type process, a recycle ratio between 20:1 and 30:1 is necessary (Aubé and Payant 1996).

The recycle rate proved to be an important variable in high density sludge production. When the recycle rate was increased, the amount of solids through the system also increased. The overall effect of recycling on the treatment process will vary depending on the properties/parameters of interest. Essentially, recycling significantly improved the solids content of the sludge up to one order of magnitude, when compared to when no recycle was used. However, recycling more sludge had only a marginal effect on the final percent solids. In fact, by introducing more solid particles in the system there is a detrimental effect on the settleability of the sludge. As the particle population in the reactors is increased, so does the probability of particle collisions. These collisions cause the particles to become abraded leading to formation of fines which are difficult to settle, often require longer polishing times and can impact on final effluent quality.

Sludge viscosity was only slightly affected by recycle rate. A small downward trend in viscosity with increased recycle was observed. Again, increased particle collisions reduced the particle size and led to a more fluid sludge. In other studies, increasing the recycle rates resulted in an increase in sludge viscosity (Aubé and Payant 1996). Differences in viscosity can be due to flocculant dosage, AMD composition, operating conditions or methods of viscosity determination.

The particle size distribution quantifies the crystallization processes occurring. The bi-modal distribution shows both particle growth and particle abrasion. The distribution actually broadens with increased recycle due to these two counter processes occurring simultaneously. While increased particle size tends to be beneficial to sludge settleability, this was not observed in this situation. The increased solids population caused a negative effect on settling rate which was not off-set by the increased particle size. The ability of a particle to settle is affected by the volume of solid particles in suspension (Smith 1998). With increased recycling the amount of particles increased and caused a reduction in the settling rate.

Metal leachability marginally increased with the recycle rate, except for zinc. Metal leachability is directly related to metal concentration and final leachate pH and thus would be expected to increase with recycling (Zinck *et al.* 1997). As the recycle rate increased, so did the metal loading in the sludge. Concurrently, the neutralization potential of the sludge decreased as lime consumption declined. Both these factors impact on metal leachability; with zinc particularly susceptible to mobilization as it is one of the last metals to precipitate during neutralization.

From these studies the optimum recycle rate to yield maximum settleability and densification, with limited metal leachability, was determined to lie between 10 to 15% sludge recycle (recycle ratio  $\approx$  10:1). Different treatment systems will yield different optimum values

for percent sludge recycle. However, these results confirm that the selection of 10% recycle as our base operating rate (Section 3.4) was valid for this process and metal strength of the water treated. Recycle ratios can vary considerable from as low as 3:1 to as much as 50:1 and depend primarily on the raw water strength and operating conditions. It is best to complete a series of tests to determine the optimum recycle required.

## 4.4 Ferric-Ferrous Ratio

### 4.4.1 Introduction

At present, the effect of iron valence in the raw water on sludge composition and stability is not fully understood. Ferric oxyhydroxides are considerably more stable than ferrous hydroxides in the generated sludge (Aubé and Payant 1997, MacDonald *et al.* 1989). Consequently, the ferric-ferrous ratio in the effluent may influence the form and degree of crystallinity of the iron oxyhydroxide precipitated, and ultimately the sludge stability. It is believed that different concentrations of ferric and ferrous iron may produce different iron compounds, such as ferrihydrite or goethite.

### 4.4.2 Methods

A series of tests were completed to determine the extent to which the ferric-ferrous ratio in the AMD stream affected sludge production, metal leachability, sludge density and sludge composition. The tests were run at a 10% (v/v) recycle rate. These tests involved varying the initial ratio of ferrous and ferric in the synthetic AMD from a 100% ferrous solution increasing in intervals of 20% until a 100% ferric solution was reached. In addition to the normal sampling routine, effluent from R1, R2, R3 and the polymer tank was collected and analyzed for ferrous iron.

### 4.4.3 Results

#### ***Visual Observations and Sludge Properties***

As the amount of ferric iron in the AMD solution was reduced, the proportion of ferrous iron increased and the sludge colour changed from light orange-brown to dark brown. Furthermore, as the ferric-ferrous ratio was decreased the sludge became more gelatinous and did not compact well in the thickener. Gypsum scaling was also a problem when treating the high ferrous iron solutions. The effect of the ferric-ferrous ratio on properties of sludge is discussed below (Table 4.4.1).

Table 4.4.1: Properties of sludge produced by treating AMD with various ferric-ferrous ratios.

Fe(III):Fe(II) (% ferric)	Polymer Dosage mg E10/ g solids	Percent Solids %	Consumption, g/min		Viscosity cP	Settling Rate m/h
			Lime	Recycle Sludge to R1		
100	0.051	36.0	56.64	393.3	21.2	6.1
80	0.050	34.1	-	355.9	23.9	5.1
61	0.067	31.9	58.11	317.0	24.7	3.5
46	0.063	35.3	52.10	222.6	24.4	4.4
22	0.072	32.5	45.55	97.1	22.3	2.4
18	0.078	23.8	48.95	80.9	21.3	2.4
0	0.073	23.9	41.96	15.8	24.3	4.4

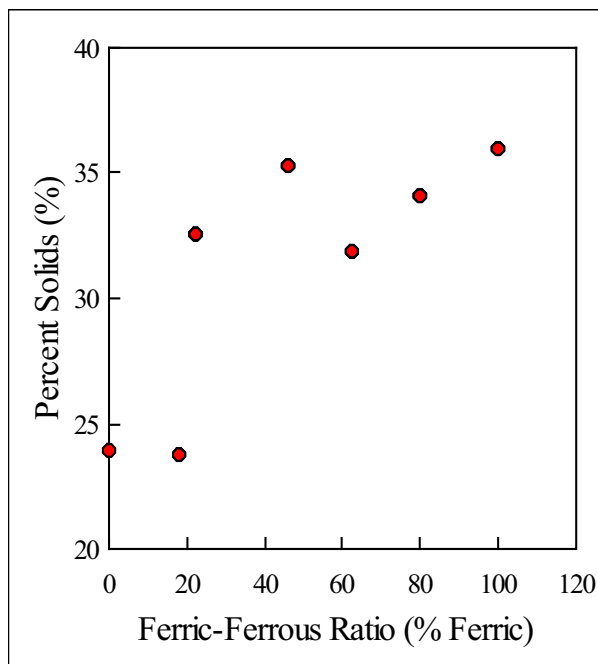
### Percent solids

The percent solids of the sludge increased as the ferric-ferrous ratio increased (Figure 4.4.1). Sludge produced from treating a solution containing 100% ferric iron contained 36% solids, while the sludge generated from an effluent with 100% ferrous iron had 24% solids. Apparently, the addition of ferric ions to the primarily ferrous solution increased the sludge density.

### Settling rate

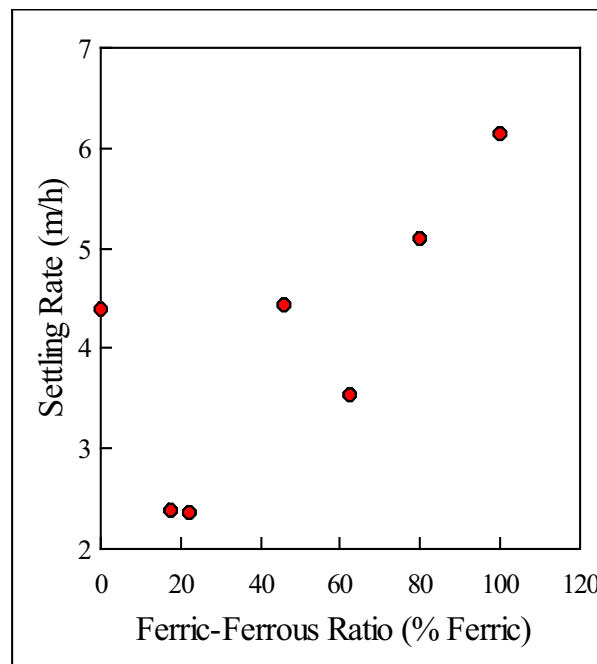
The settling rate of the sludge increased linearly with increased ferric iron addition (Figure 4.4.2). Sludge produced from a 100% ferrous iron solution settled at a rate of 4.4 m/h. The settleability of sludge produced from 20% ferric iron AMD solutions was much slower than either the 100% ferrous or 100% ferric iron AMD sludges. The fastest settling rate of 6.1 m/h was obtained with the 100% ferric iron AMD sludge.

Figure 4.4.1: Effect of ferric-ferrous ratio



on sludge density

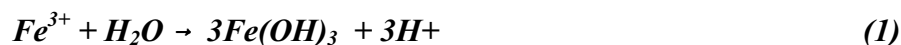
Figure 4.4.2: Effect of ferric-ferrous ratio



on sludge settleability

### Lime consumption

The lime required to treat the ferric-rich solution increased with the ferric iron content (Figure 4.4.3). During hydrolysis, acid generation ( $H^+$ ) is 50% greater for ferric than for ferrous iron. Therefore, lime consumption would be greater as these additional hydrogen ions would need to be neutralized. This simple relationship is presented in equations 1 and 2.



### Viscosity

No correlation between ferric-ferrous ratio and viscosity was found (Figure 4.4.4). The

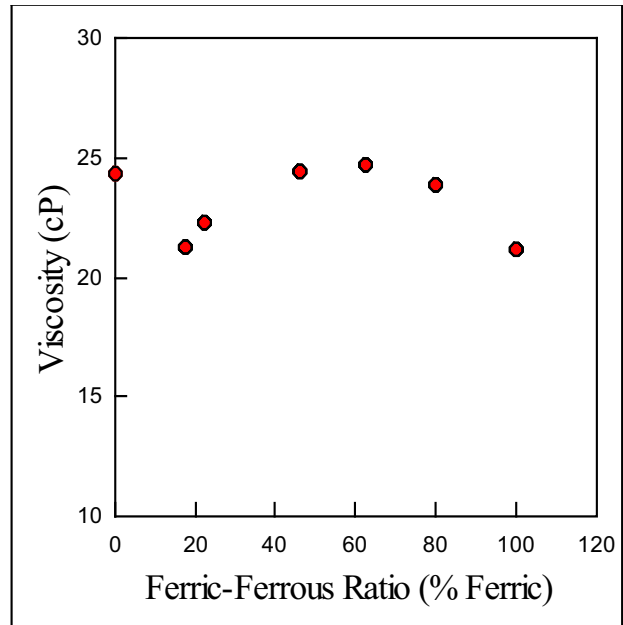
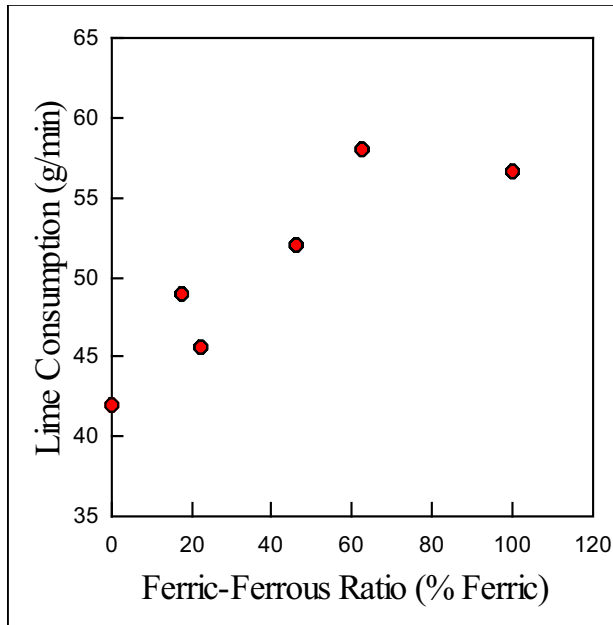


viscosity ranged from 21-25 cP, with the lower values reported for the pure ferric sludge. The sludge with the maximum viscosity was produced from a solution with a ferric-ferrous ratio of 62%.

Figure 4.4.3: Effect of ferric-ferrous ratio on lime consumption

Figure 4.4.4. Effect of ferric-ferrous ratio on sludge viscosity

**Polymer Dosage**



The amount of polymer (Percol E10) required to settle the sludge decreased as the ferric concentration was increased (Figure 4.4.5). When the polymer dosage was plotted against the sludge settling rate an inverse linear relationship was observed for all ratios, except for 0% ferric iron which had a settling rate of 4.5 m/h (Figure 4.4.6). It is possible that the polymer dosage exceeded the necessary requirement and the particles were overdosed causing them to repel and settling to be hindered.

**Particle size**

The bimodal particle size distributions for various ferric-ferrous ratios is shown in Figure 4.4.7. The peak corresponding to the small particle size fraction (5-10 $\mu$ m) shifted to larger sizes with increased ferric concentration. The second peak, centered around 110  $\mu$ m, increased in height when the ferric ratio was increased. Similarly, the more ferric iron in the solution the greater the mean particle size for the sludges (Figure 4.4.8). Lamb and Jacques (1938) found that in pure ferric salt solutions the particle size and stability of oxyhydroxides increases with the concentration of dissolved ferric iron during precipitation. As well, the particle size distribution of the 100% ferric AMD sludge was much narrower than the lower sludges produced with lower ferric ratios.

Figure 4.4.5: Relationship between polymer

Fig 4.4.6: Correlation between settling rate

dosage and ferric-ferrous ratio and polymer dosage  
 Figure 4.4.7: Effect of ferric-ferrous iron ratio on particle size distribution

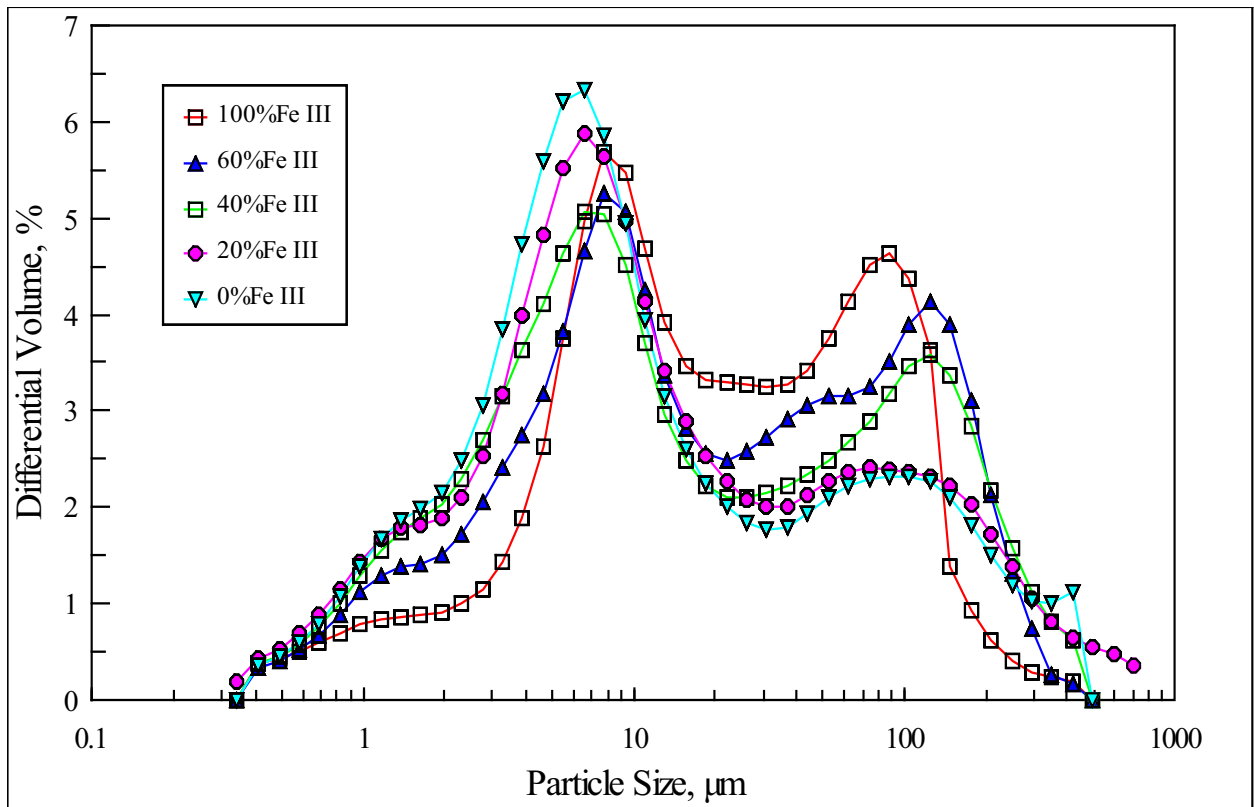
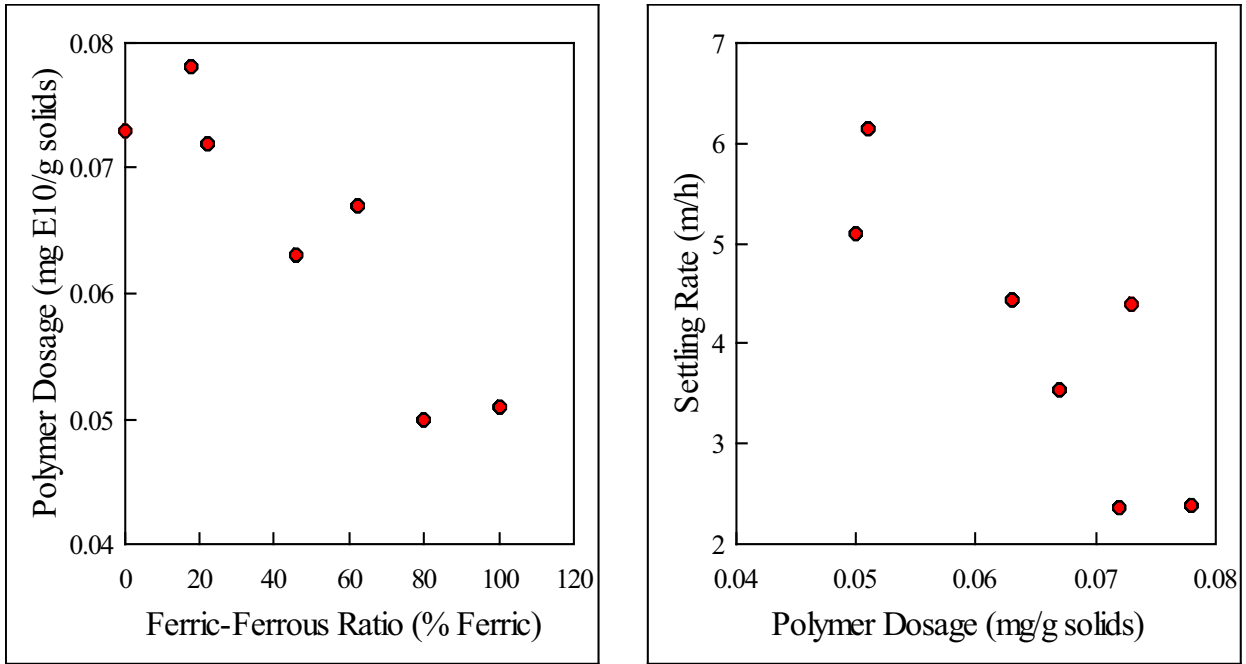


Figure 4.4.8: Effect of ferric-ferrous ratio on mean particle size

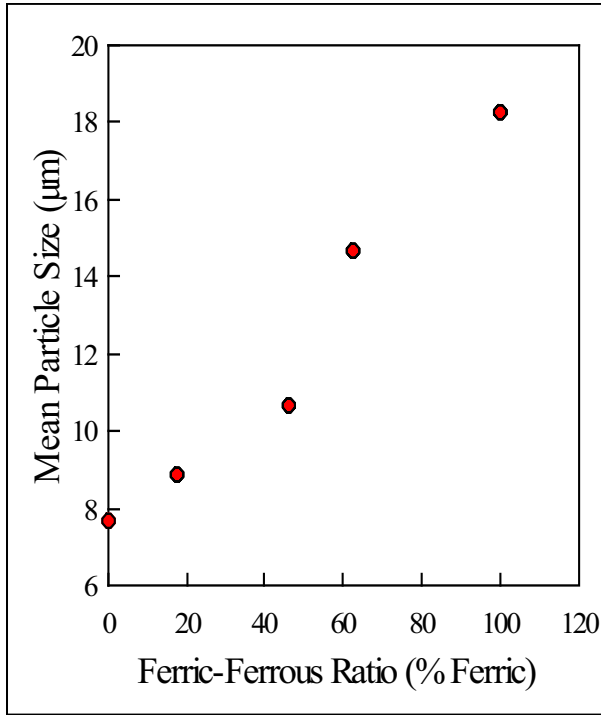
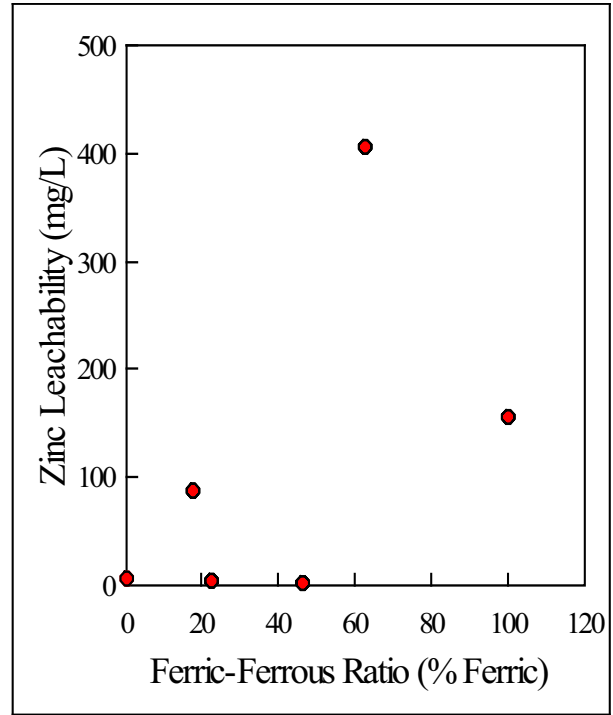


Figure 4.4.9: Effect of ferric-ferrous ratio on zinc leachability



### ***Metal leachability***

No distinct relationship between metal leachability and ferric-ferrous ratio was apparent (Table 4.4.2). However, when zinc leachability was plotted against the ferric-ferrous ratio a weak relationship was observed (Figure 4.4.9). Zinc leachability increased when the ferric iron concentration was increased, with the greatest zinc leachability observed for 100% ferric iron. All leachate concentrations were within the regulated levels for zinc. Cadmium concentrations were exceeded in some tests, however these levels did not correlate with the ferric-ferrous ratio. Further investigation should be done on factors responsible for Cd leachability.

### ***Mineralogy***

The X-ray diffraction patterns for the sludges produced at varying ferric-ferrous ratios discriminately showed peaks diagnostic of gypsum. Crystallization of the oxyhydroxide precipitates was not observed. Trace magnetite was observed in the sludge produced from treatment of the 62% ferric-ferrous ratio solution. More detailed mineralogy coupled with other characterization techniques may provide more information on the state of the iron oxyhydroxide precipitates present in the sludge.

Table 4.4.2: Metal leachability from sludges produced from AMD with varying ferric-ferrous ratios (Ontario LEP).

Fe(III):Fe(II) % ferric	Metal Leachability, mg/L			
	Cadmium	Copper	Lead	Zinc
100	4.83	0.945	<0.006	155
62	0.604	0.036	<0.006	405
46	0.240	<0.027	<0.006	2.2
22	0.379	<0.027	<0.006	3.6
18	3.83	0.373	<0.006	88
0	0.789	0.034	<0.006	6.4
Most stringent provincial regulations for sludge discharge (Zinck <i>et al</i> 1997)	0.5	10	5	5

#### 4.4.4 Discussion

The ferric-ferrous iron ratio in the AMD solution clearly affects the properties of the treatment sludge. Ferrous iron was completely oxidized and precipitated as ferric iron during the treatment process but its presence in the AMD solution influenced the final precipitate. Overall, a greater proportion of ferric iron in the AMD solution appears to improve the sludge properties, however some ferrous iron is beneficial.

Variations in the degree of crystallinity of the oxyhydroxide structures were not observed in the X-ray diffractograms, with the exception of the minor magnetite formation. This may be a factor of the AMD composition. Svanks and Shumate (1973) found that the presence of aluminum may retard the formation of ferro-magnetic sludges. To overcome this, aluminum should be precipitated prior to iron precipitation. However, this presents technical difficulties as both Al and Fe (III) hydrolysis occurs in the same pH range.

Mineralogical or morphological variations in the sludge, generated as a result of variation of the iron species, may account for the differences in the sludge properties.

Alternatively, the increase in sludge density and settling rates for the sludges precipitated from the high ferric iron solutions may be due in part to the higher concentration of calcium in solution, rather than the iron speciation. The lime requirement increased with the ferric iron concentration thus increasing the amount of Ca added to the solution. Huck *et al.* (1977) found that the cationic valence of the neutralizing agent may affect flocculation. Similarly, the concentration of the cations in solution may result in double layer compression and reduction in

forces between the polymer and the sludge particles subsequently affecting the sludge density (volume) and sludge settling rate (Black *et al.* 1965).

The observed increase in particle size with increased ferric concentration may be caused by both physical and chemical factors. For high ferric solutions, more sludge is recycled to R1 to maintain the reactor pH at 3.5. Reactor 1 neutralizes the incoming stream with recycled sludge, raising the pH to 3.5, and precipitating ferric iron. The more ferric iron in solution the greater the amount of recycled sludge required. This allows for greater particle growth as demonstrated by the increase in peak height for the larger size fraction. As the ferrous iron content rises, there is a greater probability that ferrous oxyhydroxides form initially, then rapidly oxidize to ferric oxyhydroxides; rather than ferrous iron oxidation followed by hydrolysis. The precipitation of ferrous hydroxide followed by oxidization to ferric oxyhydroxide is supported by laboratory observation. Sludge in reactor 2 was initially green and changed to brown in reactor 3 and the thickener. Thus, the different precipitation pathways could result in particle size variations.

As the iron species in the effluent was altered the final sludge colour changed from orange-brown (100% ferric iron) to dark, chocolate brown (100% ferrous iron). The observed colour variation of the sludges produced could indicate either a morphological or mineralogical variation. Matijević and Scheiner (1978) found that colour is an indication of the particle size and shape of the precipitate formed. Dispersions containing rodlike particles are yellow, while larger cubic particles give dark brown sols (1-1000 nm). Similarly, different ferric oxyhydroxide precipitates display colour variations (Schwertmann and Cornell 1991).

Upon standing, the 78, 82 and 100% ferrous sludges separated into two, roughly equal layers; a dark chocolate brown layer on the bottom, and an orange-brown layer on the top. The colour of the bottom layer became darker as the ferrous content increased. Apparently, a portion of the sludge contained a denser, darker precipitate than the normally- produced, orange-brown precipitate. However, no crystalline differences between the precipitate layers could be detected by X-ray diffractions analysis.

Zinc leachability from the sludge is strongly dependent on metal concentration (Zn) in the sludge and final pH of the leachate (GML 1987; Zinck *et al.* 1997). The final leachate pH was similar for all tests while the zinc content was slightly higher in the ferric-rich AMD sludges. However, this cannot account entirely for the significant increase in zinc leachability observed. Ferric oxyhydroxide precipitates are known for their propensity to adsorb metal ions (Erikson *et al.* 1973, Benjamin and Leckie 1981, Zinck 1993). Another explanation may be related to adsorption of zinc onto the ferric oxyhydroxide surface.

Ferric iron in the raw water would hydrolyze and precipitate in reactor 1. In this reactor, the precipitate would scavenge adsorbable metal species (Zn, Cu, Cd, etc.) onto its porous surface. As the ferric concentration in the raw water is decreased, the amount of iron precipitating in R1 would also decrease. In R2 and R3, where the high solution pH (10) would cause zinc and the other metal species to hydrolyze and precipitate from solution, metal adsorption would be minimal. In turn, these metals would not have the opportunity to be adsorbed onto the iron oxyhydroxide surface. Adsorbed metals are more readily leached than those chemically precipitated, thus stability would increase with Fe(II) concentration, as was observed with zinc leachability.

## 5.0 BATCH TESTS

### 5.1 Batch Test Procedure

The batch test unit used the components from the pilot plant configuration to duplicate process conditions as closely as possible. A 6-L acrylic reactor was filled with synthetic AMD and stirred at 400 rpm. A 20% (w/v) slurry of slaked lime was added at a flow rate of 5.0 mL/min until the pH reached 10.0. The solution was sparged with compressed air at 0.6 L/min throughout the neutralization. The mixture was left to stir for a total reaction time of 1.5 h. The agitation rate was reduced to 250 rpm and 4 mL of 0.1% (w/v) Percol E10 was slowly added to the system to obtain a final concentration of 0.1 mg E10/g solids. After 5 min, a 50 mL sample was taken for ferrous iron determination. Two liters of slurry were collected in 2 x 1-L settling cylinders and settling rates were determined for a 24 hour interval. For percent solids determination, the contents of one cylinder were collected by vacuum filtration through #3 Whatman filter paper, dried overnight at 90°C then weighed. Sulphate determinations were made on the recovered filtrate. Contents of the other settling cylinder were collected and stored at 4°C for particle size analysis.

### 5.2 Sulphate Concentration

#### 5.2.1 Introduction

The treatment of acidic mineral effluents is a site-specific process. As the composition of these effluents varies so does the ionic strength, the metal speciation and the manner in which the effluent responds to treatment. Sulphate is a major component of any AMD stream and its role in sludge production and stability is relatively unclear. Wilson (1994) surveyed Canadian mines and found the sulphate concentration in AMD streams ranged from 10-150,000 mg/L, with most of the sulphate levels in the range of 100-10,000 mg/L.

#### 5.2.2 Methods

The sulphate tests were performed on a batch scale due to the potential for gypsum scaling in the plant lines. Sodium sulphate was added to the AMD to achieve the amount of excess sulphate required for each test. The AMD, with the appropriate sulphate concentration, was then neutralized with 20% w/v slaked lime at a controlled rate until pH 9.8 was reached.

#### 5.2.3 Results

##### ***Sludge Properties***

The percent solids increased with increasing sulphate concentration (Figure 5.2.1). As the sulphate concentration increased the amount of gypsum increased until its formation was limited by the calcium concentration. The total solids produced increased from 4.5 to 10 g/L sulphate solution then leveled off when limited by the calcium concentration (Figure 5.2.2). At

4.5 g/L  $\text{SO}_4$  the limiting ion in gypsum precipitation was sulphate, however in excess sulphate concentrations (10 g/L and 30 g/L) gypsum formation was limited by the amount of calcium in the system. The bulk density of the sludge produced increased linearly with raw water sulphate concentration, in the same manner as percent solids.

Conversely, the settleability of sludge decreased linearly with increased sulphate concentration (Figure 5.2.3). The sludge generated from moderate sulphate waters (4.5, 10 g/L  $\text{SO}_4$ ) settled well with the addition of the E-10 polymer. However at high sulphate levels, the addition of the flocculant facilitated particle agglomeration and the sludge was gelatinous in appearance.

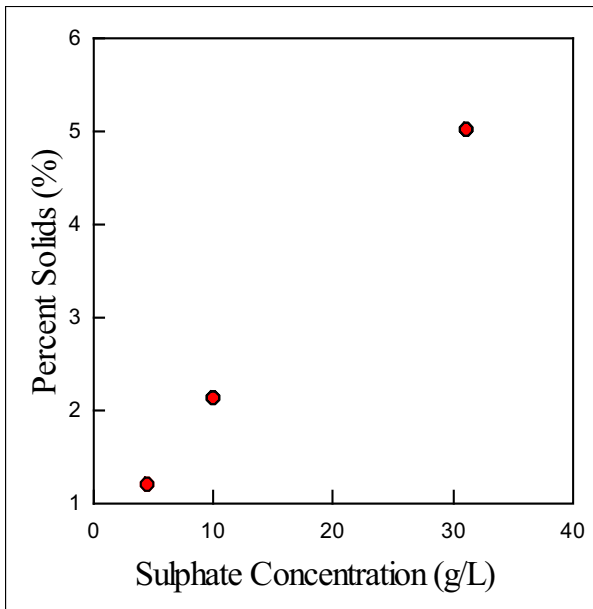
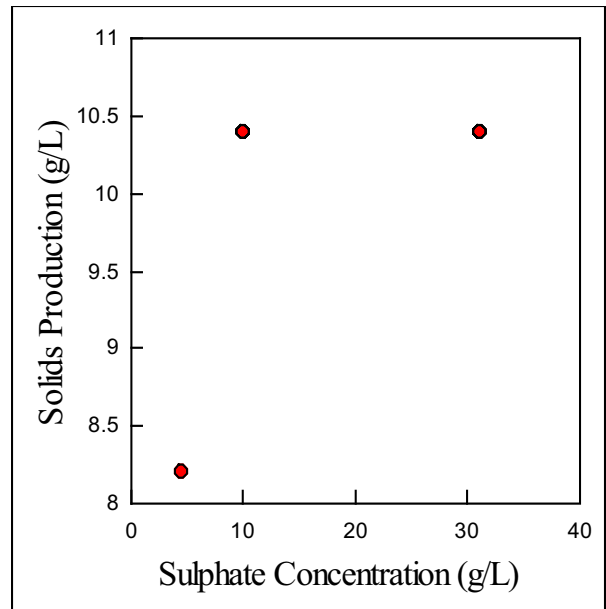
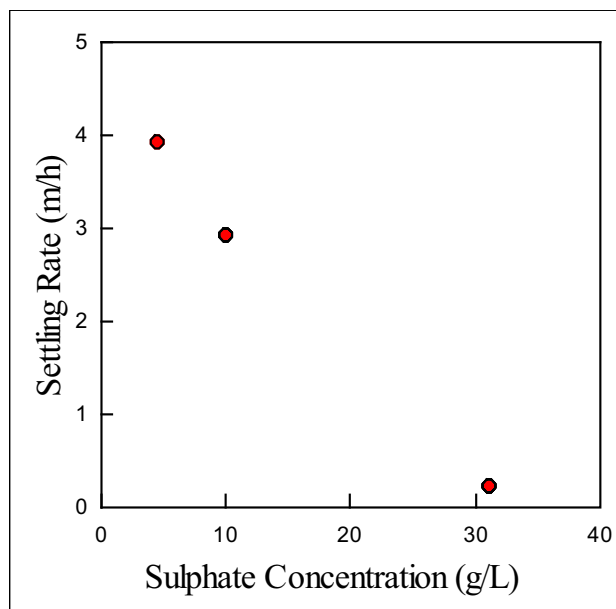


Figure 5.2.1: Effect of sulphate concentration on percent solids



5.2.2: Effect of sulphate concentration on total solids production

Figure 5.2.3: Effect of sulphate concentration on settling rate with the addition of E-10

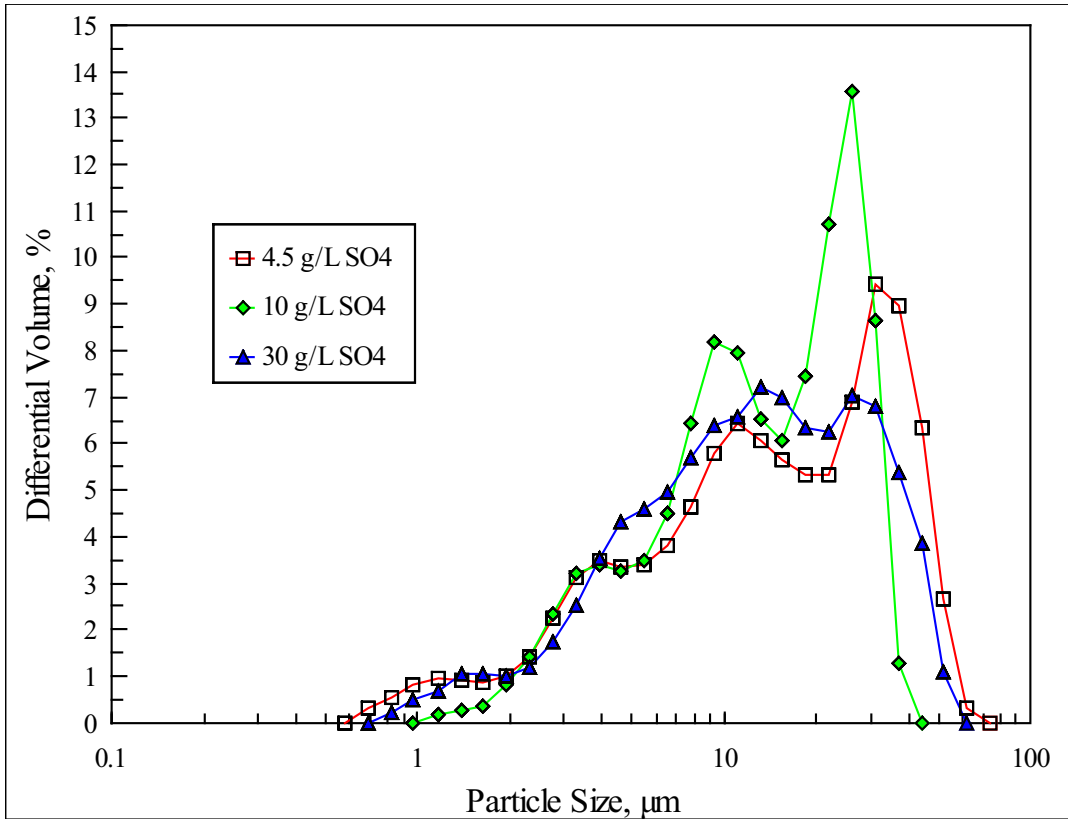


of sulphate settling rate with the polymer

### Particle Size

The particle size distributions for the 4.5 g/L, 10 g/L and 30 g/L sulphate sludge showed a weak multimodal distribution (Figure 5.2.4). The median (50%) particle size decreased when the sulphate concentration was increased from 13.43  $\mu\text{m}$  for 4.5 g/l to 12.3  $\mu\text{m}$  for 10 g/L  $\text{SO}_4$  and 11.3  $\mu\text{m}$  for 30 g/L  $\text{SO}_4$ . The entire size distribution shifted to lower size fractions with increased sulphate concentration.

Figure 5.2.4: Particle size distribution for sludge generated at various sulphate concentrations

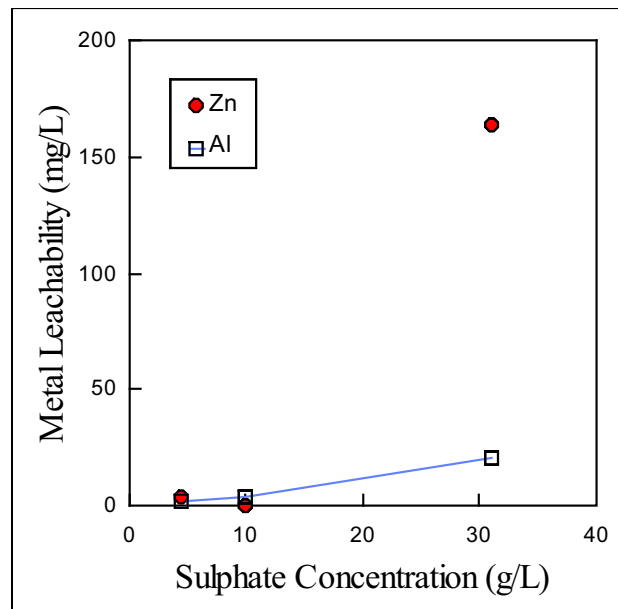




**Metal Leachability**

Metal leachability appears to be significantly affected by the sulphate content of the raw water (Table 5.2.1). Zinc and aluminum were particularly susceptible to leaching. These metals were most mobile in sludges produced from high sulphate water (Figure 5.2.5). Metal mobility appears to be exponentially dependant on AMD sulphate concentration. However, this trend could be partially due to variations in the amount of excess alkalinity present in the sludge.

Table 5.2.1: Metal of raw water



leachability as a function sulphate concentration

Sulphate Concentration (g/L)	Metal Leachability			
	Aluminum (mg/L)	Cadmium (mg/L)	Iron (mg/L)	Zinc (mg/L)
4.5	2.4	0.1	1.2	3.4
10	3.5	<0.004	0.04	0.1
30	20.9	4.2	0.5	164

Figure 5.2.5: Effect of sulphate concentration on zinc and aluminum leachability

### ***Mineralogy***

X-ray diffraction analysis of the high sulphate samples identified only gypsum. Ettringite was not identified, even in the sludge produced from the AMD containing 30 g/L sulphate. The oxyhydroxide phases were not identified due to the relative low intensity of the diffraction peaks with respect to gypsum.

### **5.2.4 Discussion**

Higher sulphate levels of AMD had a higher percent solids content primarily due to more gypsum production. Kuyucak *et al.* 1991 also found increased sulphate concentration positively impacted sludge density and they attributed this to the increase in ionic strength.

While elevated sulphate concentrations proved beneficial for sludge density it was detrimental to sludge settleability and particle growth. Elevated sulphate concentration increased the ionic strength of the solution and may have changed the precipitation precursor complexes from hydroxyl ( $M_n(OH)_z^m$ ) to sulphate species ( $M_n(SO_4)_z^m$ ). The increased ionic strength interfered with the flocculation capabilities of the polymer as seen in the reduction in settling rate. As well, the elevated sulphate levels may cause sulphate substitution and polymerization during hydrolysis. The sulphate-bearing oxyhydroxide precipitate will release sulphate ions with pH increase through deprotonation of the oxyhydroxide surface (Rose and Ghazi 1997). According to Svanks and Shumate (1973) the sulphate in the sludge is in the form of ferric hydroxysulphate, which hydrolyzes very slowly at lower pH and forms goethite. While goethite was not observed in this study, Svanks and Shumate (1973) postulate that the goethite crystals may be so tiny that they are undetected by X-ray diffraction analysis. Detailed mineralogical analysis of the samples may provide further information.

Elevated metal leachability from the sludges derived from high sulphate solutions indicated further chemical changes such as metal adsorption. The catalytic effect of  $SO_4^{2-}$  in promoting nucleation and growth at lower supersaturation levels may cause greater polymerization and trap metal-rich process water which is readily leached (Dousma *et al.* 1979).

As above, the change in the precipitation precursor may cause the zinc to precipitate as a hydroxy-sulphate type species, rather than a oxyhydroxide or hydroxy-carbonate compound, which is more readily leachable. In addition, variations in the neutralization potential of the sludges produced could also be a factor in the enhanced zinc mobility.

The greater aluminum mobility with increasing sulphate concentration may result from the dissolution of ettringite or the dissociation of the weak chemisorbed aluminum ions.

## 5.3 Rate of Neutralization

### 5.3.1 Introduction

The use of alternate neutralization processes to treat the AMD was investigated. Different rates of lime addition were studied, along with neutralization in stages to maintain a controlled supersaturation level in solution. Controlling the level of saturation ensures effective and minimal use of the neutralization reagent while promoting heterogeneous nucleation and growth (Demopoulos *et al.* 1995).

### 5.3.2 Methods

A 6-L acrylic reactor was filled with AMD and stirred at 400 rpm. A 20% (w/v) slurry of slaked lime was added at flowrates of: 2.0 mL/min (controlled neutralization); 20 mL/min (rapid neutralization); and 80 mL/min (one-step neutralization) until the pH reached 10.0. A staged neutralization process was run with lime added at 2.0 mL/min (Table 5.3.1) until the pH reached 10.0. The solution was sparged with compressed air at 0.6 L/min throughout the neutralization. The mixture was left to stir for a total reaction time of 1.5 h. The agitation rate was reduced to 250 rpm and 4 mL of 0.1% (w/v) Percol E10 were slowly added to the system to obtain a final concentration of 0.1mg E10/g solids. After 5 min, a 50 mL sample was taken for ferrous iron determination. Two liters of slurry were collected in 2 x 1-L settling cylinders and settling rates were determined for a 24 hour interval. For solids determination the contents of one cylinder were collected by vacuum filtration through #3 Whatman filter paper, dried overnight at 90°C then weighed. Sulphate determinations were made on the recovered filtrate. Contents of the other settling cylinder were collected and stored at 4°C for particle size analysis.

Table 5.3.1: Time and pH parameters for staged neutralization process

pH	Time, min
2.00 Initial	0
2.78	30
3.10	15
3.46	15
3.87	15
4.30	15
4.86	15
5.53	15
9.29	15
10.00	15
10.00 Final	Total time 2 h

### 5.3.3 Results

The method of neutralization affected sludge properties and treatment efficiencies as presented in Table 5.3.2.

Table 5.3.2: Effect of rate of neutralization on solids generation, lime consumption, settling rates and neutralization potential (NP)

Neutralization Method	Solids Generation (g/L)	Lime Consumption (mL/L)	Settling rate (m/h)	NP
Staged	7.11	16.7	4.02	80
Controlled (2.0 mL/min)	8.42	17.0	2.50	91
Rapid (20 mL/min)	9.14	18.3	1.90	100
One step (80 mL/min)	9.14	20.0	0.54	151

### 5.3.4 Discussion

The method of neutralization has a marked effect on sludge properties and treatment efficiency. Bulk (one step) or rapid neutralization is comparable to the basic treatment method and produces a voluminous sludge which has a low settling rate and dewateres slowly. A slow, controlled neutralization increased the settling rate five-fold compared with the one step process.

In staged neutralization supersaturation principles are applied, and the pH is adjusted in calculated increments based on the practical solubilities of ferric (oxy) hydroxide as a function of pH (Demopoulos *et al.* 1995). Through supersaturation control the settling rates were improved by 60% over the controlled situation. This has significant implication with respect to clarification requirements.

Lime consumption can be reduced through selection of a controlled or staged method of neutralization, reducing reagent costs by 10-15%. Efficient lime utilization, such as experienced in staged or HDS type treatment, yields sludge with a low neutralization potential and less excess alkalinity. This loss in metal buffering capacity through controlled neutralization is off-set through better precipitate crystallinity. Metal release from crystalline precipitates is generally lower than from amorphous or poorly crystalline material. Metal bonds formed during crystallization are stronger and more ordered as compared to adsorbed species or weak covalent bonds.

## 6.0 EFFECT OF EXCESS BUFFERING ON SLUDGE STABILITY

### 6.1 Introduction

The Canadian mining industry is faced with the problem of the long term stability of AMD treatment sludges with respect to environmentally acceptable disposal/storage options. Most neutralization treatments take the pH to 9.5 or higher before discharge. At this pH most metals have precipitated/coprecipitated and the effluent can be safely discharged. Sludges that contain excess lime tend to be more stable and are less likely to be leached. This study will examine the effect of excess lime on the chemical and physical properties, mineralogy and leachability of two sludges. The sludges were obtained from the CANMET pilot plant thickener and from an industrial high density sludge lime treatment plant.

### 6.2 Materials and Methods

Synthetic sludge was collected from the thickener discharge of the CANMET pilot plant facility. The industrial sludge was collected end-of-pipe from Site J7, a high density lime treatment plant (Zinck *et al.* 1997). Chemical composition, pH, bulk density and solids content of the sludges are given in Table 6.1.

Samples (6 x 100 g dry weight basis) of each sludge were placed into 500 mL glass jars. Designated amounts of lime (CaO) were combined with 50 mL (Syn) or 35 mL (J7) distilled water and added to the jars to obtain excess lime concentrations of 0 (no lime added), 5, 10, 15, 20 and 25%. The systems were thoroughly mixed then left to stand 16 h to ensure complete dissolution of the lime. The systems were analyzed for bulk density, solids content, pH, particle size, neutralization potential (NP), calcium content and CO<sub>3</sub>. The Ontario LEP 347 was performed to determine metal leachability. Mineralogy analysis was performed using XRD.

### 6.3 Results and Discussion

#### ***Percent solids and bulk density***

The addition of lime slightly increased the solids contents for both the synthetic and the J7 sludges (Table 6.2). Bulk density dropped slightly for both systems, suggesting that the sludge volume expands with lime addition. The drop in bulk density corresponds with the observation that sludges with 15%-25% excess lime formed a highly voluminous gel after standing overnight. Viscosity determinations could not be performed on these samples due to their extremely low flowabilities. The gels exhibited thixotropic behaviour (liquefying when stirred, then returning to gel form upon standing). This phenomena may be due to the formation of Mg(OH)<sub>2</sub>, which precipitates as gelatinous hydroxides at high pH-s (pH range 10-12). Additional lime raised the alkalinity of both sludge systems into this pH range. Both sludges contain several percent magnesium, 2.2% for the industrial sludge and 1.4% for the synthetic sludge. In an industrial process the formation of this magnesium hydroxide *Agel*® would be undesirable as the sludge would be difficult to transport.

At some sites, the pH is raised to ~10 then is lowered again to meet effluent discharge regulations. At these sites excess buffering would only be suitable after solid/liquid separation, where the additional lime would be added directly to the sludge.

Table 6.1: Physical characteristics and chemical composition of J7 and synthetic sludges

Sludge Source	Site J7	Synthetic
Percent Solids (wt.%)	26.3	37.58
Particle size (um, 50%)	4.18	18.18
Neutralization Potential	118	112
Bulk Density	1.19	-
pH	9.22	10.04
Chemical composition.		
Ca	13	14.2
Cu	0.077	0.13
Fe	12.8	16.7
Mg	2.2	1.37
Mn	0.47	0.16
Al	4.3	2.84
Zn	0.0031	1.87
Cd	0.0002	0.03
Co	-	0.03
Pb	<0.44	<0.02
As	<0.001	<0.01
SO <sub>4</sub>	26.71	38.4

### ***Neutralization potential***

As expected, the NP increased proportionately with the amount of added lime (Figure 6.1). However, the incremental pH increase was initially sharp, then declined at about 15% excess lime, corresponding to pH values of 10.2 (J7) and 10.8 (Syn). The maximum solubility of Ca(OH)<sub>2</sub> in water at 25°C is 1.2 g/L (pH 12.5). These systems are approaching the asymptotic limit and unreacted lime may be present. In addition, under higher pH conditions the hydroxyl ion may be consumed in other reactions, such as the formation of metal complexes i.e. ettringite or polymerizations i.e. Mg(OH)<sub>2</sub>.

Zinck *et al.* (1997) reported NP values ranging from 108 to 819 kg CaCO<sub>3</sub>/tonne sludge for eleven industrial sludges. The NP values prior to addition of lime were 153 and 112 kg CaCO<sub>3</sub>/tonne sludge for site J7 and synthetic sludge, respectively. These NP values are on the low side of the range, which is indicative of efficient lime neutralization, and consequently may have less neutralization capacity. Both sludges were stable, as defined by waste regulations, when leached using the Ontario LEP.

Table 6.2: Effect of excess lime on chemical and physical characteristics of sludge

Sludge Source	Excess Lime, %	pH	Bulk Density (g/mL)	Solids Content (%)	NP (kt)*
Site J7	0	9.30	1.20	26.78	153
	5	9.90	1.22	27.75	168
	10	10.10	1.19	28.05	182
	15	10.21	1.20	27.89	194
	20	10.28	1.17	28.00	203
	25	10.39	1.21	28.07	220
	Synthetic	0	10.04	1.25	32.62
5		10.49	1.23	32.78	123
10		10.70	1.24	33.04	136
15		10.81	1.24	33.15	145
20		10.95	1.22	33.33	153
25		11.07	1.20	33.47	161

\*kg CaCO<sub>3</sub> per tonne sludge

Neutralization potential values were lower for the synthetic sludge than the industrial sludge. This indicates that less lime was added to the pilot plant treatment to obtain neutralization and reflects the greater degree of control for operating variables such as pH regulation, mixing and slaked lime preparation. The J7 sludge is produced from an industrial HDS process; its AMD stream contained a moderately high metal and sulphate concentration, similar to that of the synthetic AMD. The low NP value for the industrial sludge indicates that the J7 plant has an efficient lime neutralization process.

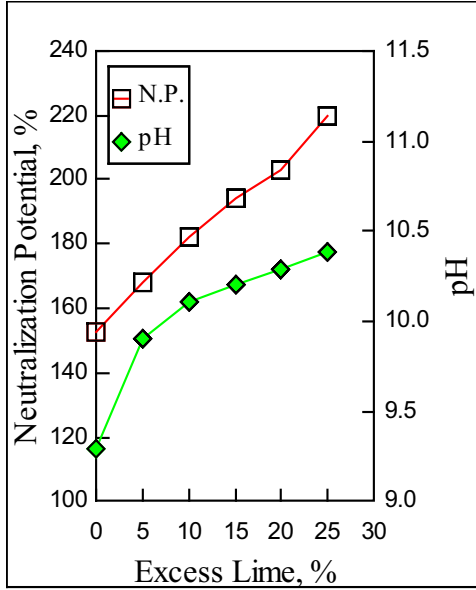
#### ***Calcium and carbonate***

Both calcium and carbonate content increased with lime addition (Figure 6.1). This was expected for calcium since it is a major component of lime. One source of carbonate could be calcium carbonate impurities in the lime.

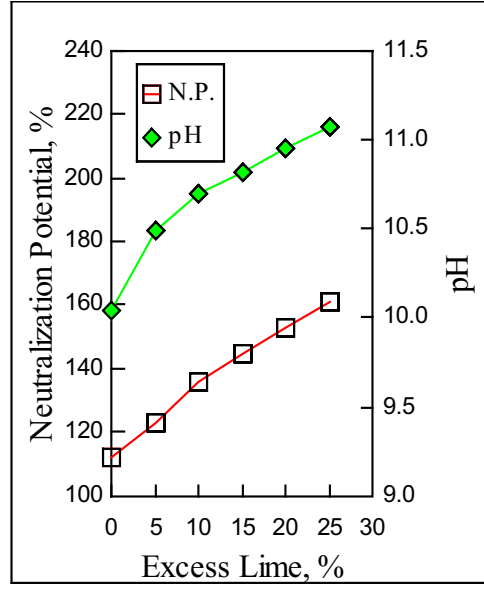


Figure 6.1: Effect of excess lime on chemical properties of sludge. a) and b) excess lime versus N.P. and pH; c) and d) excess lime versus Ca and carbonate

a) J7



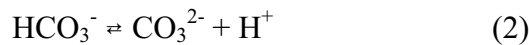
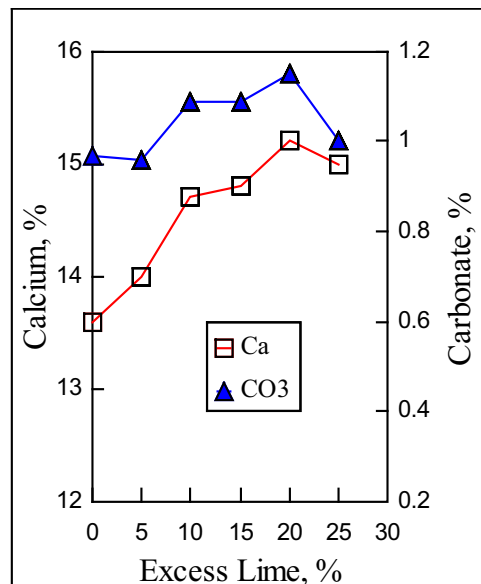
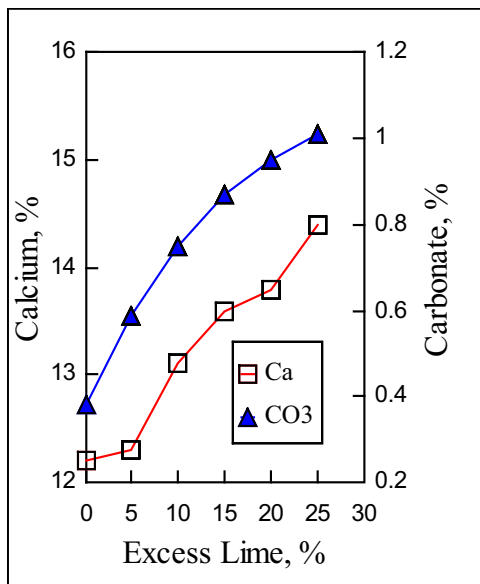
b) synthetic



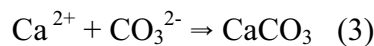
c) J7

d) synthetic

Alternatively, the increase in carbonate could also be due to dissolution of carbon dioxide at high pH and its subsequent conversion to carbonate. Carbon dioxide is introduced to the system by aeration (equations 1 and 2).



At pH 9.2 the dissolved carbon balance is roughly 93% as  $\text{HCO}_3^-$ , 7% as  $\text{CO}_3^{2-}$  and <1% as  $\text{CO}_2(\text{aq})$  (Aubé and Payant 1997). Reaction 2 is driven to the right by consumption of the carbonate to form calcite (equation 3).



### Mineralogy

X-ray diffractometry was performed on freeze-dried samples of the sludges. All samples contained a major amorphous phase that was identified as gypsum. All the J7 sludges contained major amounts of gypsum; those with 15, 20 and 25% excess lime also had traces of ettringite ( $\text{Ca}_6\text{Al}_2(\text{SO}_4)_3(\text{OH})_{12} \cdot 26\text{H}_2\text{O}$ ). Similarly, all the synthetic sludges contained major amounts of gypsum; those with 20% and 25% excess lime contained traces of ettringite. Formation of ettringite occurs at high pH, and sufficient quantities of aluminum, calcium and sulphate must be present (Mohamed *et al.* 1995). Both these sludges contained significant amounts of aluminum; 4.3% and 2.8% for J7 and synthetic respectively. The higher amounts of Al in the J7 sludge may account for the presence of ettringite at lower pH values. No calcite was detected in any of the samples. Efficient lime neutralization, as well as process conditions and chemical reactions, lead to sludges containing gypsum (low NP) rather than calcite (high NP) (Zinck *et al.* 1997).

### Leachability

The samples were leached using the Ontario LEP 347 which uses acetic acid to mimic organic acids expected to be present in a municipal landfill and assumes codisposal of mineral processing and municipal wastes. For disposal of sludge in a landfill the amount of acidification contributed by rainwater percolation must be considered when assessing sludge leachability. Rainwater is only marginally acidic (pH 4-6). A 3-m sludge bed containing 40% solids and 10% free  $\text{CaCO}_3$  would contain 0.2 tonnes of  $\text{CaCO}_3$  that would be available to consume acidity from about 40,000 yrs of incident rainfall (Orava *et al.* 1995). Although some pH depression would occur, no major metals mobility is expected if lime is used as the neutralization agent. Sodium hydroxide or soda ash (sodium carbonate) present potential problems, as these reagents are highly pure and react fully, leaving no excess alkalinity to buffer any potential acidification (Senes 1994). In addition, except for use with low metal effluents, these reagents are too costly.

All the sludges tested with the Ontario LEP reported leachate below the regulated limits for sludge leachability for iron, zinc, cadmium, copper and lead (Table 6.3). Leachability of the non-regulated metals, aluminum and magnesium, was low. The leachability of magnesium dropped as the pH increased for both sludge systems. Its increased stability is likely due to the formation of magnesium hydroxide at the higher pH values. Increased amounts of aluminum were leached out of the synthetic sludge at pH values greater than 10.7, this effect was not seen with industrial sludge which did not reach as high a pH as the synthetic sludge. When the alkalinity of the solution is increased beyond pH 9.5 the solubility of aluminum hydroxide increases (OISTL Design Manual, U.S. Environmental Protection Agency, 1983). Some of the resolubilized aluminum appeared to be captured as ettringite while a portion remained in solution. The Ontario LEP includes the sludge waters with the solids, so any resolubilized metals would be included in the determination along with any leached metals.

Table 6.3: Effect of excess lime on sludge leachability

Sludge Source	Excess Calcium %	pH	Ontario Leachate Extraction Procedure 347						
			Fe	Mg	Zn	Al	Cd	Cu	Pb
			mg/L	mg/L	mg/L	µg/L	µg/L	µg/L	µg/L

Site J7	0	9.30	<0.04	465	0.05	<45	<2	<55	0.7
	5	9.90	<0.04	394	0.07	99.9	3.7	<55	1.5
	10	10.10	<0.04	311	0.05	96.8	3.0	<55	<0.7
	15	10.21	<0.04	282	0.03	<45	<2	<55	<0.7
	20	10.28	<0.04	297	0.04	<45	<2	<55	<0.7
	25	10.39	<0.04	267	0.03	<45	<2	<55	<0.7
Synthetic	0	10.04	<0.04	130	0.10	79.8	15.9	<55	<0.7
	5	10.49	<0.04	222	0.45	<45	69.5	<55	<0.7
	10	10.70	<0.04	162	0.20	<45	41.4	<55	1.3
	15	10.81	<0.04	92	0.04	192.9	10.8	<55	1.7
	20	10.95	<0.04	34	0.04	587.5	4.5	<55	0.9
	25	11.07	<0.04	15	0.03	1107.7	2.4	<55	1.2
Most stringent Canadian regulated limit (Zinck <i>et al.</i> 1997)			1000		500		500	10000	5000

### ***Particle size distribution***

Particle size analysis were done on both sludge systems (Figure 6.2). Both sludges exhibited a bimodal particle size distribution pattern. Additional lime caused a relative drop in the larger particle size peak and an increase in the smaller particle size peak for both sludge systems; this effect was more pronounced for the synthetic sludge. Statistical analyses of the particle size distribution were done (Table 6.4). These values indicate that the average particle size (50%,  $\mu\text{m}$ ) drops as lime is added. The effect is more evident for the synthetic sludge. The other statistical data, 90%  $\mu\text{m}$ , mv, mn and ma correlates this drop. The calculated specific surface area, cs, increased with additional lime, indicating a larger number of smaller particles are present. This was likely a simple dilution effect, with the addition of smaller lime particles shifting the size distribution downwards.

### ***Use of excess lime***

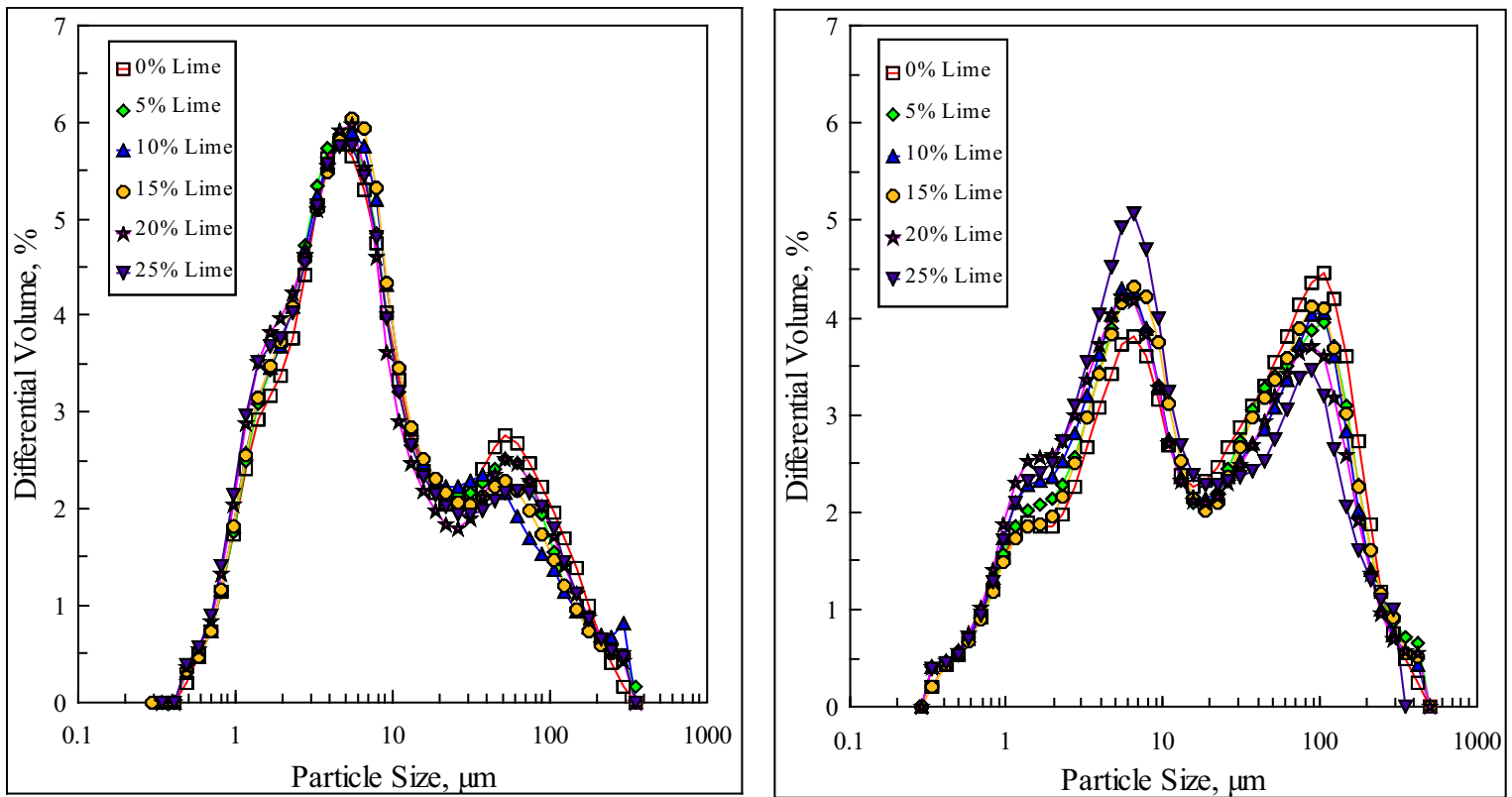
The addition of lime to the sludge did not benefit sludge properties or sludge leachability. At high concentrations it had a detrimental effect on sludge density, as it increased the volume of the sludge. Although aluminum is not currently regulated in Canada under leachate regulation, it was noted that high concentrations of lime increased its leachability.

Figure 6.2: Particle size distribution for a) J7 sludge and b) synthetic sludge treated with excess lime

a)

b)

Table 6.4: Particle size distribution for industrial and synthetic sludges treated with excess lime



Sludge Source	Excess Lime %	Particle Size Distribution Statistics					
		50%, $\mu\text{m}$	90%, $\mu\text{m}$	mv, $\mu\text{m}$	mn, $\mu\text{m}$	ma, $\mu\text{m}$	cs, $\text{m}^2/\text{cc}$
Site J7	0	6.19	71.50	23.30	0.97	3.68	1.641
	5	5.72	63.75	22.13	0.93	3.49	1.720
	10	5.74	59.92	21.92	0.94	3.46	1.730
	15	5.74	60.59	20.96	0.93	3.46	1.734
	20	5.40	67.20	22.18	0.91	3.29	1.825
	25	5.49	67.57	21.95	0.90	3.26	1.838
Synthetic	0	18.18	129.58	46.52	0.61	4.38	1.368
	5	13.45	126.58	45.01	0.56	4.01	1.495
	10	11.09	118.12	41.41	0.58	3.79	1.582
	15	13.40	125.39	44.50	0.62	4.28	1.401
	20	9.96	115.16	40.00	0.59	3.62	1.661
	25	8.38	104.43	31.72	0.72	3.83	1.565

mv: based on center of gravity of particles; mn: mean particle diameter based on the number frequency distribution; ma: mean diameter of the area distribution; cs: calculated specific surface area  $\text{m}^2/\text{cm}^3$

## 7.0 SLUDGE AGING

Aging directly affects the volume, physical properties and leachability of the treatment

sludge. While several studies comment on the effect of aging on sludge characteristics, few studies have examined sludge aging in controlled environments. A laboratory study was conducted at CANMET to examine the effect of aging on the stability and physical properties of AMD treatment sludge. The purpose of the sludge aging study was threefold:

- # to monitor the rate at which aging takes place;
- # to determine the extent to which gypsum recrystallization occurs; and
- # to assess the role aging plays in sludge stability and metal mobility.

## 7.1 Materials and Method

Two fresh industrial sludges (high density sludge: W-8; low density: S-6) and one freshly prepared synthetic sludge were used for the study. The synthetic sludge was generated with the multi-reactor, continuous mini-plant system. Chemical and physical properties of the sludges are presented in Table 7.1. Further details on the mineralogy and leaching characteristics of the industrial sludges, W-8 and S-6, can be found in Zinck *et al.* (1997).

Table 7.1: Physical characteristics and chemical composition of W-8, S-6 and synthetic sludges

Characteristic		Site W-8	Site S-6	Synthetic
Percent Solids (wt.%)		32.2	3.4	37.58
Particle size (um, 50%)		4.19	6.67	18.18
Neutralization Potential		142	471	112
Bulk Density (g/cm <sup>3</sup> )		1.26	1.08	
pH		10.04	10.85	10.04
Chemical composition (%)	Ca	3.8	17.2	14.2
	Cu	0.12	0.15	0.13
	Fe	15.0	16.1	16.7
	Mg	3.13	5.7	1.37
	Mn	-	-	0.16
	Al	3.9	1.3	2.84
	Zn	14.2	8.5	1.87
	Cd	0.0137	0.0674	0.03
	Pb	<0.43	<0.42	<0.02
	As	0.0248	0.0056	<0.01
SO <sub>4</sub>	11.8	6.90	38.4	

The sludge samples were aged under two moisture environments, saturated (under water

cover) and atmospheric (exposed to air) and three different temperatures, 4°C, 25°C and 60°C. The sludges were aged at 60°C to accelerate the aging processes that occur over a longer period of time at lower temperatures. Samples of the aged sludge were collected at intervals of 1, 6 and 12 months. Table 7.2 outlines the tests that were completed.

Leaching tests (Ontario LEP) were used to evaluate metal leachability from the aged sludges. This information, coupled with mineralogical and chemical analysis, was used to assess sludge stability.

Table 7.2: Summary of sludge aging tests performed on fresh industrial sludges and fresh synthetic sludge

Moisture		Temperature		
Atmospheric	Saturated	4°C	25°C	60°C
X		X		
X			X	
X				X
	X	X		
	X		X	
	X			X

## 7.2 Metal Leachability

The sludges were leached using the Ontario LEP. The leachate concentrations are presented in Tables 7.3, 7.4 and 7.5 for high density (W-8), low density (S-6) and the synthetic sludge samples, respectively. The samples showed a marked reduction in metal mobility with aging. The minimum metal concentration was observed in leachates from sludge samples aged 12 months. Similar behaviour was observed for all the sludge types.

Leachate concentrations indicated metal leachability was slightly affected by the presence or absence of a water cover, particularly after 12 months. Overall, leachate results from sludges aged in an atmospheric environment (without a water cover) were more consistent and displayed stronger aging trends.

The leachate concentrations indicated a significant reduction in metal leachability with increased aging temperature. This trend was particularly apparent for zinc from high density sludge (Figures 7.1 and 7.2). As well, the qualitative rate of aging was faster at 60°C than 4°C and 25°C as suggested by zinc leachability over time (Figure 7.1).

Table 7.3: Leachate concentration from Ontario LEP for the high density sludge (W-8)

Temp. °C	Time mos	Cover	Metal concentration, µg/L													
			Hg	B	Fe	Zn	Ag	As	Ba	Cd	Cr	Cu	Ni	Pb	Se	
4	1	Atm	<0.16	210	<40	151000	<50	<460	73	230	<60	100	160	<350	<480	
		Sat	<0.16	170	<40	197000	<50	<460	82	240	<60	120	230	<350	1200	
	6	Atm	<0.18	400	<40	279300	<2	<6	85	452	34	223	453	79	<33	
		Sat	<300	<40	200	<2	<6	53	2	<15	<14	<37	13	<33		
12	Atm	<0.26	200	<80	21900	<2	<13	64	51	17	33	64	<3	<35		
	Sat	<0.26	<200	<80	1100	<2	<13	53	8	13	19	41	<3	<35		
25	1	Atm	<0.16	160	<40	180000	<50	<460	79	220	<60	90	220	<350	880	
		Sat	<0.16	150	<40	187000	<50	<460	80	230	<60	100	250	<350	930	
	6	Atm	<0.18	500	<40	248200	<2	<6	10	394	38	225	444	46	<33	
		Sat	<0.18	300	<40	480	<2	<6	51	4	<15	19	<37	1	<33	
12	Atm	<0.26	200	<80	15100	<2	<13	53	27	24	29	58	<3	<35		
	Sat	<0.26	200	<80	6000	<2	<13	65	30	13	18	42	<3	<35		
60	1	Atm	<0.20	<50	90	160900	<4	<5	90	205	<31	209	311	23	<306	
		Sat	<0.20	<50	80	102400	<4	<5	84	124	<31	141	188	15	<306	
	6	Atm	<0.18	300	160	3870	<2	<6	54	12	52	<81	<88	<31	<48	
		Sat	<0.18	200	90	2500	<2	<6	72	11	46	<81	<88	<31	<48	
12	Atm	<0.6	<100	<90	80	3	<12	31	7	23	11	<49	1	<71		
	Sat	<0.26	<200	<80	<40	<2	<13	53	27	24	30	58	<3	<35		



Table 7.4: Leachate concentration from Ontario LEP for the low density sludge (S-6)

Temp. °C	Time, mos	Cover	Metal Concentration, µg/L												
			Hg	B	Fe	Zn	Ag	As	Ba	Cd	Cr	Cu	Ni	Pb	Se
4	1	Atm	<0.16	70	<40	471000	<50	<460	84	3060	<60	50	6000	<350	2580
		Sat	<0.16	50	<40	308000	<50	<460	83	2430	<60	2240	3570	<350	1800
	6	Atm	<0.18	<300	<40	770	<2	<6	91	4810	44	816	15300	15	194
		Sat	<0.18	<300	<40	1090000	<2	<6	38	31	<15	21	<37	2	84
	12	Atm	<0.26	<200	<80	2300	<2	<11	54	23	15	33	101	<3	105
		Sat	<0.26	<200	<80	<40	<2	<11	23	<5	<5	16	<39	<3	124
25	1	Atm	<0.16	80	<40	639000	<50	<460	130	4320	<60	670	6880	<350	3350
		Sat	<0.16	60	<40	465000	<50	<460	120	3550	<60	3320	5120	<350	2540
	6	Atm	<0.18	<300	<40	447100	<2	<6	93	2300	28	241	7800	11	160
		Sat	<0.18	<300	<40	1470	<2	<6	41	47	<15	20	40	3	91
	12	Atm													
		Sat	<0.26	<200	<80	<40	<2	<11	25	<5	<5	12	<39	<3	136
60	1	Atm	<0.20	<0.05	50	545									
		Sat	<0.20	<0.05	<40	304									
	6	Atm	<0.18	200	100	295500	<2	<6	91	632	48	387	4571	<31	383
		Sat	0.33	100	<20	191000	<2	<6	87	1262	41	312	4214	<31	270
	12	Atm	<0.26	<200	<80	116000	<2	<11	118	45	14	82	2017	4	80
		Sat	<0.26	<200	<80	<40	<2	<11	28	6	<5	52	<39	<3	290

Some samples were not available for leaching analyses.

Table 7.5: Leachate concentration from Ontario LEP for the synthetic sludge

Temp. °C	Time, mos	Cover	Metal concentration, µg/L													
			Hg	B	Fe	Zn	Ag	As	Ba	Cd	Cr	Cu	Ni	Pb	Se	
4	1	Atm	110	<20	<5	<10	<10	<30	161	<4						
		Sat	110	<20	<5	<10	<10	<30	147	<4						
	6	Atm														
		Sat														
	12	Atm	<0.26	<100	<90	<50	<1	<12	1	<6	17	<9	<49	<0.8	<71	
		Sat	<0.26	<100	<90	<50	<1	<12	1	<6	16	<9	<49	<0.8	<71	
25	1	Atm	<50	<20	<5	<10	<10	<30	142	<4						
		Sat	<50	<20	<5	<10	<10	<30	153	<4						
	6	Atm	<0.17	<200	50	<20	<2	<6	1	<2	42	<81	<88	<31	<48	
		Sat	<0.17	<200	60	<20	<2	<6	1	<2	<40	122	<88	<31	<48	
	12	Atm	<0.26	<100	<90	<50	<1	<12	0	<6	24	<9	<49	<0.8	<71	
		Dupl	<0.26	<100	<90	<50	<1	<12	1	<6	20	<9	<49	<0.8	<71	
60	1	Atm	<0.26	<100	<90	<50	<1	<12	1	<6	18	<9	<49	1	<71	
		Sat	<20	<230	<6	<6	<6	<6	1	<6	<8	<112	<112	<1	<1	
	6	Atm	<20	<230	<6	<6	<6	<6	<0.3	<0.3	<8	<112	<112	<1	<1	
		Sat	<20	<230	<6	<6	<6	<6	<0.3	<0.3	<8	<112	<112	<1	<1	
	12	Atm	<0.17	<200	<50	<20	<2	<6	<0.6	2	53	<81	<88	<31	<48	
		Sat	<0.26	<100	<90	<50	<1	<12	<0.1	<6	39	<9	<49	<0.8	<71	
		Sat	<0.26	<100	<90	<50	<1	<12	<0.1	<6	44	<9	<49	<0.8	<71	

Some samples were not available for leaching analyses.

Figure 7.1: Zn leachability versus time at different temperatures for the high density sludge aged under atmospheric conditions

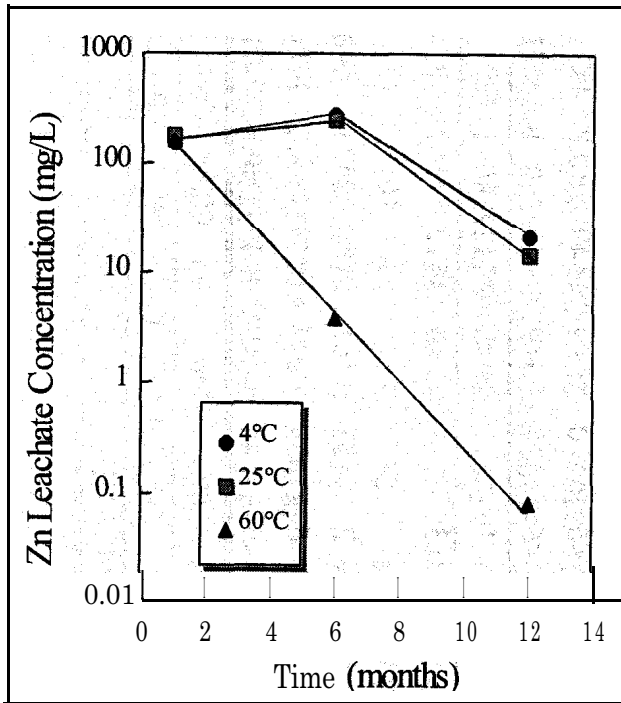
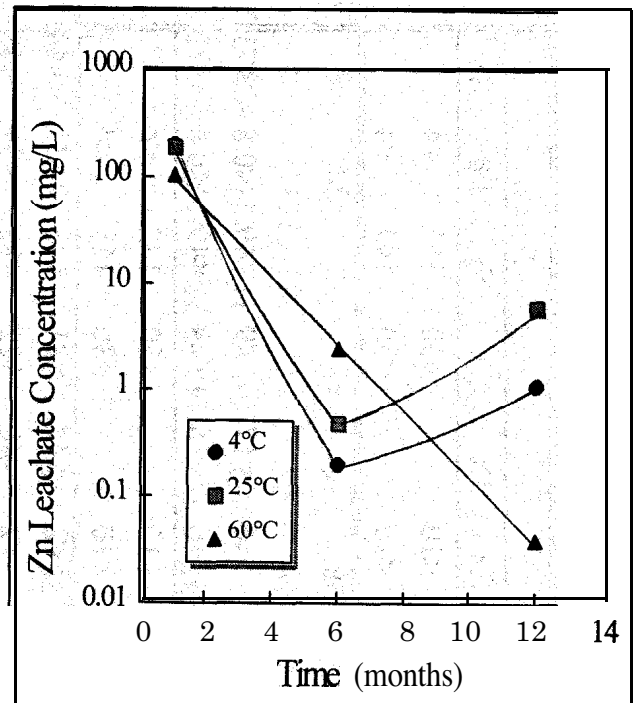


Figure 7.2: Zn leachability versus time at different temperatures for the high density sludge aged under saturated conditions



## 7.3 Mineralogy

### 7.3.1 X-Ray Diffraction Analysis

X-ray diffraction analysis was completed on the aged sludge samples to identify new phases and changes in precipitate crystallinity. The X-ray diffraction results are summarized in Table 7.6 for the low density and synthetic sludges HDS and Table 7.7 for the industrial high density sludge. For reference, the diffraction patterns are appended (Appendix A).

Minor marked differences were observed in the XRD patterns of the aged low density sludge. With increased temperature after 12 months aging there appeared to be more calcite recrystallization. This trend was observed with aging time, where the calcite diffraction pattern was more intense after 12 months aging. This was particularly apparent for sludge aged in the saturated environment.

The HDS sludge showed sharp differences in composition with aging time and temperature. More calcite, relative to gypsum, was observed with low temperature aging. With increased aging temperature the intensity of gypsum, relative to calcite increased. As well, there was a reduction in the proportion of ettringite in the sludge with increased aging temperature and aging time. The aging environment did not affect the XRD for the HDS sludge.

The only crystalline phase identified in the fresh synthetic sludge sample was gypsum.

Table 7.6: Summary of XRD findings after aging low density and synthetic sludge samples

Sample	Low Density Sludge - S-6	Synthetic Sludge
4-S-1	Calcite>gypsum>quartz>clinochlore>albite>muscovite	Gypsum
4-A-1	Calcite>gypsum>quartz>clinochlore>albite>muscovite	Gypsum
4-S-12	Calcite>gypsum>quartz>clinochlore>muscovite	Gypsum
4-A-12	Calcite>gypsum>quartz>clinochlore>muscovite>albite	Gypsum>ettringite
25-S-1		Gypsum>ettringite
25-A-1	Calcite>gypsum>quartz>clinochlore>anorthite>muscovite	Gypsum>ettringite
25-S-12	Calcite>gypsum>quartz>clinochlore>muscovite>albite>dolomite	Gypsum>ettringite
25-A-12		Gypsum>ettringite
60-S-1	Calcite>gypsum>quartz>clinochlore>muscovite>albite	Ettringite>gypsum
60-A-1		Gypsum>ettringite
60-S-12	Calcite>gypsum>clinochlore>quartz>muscovite>albite	Gypsum
60-A-12		

After aging the sludge at 4°C for one month gypsum was still the only crystalline phase identified. However, after aging for one month at 25°C and 60°C ettringite was identified. Furthermore, ettringite was identified in all the synthetic sludge samples aged for 12 months, except for the sample aged at 60°C in a saturated environment. This absence of ettringite at 60°C was also observed in the HDS sludge from both disposal environments.

### 7.3.2 Detailed Mineralogy - High Density Sludge

Detailed mineralogical analysis of the aged high density sludge samples were completed. These detailed results are presented in Appendix B and summarized below. Sixteen freeze-dried sludge samples labelled as: W8-4A1, W8-4A6, W8-4A12, W8-25A1, W8-25A6, W8-25A12, W8-60A1, W8-60A6, W8-4S1, W8-4S6, W8-4S12, W8-25S1, W8-25S12, W8-60S1, W8-60S6 and W8-60S12 were examined. The coding used to identify each sample is as follows: the first two digits are for the mine site (i.e. W8), the next digit is the temperature at which the sludges were aged (i.e. 4, 25 or 60°C), the following digit is the moisture environment (i.e. A for atmospheric and S for saturated) and the last digit is for the aging duration (i.e. 1, 6 or 12 months).

Polished sections were prepared from subsamples of each sludge. The polished sections were first examined by optical microscopy under reflected light, followed by scanning electron microscopy (SEM) in the back-scattered electron (BE) mode, with a JEOL 820 SEM operated at 20 kV, with a beam current of 1 nA. Identifications were done by Energy Dispersion Spectrometry (EDS), using a Link ISIS series 300 system. Also, the samples were submitted for X-ray diffraction analysis (XRD), as a complementary technique for mineral identification.

The findings of the mineralogical characterization for this series of samples are summarized in Table 7.7. With the exception of two samples (W8-60S6 and W8-60S12), the major phase (*phase M*) was observed in all the sludges studied.

*Phase M* consists of a Ca-Mg-Fe sulfate hydroxide hydrate with lower contents of Zn, Mn, Al, Si and C; it is typically non-homogeneous and has poor crystallinity, so it does not diffract well. It is presumably a member of the hydrotalcite group, a variant of the mineral desautelsite. The composition of *phase M* from sample W8-60S12, shows an increase in Si content compared to average composition obtained in other samples.

Gypsum and calcite were observed as minor constituents in all but two samples (W8-60S6 and W8-60S12), where they appeared as major phases. Crystallization of gypsum was observed to various extents in all samples, with one exception (W8-4S6), whereas crystallization of calcite was rarely observed.

Ettringite which is found as small euhedral laths within *phase M*, was identified in eleven samples by SEM-EDS and in twelve samples by XRD technique, from a total of sixteen samples studied.

Sulphides particles are found in all samples as small grains rarely

exceeding 50  $\mu\text{m}$  in maximum dimension, often free but sometimes attached or included in the major phase. Most grains were identified as pyrite, but sphalerite, chalcopyrite, pyrrhotite and arsenopyrite were also found. A distinct feature is that sulphide particles from the sludge samples that were subjected to high temperatures (60°C) often showed alteration rims of goethite.

In summary, the major phase in the sludges is *phase M*, which is a Ca-Mg-Fe sulfate hydroxide hydrate; gypsum and calcite are the minor phases with traces of other minerals often trapped as small particles in the major phase of the sludge. Treatment at 60°C accelerated the aging of the sludges. After heating and exposing the sludge to humidity-saturated atmosphere for six and twelve months (samples W8-60S6 and W8-60S12), gypsum and calcite become the phases of major abundance probably at the expense of *phase M* which became a phase of medium abundance. Also, the sludge loses some of its protective anti-oxidative role on the entrapped sulfide particles, for example, pyrite and pyrrhotite particles show layers of oxides-goethite (samples W8-60A6, W8-60S6 and W8-60S12).

#### 7.4 Field Study

The characterization results from a field study that examined fresh and aged lime sludges (Zinck *et al.* 1997) indicated some interesting trends regarding the effect of sludge aging on sludge density and sludge stability. Generally, the sludges tended to densify with age though natural dewatering and freeze-thaw. The degree of densification with time was found to be directly dependent on the amount of moisture present in the sludge. Particle size increased with aging as the calcite crystals recrystallized, leading to particle growth. As well, there was evidence of this recrystallization from the mineralogical analysis.

Metal leachability from the sludges appeared to decrease with aging. When fresh sludge failed the leaching protocol, the corresponding aged material was found to be stable and leach considerable less metal. Mineralogical analysis determined that mineral recrystallization stabilizes metal species.

Table 7.7: Summary of mineralogical findings after aging high density sludge (W-8)

Sample	Major	Minor	Trace	XRD
W8-4A1	Phase M	Gypsum <sup>R</sup> , Calcite, Fe-rich phase**	Ettringite <sup>R</sup> , Ca silicate, Ca-Mn oxide, pyrite, chalcopyrite, apatite, Mn>Ba oxide and magnetite	Calcite>gypsum>quartz>ettringite+desautelsite-like compound
W8-4A6	Phase M	Gypsum <sup>R</sup> , Calcite, Fe-rich phase	Ettringite <sup>R</sup> , quartz, pyrite, chalcopyrite, sphalerite, pyrrhotite, arsenopyrite, Mn oxide and barite	Gypsum>calcite>ettringite>bassanite>quartz+desautelsite-like compound
W8-4A12	Phase M	Gypsum <sup>R</sup> , Calcite <sup>R</sup> , Fe-rich phase	Ettringite <sup>R</sup> , pyrite, Mn-Ca oxide and Ca-Al silicate <sup>R</sup>	Calcite>gypsum>quartz>ettringite>bassanite+desautelsite-like compound
W8-25A1	Phase M	Gypsum, Calcite, Fe-rich phase	Ettringite <sup>R</sup> , quartz, pyrite, pyrrhotite and Ca-Al silicate	Calcite,gypsum>quartz>ettringite>bassanite+ fair amount of desautelsite-like compound
W8-25A6	Phase M	Gypsum <sup>R</sup> , Calcite, Fe-rich phase	Pyrite, barite, Mn oxide	Gypsum>calcite>quartz>ettringite+desautelsite-like compound
W8-25A12	Phase M	Gypsum <sup>R</sup> , Calcite	Quartz, Fe-rich phase, Ti oxide, Mn oxide, barite, Na-Al silicate, Ca-Si sulfate/hydroxide(?)	Gypsum,calcite>quartz>ettringite+desautelsite-like compound
W8-60A1	Phase M	Gypsum <sup>R</sup> , Calcite	Ettringite <sup>R</sup> , Fe-rich phase, pyrite, Na-Ca-Al silicate	Gypsum>calcite>ettringite>quartz+desautelsite-like compound
W8-60A6	Phase M	Gypsum <sup>R</sup> , Calcite <sup>R</sup>	Fe-rich phase, Ca-Mn oxide, pyrite, sphalerite, goethite	Gypsum,calcite>quartz+desautelsite-like compound
W8-4S1	Phase M	Gypsum <sup>R</sup> , Calcite, Fe-rich phase(s)	Quartz, Ca and Ca-Al silicate <sup>R</sup> , ettringite <sup>R</sup> , apatite, pyrite, sphalerite and chalcopyrite	Gypsum,calcite>quartz+desautelsite-like compound
W8-4S6	Phase M	Fe-rich phase, Calcite	Gypsum , quartz, Ca-Al silicate, Mn oxide,ettringite <sup>R</sup> , pyrite, sphalerite, chalcopyrite, arsenopyrite and barite	Calcite>ettringite,bassanite,pyroaurite (member of the hydrotalvite group)
W8-4S12	Phase M	Gypsum <sup>R</sup> , Fe-rich phase, Calcite	Ettringite <sup>R</sup> , pyrite, sphalerite, Mn oxide, apatite and quartz	Calcite>gypsum>bassanite>quartz> ettringite+desautelsite-like compound
W8-25S1	Phase M	Gypsum <sup>R</sup> , Calcite	Fe-rich phase, ettringite <sup>R</sup> , pyrite, barite	Calcite>gypsum>ettringite,quartz, bassanite+desautelsite-like compound
W8-25S12	Phase M	Gypsum <sup>R</sup> , Calcite, Fe-rich phase	Quartz, ettringite <sup>R</sup> , pyrite, Mn oxide	Calcite, gypsum>quartz, bassanite, ettringite+desautelsite-like compound
W8-60S1	Phase M	Gypsum <sup>R</sup> , Fe-rich phase, Calcite	Ettringite <sup>R</sup> , pyrite	Calcite,gypsum>quartz, ettringite+desautelsite-like compound
W8-60S6	Gypsum <sup>R</sup> , Calcite <sup>R</sup>	Phase M, Fe-rich phase	Pyrrhotite, pyrite, chalcopyrite, goethite and magnetite	Calcite,gypsum>quartz, ettringite+desautelsite-like compound
W8-60S12	Gypsum <sup>R</sup> ,	Phase M, Fe-rich phase	Pyrite, goethite, magnetite	Calcite,gypsum >quartz+desautelsite-like compound



Sample	Major	Minor	Trace	XRD
	Calcite <sup>R</sup>			

\* Phase M = Ca-Mg-Fe sulfate hydroxide with lower contents of Zn,Mn, Al,Si and C; \*\* Fe-rich phase = Fe-rich variant of phase M;

<sup>R</sup> = Phases which shows recrystallization

## 7.5 Discussion

A key factor in assessing long-term sludge stability is the sludge aging process. As sludges age they tend to undergo some degree of recrystallization and transformation of neutralization by-products. Results from the field study (Zinck *et al.* 1997) discussed above found that aged sludges seem to have a somewhat lower propensity for metal leachability than fresh sludges. However, variation in raw water chemistry or other site factors make the results from a strict field comparison limited by several assumptions; such as similar starting material, similar aging conditions, etc. This complementary study focused on assessing sludge aging under controlled conditions. For the most part, the trends observed in the field study (Zinck *et al.* 1997) were substantiated by this laboratory aging study.

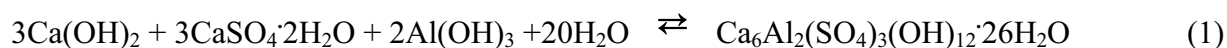
The degree of metal mobility from the sludge declined with aging time. After one year of aging, at all temperature conditions, there was a significant drop in leachate concentration. This was particularly apparent for zinc mobility which declined by several orders of magnitude after aging only one year.

Mineralogical examination of the aged sludge samples showed changes in composition with time. The proportion of calcite and gypsum in the sludge samples increased over time. This was accomplished through a process of dissolution and recrystallization of the sludge components. This process was accelerated in a saturated environment as observed in the detailed analysis of the high density sludge samples. These observations support the theory presented by Zinck *et al.* 1997 that the calcite and gypsum are the >final< phases of the aged sludge and in the long term (millennia), the sludge may transform into a carbonate rock with a minor iron oxide phase. The ferric oxyhydroxide present in the sludge will slowly transform into hematite.

Ettringite ( $\text{Ca}_6\text{Al}_2(\text{SO}_4)_3(\text{OH})_{12}\cdot 26\text{H}_2\text{O}$ ) was observed in both the fresh and aged high density sludge samples and in most of the aged synthetic sludge samples. This mineral was not observed in other sludges characterized previously (Zinck *et al.* 1997). Ford *et al.* (1998) also found ettringite to be a minor phase in the sludges characterized from the Climax Molybdenum Mine.

Ettringite is a calcium, aluminum, hydroxy-sulphate hydrate which is commonly observed in the concrete industry. This mineral phase is stable in the pH range 11.5 to 12.5 and has limited dissolution at pH 10 and complete dissolution at pH 2 (Ford *et al.* 1998). The hydrous nature of ettringite is apparent in its low specific gravity,  $1.8 \text{ g/cm}^3$ . Thus, the formation of ettringite would cause an increase in sludge volume.

As the sludge ages it appears that sludge components recrystallize into ettringite as outlined below [1].



Ettringite decomposes at elevated temperatures ( $>70^\circ\text{C}$ ) into gypsum and aluminum hydroxide (Albino *et al.* 1997; Kuzel 1996). This was observed in the sludges aged for 12 months at  $60^\circ\text{C}$ . This decomposition would explain the increase in gypsum concentration in the sludges with aging time/temperature.

The formation of ettringite appears beneficial to the stabilization of metal contaminants in

the sludge. Ferric iron can replace  $\text{Al}^{3+}$  in the ettringite lattice. Other cationic substitutions can occur as bivalent ions such as  $\text{Mg}^{2+}$ ,  $\text{Zn}^{2+}$ ,  $\text{Mn}^{2+}$ ,  $\text{Fe}^{2+}$ ,  $\text{Co}^{2+}$  and  $\text{Ni}^{2+}$  can replace  $\text{Ca}^{2+}$  in the crystal lattice to variable extents (Albino *et al.* 1997). Furthermore, the zero point charge of ettringite make it a good adsorbent of positively charged metal species (Mohamed *et al.* 1995).

The presence of the desautelsite-compound commonly found in these sludges also appears to impact on metal leaching. It has been previously suggested (Zinck *et al.* 1998) that the degree of metal leaching is related to the occurrence and stability of desautelsite in the sludge. Baltpurvins *et al.* (1997) suggested that aging amorphous ferric hydroxide precipitates in the presence of magnesium above pH 9 produced a multi-component phase related to the mineral pyroaurite. Both pyroaurite and desautelsite are members of the water-bearing-carbonate, hydrotalcite group of minerals. Unlike ferrihydrite or other iron oxyhydroxides, pyroaurite is not a precursor in the formation of goethite or hematite. Pyroaurite occupies relatively less volume than either ferrihydrite or goethite (Baltpurvins *et al.* 1997).

Another interesting feature observed with sludge aging was the oxidation rims of goethite and magnetite which formed around sulphide particles present in the sludge. These secondary phases suggest that long-term codisposal of sludge and tailings may be beneficial in terms of both waste management and metal leachability. The oxidation rim around the tailings would provide a physical barrier that may reduce acid-generating potential. The high elevated temperature accelerated the aging process and in reality the iron oxide rims may take hundreds of years to form, possibly longer than the time required for the excess alkalinity to be consumed and the tailings to turn acid.

## 8.0 CONCLUSIONS

Several treatment parameters significantly impact sludge production and the geochemical stability of lime sludge. Through minor modifications to the treatment process the properties of the generated sludge can be tailored to the plant or site operating priorities.

### 8.1 Process Parameters

Suitable agitation rates and impeller designs must be selected to discourage particle abrasion in the continuous stirred tank reactor (CSTR) which often leads to the production of fines. The rate should allow the particles to remain suspended for maximum growth while limiting unnecessary particle collisions and excessive energy demands. Unmixed pockets within the reactors will limit the degree of particle growth and will broaden the particle size distribution.

Rapid agitation tends to rework fragile porous precipitates into dense, compact aggregations with improved settling rates (Zinck 1993). This is particularly true for a batch process where particle overcrowding is not a factor. However, sludge recycling in a high hydrodynamic shear environment is detrimental to the formation of large, compact particles as particle abrasion and particle growth processes occur counterproductively.

Ultimately, the optimum rate of mixing during AMD treatment will depend on the amount of sludge recycled through the system. Recycling is a key factor in producing high density sludges. The optimum degree of recycling will depend on site specific factors such as raw water composition and treatment plant configuration. This study has found recycling affects several treatment related parameters and can impact on long term sludge stability as well as intermediate concerns such as sludge density. Increased recycling, while beneficial in terms of plant efficiency and reagent costs, serves to increase the heavy metal content of the sludge. This coupled with the lower net neutralization potential commonly observed with HDS type sludges provides the opportunity for metal leaching (Zinck *et al.* 1997).

The method of neutralization was found to impact on sludge properties and treatment efficiency. Bulk or rapid neutralization is comparable to the basic treatment method and results in the formation of voluminous sludges which dewater slowly and have low settling rates (Zinck *et al.* 1997). Slow, controlled neutralization was shown to increase settling rates by five-fold. This has significant implications with respect to clarification requirements. Through supersaturation control, as with staged-neutralization, settling rates can be further increased by 50%. Furthermore, lime consumption can be reduced through selection of a controlled or staged method of neutralization, reducing reagents costs by 10-15%. Efficient lime utilization yields sludge with low neutralization potential values and less excess alkalinity. This loss in metal buffering capacity of the sludge through controlled neutralization is off-set through better precipitate crystallinity. Metal release from crystalline precipitates is generally lower than from amorphous or poorly crystalline material.

### 8.2 Raw Water Composition

Presently, the raw water is collected for treatment and its composition may vary

significantly. However, knowledge of sludge generation under specific effluent conditions (e.g. high sulphate) will allow operators to better understand the limitations of their treatment process and suggest probable treatment by-products based on raw water chemistry. This study examined three effluent components; ferric-ferrous iron ratio, sulphate concentration and suspended solids.

Results suggest that a greater proportion of ferric iron in solution enhances sludge density and settleability, however some ferrous iron was found to be beneficial. The mineralogical and morphological variations in the sludge appear to be due to the increased amount of recycled sludge required for neutralization of the AMD stream. This increased amount of recycled sludge in reactor 1 (pH 3.5) acts as seeds for ferric hydroxide precipitation and allows for greater particle growth.

The amount of zinc leached from the sludge increased with increasing ferric iron concentration in the raw water. In the ferric form, iron precipitates as ferric oxyhydroxide which has a known propensity to adsorb metal ions (Erikson *et al.* 1973; Benjamin and Leckie 1981; Zinck 1993). Adsorbed metals are more readily leached than those chemically precipitated, thus stability was found to increase with Fe(II) concentration. In general, it was found that a solution containing a mixture of both ferric and ferrous iron produced the best results, with the sludge handling properties improving with a greater relative proportion of ferric and sludge stability increasing as the portion of ferrous in the solution increased.

Higher sulphate levels yield higher sludge densities primarily due to greater gypsum production. Conversely, elevated sulphate concentrations were detrimental to sludge settleability and particle growth. Elevated sulphate concentrations increases the ionic strength of the solution and changes the precipitation precursor complexes from hydroxyl ( $M_n(OH)_z^m$ ) to sulphate species ( $M_n(SO_4)_z^m$ ) affecting both the flocculation capabilities of the polymer and metal hydrolysis mechanisms. Also, sludges precipitated from high sulphate solutions demonstrated higher levels of metal leachability. Greater polymerization of the oxyhydroxide phase traps metal rich raw water which is readily leached. The greater aluminum mobility with increasing sulphate concentration was thought to result from the dissolution of ettringite or the dissociation of the weak chemisorbed aluminum ions.

### **8.3 Excess Alkalinity**

The addition of excess lime to HDS-type treatment sludges resulted in lower metal leachability, however, the physical properties of the sludge were adversely affected. In both sludges, ettringite formed at high levels of lime addition and at high pH values (>10). While ettringite served to stabilize other metals, aluminum, which is not regulated in Canada, saw increased mobilization as the stabilized, ettringite-containing sludge decomposed under leaching conditions. This potential method of remediation is not cost-effective relative to its limited benefits.

## 8.4 Sludge Aging

The degree of metal mobility from sludge declined with aging time in both this laboratory study and the field study. Mineralogical examination of the aged sludge samples showed changes in composition with time. The proportion of calcite and gypsum in the sludge samples increased over time. This was accomplished through a process of dissolution and recrystallization of the sludge components, supporting the theory presented by Zinck *et al.* (1997) that the calcite and gypsum are the >final< phases of the aged sludge and in the long term (millennia), the sludge may transform into a carbonate rock with a minor iron oxide phase.

Ettringite was observed in both the fresh and aged high density sludge samples and in most of the aged synthetic sludge samples. The formation of ettringite was beneficial to the stabilization of metal contaminants in the sludge. Furthermore, mineralogical evidence suggests the degree of metal leaching is related to the occurrence and stability of desautelsite in the sludge.

Oxidation rims of goethite and magnetite which formed around sulphide particles present in the sludge suggest that long-term co-disposal of sludge and tailings may be beneficial in terms of both waste management but also metal leachability. The oxidation rim around the tailings would serve to provide a physical barrier that may reduce acid-generating potential.

From this study it appears that several factors impact the metal leachability of lime sludges as well as sludge properties. Optimization of treatment conditions and appropriate disposal methods can yield dense, stable sludge with little or no additional expenditure.

## **9.0 RECOMMENDATIONS**

### **9.1 Plant Practice**

- ▶ Lime neutralization treatment should utilize a process of sludge recycle and supersaturation control to minimize metal leachability and sludge production.
- ▶ Excess lime addition is not a cost-effective method to stabilize sludge. Plant and crystallization control are more effective in reducing sludge volumes and stabilizing heavy metals.
- ▶ Excessive agitation and recycle should be avoided as they lead to particle abrasion, poor settling and increased metal leachability.

### **9.2 Further Work**

- ▶ Further investigations are necessary to study the long term environmental stability and mechanisms responsible for metal mobility from ettringite and desautelsite since the presence of these sludge compounds appears to impact on long term sludge stability
- ▶ Aging tests should be correlated with a complementary, controlled field study and the aggressive aging treatments should be related to actual aging conditions and times
- ▶ The tests applied in this study roughly simulate long term sludge disposal in a pond-type environment. As many sites elect to dispose of lime sludge with tailings, metal leachability and sludge aging should be studied for this disposal environment.
- ▶ Modelling studies should be conducted on the data obtained and applied to operating plants to optimize current lime treatment processes.

## 10.0 REFERENCES

Albino, V., R. Cioffi, M. Marroccoli and L. Santoro, Potential application of ettringite generating systems for hazardous waste stabilization, *Journal of Hazardous Materials*, **51**(1):241-252, 1997.

Allied Colloids, Percol E-10 Report and Material Safety Data Sheet.

ASG Quality Manual 1996-1997. Analytical Services Group, Materials, Processing and Services Laboratories, Minerals and Mining Services Laboratories, NRCan, Ottawa.

Aubé, B. and S. Payant, Engineering and Process Summary of the Treatment Pilot Program at Heath Steele, Noranda Technology Centre, May, 1996.

Aubé, B. and S. Payant, The Geco Process: A New High Density Sludge Treatment for Acid Mine Drainage. In: *Proceedings of the Fourth International Conference on Acid Rock Drainage*, Vancouver, BC, May 31-June 6, 1997.

Baltpurvins, K.A., R.C. Burns and G.A. Lawrence, Effect of  $\text{Ca}^{2+}$ ,  $\text{Mg}^{2+}$  and anion type on aging of Fe(III) hydroxide precipitates., *Environmental Science and Technology*, **31**:1024-1032, 1997.

Benfield, L.D., J.F. Judkins and B.L. Weand. Process Chemistry for Water and Wastewater Treatment. Prentice-Hall, Inc., New Jersey, 1982.

Benjamin, M.M. and J.O. Leckie, Multiple-site adsorption of Cd, Cu, Zn, and Pb on amorphous iron oxyhydroxide., *J. Colloid and Interface Science*, **79**(1):209-222, 1981.

Black, A.P., F.B. Birkner and J.J. Morgan, Destabilization of dilute clay suspensions with labelled polymers., *JAWWA*, **57**(12):1547-1600, 1965.

Demopoulos, G.P., J.M. Zinck and P.D. Kondos, Production of Super Dense Sludges with a Novel Neutralization Method, In: *Waste Processing and Recycling in Mineral and Metallurgical Industries II*. (Eds. S.R. Rao, L.M. Amaratunga, G.G. Richards and P.D. Kondos), Vancouver, B.C. Aug. 20-24, 1995. pp 401-411.

Dinardo, O., P.D. Kondos, D.J. MacKinnon, R.G.L. McCready, P.A. Riveros and M. Skaff, 1991. A Study on Metals Recovery/Recycling from Acid Mine Drainage. MEND Project Report, 3.21.1(a), July 1991.

Dousma, J., D. den Ottenander and P.L. de Bruyn, The influence of sulphate ions on the formation of iron(III) oxides., *Journal of Inorganic and Nuclear Chemistry*, **41**:1565-1568, 1979.

EPA, Neutralization of Acid Mine Drainage, Design Manual, January 1983.



Erikson, L., E. Matijević and S. Friberg, Desorption of hydrolyzed metal ions from hydrophobic interfaces. I. Latex-aluminum nitrate systems., *J. Colloid and Interface Science*, **43**(3):519-598, 1973.

Flynn, C.M., Jr. 1990. Dense Hydrolysis Products from Iron(III) Nitrate and Sulphate Solutions. *Hydrometallurgy*, Volume 25, pp. 257-270.

Ford, R.C, J.L. Clapper and B.R. Roming, Stability of Water Treatment Sludge, Climax Mine, Colorado, Part I and Part II. *Tailings and Mine Waste* 98, pp. 645-667, 1998.

Gionet, Mellor, Liebich Associates Limited (GML) 1987. "Generation and Stability of Canadian Mine/Smelter Treatment Sludges". DSS Contract No. 15SQ. 23440-5-9161, GML Project 7227-R-1, July 7, 1987.

Government of Ontario 1994. General-Waste Management Regulation. Ontario Regulation 347, Environmental Protection Act.

Huck, P.M., K.L. Murphy and B.P. LeClair, Scavenging and flocculation of metal-bearing wastewaters using polyelectrolytes., Environmental Protection Service Report No. EPS 4-WO-77-7, November, 1977.

Jeffery, G.H., J. Bassett, J. Mendham and R.C. Denney. Vogel's Textbook of Quantitative Chemical Analysis, Fifth Edition. Longman Scientific and Technical, Great Britian, 1989

Kuit, W.J. 1980. Mine and Tailings Effluent Treatment at the Kimberley, B.C. Operations of Cominco Ltd. *CIM Bulletin*, Volume 73, December, pp 105-112.

Kuyucak, N., T.W. Sheremata and K.G. Wheeland, 1991. Evaluation of Improved Lime Neutralization Processes. Part I: Lime Sludge Generation and Stability. In: Proceedings of the Second International Conference on the Abatement of Acidic Drainage, Volume 2, pp. 1-13. September 16-18, 1991, Montréal, Québec.

Kuzel, H.J., Initial hydration reactions and mechanisms of delayed ettringite formation in Portland cements., *Cement and Concrete Composites*, **18**(3):195-2034, 1996.

Lamb, A.B. and A.G. Jacques, The slow hydrolysis of ferric chloride in dilute solutions. II. The change in hydrogen ion concentration., *J. American Chemical Society*, **60**:1215-1225, 1938.

Lawrence, R.W. and P.B. Marchant, 1991. Acid Rock Drainage Prediction Manual. MEND Report 1.16.1b.

MacDonald, R.J.C., P.D. Kondos, S. Chevier, P. Rubinsky and M. Wasserlauf, 1989. **Generation of, and Disposal Options for Canadian Mineral Industry Effluent Treatment Sludges**. In: Tailings and Effluent Management Symposium, August 20-24, 1989, Halifax, Nova Scotia.

Matijević, E. and P. Scheiner, Ferric Hydrous Oxide Sols III. Preparation of uniform particles by hydrolysis of Fe(III)-chloride, -nitrate, and -perchlorate solutions., *J. Colloid and Interface Science*, **63**(3):509-524, 1978.

Mohamed, A.M.O, J.F. Boily, M. Hossein and F.P. Hassani 1995. Ettringite formation in lime-remediated mine tailings. CIM Bulletin, Volume 88, November/December, pp 69-75.

OISTL Design Manual, Neutralization of Acid Mine Drainage, U. S. Environmental Protection Agency Office of Research and Development Industrial Environmental Research Laboratory, University of Kentucky, EPA-600/2-83-001. Jan., 1983.

Orava, D., C.E. Hallam and R. Swider. 1995. Evaluating alternative long-term strategies for treatment of acid mine drainage (AMD). In: Proceedings of Sudbury '95, Conference on Mining and the Environment, Volume 2, pp 504-514 May 28-June 1, 1995, Sudbury, ON

Rose, S. and A.M. Ghazi, Release of sorbed sulphate from iron oxyhydroxides precipitated from acid mine drainage associated with coal mines., *Environmental Science and Technology*, **31**:2136-2140, 1997.

Schwertmann, U. and R.M. Cornell, Iron Oxides in the Laboratory., VCH, Weinheim, Germany, 1991.

Senes Consultants Limited, 1994. **Acid Mine Drainage - Status of Chemical Treatment and Sludge Management Practices**. DSS Contract No. 015SQ.23440-3-9140, June 1994

Smith, T.N., A model of settling velocity., *Chemical Engineering Science*, **53**(2):315-323, 1998.

Svanks, K. and K.S. Shumate, **Factors Controlling Sludge Density During Acid Mine Drainage Neutralization**. Water Resources Center, Ohio State University, 1973.

Vachon, D., R.S. Siwik, J. Schmidt. and K. Wheeland, 1987. **Treatment of Acid Mine Water and the Disposal of Lime Neutralization Sludge**. In: Proceedings of Acid Mine Drainage Seminar/Workshop, Halifax, Nova Scotia, Environment Canada, March 23-26, 1987, pp. 537-564.

WQA, Glossary of Terms, 3rd Edition Copyright 1997 by the Water Quality Association

Wilson, L.J. "Canada-Wide Survey of Acid Mine Drainage Characteristics". MEND Report 3.22.1, December, 1994.

Zeta Meter, Inc, "Everything you want to know about Coagulation & Flocculation ...", Zeta-Meter, Inc. Staunton, Virginia. Fourth Edition. April 1993

Zinck, J.M. "An Investigation into the Hydrolytic Precipitation of Iron(III) from Sulphate-Bearing Effluents", M.Eng. Thesis, McGill University, 1993.

Zinck, J.M., L.J. Wilson, T.T. Chen, W. Griffith, S. Mikhail and A.M. Turcotte, "Characterization and Stability of Acid Mine Drainage Treatment Sludges", MEND Report 3.42.2, May 1997.

Zinck, J.M., C.M. Hogan and W. Griffith, "CANMET's High Density Sludge Pilot Plant Facility". Poster Display presented at 36<sup>th</sup> Conference of Metallurgists, Sudbury, August, 1997b.

Zinck, J.M., W.F. Griffith, G. Laflamme, S. Mikhail and A.M. Turcotte, Client Report. Mining and Mineral Sciences Laboratories Report 97-086 (CR), March 1998.

## **APPENDIX A**

MINING AND MINERAL SCIENCES LABORATORIES

MINERALOGICAL CHARACTERIZATION GROUP

REPORT M - 5280

**TITLE:** Mineralogical characterization of a series of high density sludge samples (**W8-series**).

**INVESTIGATOR:** J.H.G. Laflamme



**PROJECT NO.:** 1144

**SAMPLE:** Sixteen freeze-dried sludge samples, each weighing between 1 to 18 g, were received in sealed bags, by M C. Hogan (MMSL) in October 1997. The samples came from Brunswick Mining and Smelting's high density sludge plant (Bathurst N.B.), and were **labelled** as: **W8-4S1(A), W8-4A6, W8-4A12, W8-25A1, W8-25A6, W8-25A12, W8-60A1, W8-60A6, W8-4S1(B), W8-4S6, W8-4S12, W8-25S1, W8-25S12, W8-60S1, W8-60S6** and **W8-60S12**. Samples **W8-4S1(A)** and **W8-4S1(B)** are believed to be **W8-4A1** and **W8-4S1** respectively. The coding used to identify each sample is the following: the first two digits are for the mine site (i.e. **W8**), the next digit is for the temperature of a heat treatment at which the sludges have been submitted in °C (i.e. 4, 25 and 60), the following digit is for the moisture environments (i.e. A, for atmospheric and S for saturated) and finally the last digit is for the aging duration in months (i.e. 1, 6 and 12). Two samples are apparently missing to complete the series, i.e. **W8-25S6** and **W8-60A12**.

**PURPOSE:** To perform mineralogical characterization of the sludge samples as part of a more detailed aging study. The sludges have been submitted to a heat treatment at different temperatures and exposed to different moisture environments for various lengths of time. The emphasis should be on mineral recrystallization and/or replacement, on the dissolution of gypsum, on the formation of ettringite [ $\text{Ca}_3\text{Al}_2(\text{SO}_4)_3(\text{OH})_{12}\cdot 26\text{H}_2\text{O}$ ] and on any morphological changes observed in general.

**METHOD OF INVESTIGATION:** Polished sections were prepared from sub-samples of each sludge. The polished sections were first examined by optical microscopy under reflected light, followed by scanning electron microscopy (SEM) in the back-scattered electron (BE) mode, with a JEOL 820 SEM operated at 20 kV, with a beam current of 1 nA. Identifications were done by Energy Dispersion Spectrometry (EDS), using a Link ISIS series 300 system. Also, part of the samples were submitted for X-ray diffraction analysis (XRD), as a complementary technique for mineral identifications.

.../2

Signed  Date 3/02/98 Approved  Date 3-Feb.-98  
INVESTIGATOR Rolando Lastra

1. C. Hogan 2. J. Zinck 3. Section Files

ORIGINATOR (2 copies)

PROJECT LEADER

4. \_\_\_\_\_

PLEASE NOTE: THIS REPORT NOT TO BE REFERENCED IN PUBLICATIONS  
PLEASE ACKNOWLEDGE THIS WORK IN FINAL REPORT

**RESULTS:** Details of the mineralogical findings are described for each sample, followed by **photomicrographs** referred in the text by their plate number. XRD **diffractogram** for each sample is also included, as well as a summary of the mineralogical findings done by SEM-EDS and XRD (Table 1). Some of the compounds observed in the sludges were not characterized enough to give an accepted mineral name; therefore for these compounds, the more generic term “phase” is used. In most of these samples the compound of major abundance is a phase corresponding to a Ca-Mg-Fe sulfate hydroxide hydrate with lower contents of **Zn, Mn, Al, Si** and **C**. This compound is referred as **“phase M”**. Abbreviations used in the photomicrographs are the following: “Fe-rich” and “Fe-O” are variants of **“phase M”**, the second with higher Fe content than the first; **cal=calcite; gp=gypsum; Ca sil=Ca silicate** phase; **qtz=quartz; py=pyrite; sp=sphalerite; po=pyrrhotite; apy=arsenopyrite; brt=barite; Mn-O=Mn oxide** phase; **Ca-Mn-O=Ca-Mn oxide** phase; **Ca-Al sil=Ca-Al silicate** phase; **ap=apatite; Na-Ca-Al sil=Na-Ca-Al silicate** phase; **Ca-Si-S=Ca-Si sulfate/hydroxide** phase.

#### **W8-4S1(A):**

This sample is probably mislabelled and perhaps should correspond to **W8-4A1**. Examination of this fresh sludge sample reveals great variability in grain size, which ranges from **< 5µm** to roughly **700µm** (Plate **000**), although in general the particle size is relatively coarse. The major constituent was identified by SEM-EDS as a Ca-Mg-Fe sulfate hydroxide hydrate, containing lower contents of **Zn, Mn, Al, Si** and **C** (Fig. **1A**), which shows inhomogeneity from spot to spot. As previously indicated, this major phase will be referred simply as **“phase M”**. **Gypsum** and **calcite** are observed as **minor** constituents, either free, attached or included within the major phase (Plates **000, 001** and **002**); the larger grains of gypsum are often showing crystallization. An Fe-rich phase (Fig. **1b**), that could be a variant of **“phase M”** with higher Fe content, was also observed in small amount. These Fe-rich phase particles are relatively small in size, often free but also attached to **“phase M”**. Observed in even lesser amounts are ettringite, **Ca silicate**, **Ca-Mn oxide**, **pyrite**, **chalcopryrite**, **apatite**, an oxide phase with **Mn > Ba** and **magnetite**. **Ettringite** (Fig. **1c**), is found as small **euohedral** laths within the major constituent (Plate **007**). **Pyrite** is the predominant sulfide observed; the particles are rarely exceeding **50 µm** in size, and are found either free or attached to the major constituent.

**XRD** analysis (Fig. **2**) indicates that this sludge consists of crystalline **calcite**, **gypsum**, **quartz**, **ettringite** and of a major amount of poorly crystalline material. It is assumed that this poorly crystalline material, is in fact the most important constituent observed and identified by SEM-EDS in the sample, i.e. **“phase M”**; this material is most probably another variant of the poorly crystallized **desautelsite-like** compound (a member of the **hydrotalcite** group), identified by XRD and reported for **Mattabi** (report **M-5236**) and for **Heath Steele** (report **M-5265**).

#### **W8-4A6:**

Examination of this 6 months aged sample generally shows much finer **grained** particles (Plates **023** and **024**), although some quite large particles (almost **2mm** in maximum dimension, Plate **021**) were also observed. As observed in the previous sample, the major constituent was identified as **“phase M”**, which shows inhomogeneity from spot to spot as shown by SEM-EDS (Figs **3a** and **3b**). **Gypsum** which shows nice crystallization (Plate **024**) is a minor constituent, it is generally found free, but also attached or included within the major constituent. **Calcite** is also observed in minor amount, generally included in the major phase, but also within gypsum (Plate **024**). Numerous grains of the Fe-rich phase described in the previous sample are also present, sometimes free but also within the major phase. Numerous sulfides particles are found, of which **pyrite** is the most common, but **chalcopryrite**, **sphalerite**, **pyrrhotite** and **arsenopyrite** were also identified by SEM-EDS. **Quartz** and **Mn oxide** particles were also observed included within the major phase (Plates **021** and **022**). **Ettringite** was found as extremely fine laths, **within the** major phase (Plate **022**). Few small particles of **barite** were found free (Plate **024**).

**XRD** analysis (Fig. **4**) indicates that this sludge consists of crystalline **calcite**, **gypsum**, **bassanite**, **ettringite**, **quartz** and of a poorly crystalline phase. Once more, it is obvious that the major phase identified by SEM-EDS is poorly crystalline, therefore not diffracting well and most probably consists of a **desautelsite-like** compound. Although identified by **XRD**, **bassanite (2CaSO<sub>4</sub>·H<sub>2</sub>O)** was not identified by SEM-EDS because of similarity with **gypsum (CaSO<sub>4</sub>·H<sub>2</sub>O)** in terms of composition.

### **W8-4A12:**

Examination of this 12 months aged sludge also shows quite a variability in term of grain size as shown in Plate 040. Once more, the major phase present is "**phase M**", which shows inhomogeneity (Figs **5a** and **5b**), and carries fine-grained calcite particles disseminated throughout the matrix (Plates 041, 042 and 044). **Gypsum** which is a minor constituent, shows crystallization (Plate **040**), and is generally present as free grains, but also attached or included within the major phase (Plate 041). **Calcite** particles are also found free or **attached**(Plates 040,042 and **044**), sometimes showing crystallization. The Fe-rich phase previously described is also present in this sample (Plate 040). Numerous sulfides particles are present, either free or included within the major phase (e.g. pyrite, Plate 042). **Ettringite** is once more present as thin laths within the major phase (Plate 044). A Ca-Al silicate phase was also observed as needles (Plate 041) within the major phase, together with a **Mn-Ca** oxide phase (Plate 042).

XRD diffractogram (Fig. **6**), indicates crystalline calcite, gypsum, **bassanite, quartz, ettringite** and a poorly crystalline material (desautelsite-like compound).

### **W8-25A1:**

Examination of this fresh sludge, submitted to a heating treatment of **25°C**, reveals some variability in terms of grain sizes, although generally coarser and somewhat similar to **W8-4A1** sample. The major phase is once **more "phase M"**, observed in the previous samples. **Gypsum** particles are present in minor amounts, generally as free euhedral particles (Plate **008**), but also as smaller grains enclosed within the major phase. **Calcite** is observed in lesser amount as free grains (Plates **008** and **009**), but also as locked particles within the major phase (Plates **008, 009, 010** and 011). The Fe-rich phase described in previous samples is also present as free grains or included within the major phase (Plates 008 and 009). **Ettringite** is once more identified in this sample as thin laths (Plate 010 and 011) within the major phase. Quartz (Plate 011) and Ca-Al silicate were also observed within the major phase. **Numerous** sulfides particles **are** present, although pyrite is the most common, either as free grain or locked within the major phase (Plate 009); pyrrhotite was also identified (Plate 010).

XRD diffractogram (Fig. **7**), indicates that this sludge consists of crystalline calcite, gypsum, quartz, ettringite and a large amount of poorly crystalline material (a desautelsite-like compound).

### **W8-25A6:**

Examination of this 6 months aged sludge shows a relatively fine **grained** sample, with only a few relatively coarse grains. The major phase is identified **as "phase M"**. **Gypsum** and **calcite are** minor constituents, observed free, attached or included within the major phase ( Plates 029, 030 and 031). **Gypsum** shows crystallization (Plates 029 and **031**), whereas calcite is mainly found as small disseminated grains within the major phase. Few particles of the Fe-rich phase are present as free grains but some were also found enclosed within the major phase. Numerous sulfides, of which the most common is pyrite are present, often free, but also included within the major phase. Ettringite and quartz were not observed during SEM examination, even though they were reported by XRD. Few barite and Mn oxide grains were observed as free particles (Plate 031).

XRD diffractogram (Fig. 8) indicates the presence of crystalline gypsum, calcite, quartz, ettringite and poorly crystalline material (desautelsite-like compound).

### **W8-25A12:**

**Examination** of this aged sludge sample treated at **25°C**, shows some variability in terms of grain sizes (Plate 049). The major phase is once more "**phase M**", which hosts a wide variety of **fine-grained** disseminated minerals, i.e. calcite, gypsum, quartz, Ti oxide, pyrite, an undefined Ca-Si and S-bearing mineral and the Fe-rich phase (Plates 050,051 and 052). Plate 049, also shows a Na-Al silicate enclosed with the **major** phase. A fair amount of gypsum was observed as large euhedral grains (Plate **049**), Mn oxide coexisting with barite was also observed (Plate **049**). Numerous sulfides particles are also present either as free grains or included or attached to major phase. Once more, even though ettringite is reported by XRD, it was not observed during SEM examination.

XRD diffractogram (Fig. **9**), indicates the presence of crystalline gypsum, calcite, quartz, ettringite and poorly crystalline desautelsite-like compound.

### **W8-60A1:**

Examination of this fresh sludge submitted to a heating treatment of **60°C**, reveals a wide variability in terms of grain sizes, with particles generally small and widely dispersed, although fairly large crystallized grains of gypsum are observed (Plates 016 and 017). Gypsum is also found attached or included within "**phase M**", which is a major constituent. Much lesser amounts of **calcite**, the Fe-rich phase are also found either free, attached or included within the major phase. **Ettringite** was observed as small **euhedral** laths within the major phase (Plate 018). Numerous sulfides particles present, of which pyrite is the predominant sulfide, either as free grains or included within the major phase. (Plate **017**). Also present is a Na-Ca-Al silicate phase that was found as free grain.

XRD diffractogram (**Fig.10**) indicates the presence of gypsum, calcite, ettringite, quartz and poorly crystalline desautelsite-like phase.

### **W8-60A6:**

Examination of this sample shows wide variability in terms of grain size, with particles ranging from **c 5 μm** to **800 μm** although they are generally quite fine. Again, the most common is "**phase M**". Fair amount of **gypsum** particles are showing crystallization (Plates 033 and 034), as well as **calcite** which also shows some crystallization (Plate 035). Numerous sulfides particles observed, either free or attached; pyrite is the most common often showing alteration rim of goethite (Plate 032), which also shows sphalerite attached. Particles of a Ca-Mn oxide phase are also present.

XRD diffractogram (Fig. 11), indicates the presence of gypsum, calcite, quartz and poorly crystalline desautelsite-like phase.

### **W8-4S1(B):**

**This** sample is probably mislabelled and perhaps should correspond to W8-4S 1. Examination of this sample reveals great variability in terms of grain size, with average particle size that is relatively coarse, somewhat similar to observations done for sample W8-4S1(A). The major constituent identified by SEM-EDS is also "**phase M**". Gypsum and **calcite** are minor constituents, observed either free, attached or included within the major phase (Plates 003, 004, 005 and 006). Particles of the Fe-rich phase ( a variant of "**phase M**", but richer in Fe content) are also present, as well as another Fe-rich phase which shows even higher Fe content than the previous phase (Fig. 12b, Plate 003). Observed in lesser amounts are quartz, Ca and Ca-Al silicates, ettringite, apatite and numerous sulfides (mainly pyrite, sphalerite **and** chalcopyrite). **Ettringite** (Fig. 12c and a Ca-Al silicate phase are observed as small laths within "**phase M**" (Plates 005 and 006). The sulfides particles were found either free, attached or included in the major phase, as observed in sample W8-4S1(A), ( presumably W8-4A1).

XRD diffractogram (Fig. 13) indicates crystalline calcite, gypsum, quartz and a poorly crystalline material, most probably a variant of a desautelsite-like mineral.



### **W8-4S6:**

Examination of this sample reveals in general a much finer grain size than previous sample, although large particles are observed (Plates 025 to **027**), as found in sample **W8-4A6**. From a mineralogical point of view, this sample is not any different from **W8-4A6**, with the exception of **gypsum**; in sample **W8-4A6**, fairly large euhedral grains of gypsum were observed, whereas only a few small grains were observed in the present sample. The major phase ("phase **M**") shows inhomogeneity (Figs **14a**, **14b** and **14c**), and hosts various minerals such as quartz, **calcite**, a **Ca-Al** silicate phase, a Mn oxide phase, **ettringite** and sulfides particles (pyrite > sphalerite, chalcopyrite and arsenopyrite), as shown in Plates 025 to 027. Particles of Mn oxide and barite were also found liberated.

XRD diffractogram (Fig. **15**), indicates that this sludge consists of crystalline calcite, ettringite, bassanite, pymaurite and/or desautelsite ( members of the hydrotalcite group). As mentioned previously, identification of bassanite is not obvious by SEM-EDS because of compositional similarity with gypsum.

### **W8-4S12:**

Examination of this sample shows quite a variability in terms of grain sizes (Plates 045 and **048**), as observed for sample **W8-4A12**. "**Phase M**" is also the major constituent, and a few large euhedral grains of **gypsum** were found. **Calcite** is found either as free or attached particles, although generally as fine-grained particles enclosed in the major phase (Plates 045 to **048**), and sometimes with gypsum. Minor amount of the Fe-rich phase is present, either as free or attached particles; other constituents observed and often included within the major phase are sulfides (pyrite >> sphalerite grains were identified, Plate **046**), a Mn oxide phase, apatite and quartz. **Ettringite** is present as finely dispersed laths within the major phase (Plate 047).

XRD diffractogram (Fig. 16) indicates crystalline calcite, gypsum, bassanite, quartz, ettringite and a large amount of poorly crystalline phase (desautelsite-like compound).

### **W8-25S1:**

Examination of this sample reveals a lot of similarities with sample **W8-25A1**, i.e. with "**phase M**" as the major constituent and much lesser amounts of **gypsum**, generally observed as free grains showing crystallization (Plate **012**), but also as smaller particles enclosed within the major phase. **Calcite** is found either as free grains but also as locked particles within the major phase, together with **ettringite** (Plates 013 to 015) occurring as small laths, and sulfides particles (mainly pyrite). Other constituents present are the Fe-rich phase, observed as free or locked particles, and barite observed liberated.

XRD diffractogram (Fig. 17) indicates calcite, gypsum, ettringite, quartz, bassanite and a fair amount of poorly crystalline material (desautelsite-like compound).

### **W8-25S12:**

This sample shows a lot of similarities with sample **W8-25A12**; particle size is generally small (Plates 053 and **056**), although some grains observed are fairly large in size (Plate 054). **Gypsum** particles are generally free, showing euhedral outlines, but are also found attached or included within the major constituent, as observed for **calcite**. Other constituents present are the Fe-rich phase, generally observed free, and quartz which was found as small particles enclosed within "**phase M**". Numerous sulfides particles were found, mainly included within the major phase; also found within "**phase M**" are thin laths of **ettringite** (Plate 055). Mn oxide particles are also found liberated.

XRD diffractogram (Fig. 18) indicates the presence of crystalline calcite, gypsum, bassanite, quartz, ettringite and a poorly crystalline phase identified as a desautelsite-like compound.

### **W8-60S1:**

Very similar to sample **W8-60A1** with fairly wide variability in terms of grain size, and "**phase M**" as the major constituent. **Gypsum** generally shows crystallization (Plate **019**), and the particles are generally free, but also attached or included within the major phase. **Calcite** particles are much smaller in size, and also found either free, attached or included in "**phase M**" (Plates 019 and 020). Few particles of the Fe-rich phase were found, either free or attached. Numerous sulfides particles (mainly pyrite) were found often enclosed within "**phase M**". **Ettringite** was observed as small laths in the major phase (Plate 020).

XRD diffractogram (Fig. 19) reveals the presence of crystalline calcite, gypsum, ettringite, quartz and of a fair amount of poorly crystalline desautelsite-like compound.

### **W8-60S6:**

As **observed** in sample **W8-60A6**, this sample consists of often large euhedral grains of **gypsum** generally free (Plates 036,037 and **039**), and of fairly large grains of **calcite** also showing crystallization as shown in Plate 037. "**Phase M**" which appears to be a minor constituent in this sample is very fine **grained**. Large grains of the Fe-rich phase were observed (Plate 036). Numerous sulfides particles (pyrite, pyrrhotite and chalcopyrite) are found either free or attached, and furthermore, as found in sample **W8-60A6**, sulfides particles are showing alteration to goethite-like compound (Plate 039). A few small particles of magnetite were observed liberated.

XRD diffractogram (Fig. **20**), indicates crystalline calcite, gypsum, quartz and a poorly crystalline phase.

### **W8-60S12:**

**This** sample shows wide variability in terms of grain size, with gypsum and calcite as the major constituents, which are often free and show nice crystallization (Plates 057 and 059). These minerals are also present as small particles enclosed in "**phase M**", which is typically Si-rich compared to average composition obtained in previous samples, as shown on EDS spectra (Figs 21a and 21 b). Pyrite particles observed are generally free, and also show alteration rims of goethite (Plate 058). A few small grains of magnetite were found.

XRD diffractogram (Fig.22) indicates crystalline gypsum, calcite, quartz and some poorly crystalline material.

### **CONCLUSION:**

- With the exception of two samples (**W8-60S6** and **W8-60S12**), the major phase (**phase M**) observed in all the sludges studied, consists of a **Ca-Mg-Fe** sulfate hydroxide hydrate with lower contents of **Zn**, Mn, Al, Si and C; it is typically non-homogeneous and of poor crystallinity, **therefore** not diffracting well. It is presumably a member of the hydrotalcite group, a variant of the mineral desautelsite. Composition of **phase M** from sample **W8-60S12**, shows an increase in Si content compared to average composition obtained in other samples.
- Gypsum and calcite were observed as minor constituents in all but two samples (**W8-60S6** and **W8-60S12**), where they appear as major phases; crystallization of gypsum was observed to various extent in all samples, with one exception (**W8-4S6**), whereas crystallization of calcite was more rarely observed.

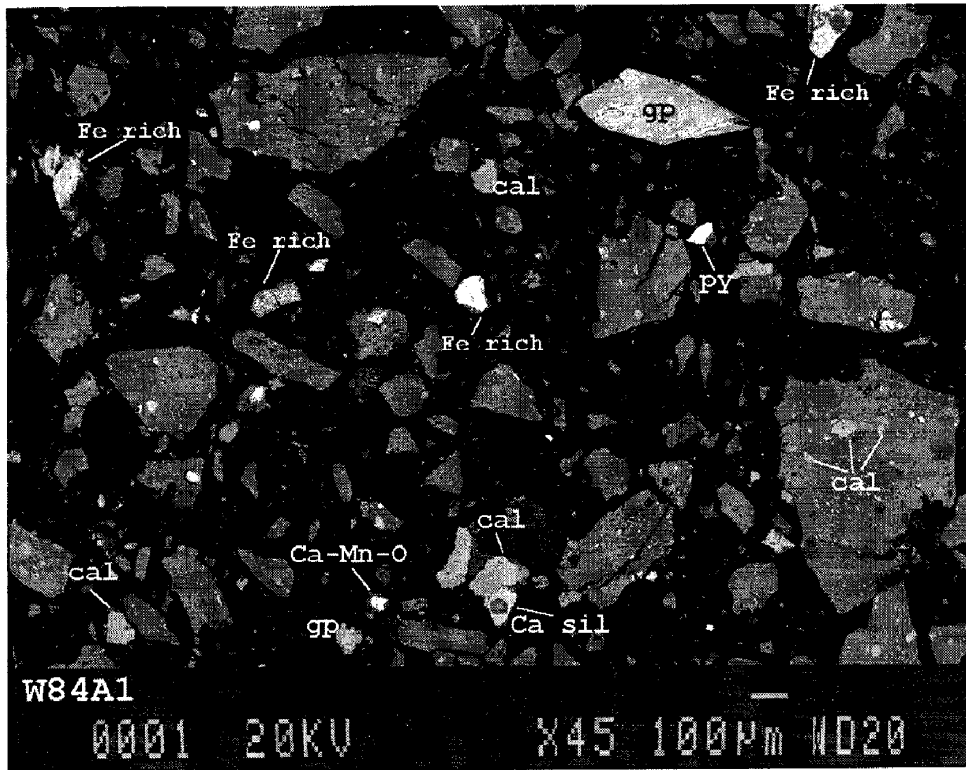
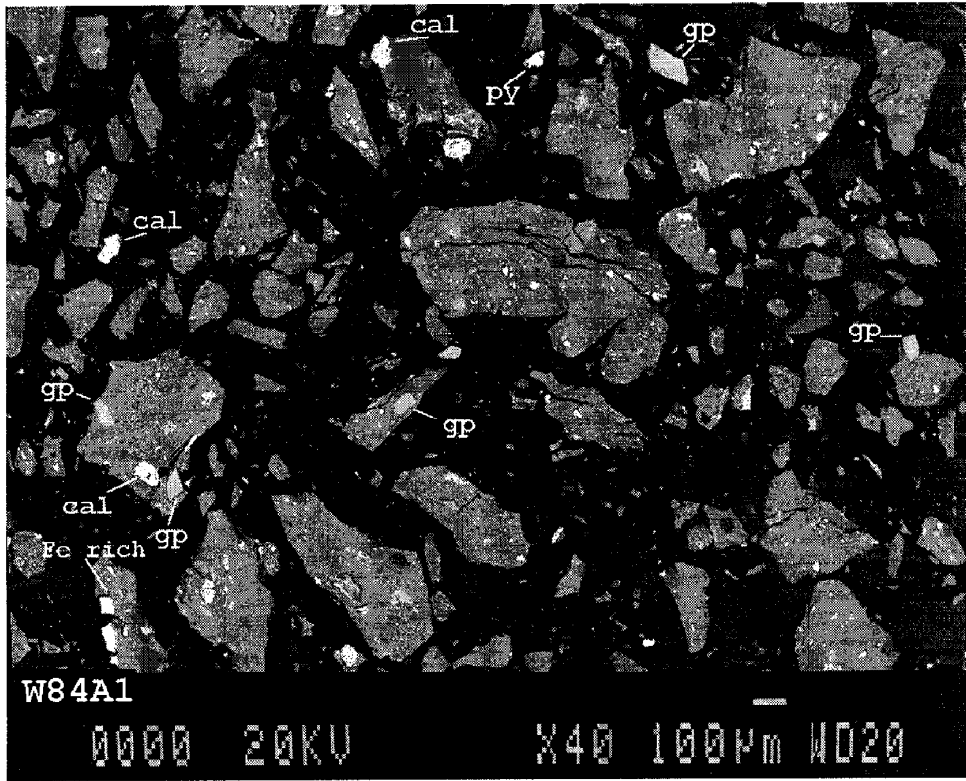
- Ettringite which is found as small euhedral laths within "**phase M**", was identified in eleven samples by SEM-EDS, and in twelve samples by XRD technique, **from** a total of sixteen samples studied.
- There is wide variability in terms of particle size, and the only explanation appears to be the way the samples have been prepared, i.e. the grain size of the starting materials.
- Sulfides particles are found in all samples as small grains rarely exceeding **50 $\mu$ m** in maximum dimension, often free but sometimes attached or included in the major phase; most grains were identified as pyrite, but sphalerite, chalcopyrite, pyrrhotite and arsenopyrite were also found. A distinct feature is that sulfide particles from the sludge samples that were submitted to high temperature (**60°C**), often show alteration rims of goethite.

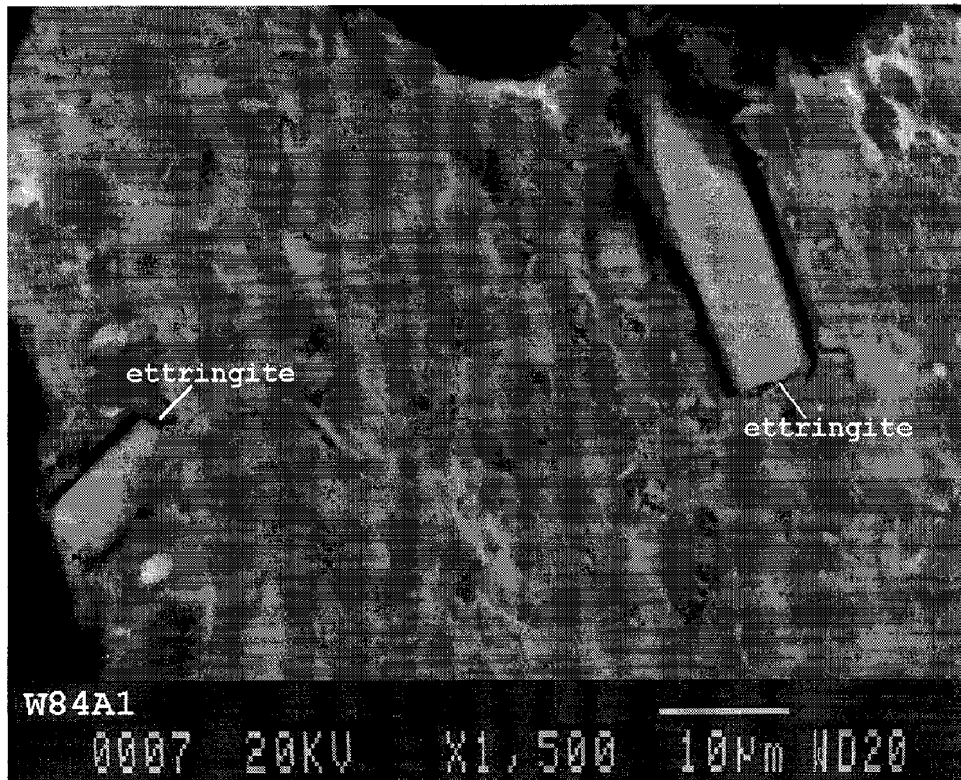
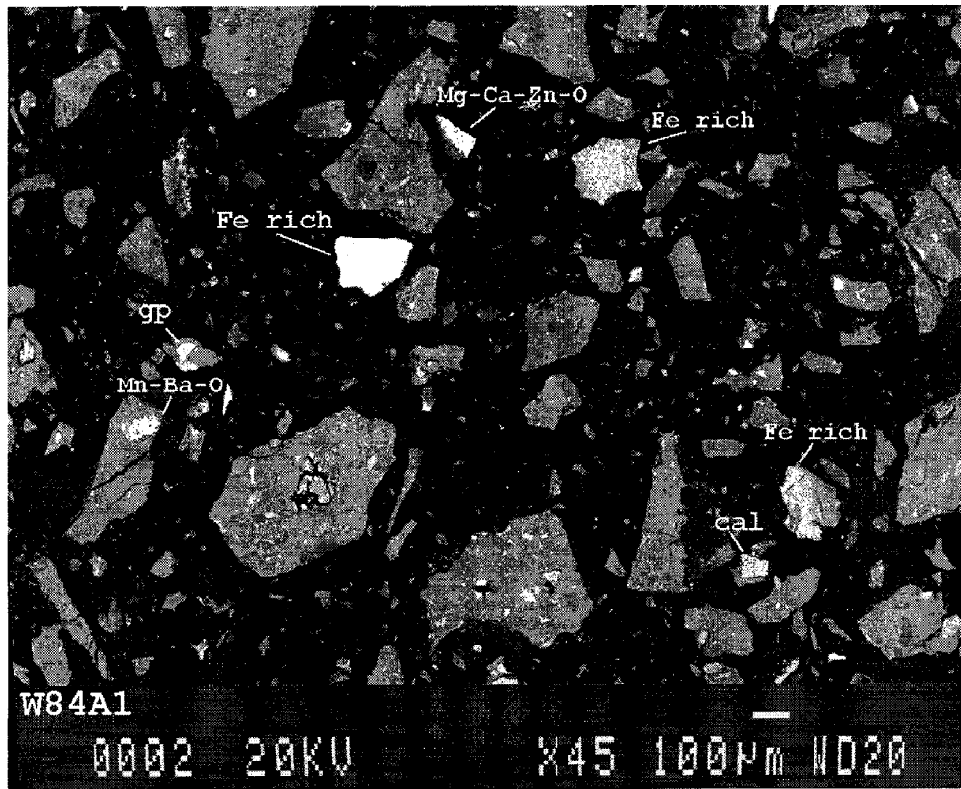
### **Additional comments:**

It seems that this series of samples is related to experiments to assess the **longterm** stability of the high density sludges. The findings of the mineralogical characterization of this series of samples are summarized in Table 1. The major phase in the sludges is "**phase M**", which is a Ca-Mg-Fe sulfate hydroxide hydrate; gypsum and calcite are the minor phases with traces of other minerals often trapped as small particles in the major phase of the sludge. It is obvious to observe that subjecting the sludges to a heat treatment at a temperature of 60°C increases the aging of the sludge. 'After this kind of heat treatment and exposing the sludge to humidity-saturated atmosphere for six and twelve months (samples **W8-60S6** and **W8-60S12**), gypsum and calcite become the phases of major abundance probably at the expense of **phase M**" which becomes a phase of medium abundance. Also the sludge losses some of its protective anti-oxidative role on the entrapped sulfide particles, for example, pyrite and pyrrhotite particles show layer of oxides-goethite-(samples **W8-60A6**, **W8-60S6** and **W8-60S12**). It would be interesting to calculate what would be the equivalent aging under average environmental conditions that would be related to these aggressive aging treatments.

### **ACKNOWLEDGMENTS:**

**Michel** Beaulne and Paul **Carrière** are greatly acknowledged, for the preparation of polished sections from difficult samples, and the X-ray diffraction work respectively. Thanks are extended to Rolando Lastra for helpful comments.





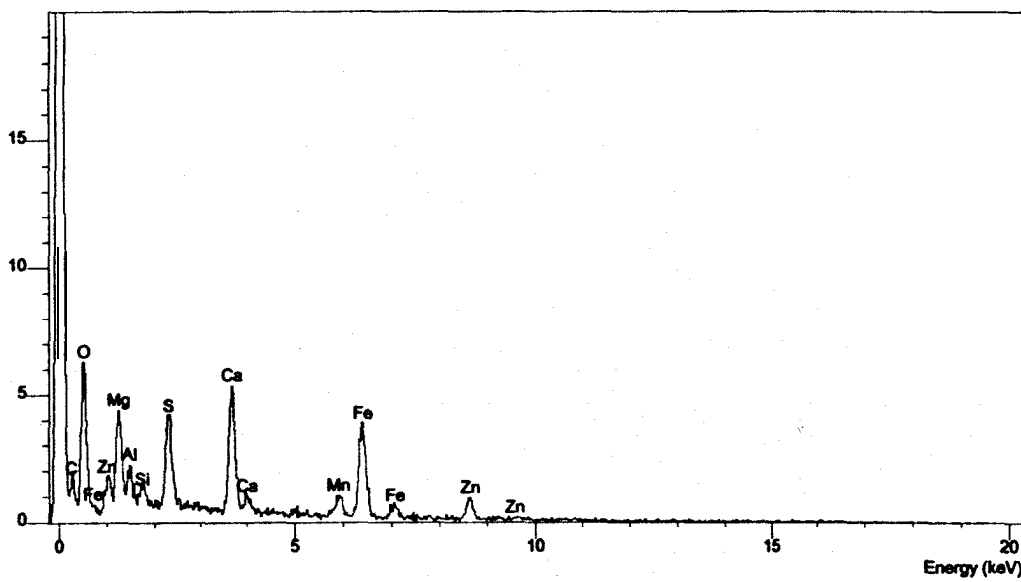


Fig. 1a. EDS of Ca-Mg-Fe sulfate hydroxide hydrate (*phase M*); area 1, W8-4A1.

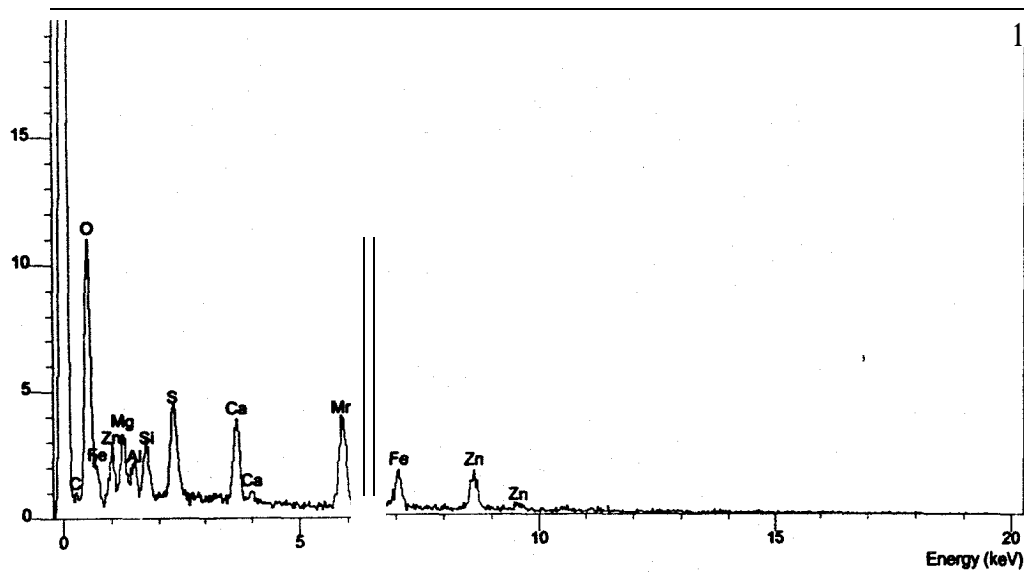


Fig. 1b. EDS of Fe-rich *phase M*; area 2, W8-4A1.

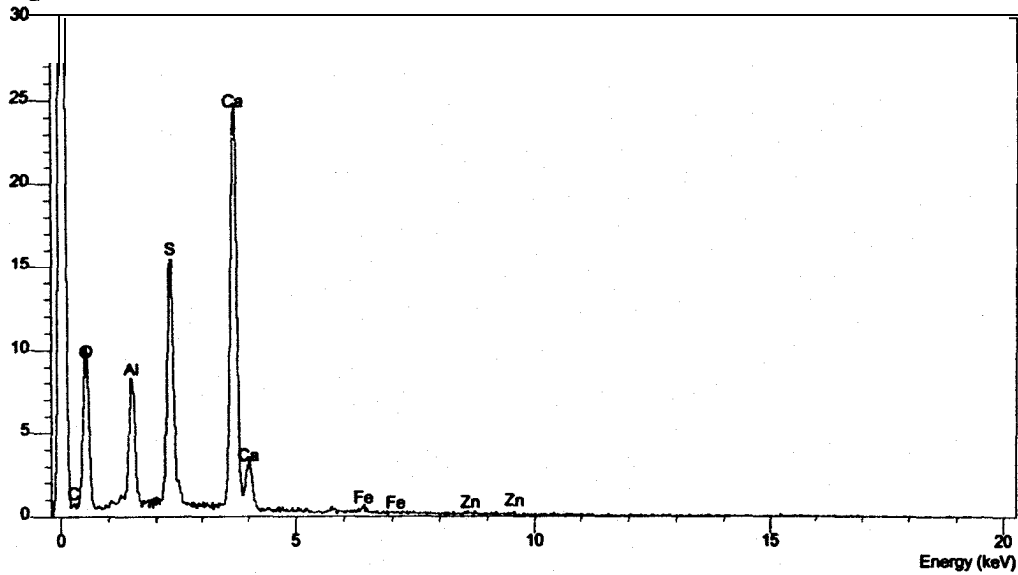


Fig. 1c. EDS of a lath of ettringite; W8-4A1.

ID: HOGAN W8-4S1 A, 21-OCT-97@10:38  
 File: Z04318.RAW Scan: 5-90/.05/ 1/#1701, Anode: CU

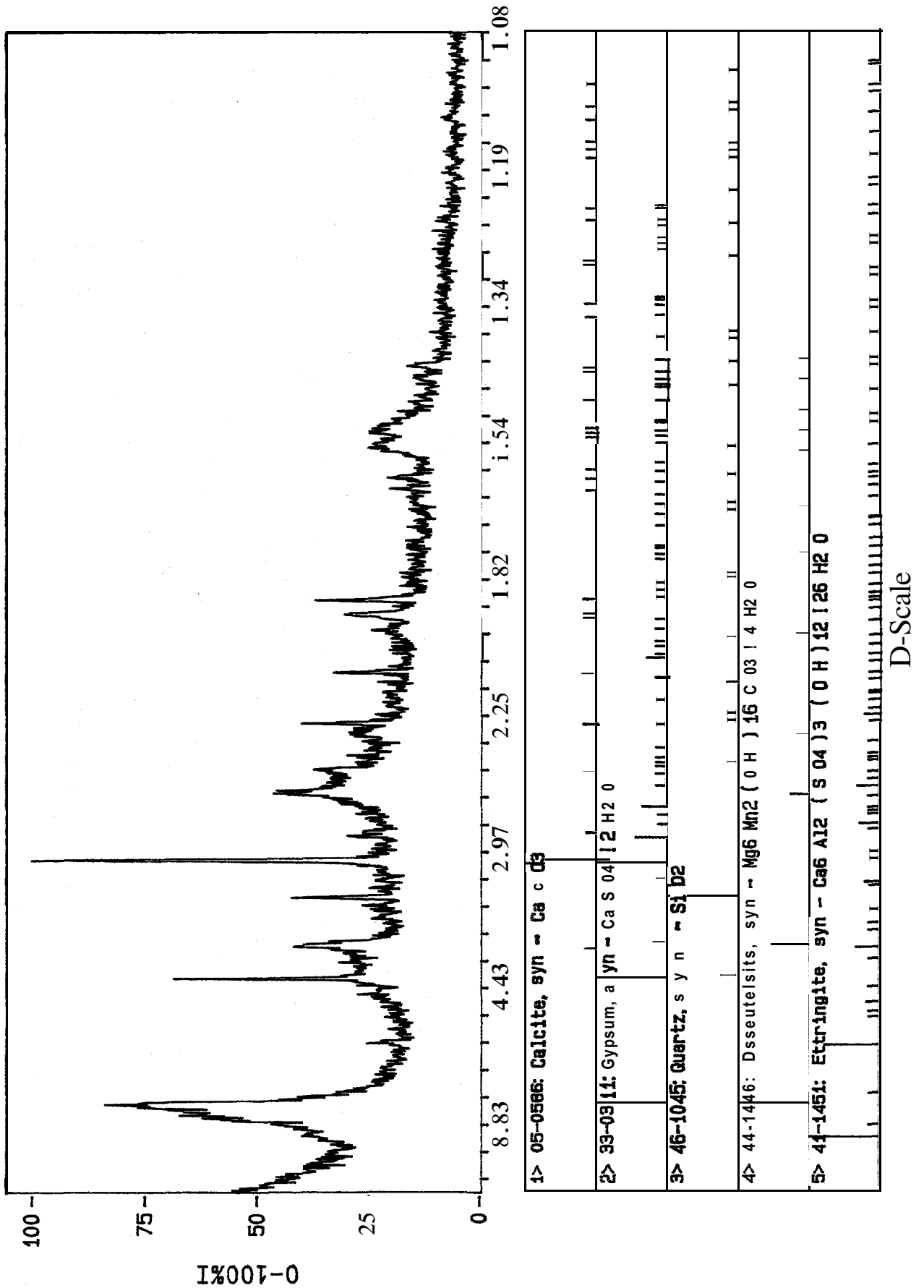
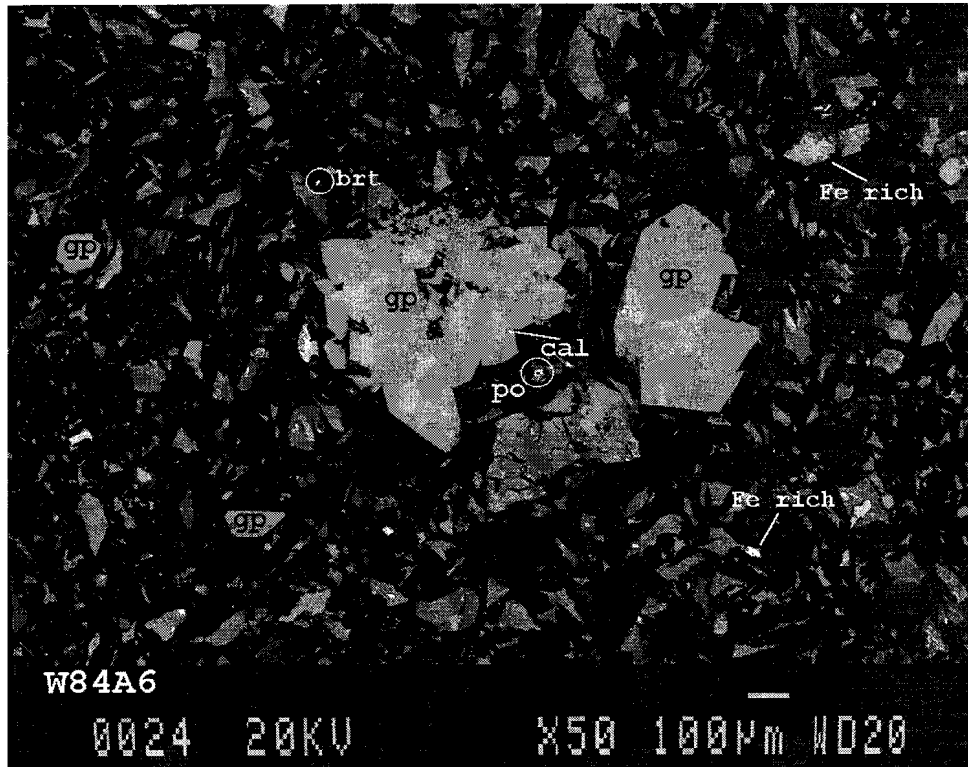
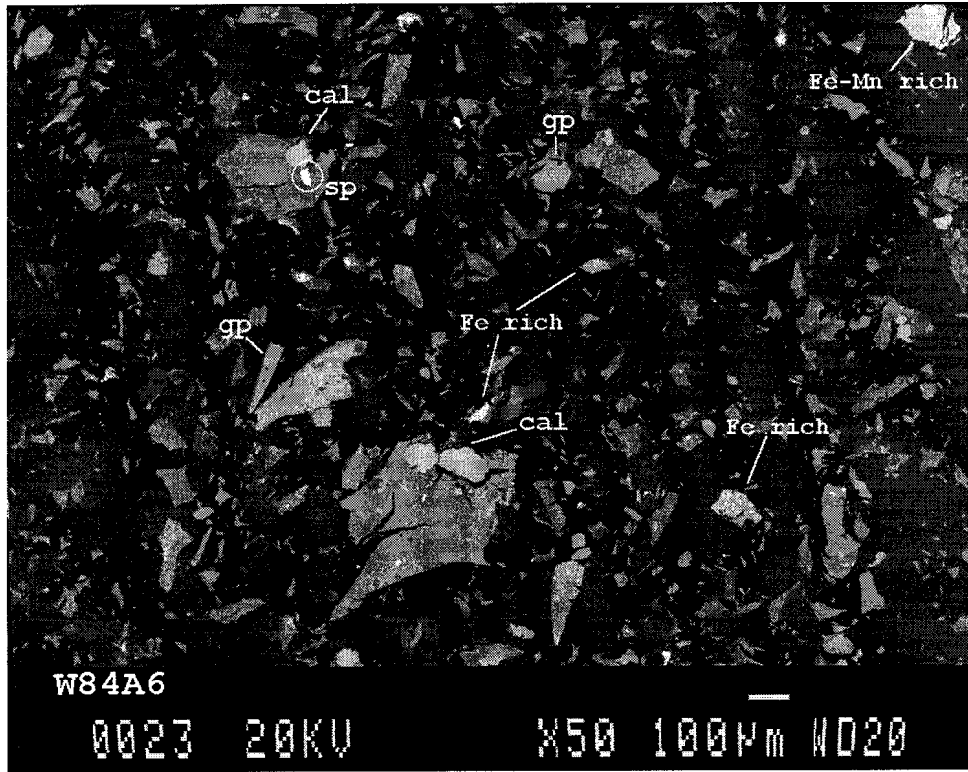
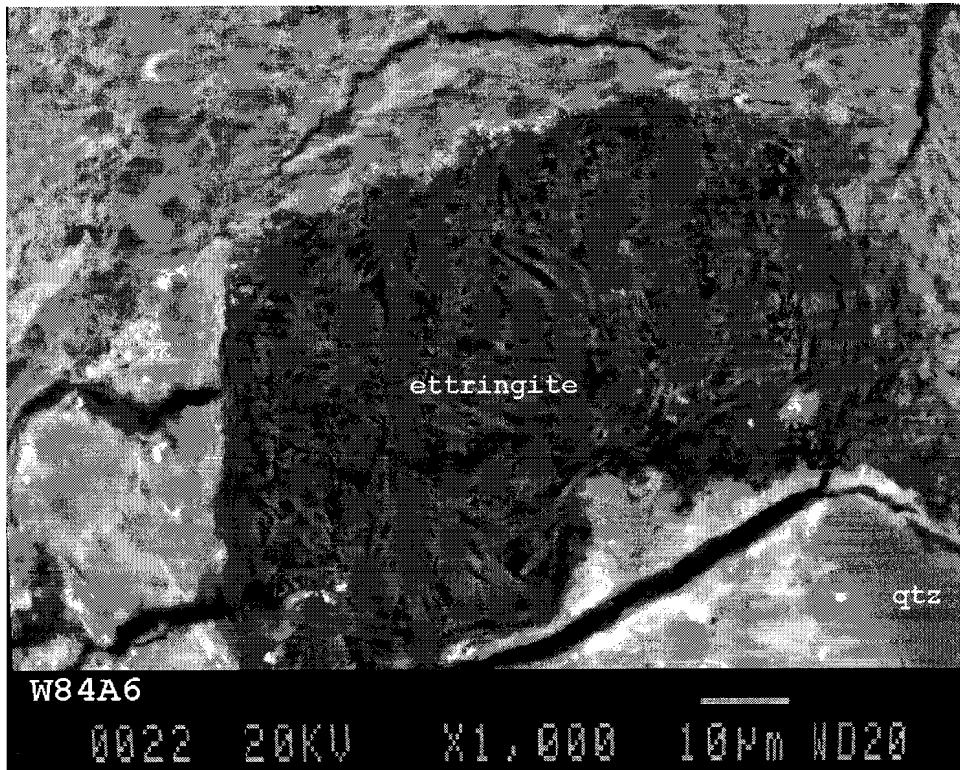
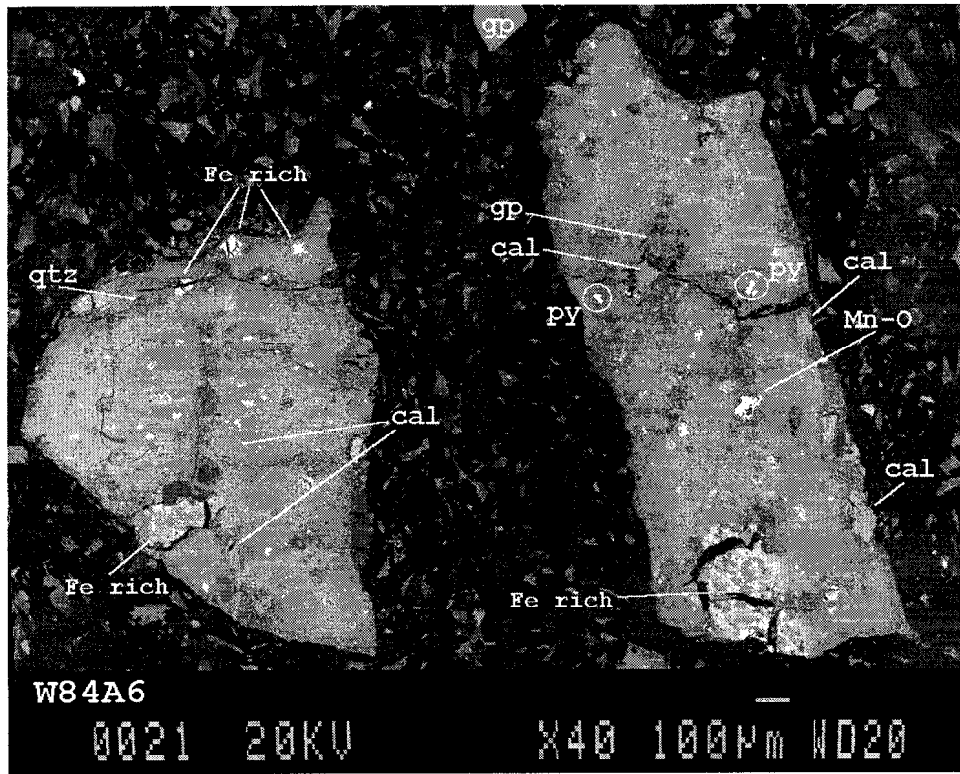


Fig. 2. X-ray diffractogram of sample W8-4S1.







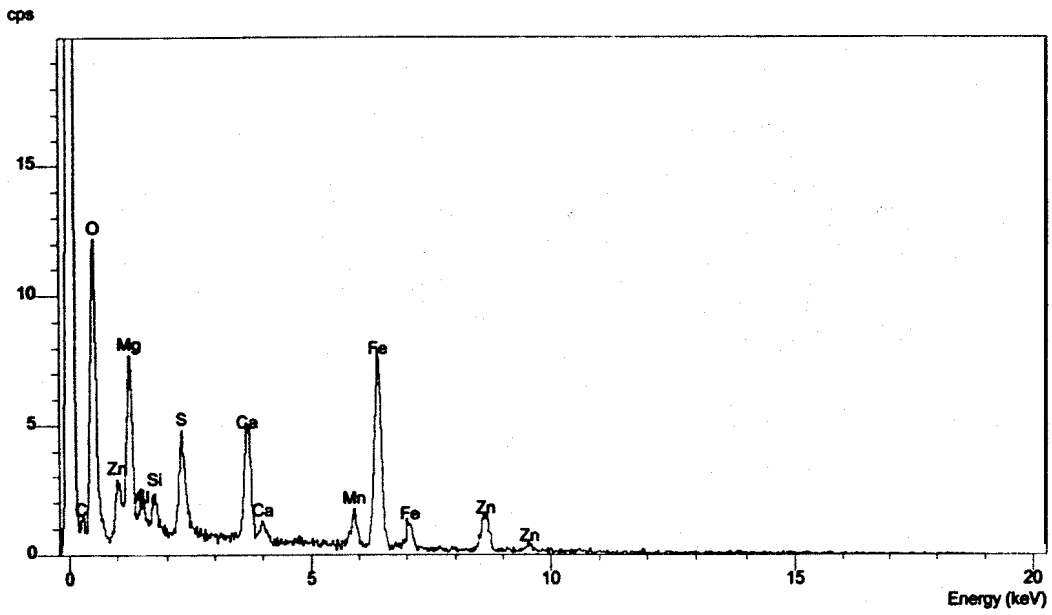


Fig. 3a. EDS of Fe-rich *"phase M"*; area 1, W8-4A6.

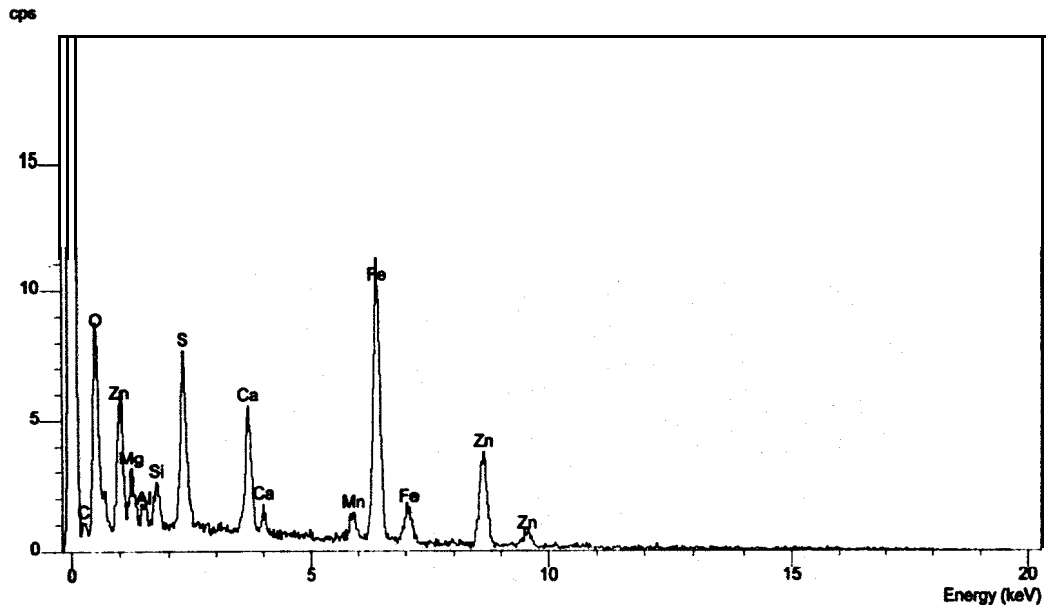


Fig. 3b. EDS of Fe-rich variant of *"phase M"*; area 2, W8-4A6.

ID: GRIFFITH W8-4A6, 21-APR-97@11: 27  
 File: Z03876.RAW Scan: 5-90/.05/ 1/#1701, Anode: CU

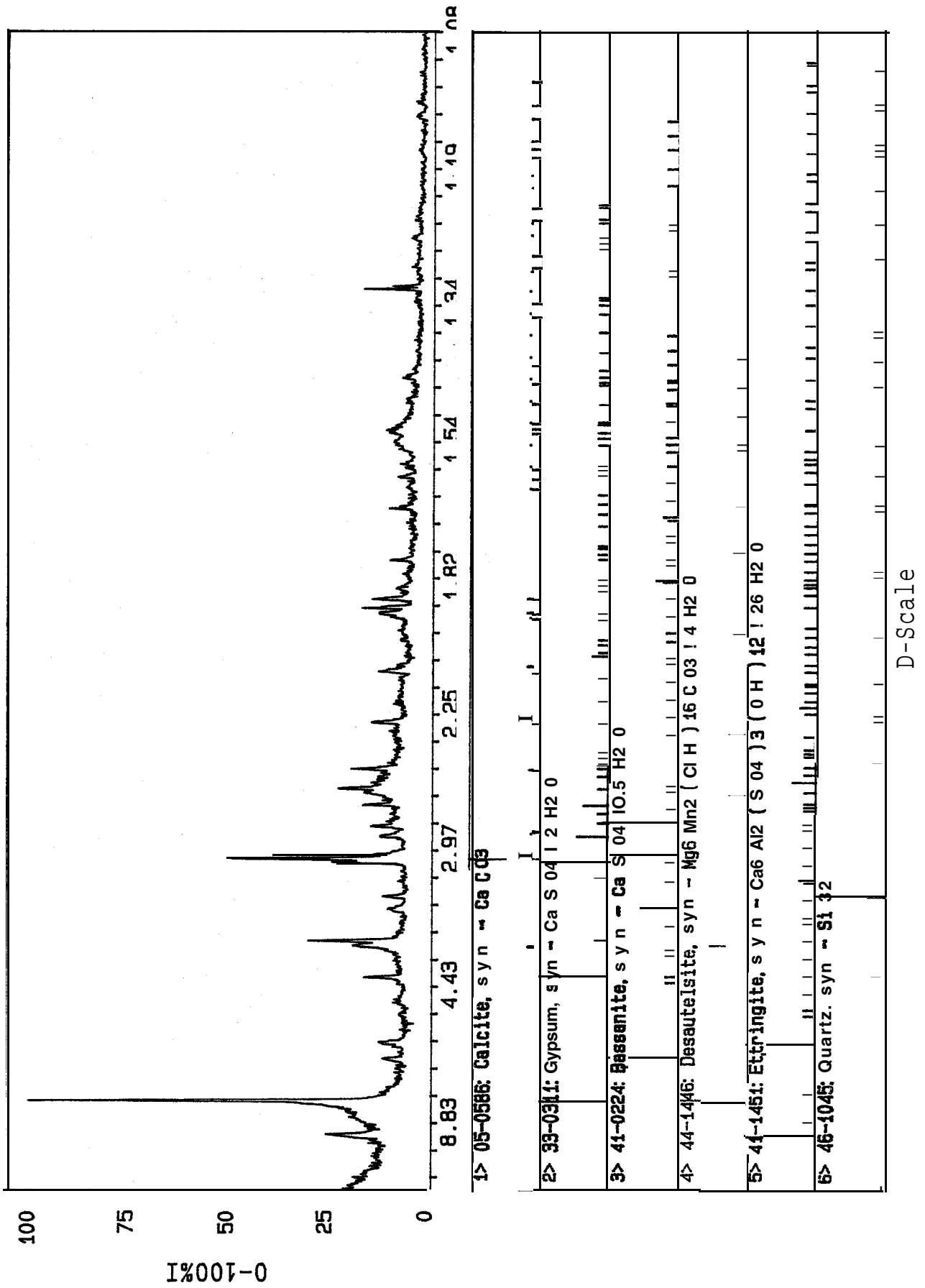
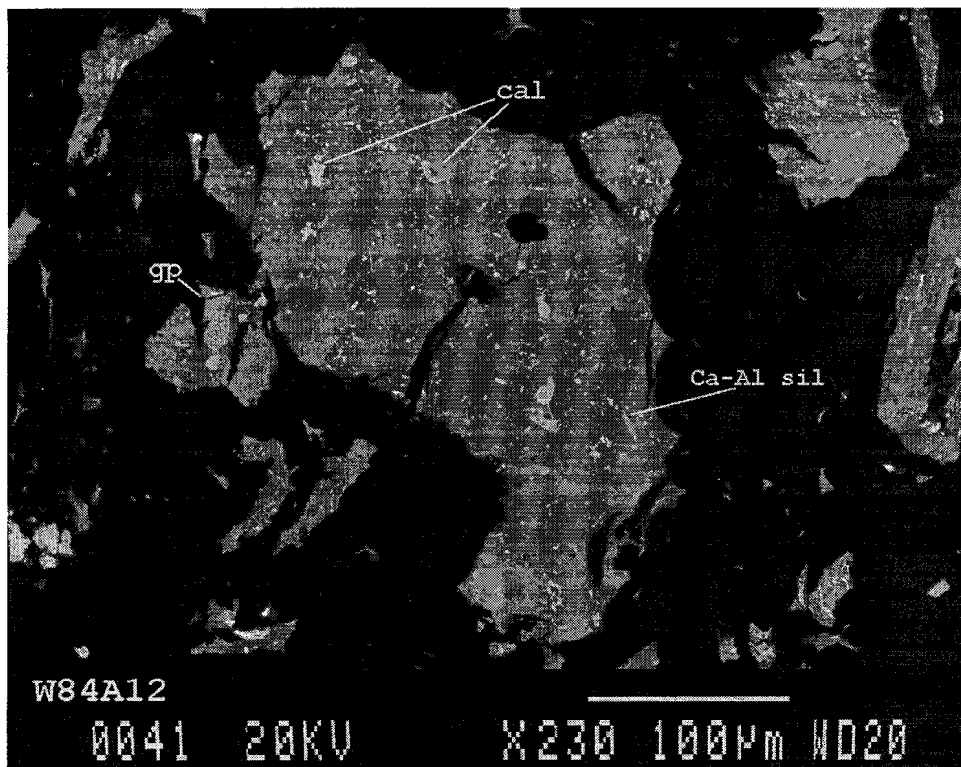
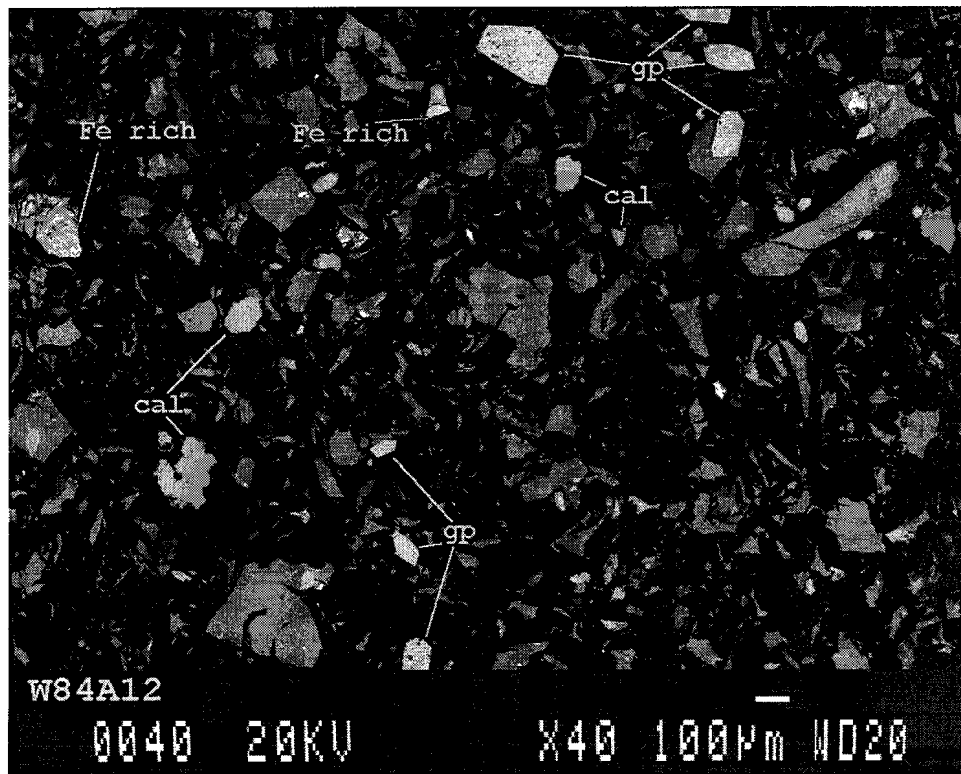
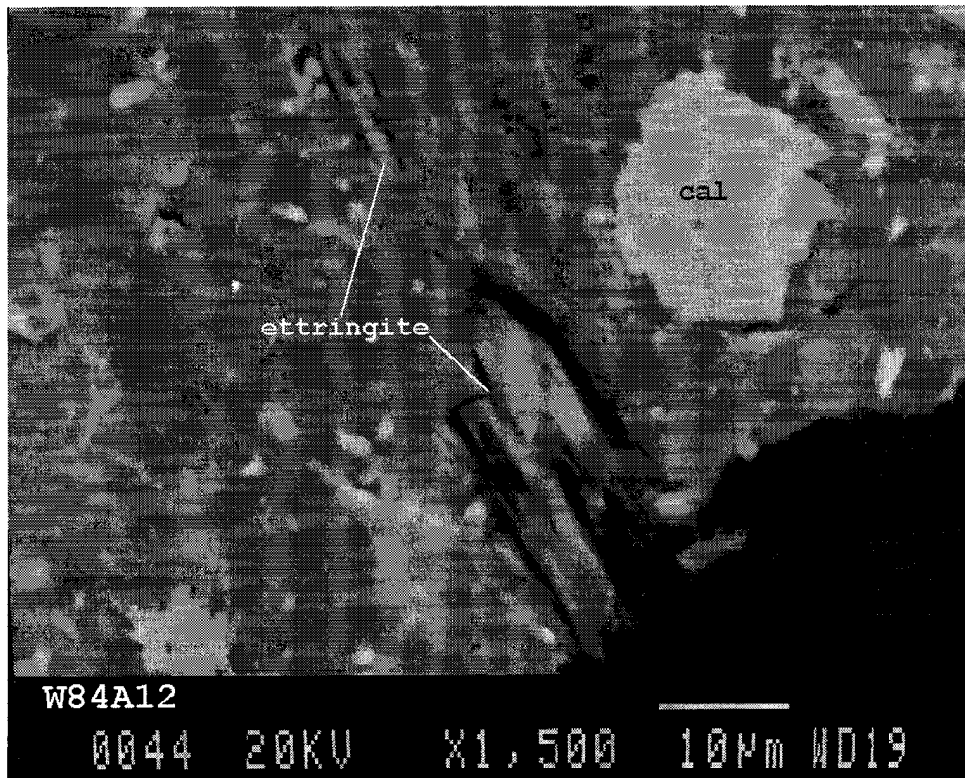
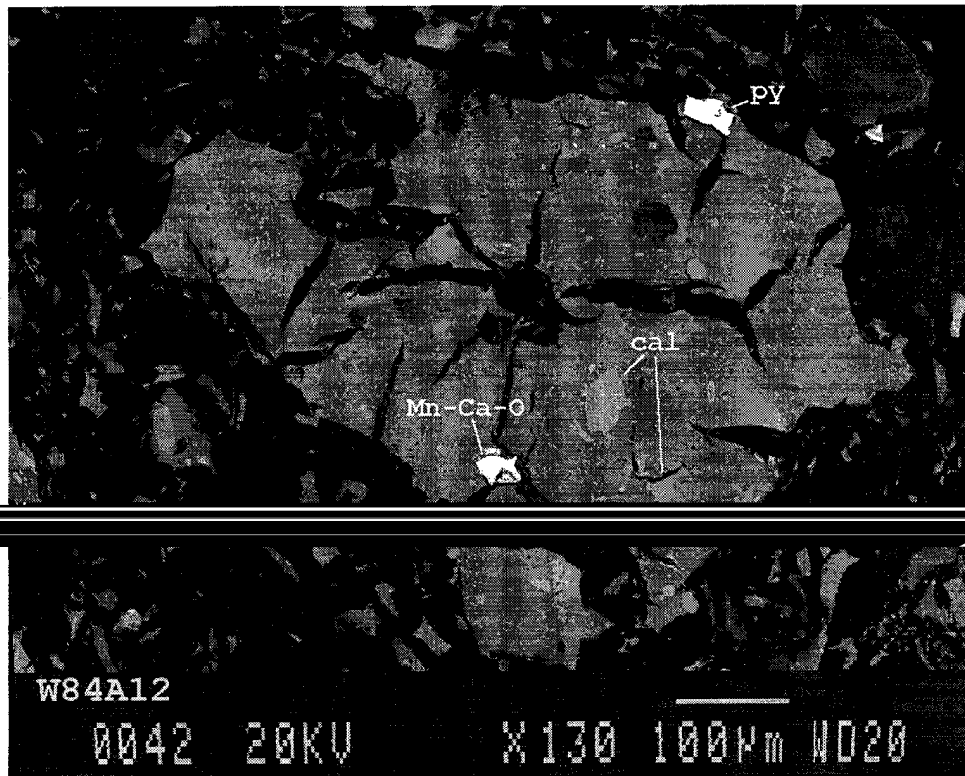


Fig. 4. X-ray diffractogram of sample W8-4A6.





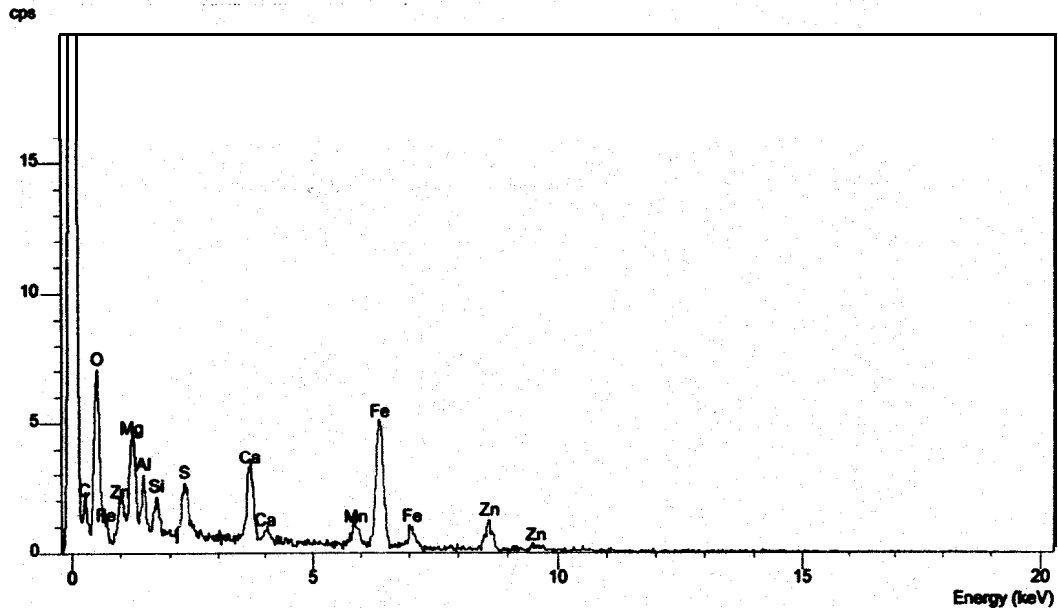


Fig. 5a. EDS of "phase M"; area 1, W8-4A12.

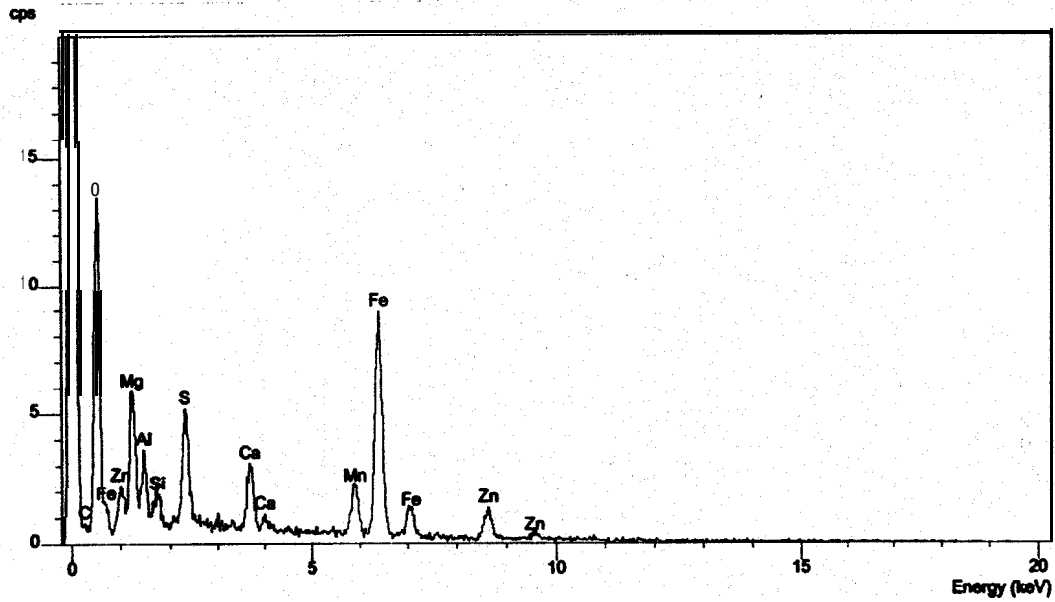


Fig. 5b. EDS of Fe-rich "phase M"; area 2, W8-4A12.

ID: HOGAN W8-4A-12, 21-OCT-97@11:55  
 File: Z04329.RAW Scan: 5-90/.05/ 1/#1701, Anode: CU

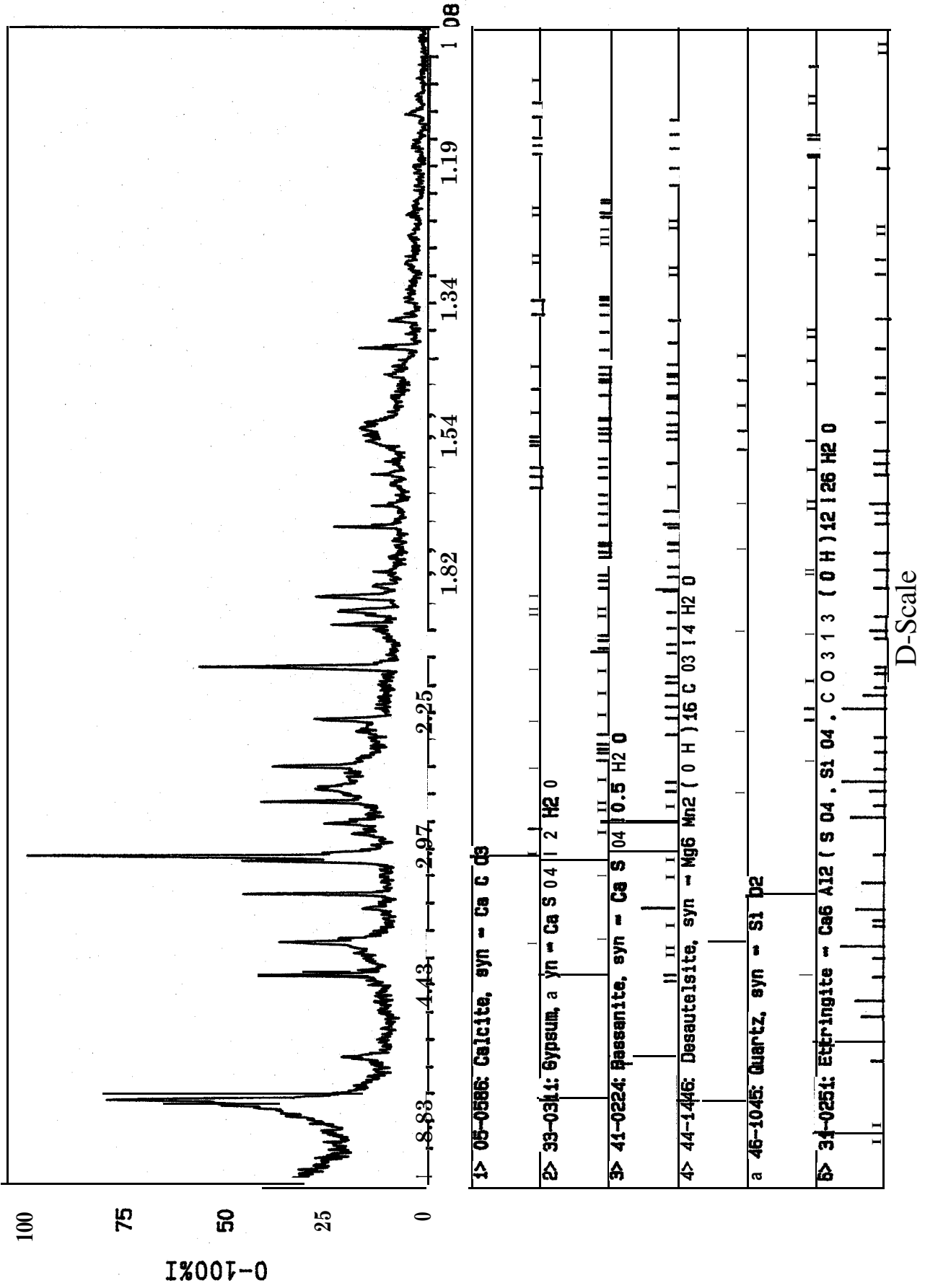
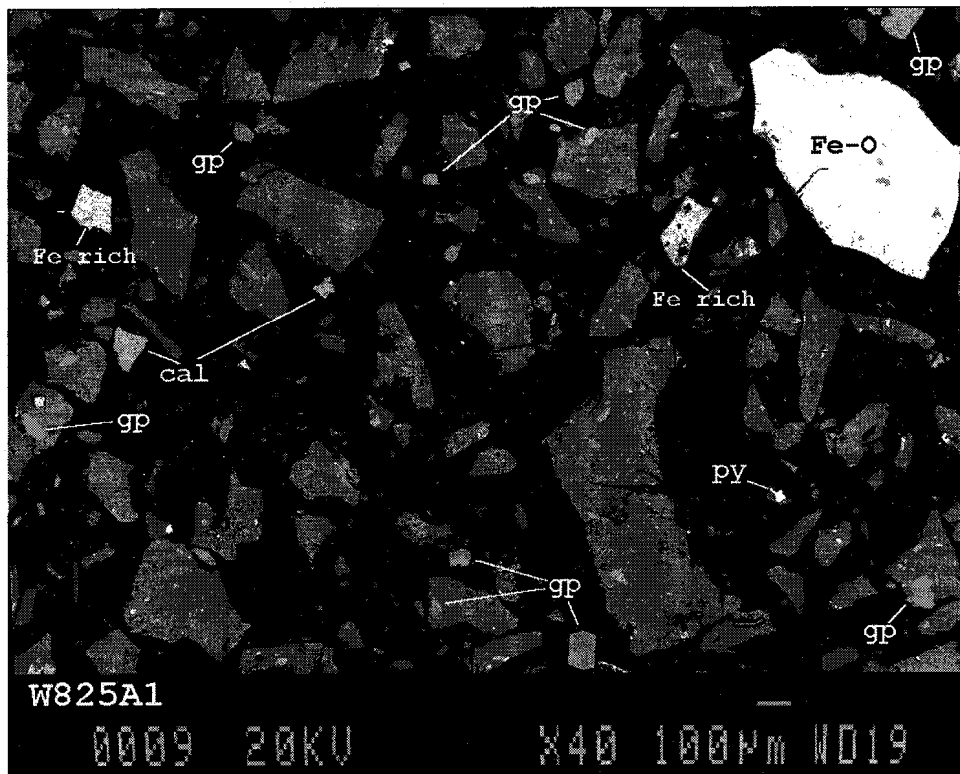
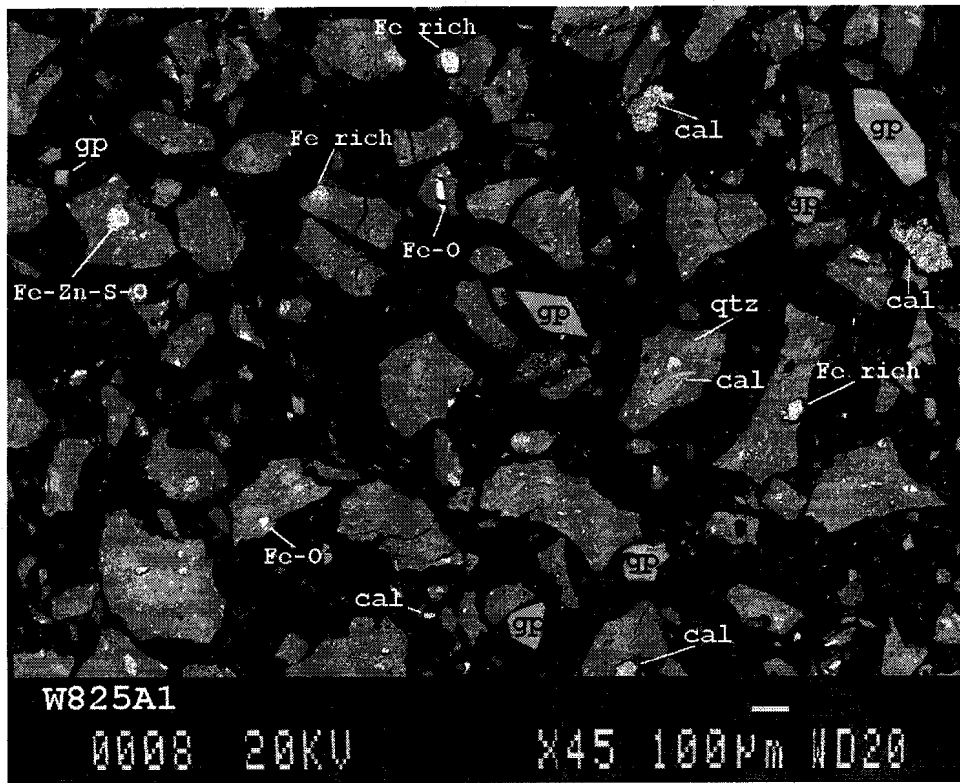
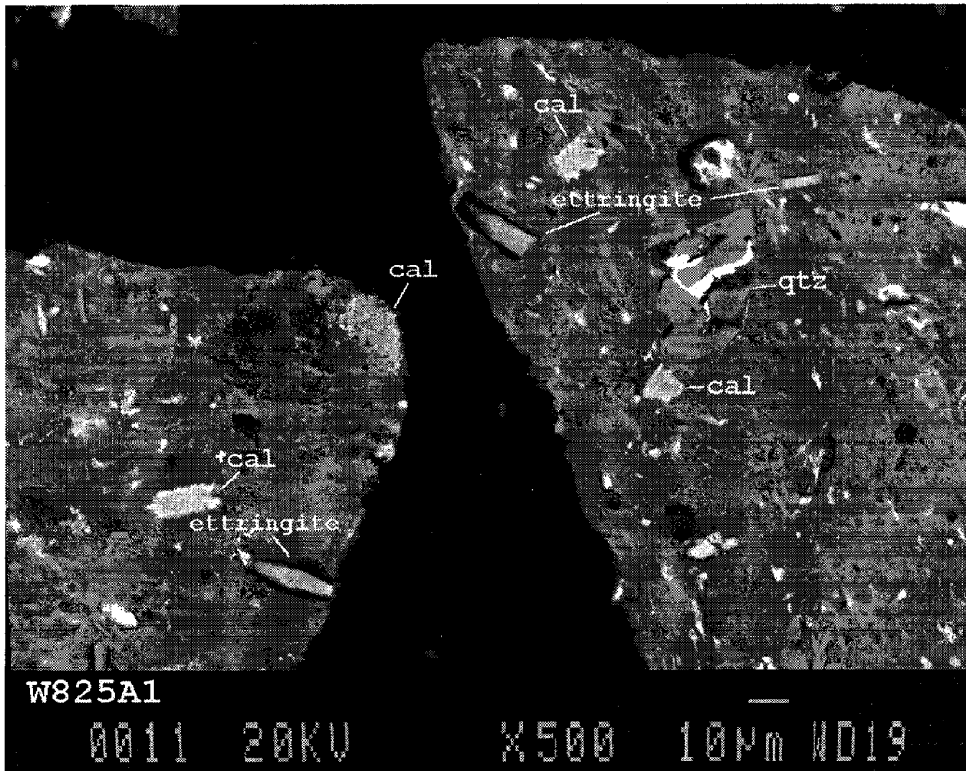
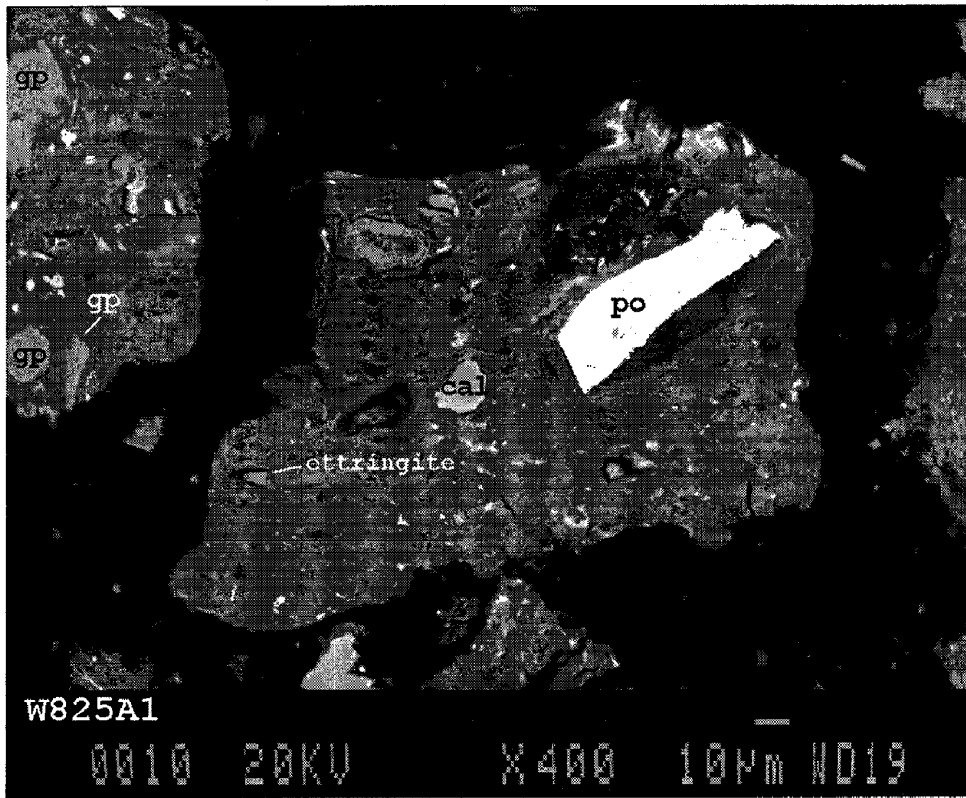


Fig. 6. X-ray diffractogram of sample W8-4A12







ID: HOGAN W8-25A1, 21-OCT-97@10:38  
 File: Z04320.RAW Scan: 5-90/.05/ 1/#1701, Anode: CU

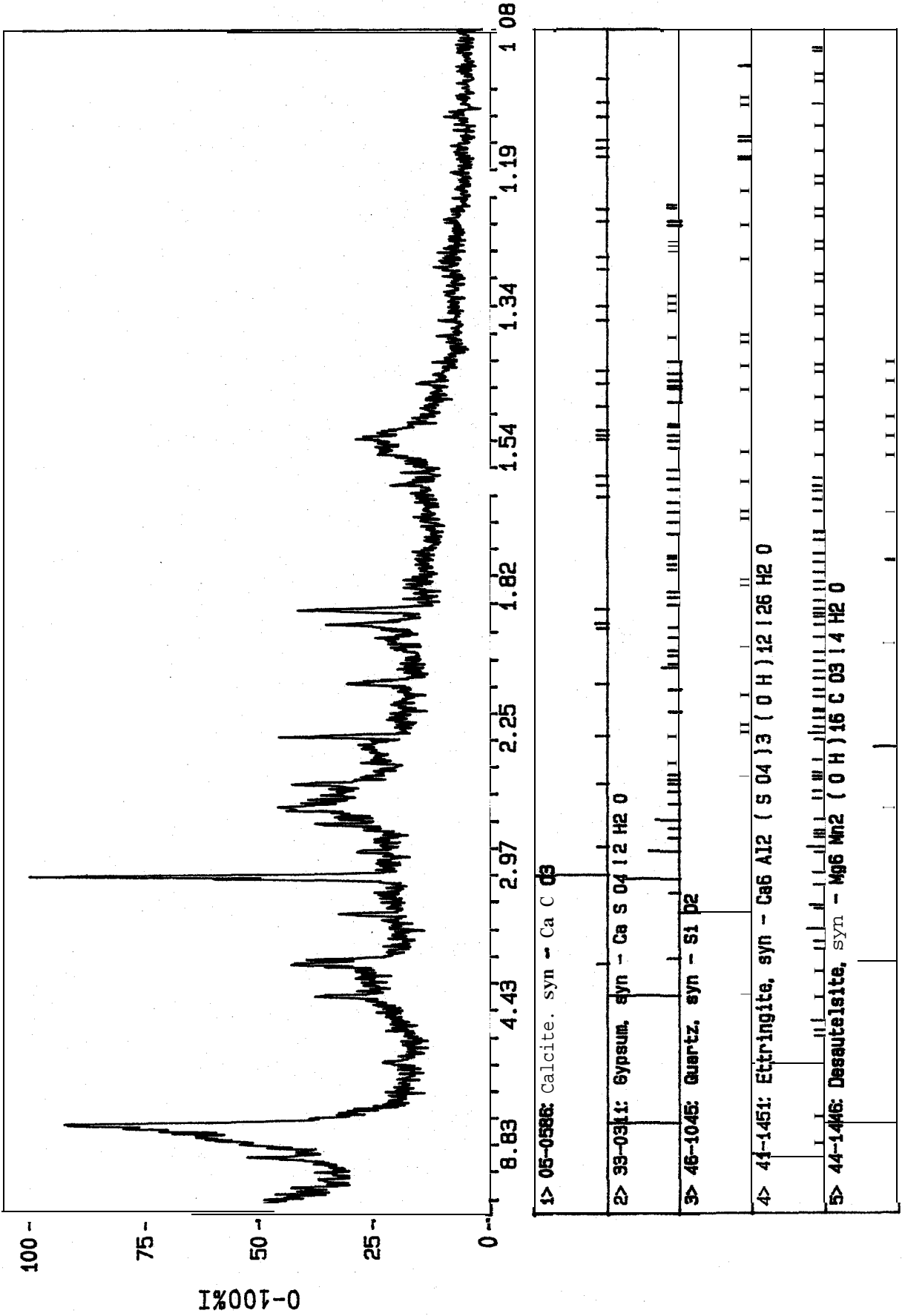
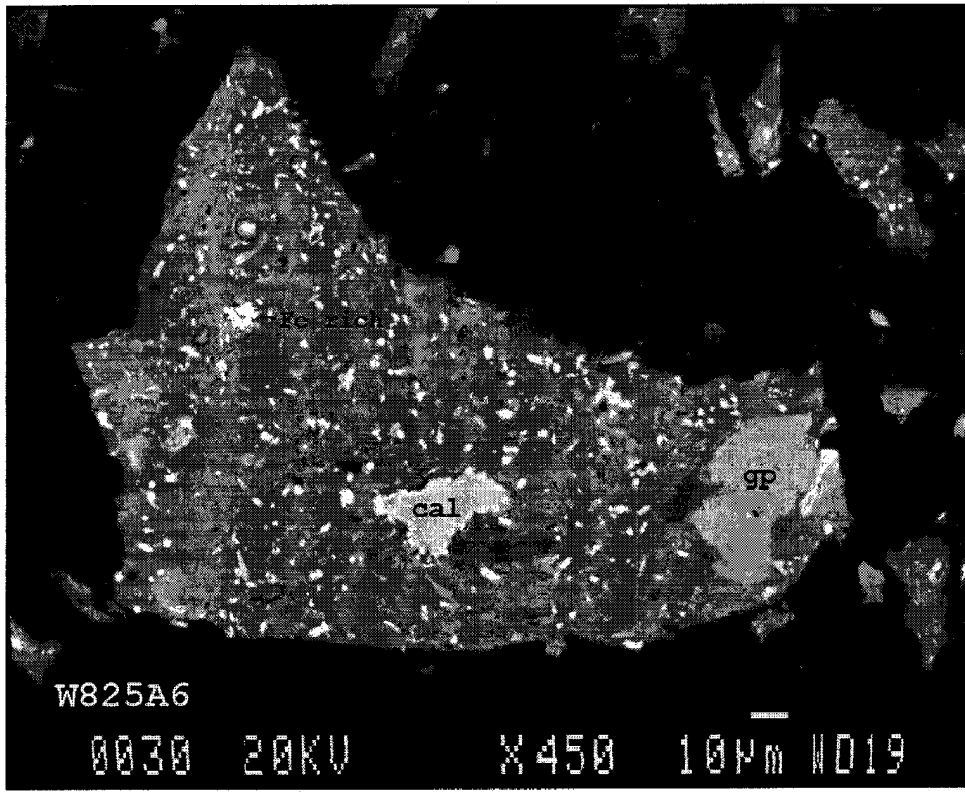
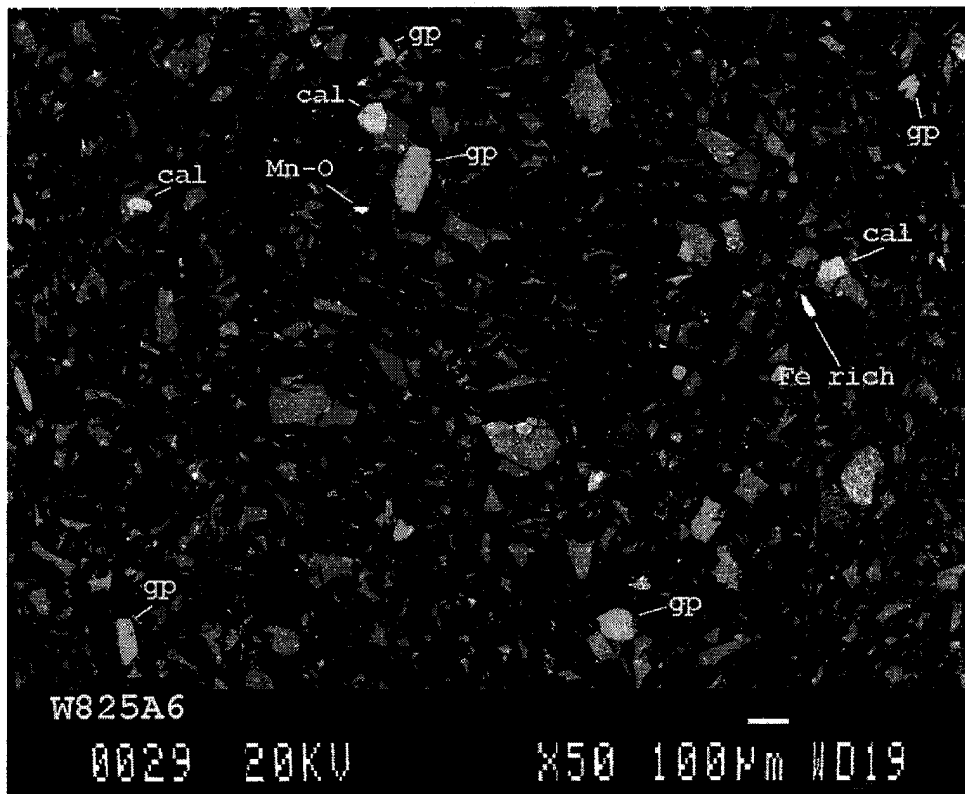
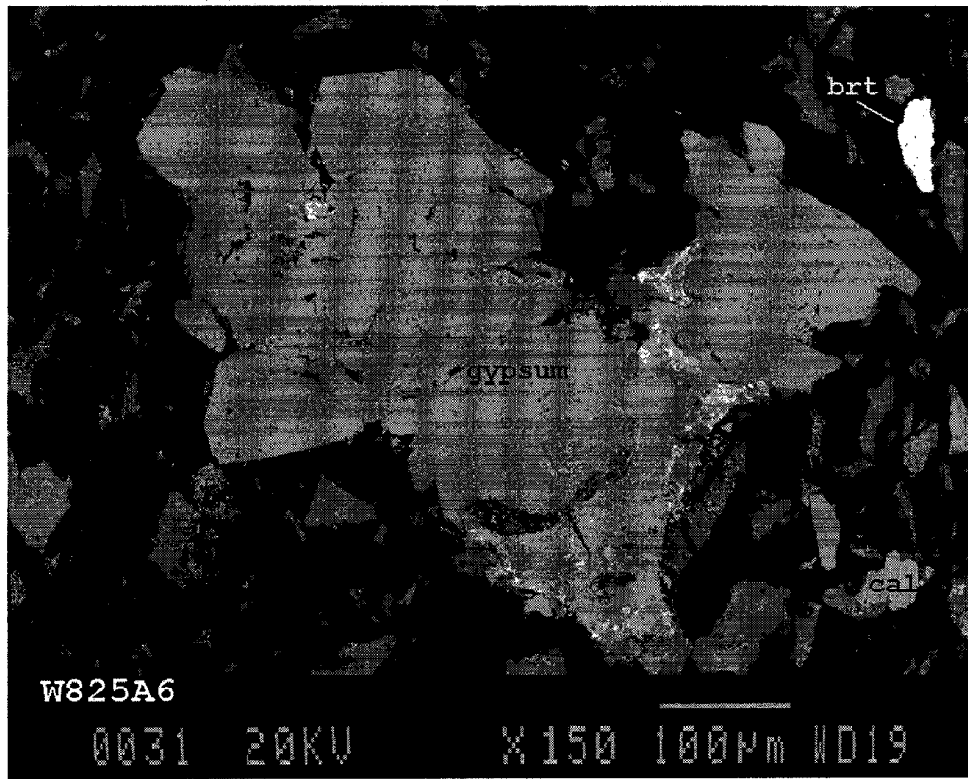


Fig. 7. X-ray diffractogram of sample W8-25A1.





IO: GRIFFITH W8-25A6, 21-APR-97@11: 27  
 File: Z03877.RAW Scan: 5-90/.05/ 1/#1701, Anode: CU

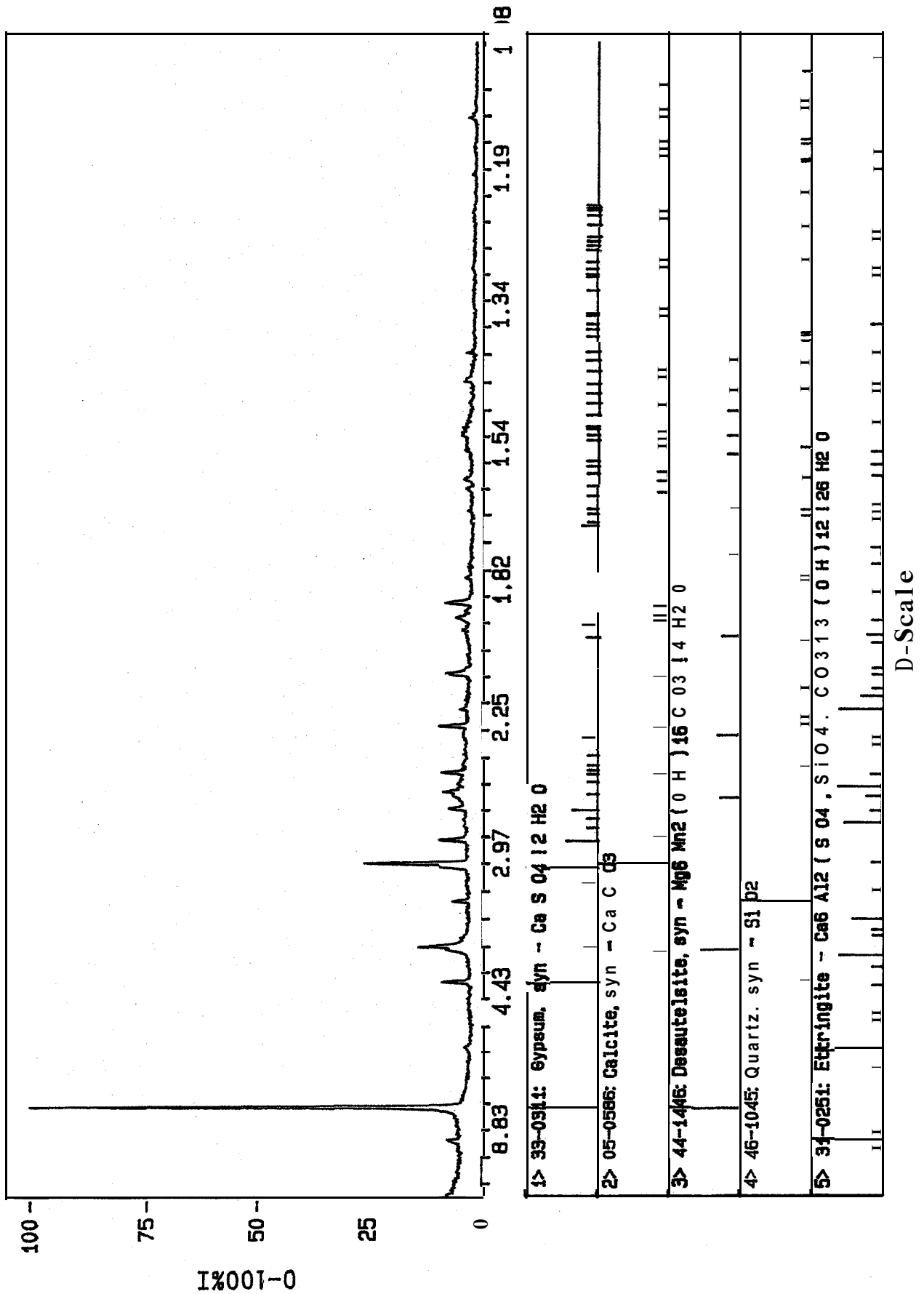
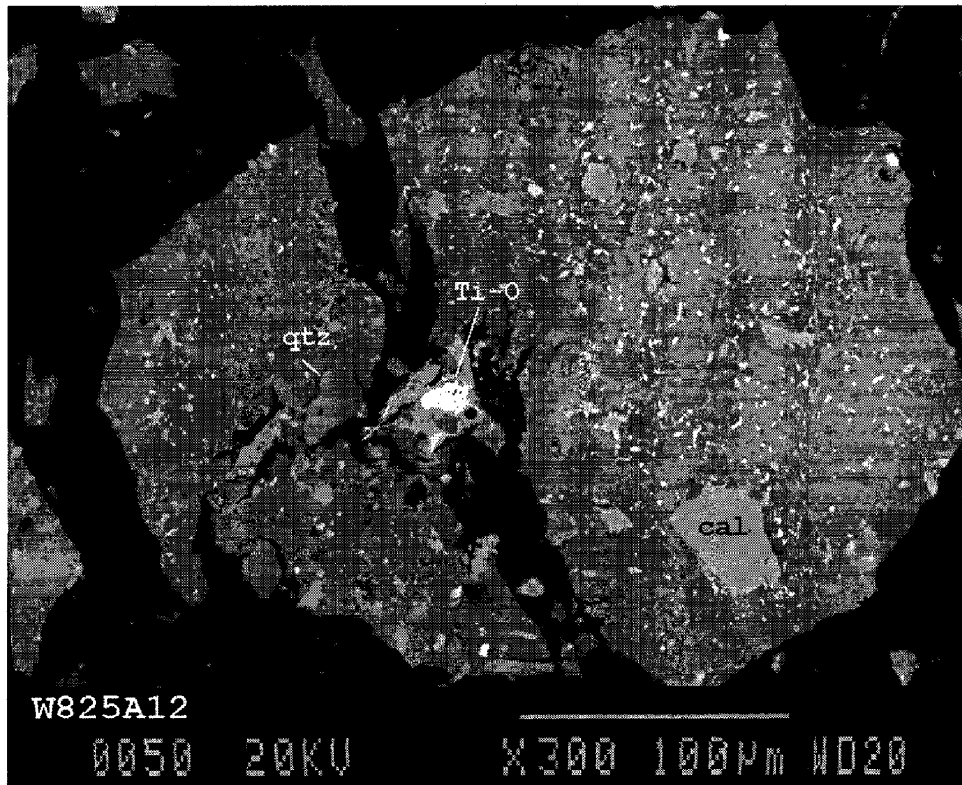
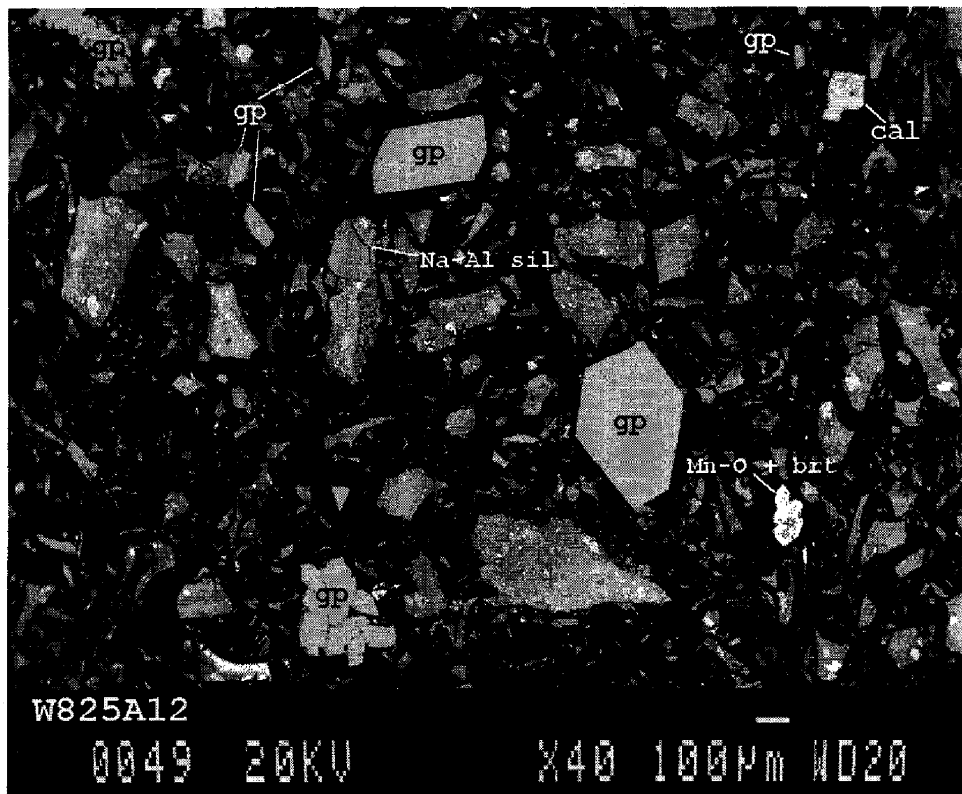
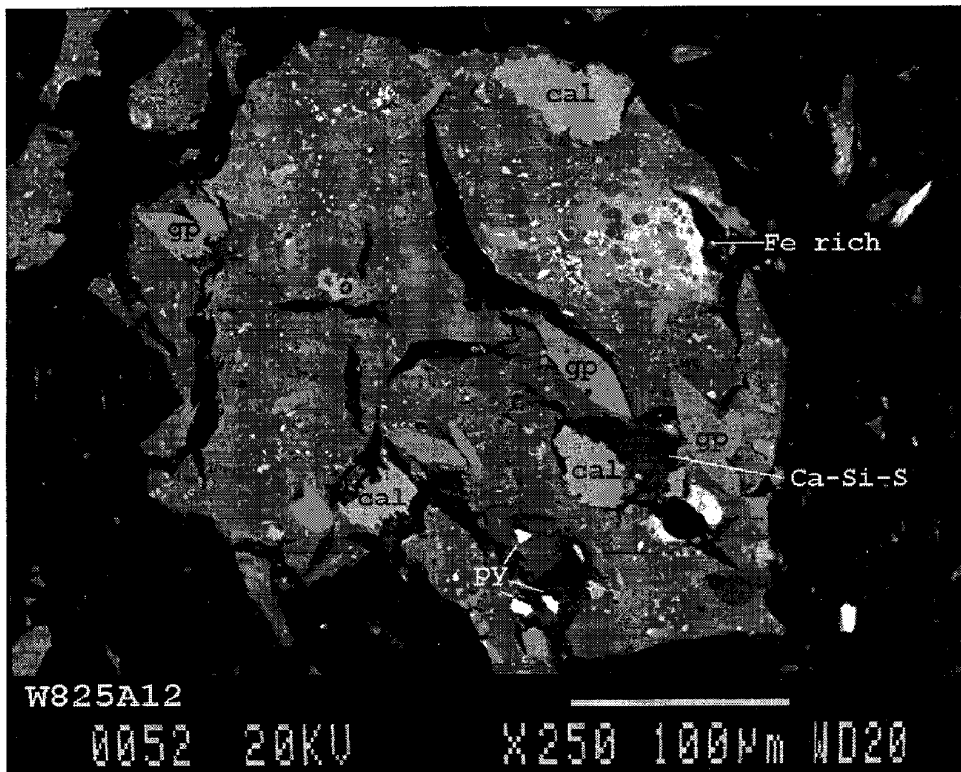
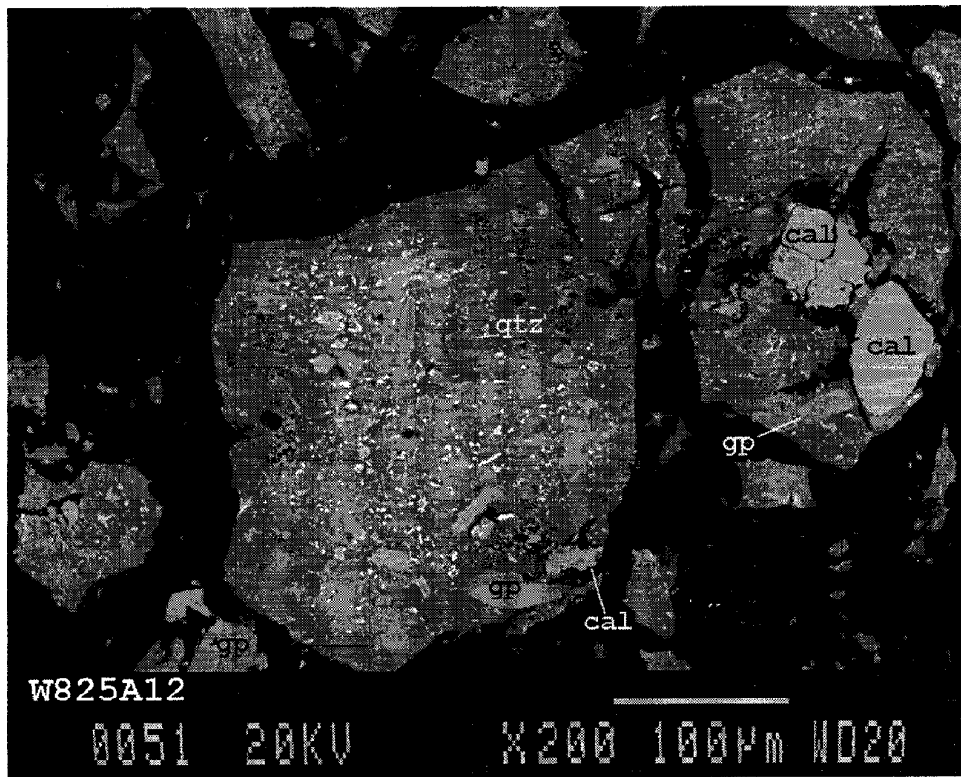


Fig. 8. X-ray diffractogram of sample W8-25A6.





ID: HOGAN W8-25A-12, 21-OCT-97@13: 30  
 File: Z04331.RAW Scan: 5-90/.05/ 1/#1701, Anode: CU

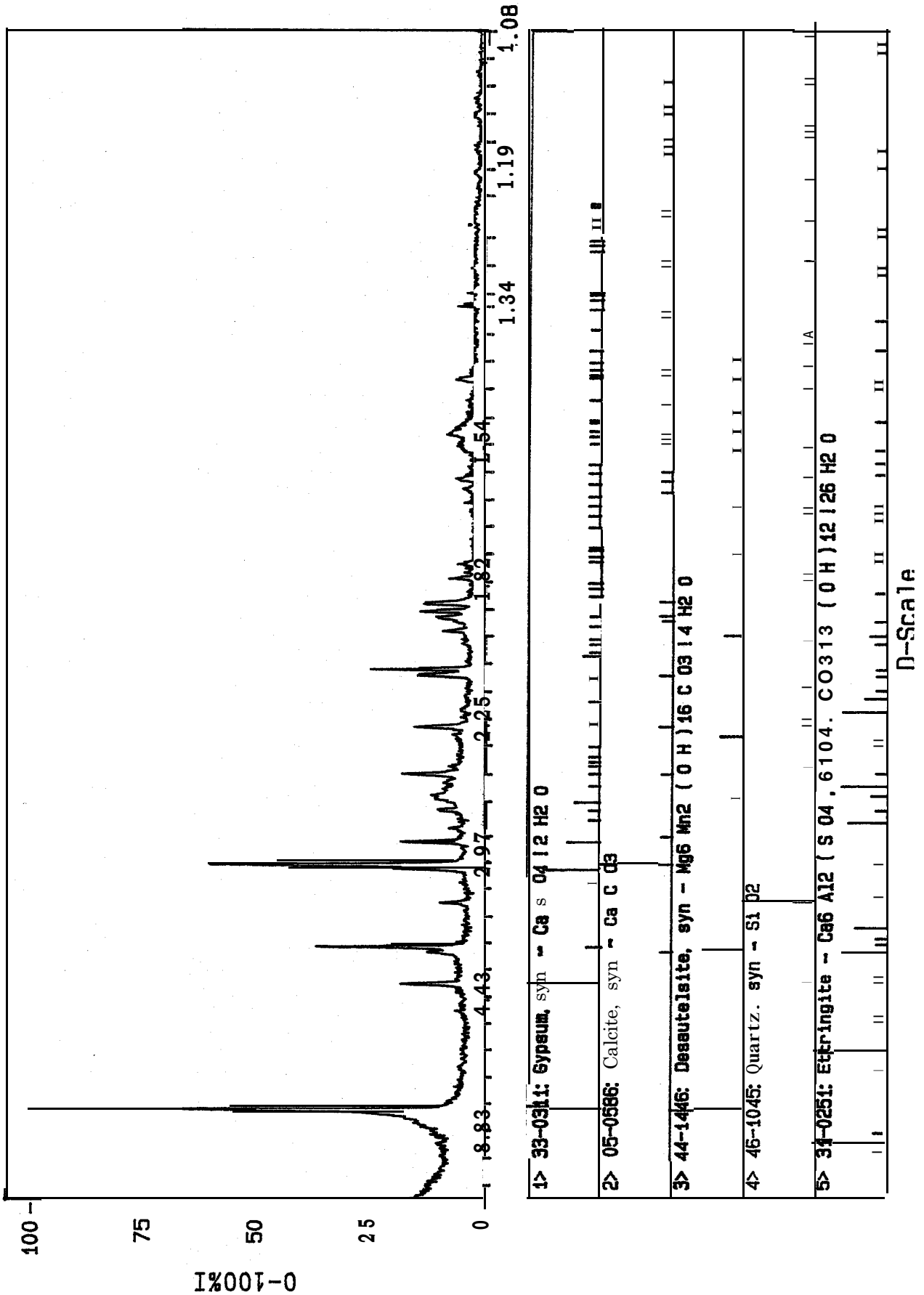
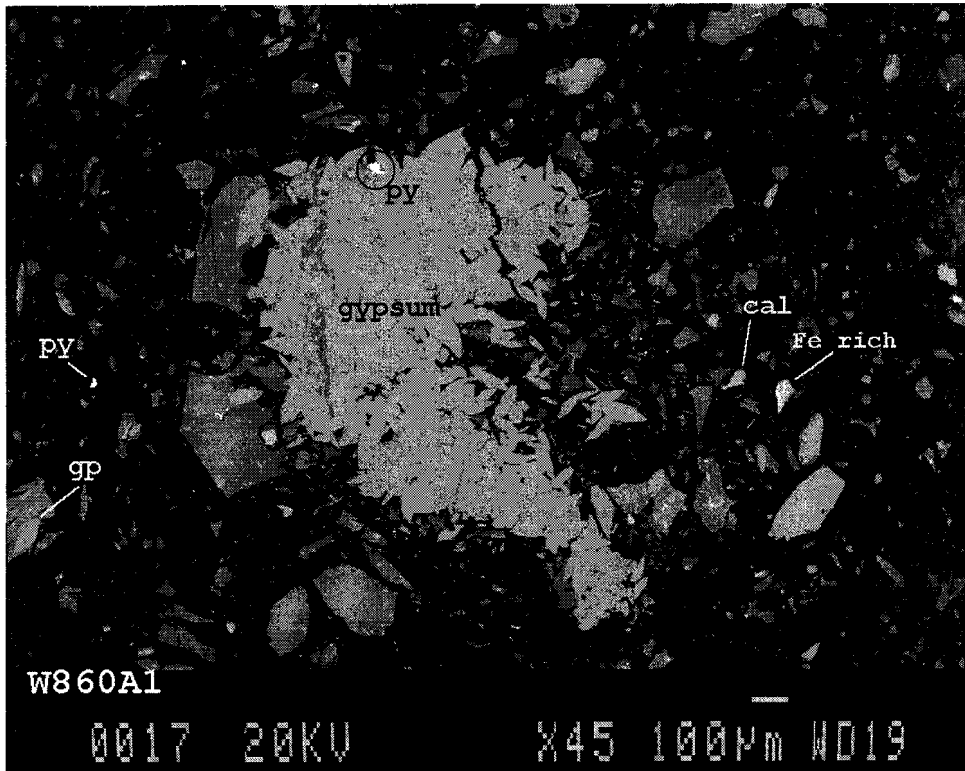
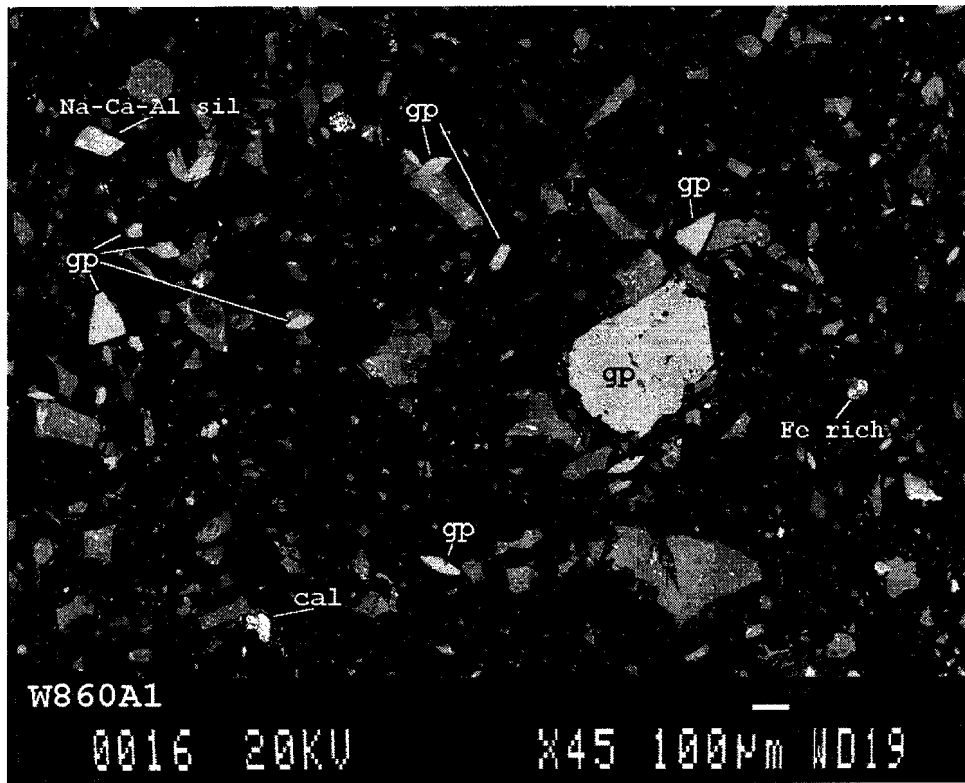
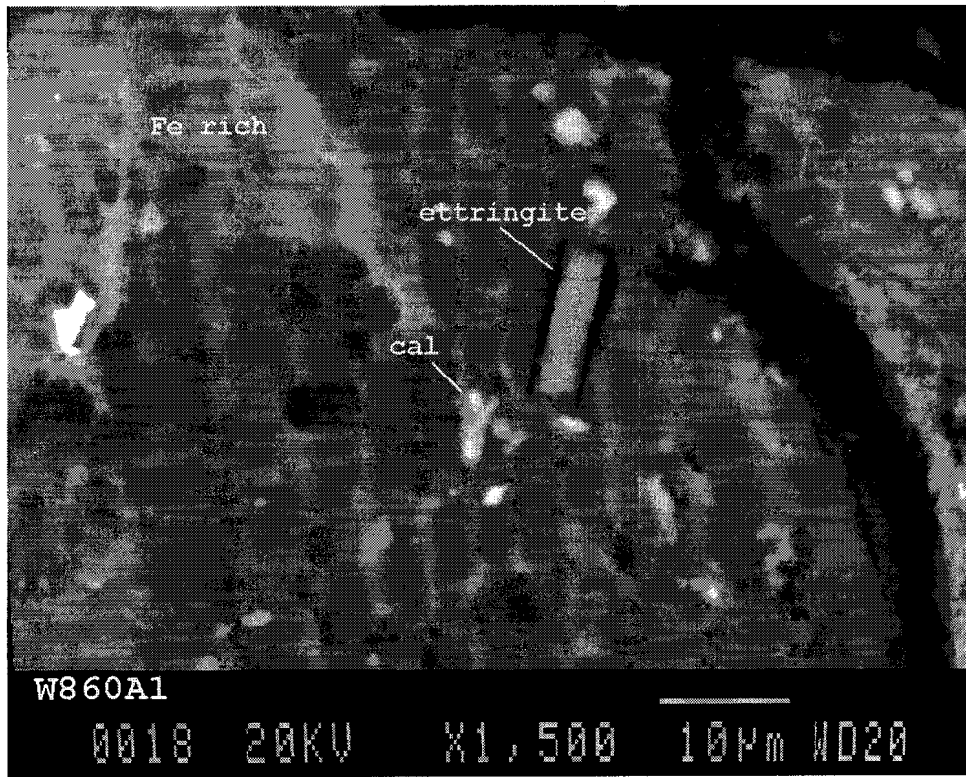


Fig. 9. X-ray diffractogram of sample W8-25A12.







ID: HOGAN W8-60A1, 21-OCT-97@10: 38  
 File: Z04322.RAW Scan: 5-90/.05/ 1/#1701, Anode: C

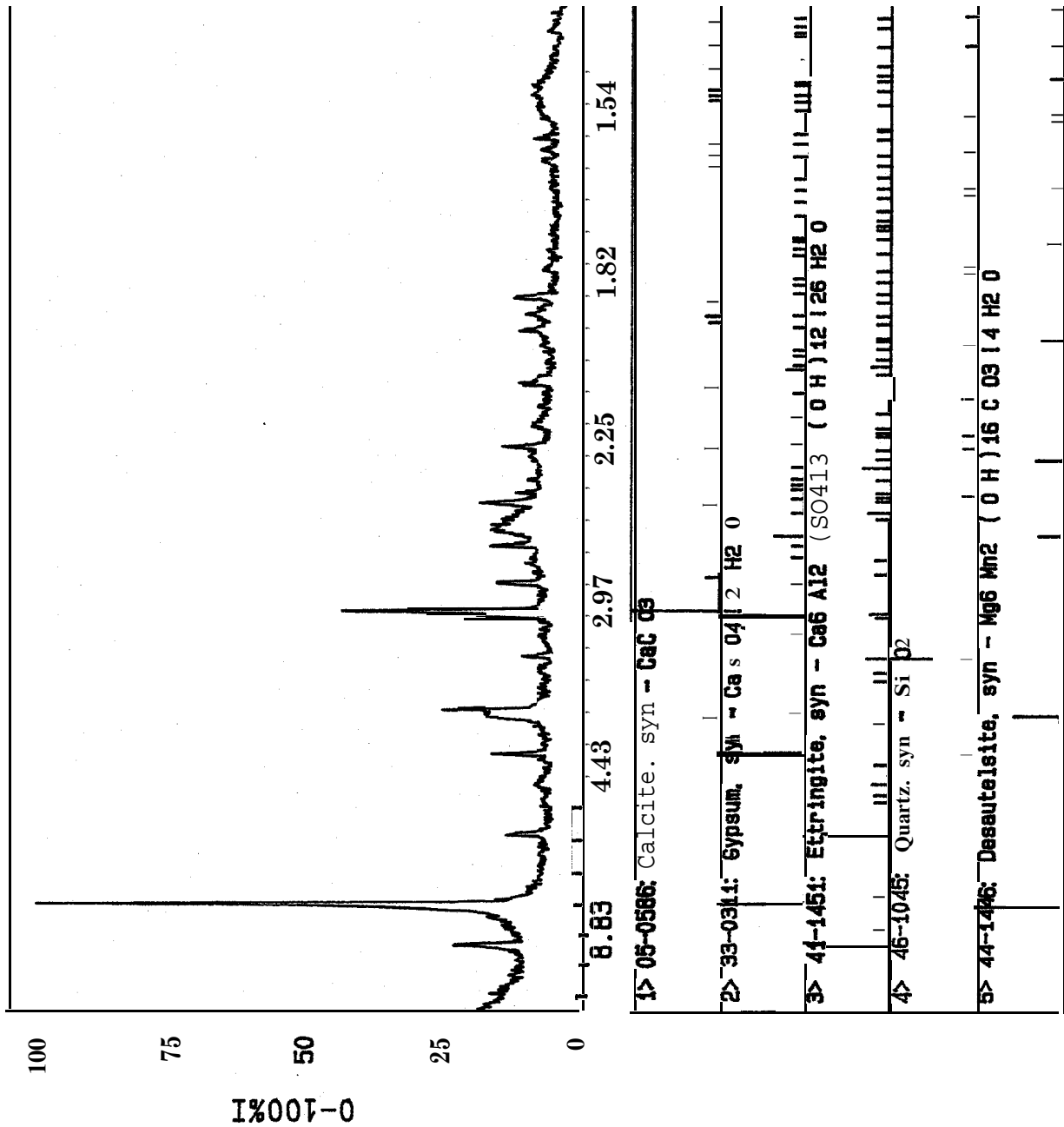
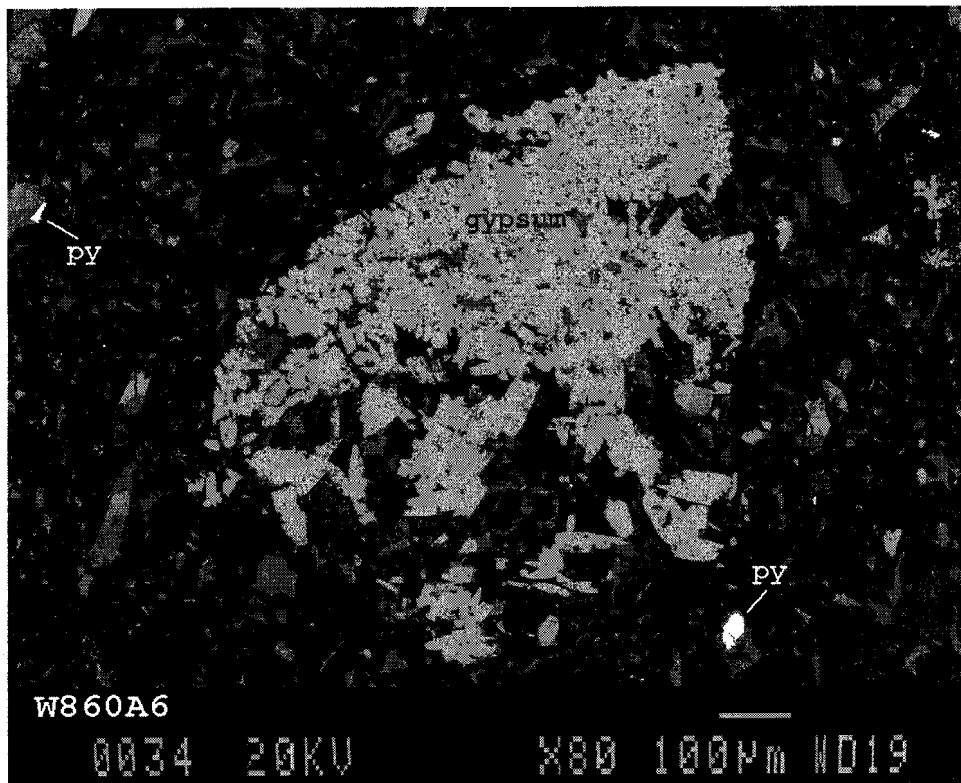
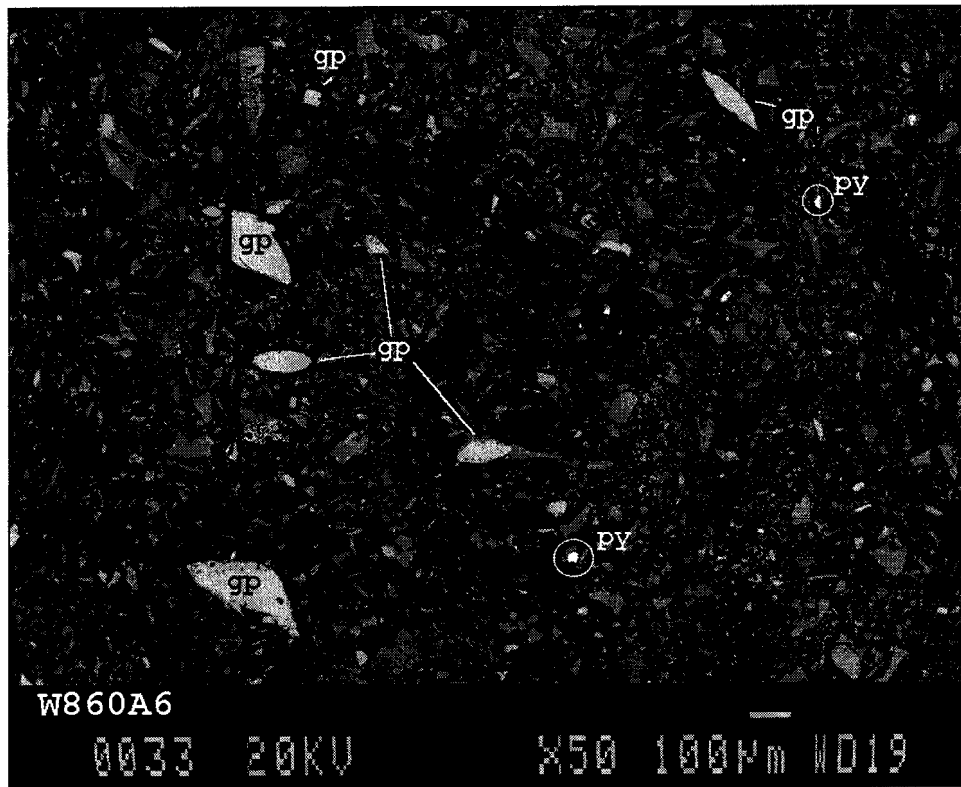
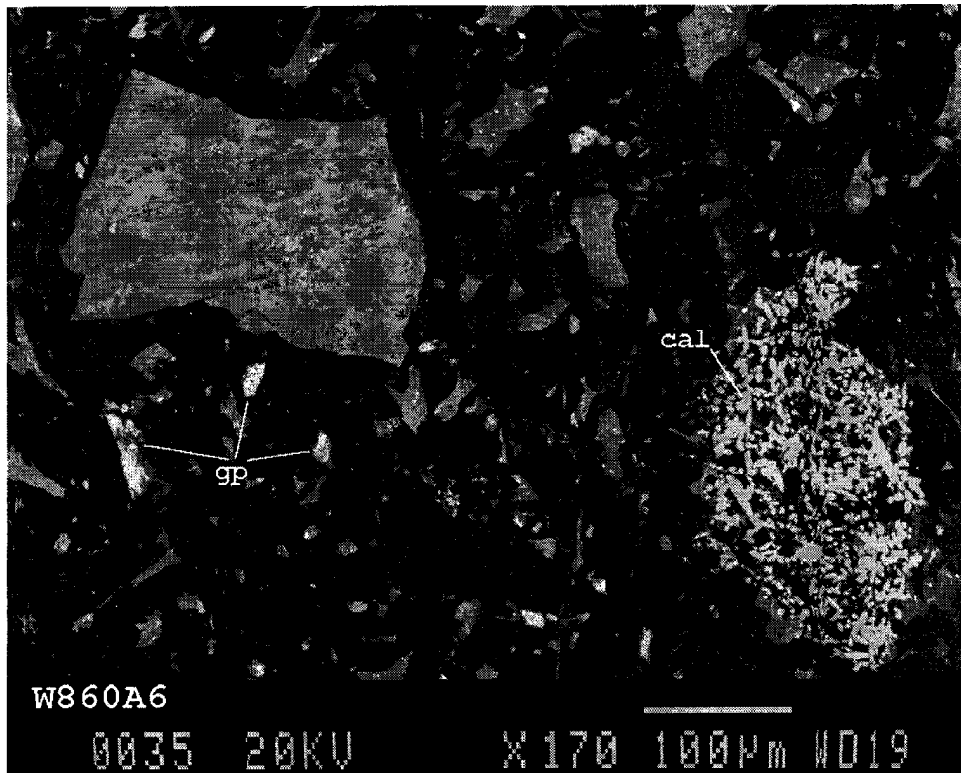
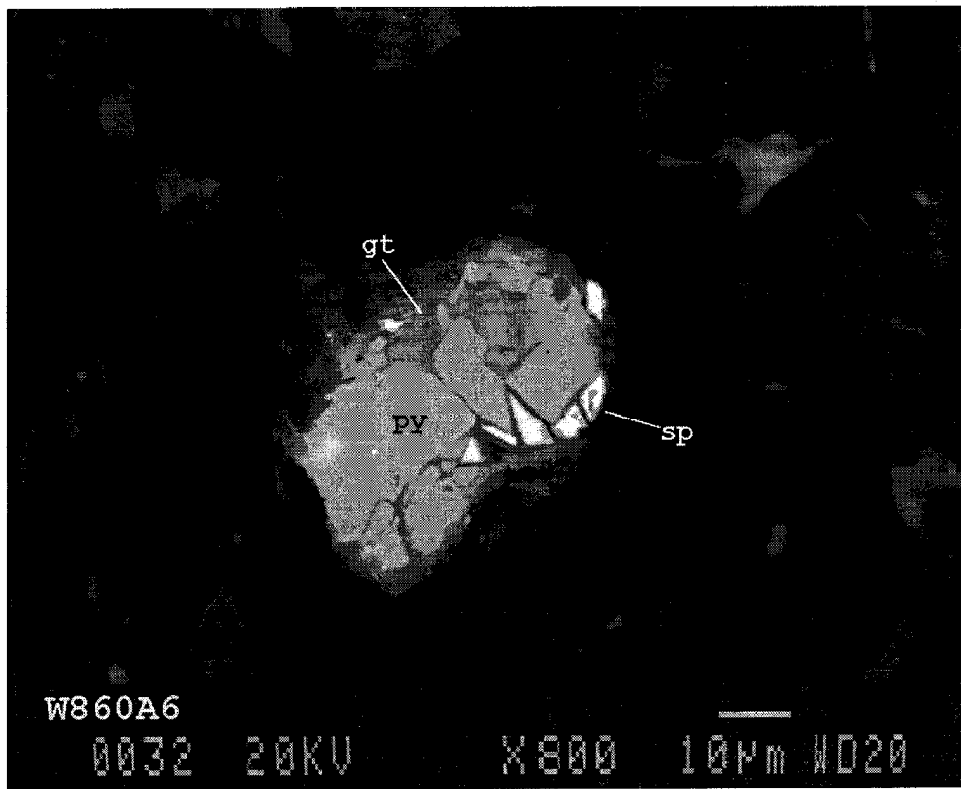


Fig. 10. X-ray diffractogram of sample W8-60A1.





ID: GRIFFITH W8-60A6, 21-APR-97@11: 27  
 File: Z03879.RAW Scan: 5-90/.05/ 1/#1701, Anode: CU

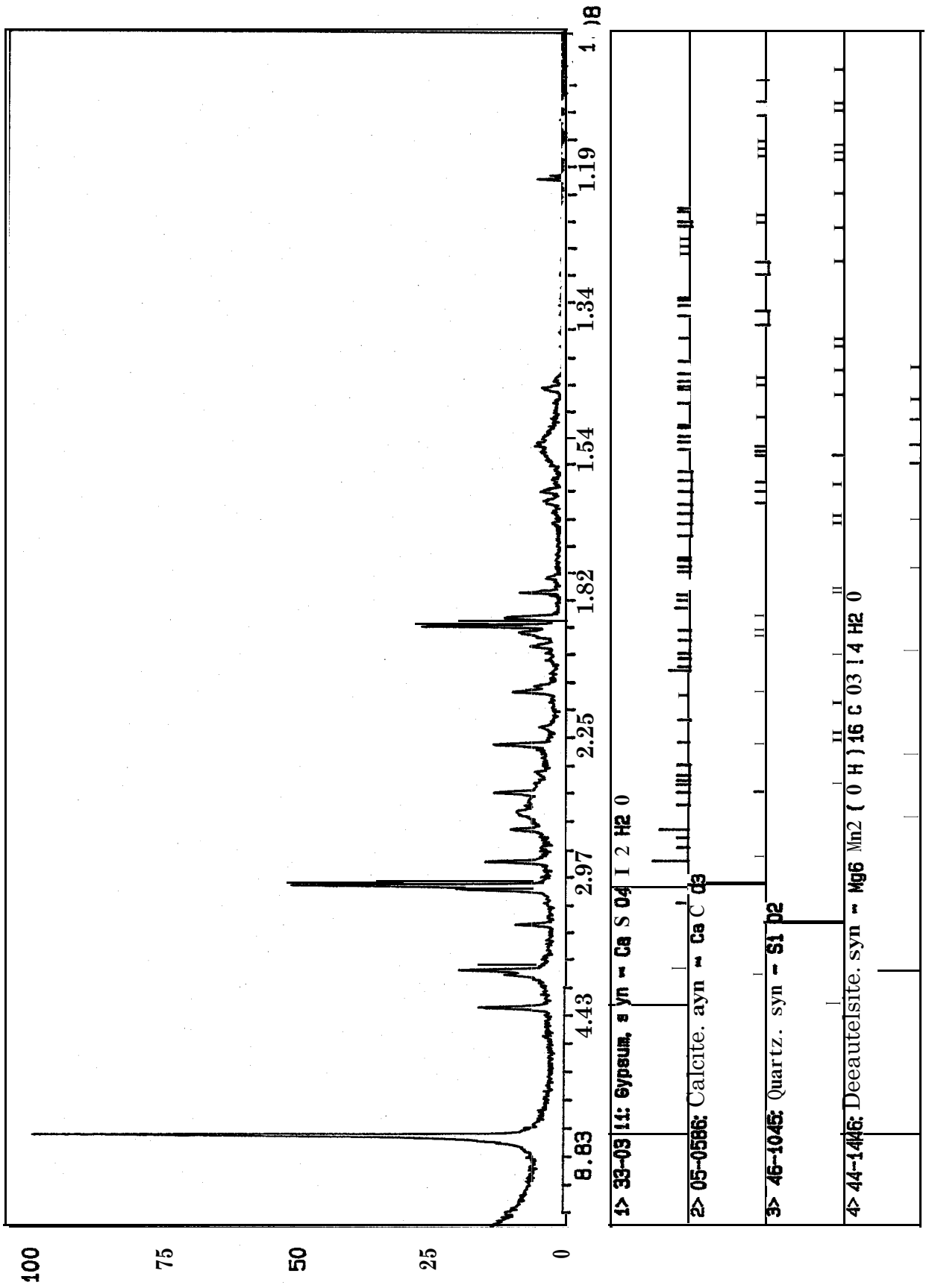
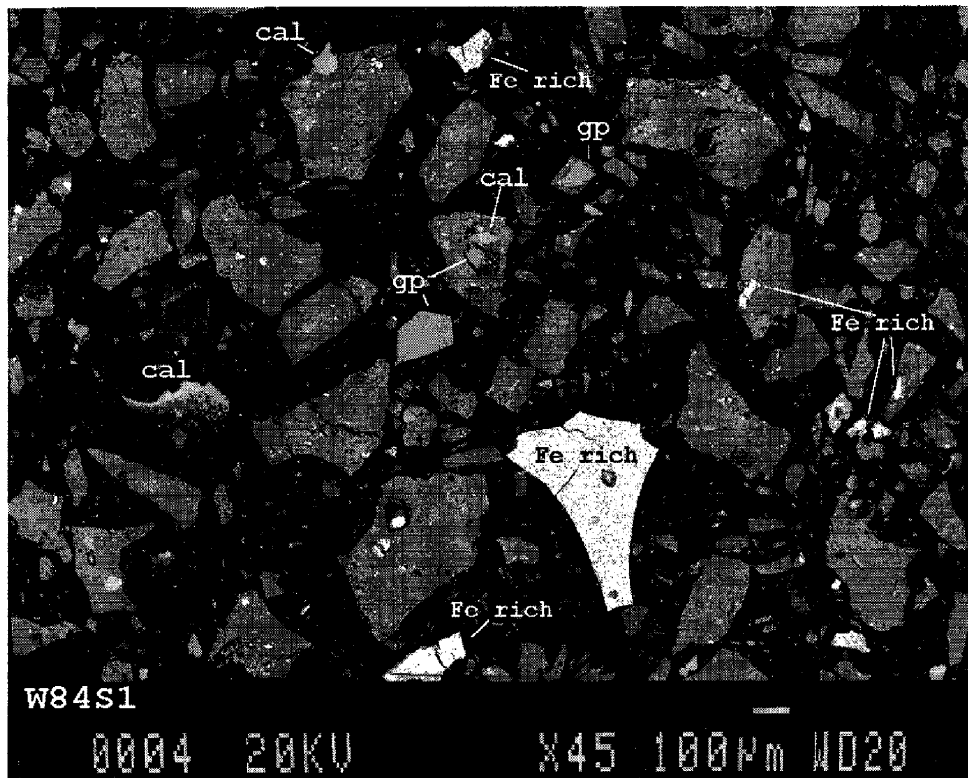
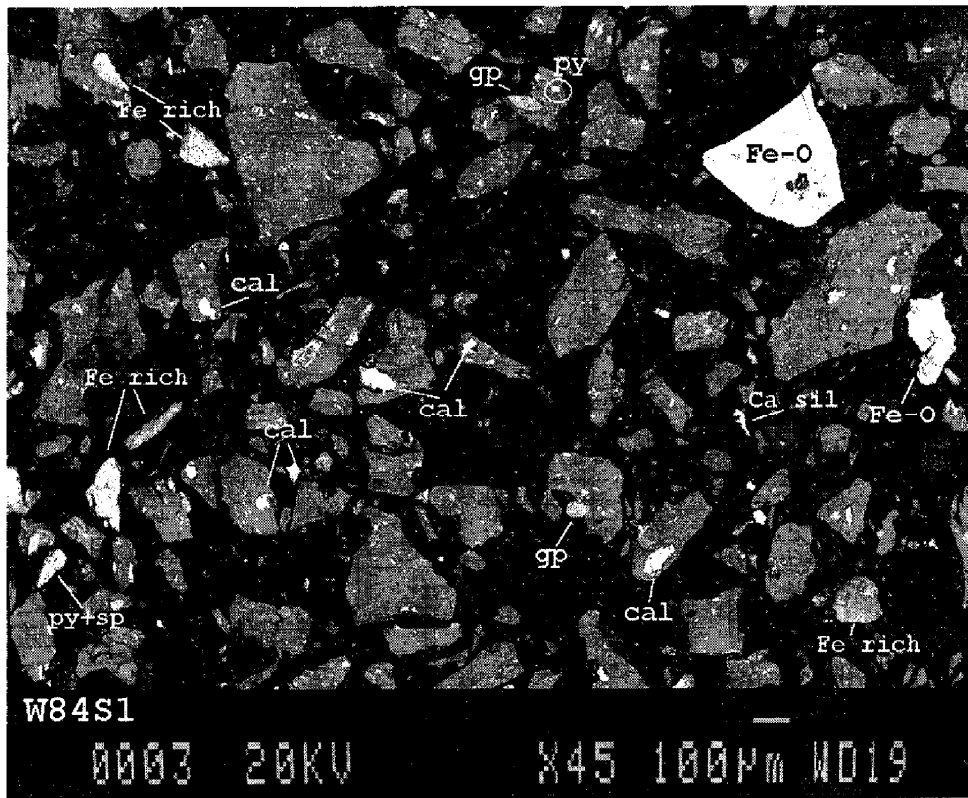
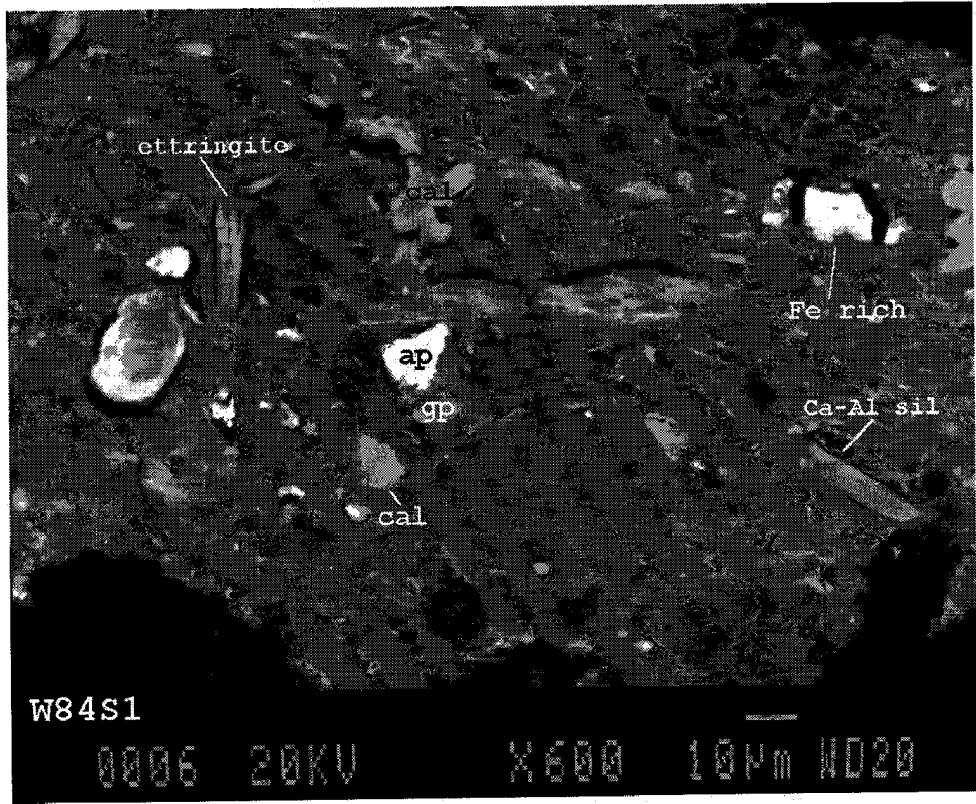


Fig. 11. X-ray diffractogram of sample W8-60A6.







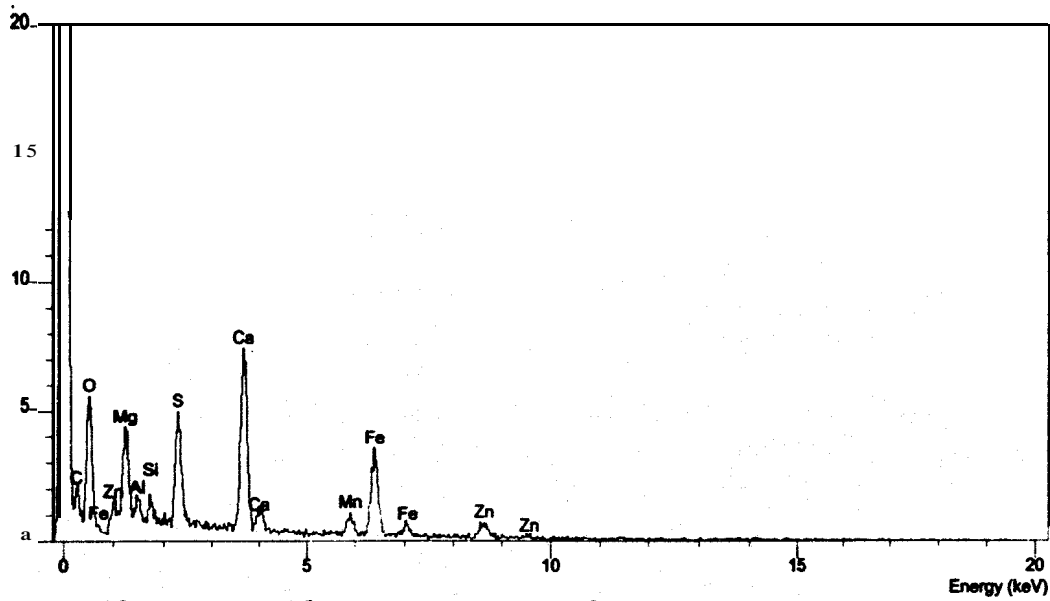


Fig. 12a. EDS of "phase M"; area 1, W8-4S1.

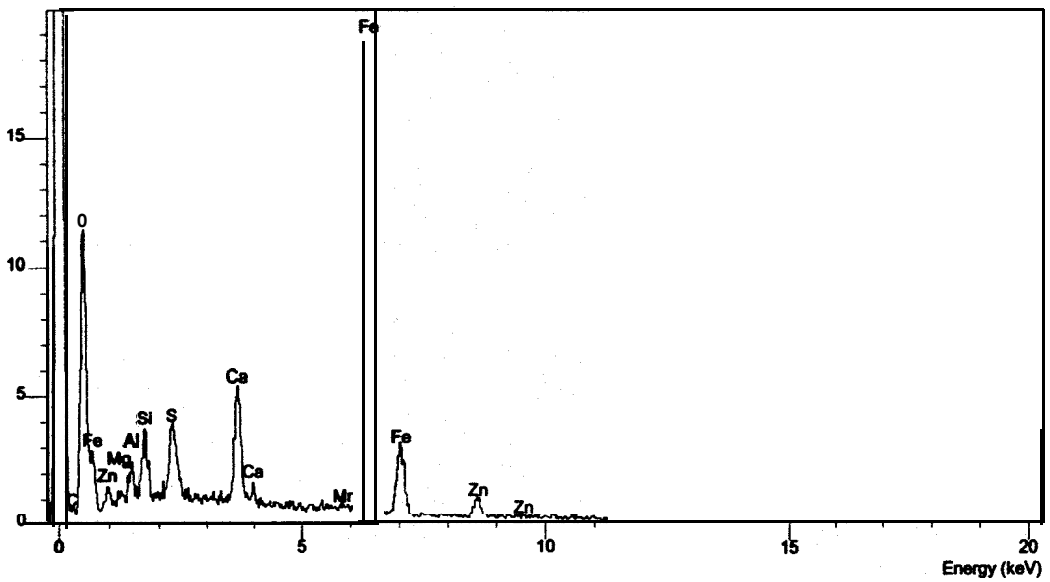


Fig. 12b. EDS of Fe-rich variant of "phase M"; area 2, W8-4S1.

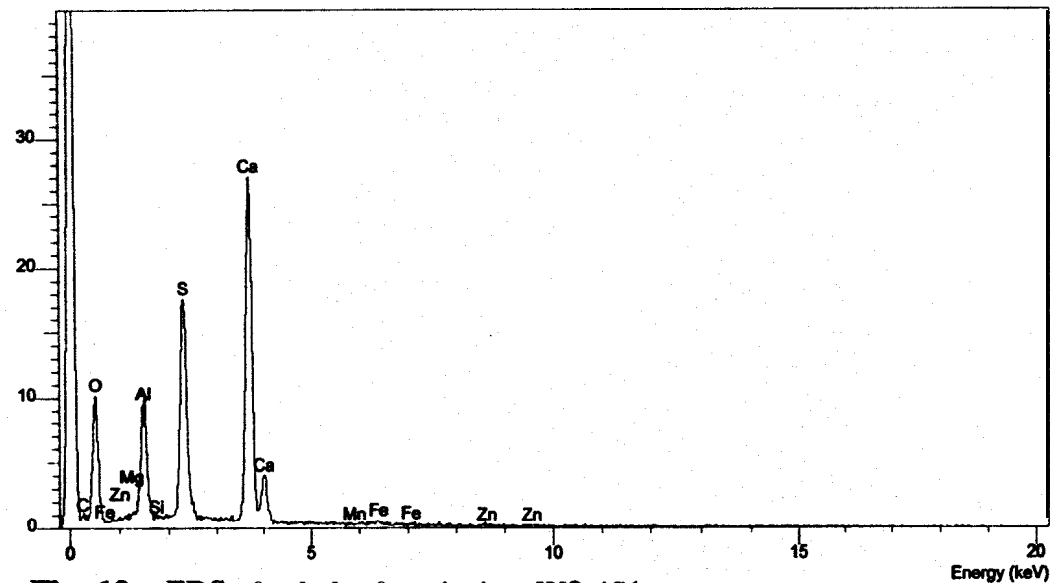


Fig. 12c. EDS of a lath of ettringite; W8-4S1.

ID: HOGAN W8-4S1 B, 21-OCT-97@10:38  
 File: Z04319.RAW Scan: 5-90/.05/ 1/#1701, Anode: CU

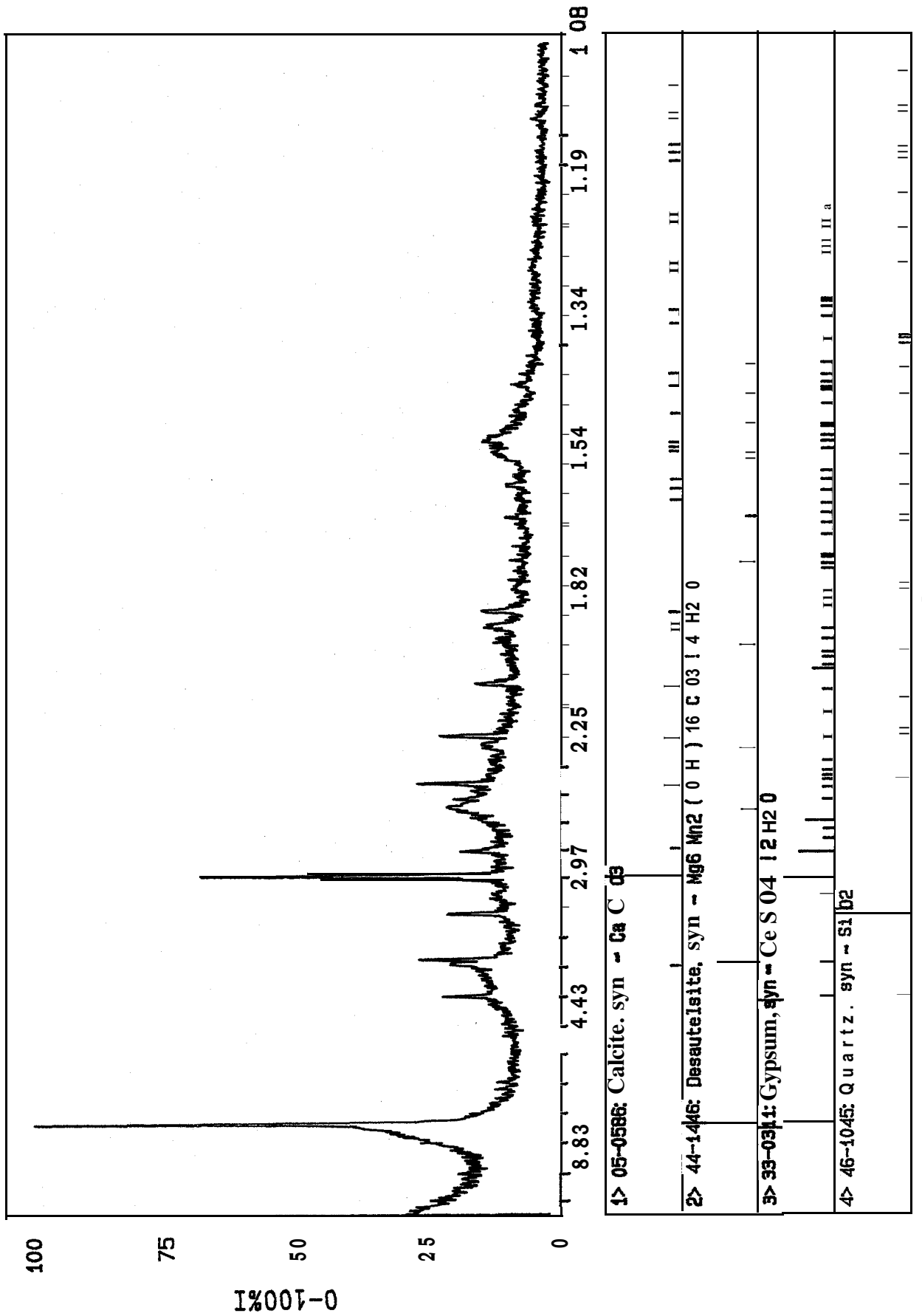
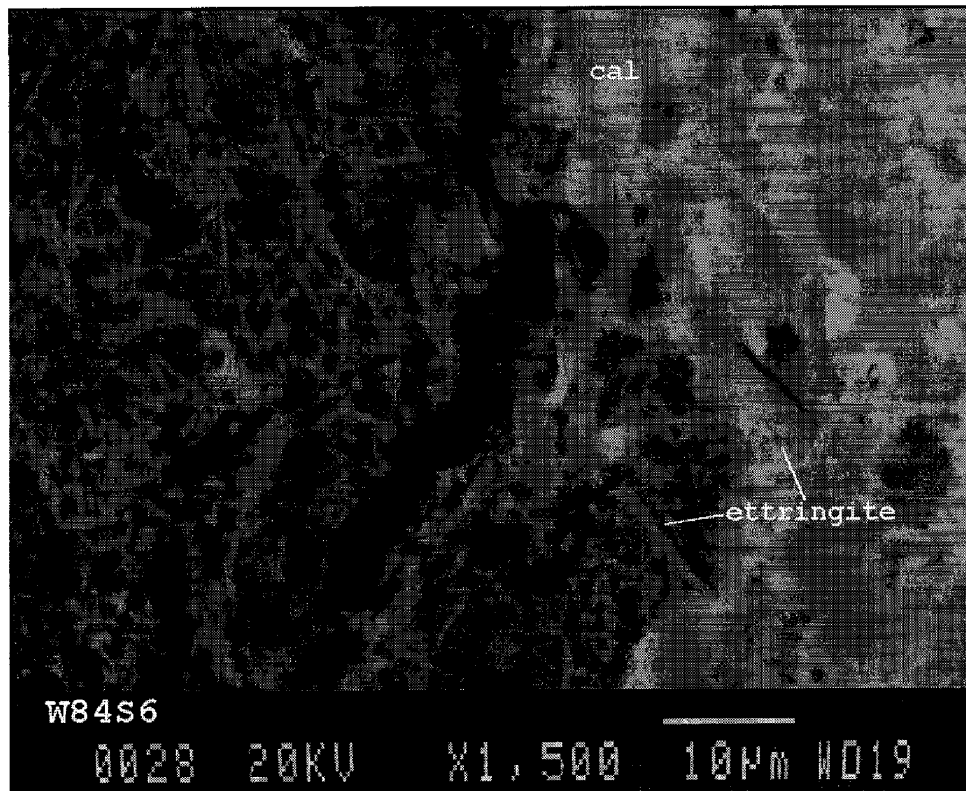
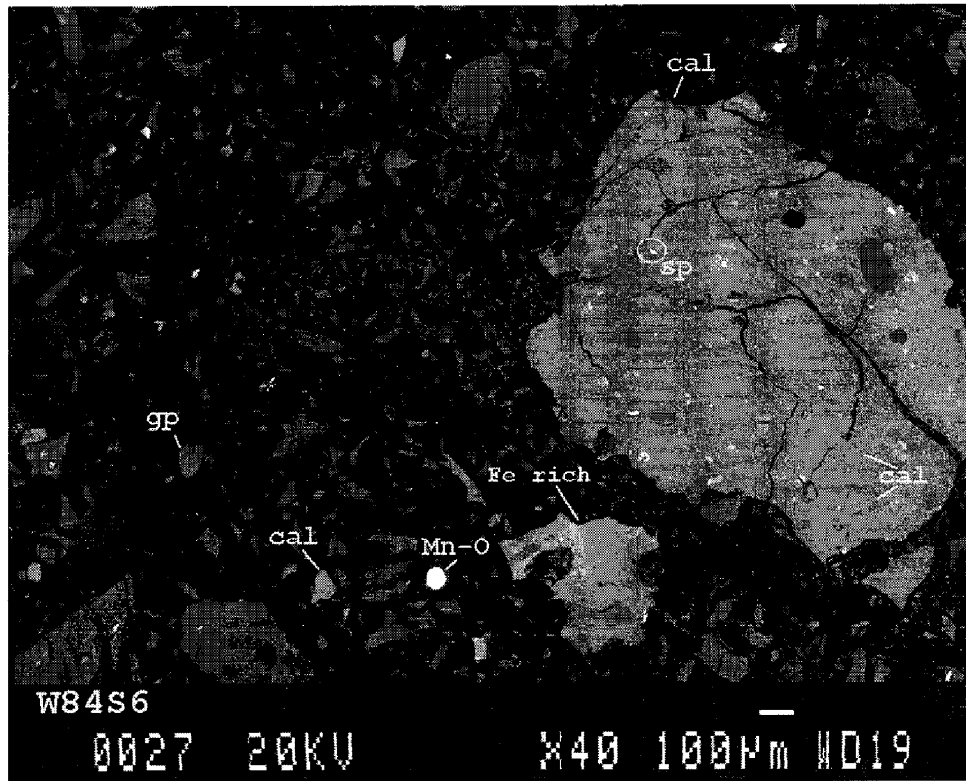
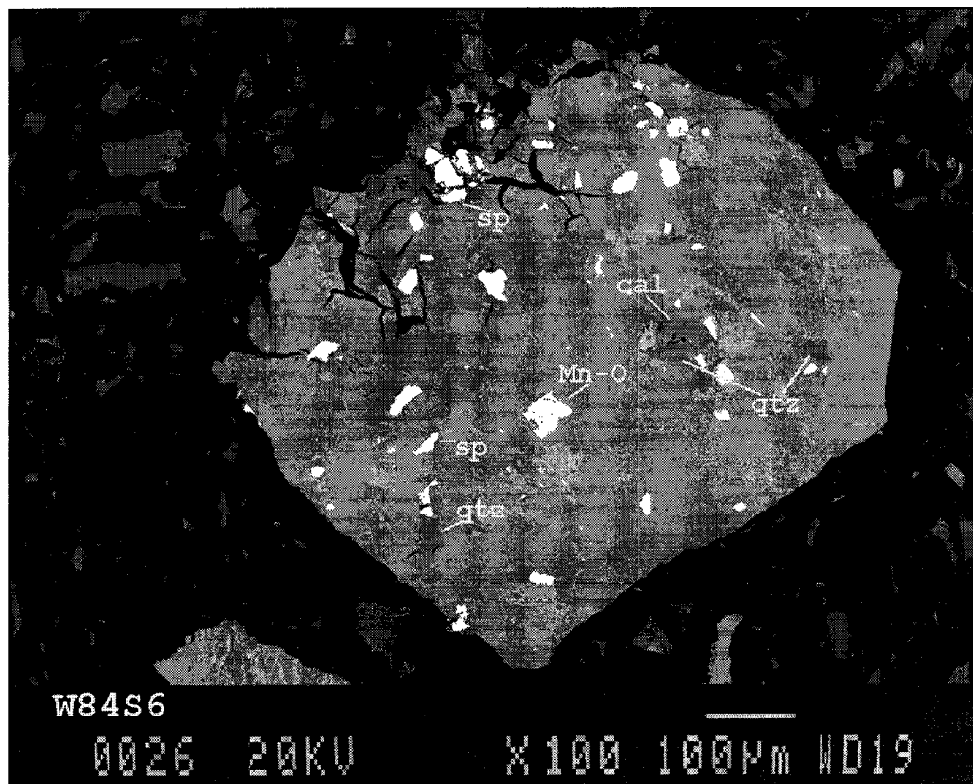
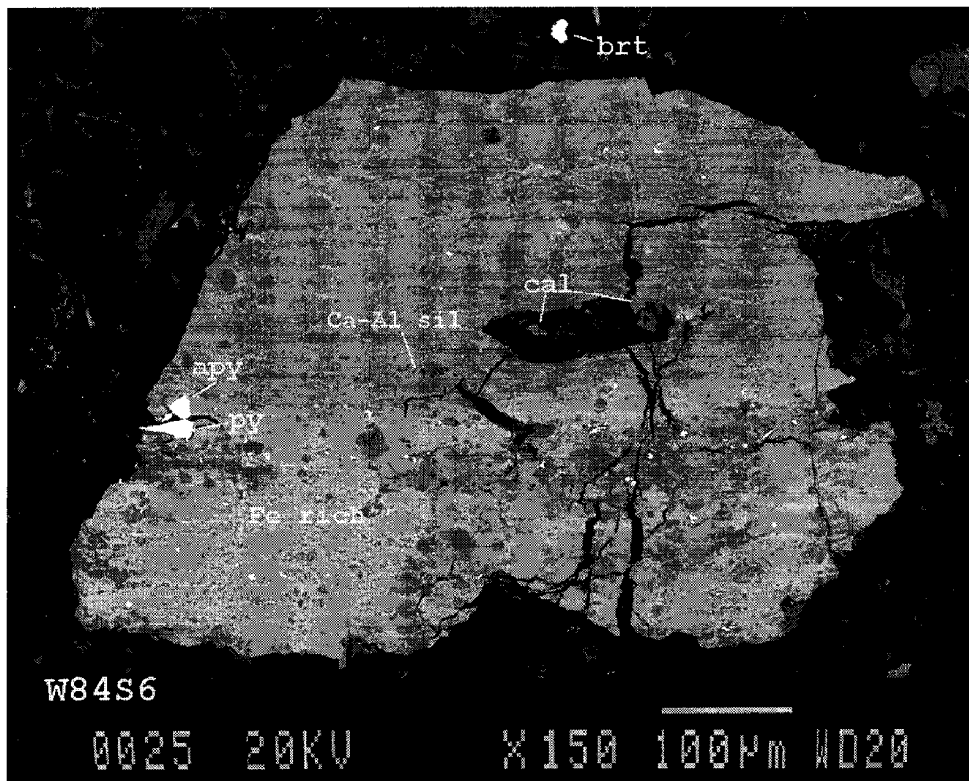


Fig. 13. X-ray diffractogram of sample W8-4S1.





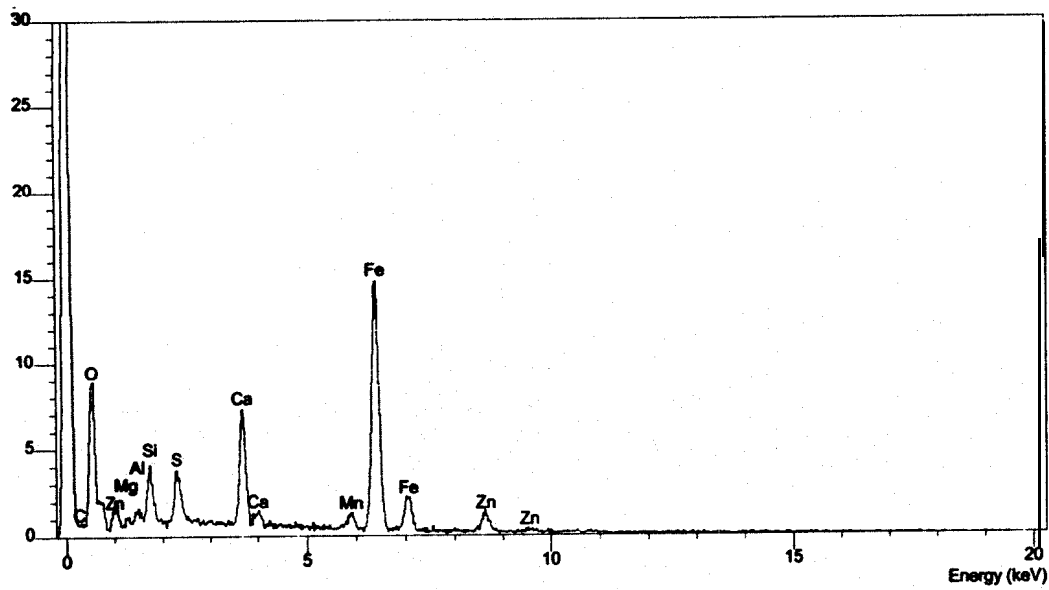


Fig. 14a. EDS of Fe-rich variant of "phase M" ; area 1, W8-4S6.

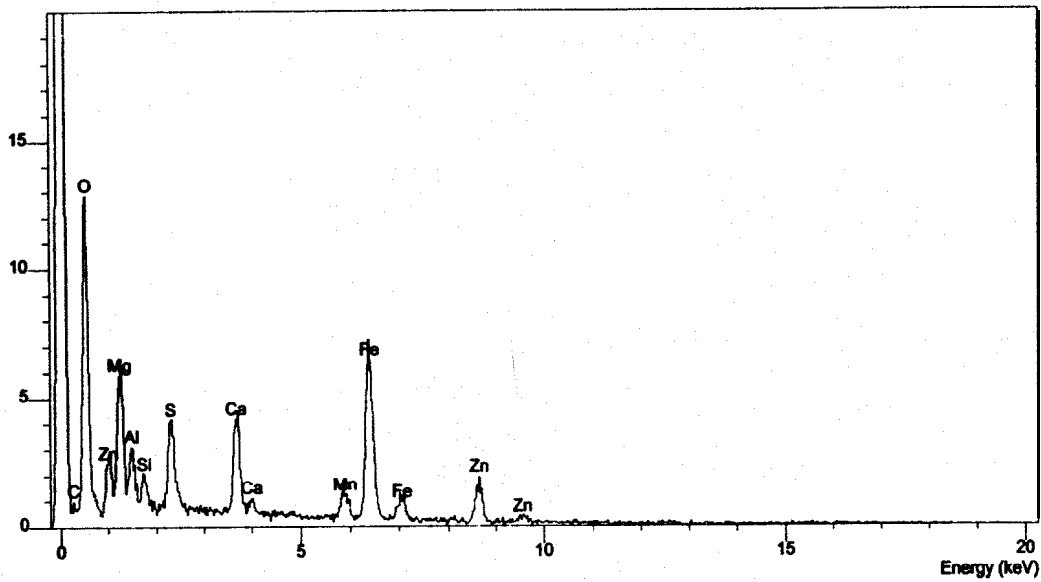


Fig. 14b. EDS of Fe-rich "phase M" ; area 2, W8-4S6.

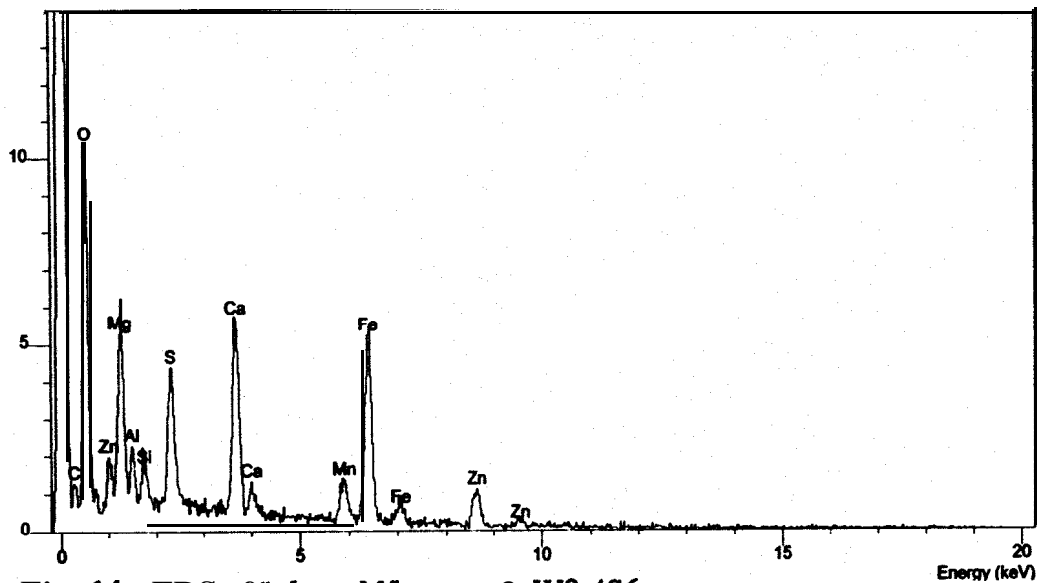


Fig. 14c. EDS of "phase M" ; area 3, W8-4S6.

ID: GRIFFITH W8-4S6, 21-APR-97@11: 27  
 File: Z03878.RAW Scan: 5-90/.05/ 1/#1701, Anode: CU

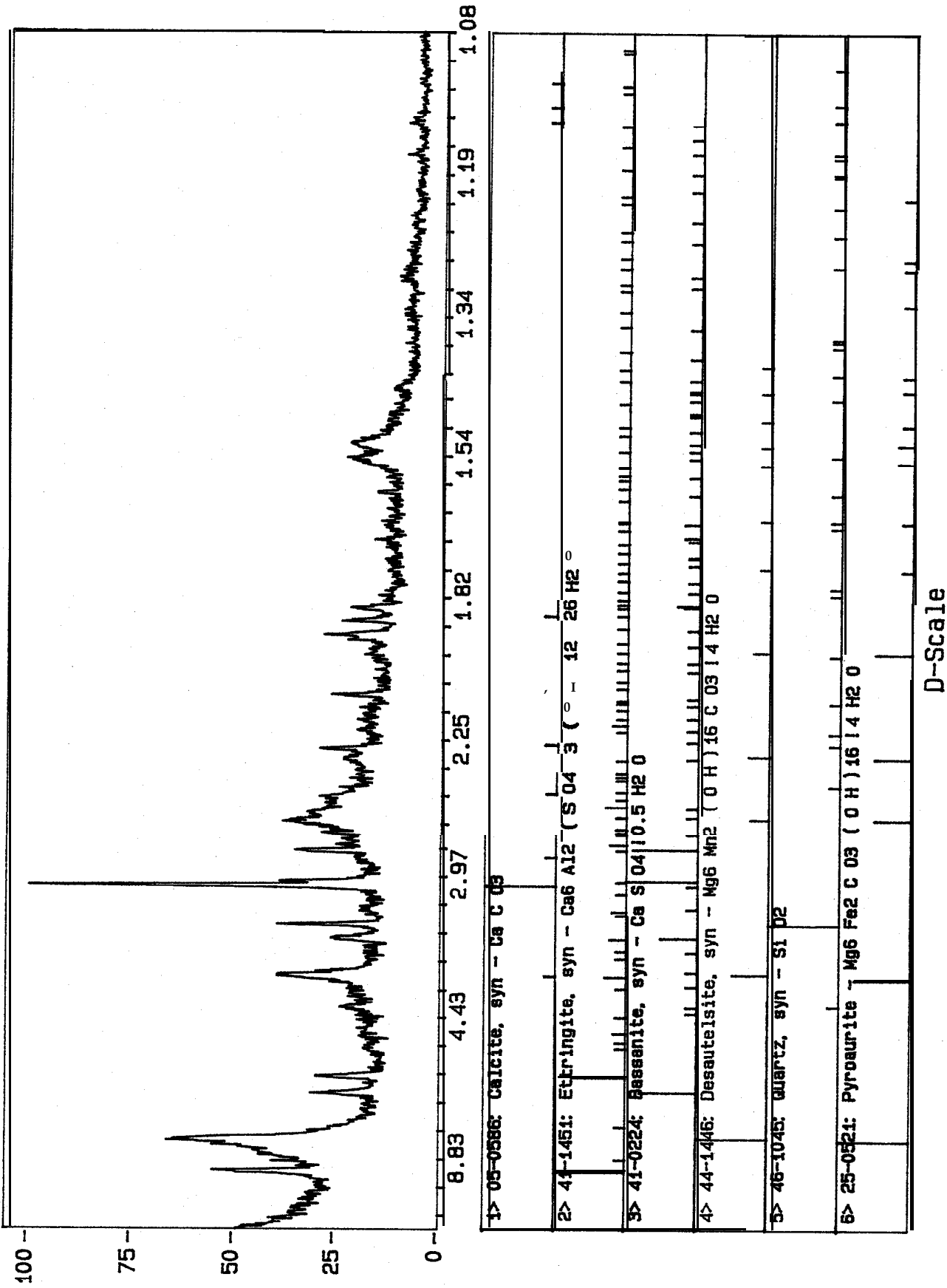
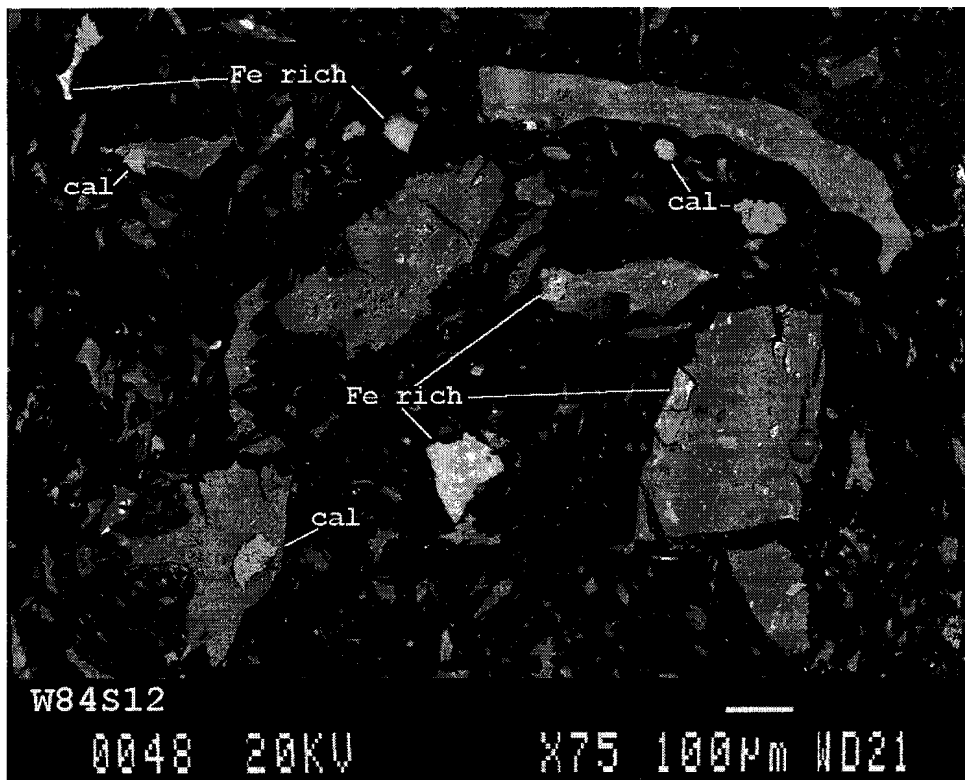
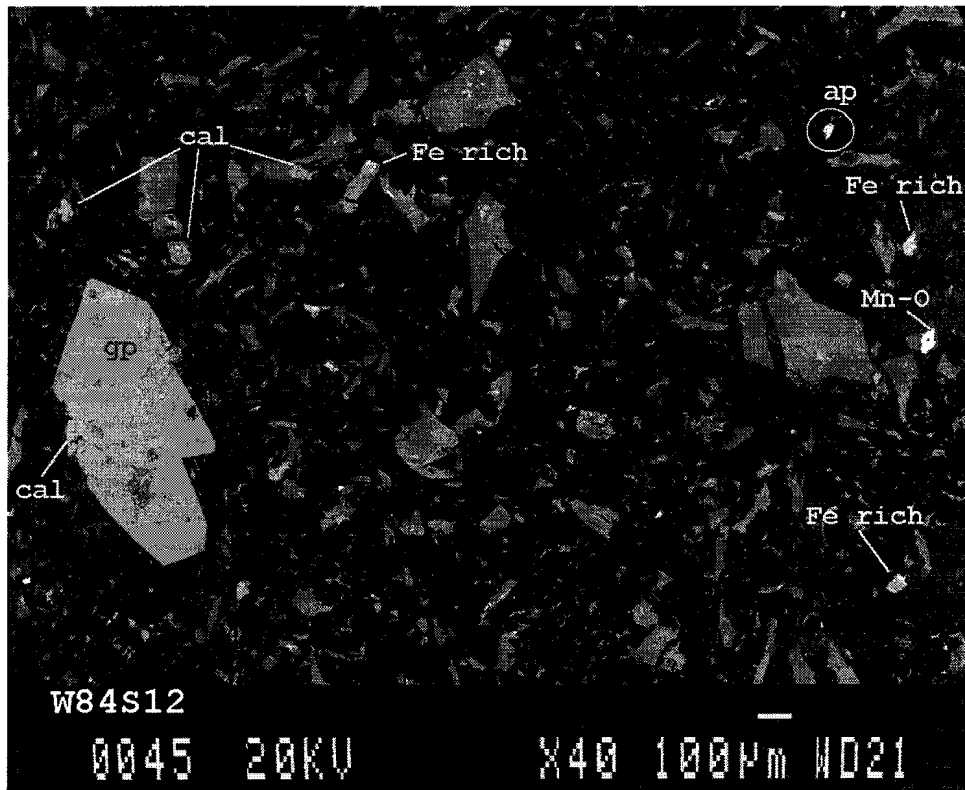
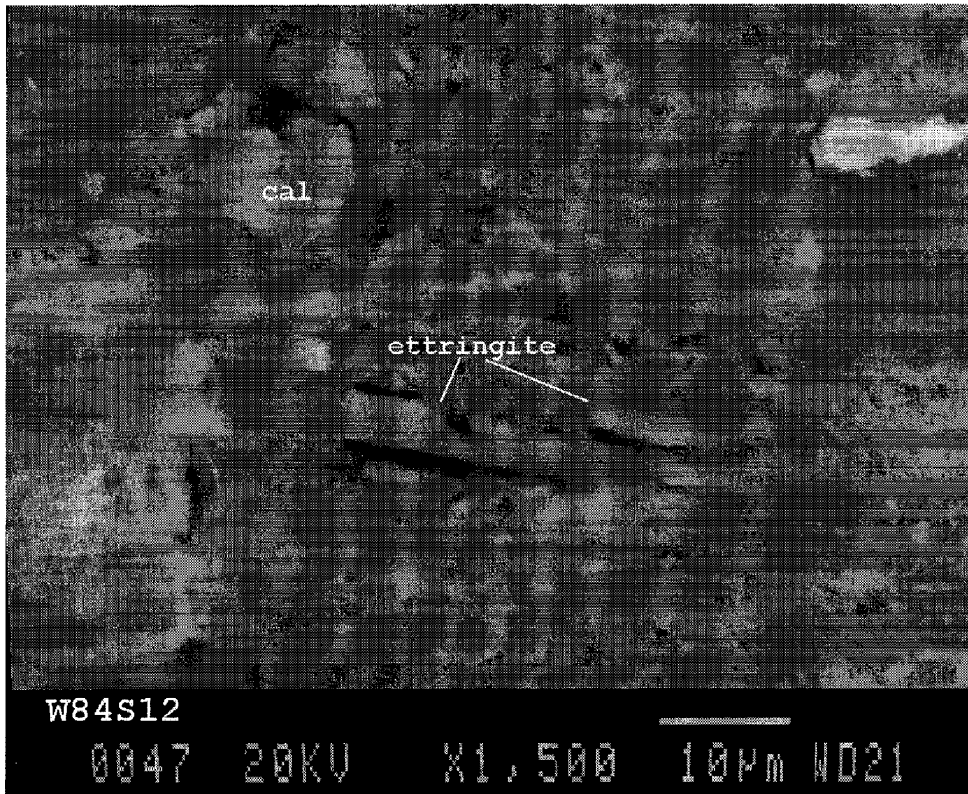
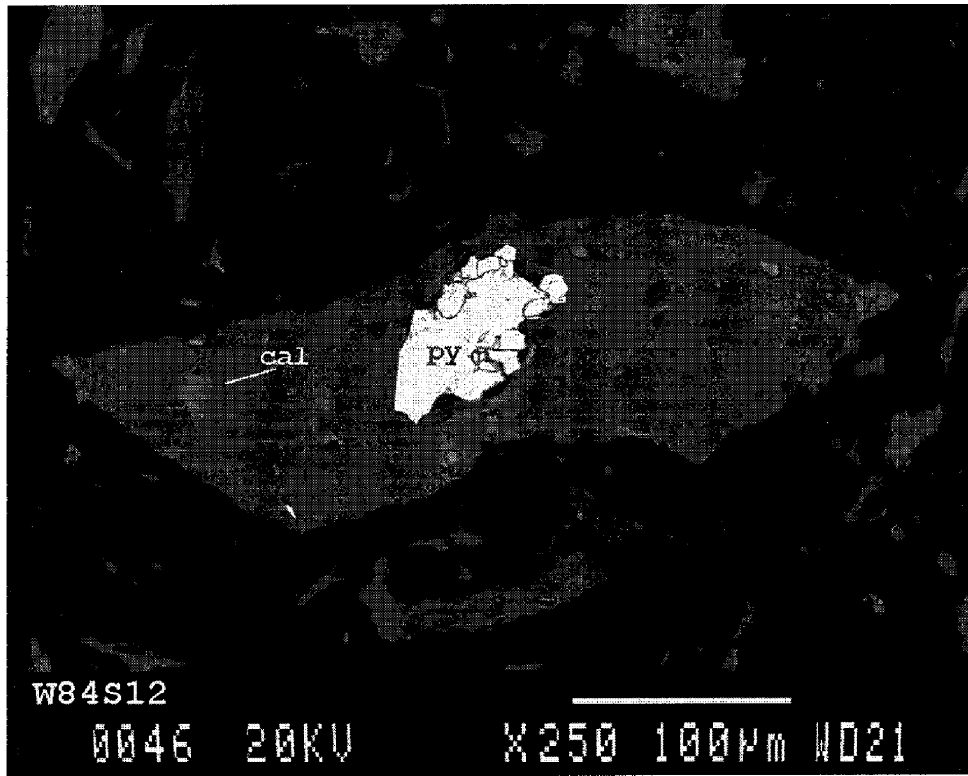


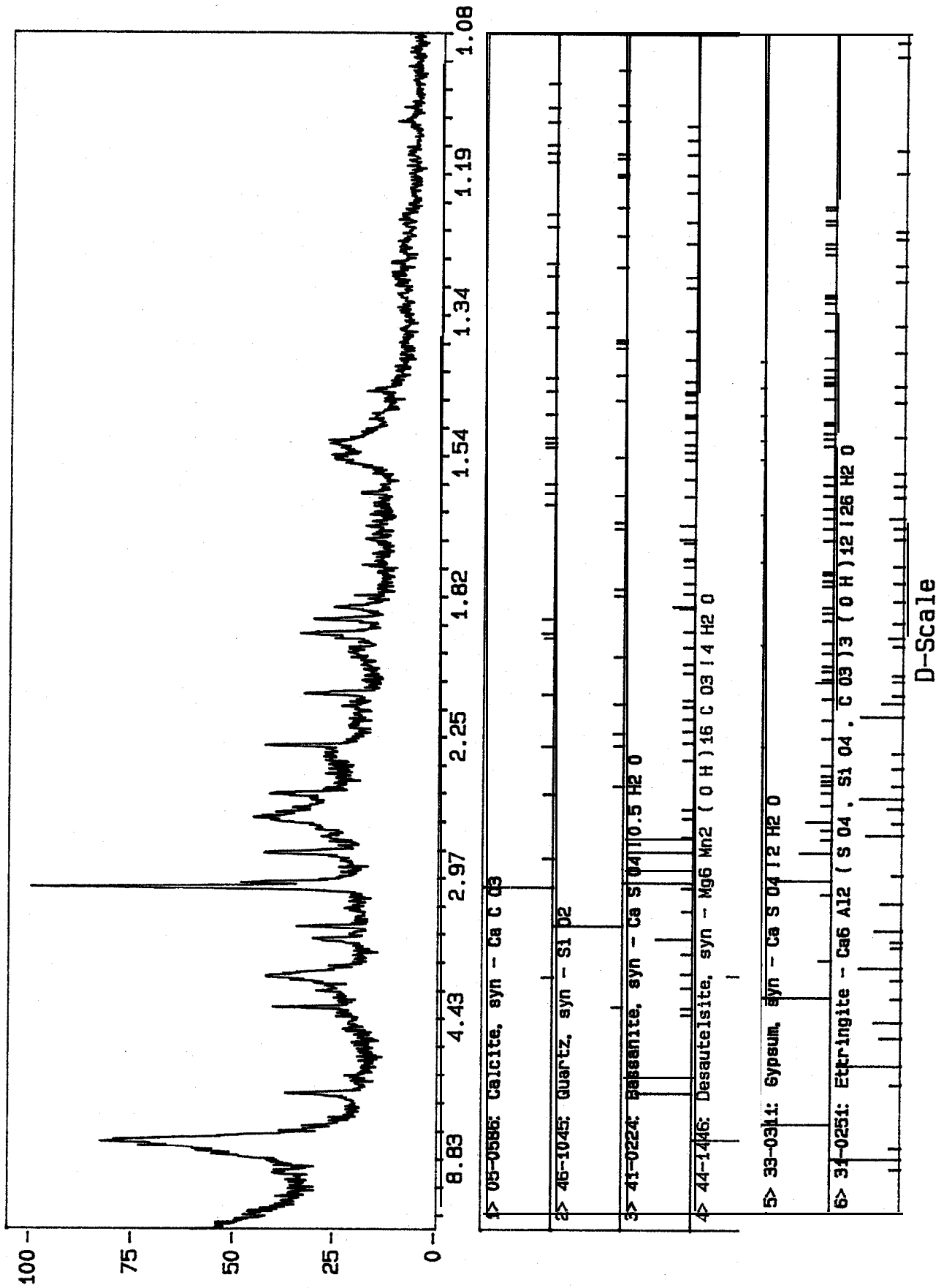
Fig. 15. X-ray diffractogram of sample W8-4S6.



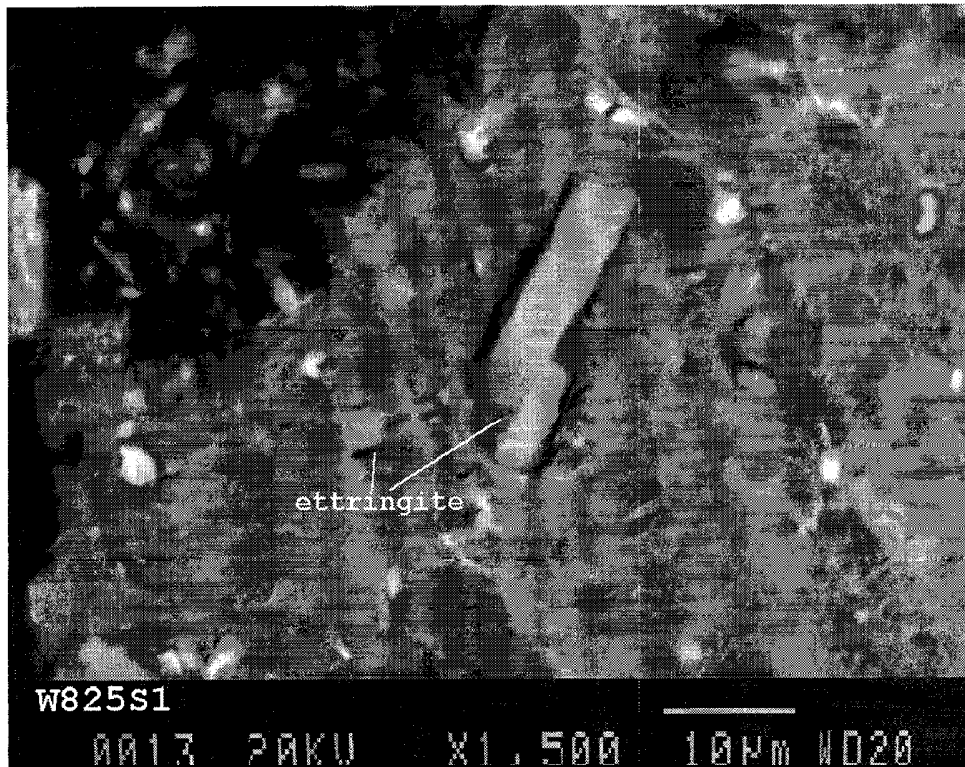
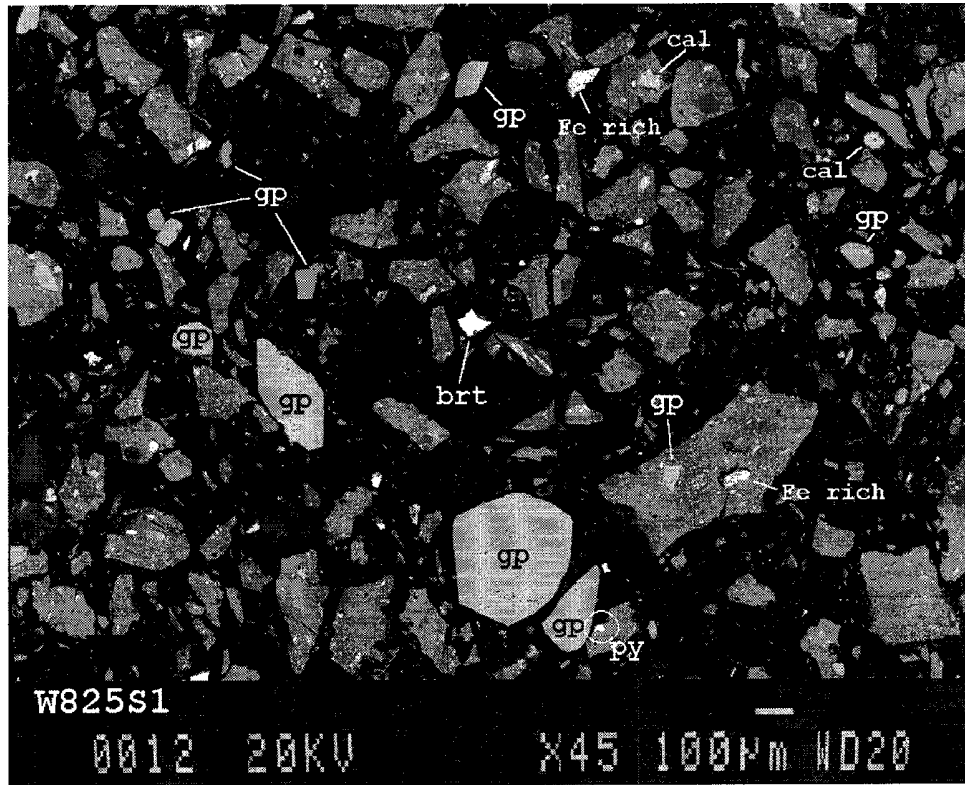


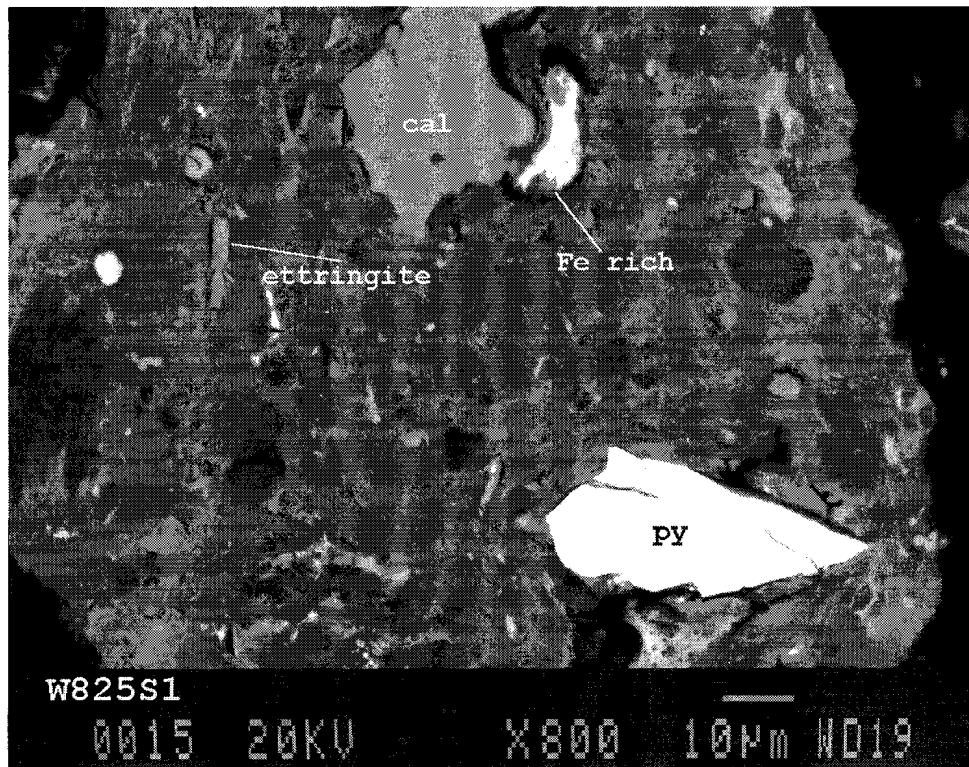
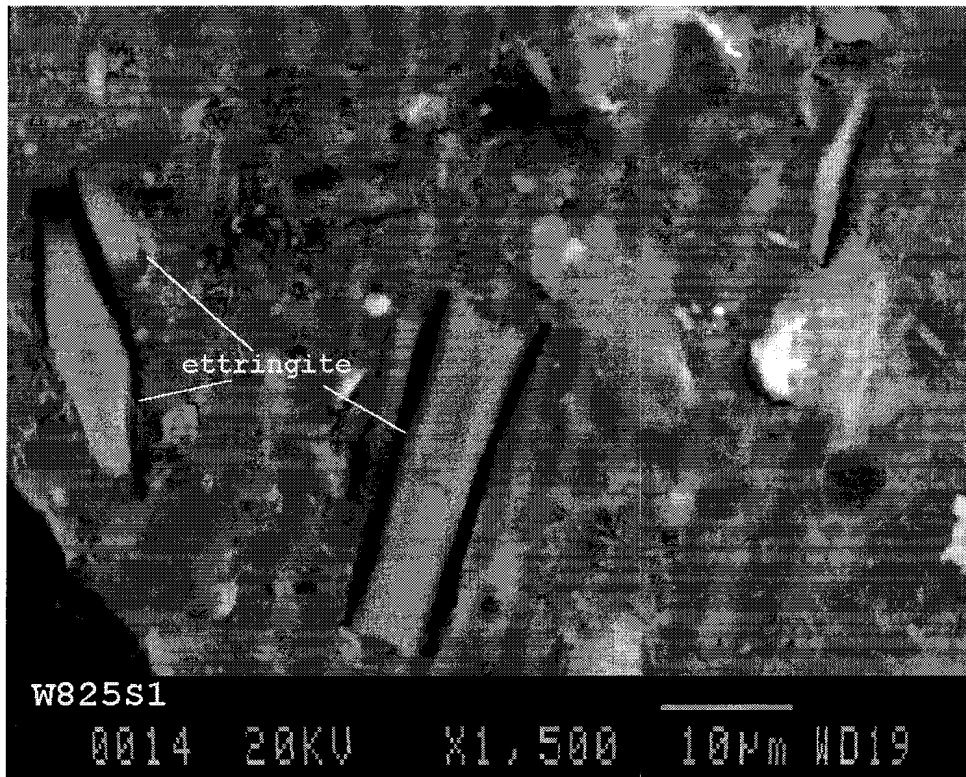


ID: HOGAN W8-4S-12, 21-OCT-97@11:55  
 File: Z04328.RAW Scan: 5-90/.05/ 1/#1701, Anode: CU



0-100% I  
 Fig. 16. X-ray diffractogram of sample W8-4S12.





ID: HOGAN W8-25S., 21-OCT-97@10:38  
 File: Z04321.RAW Scan: 5-90/.05/ 1/#1701, Anode: CU

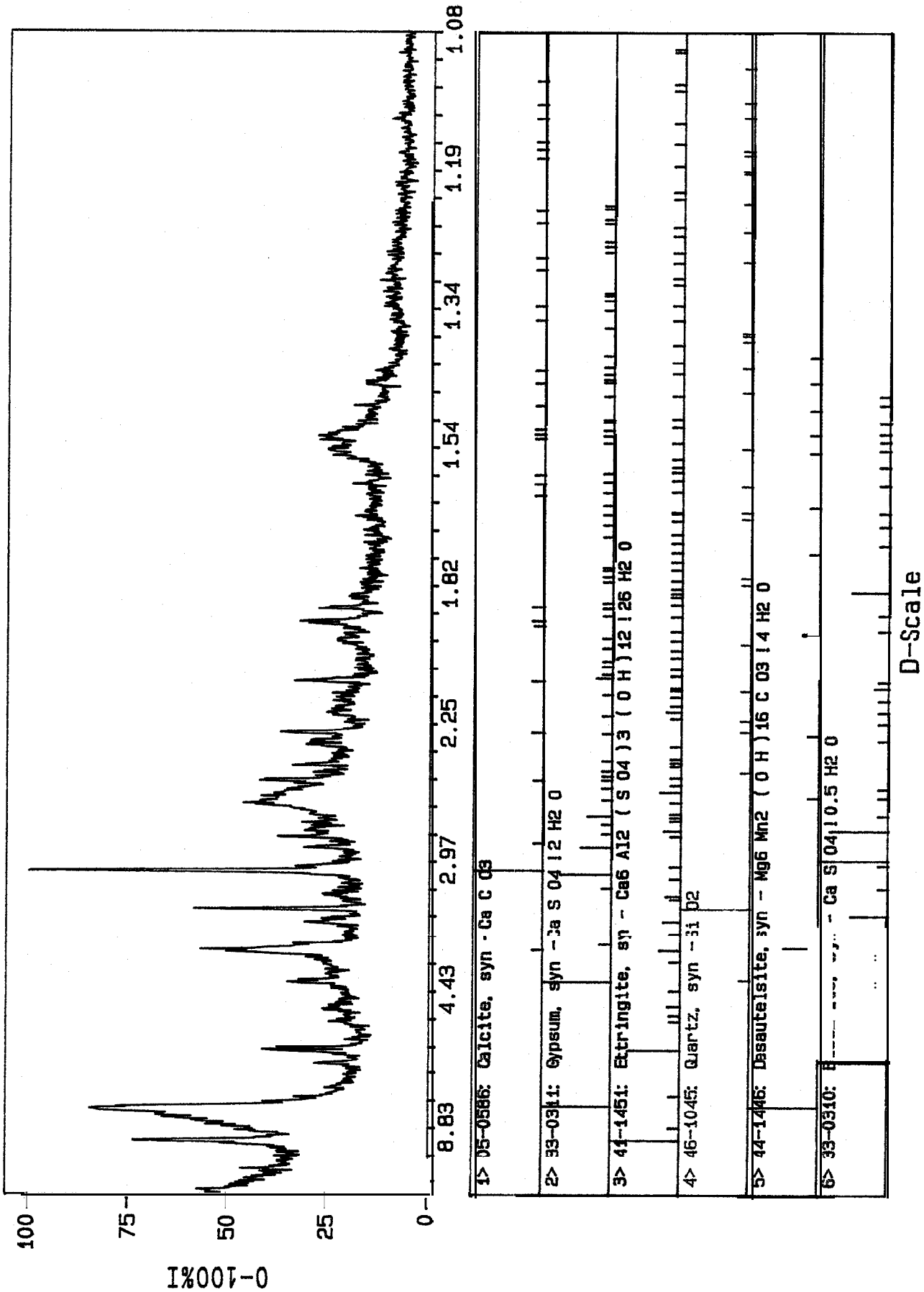
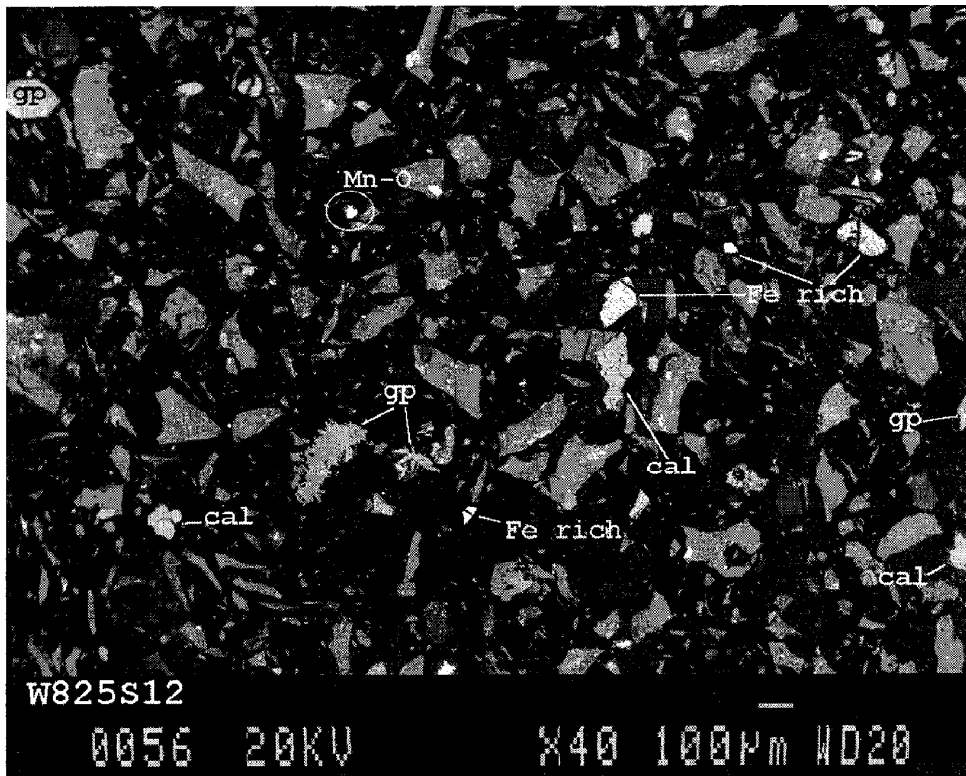
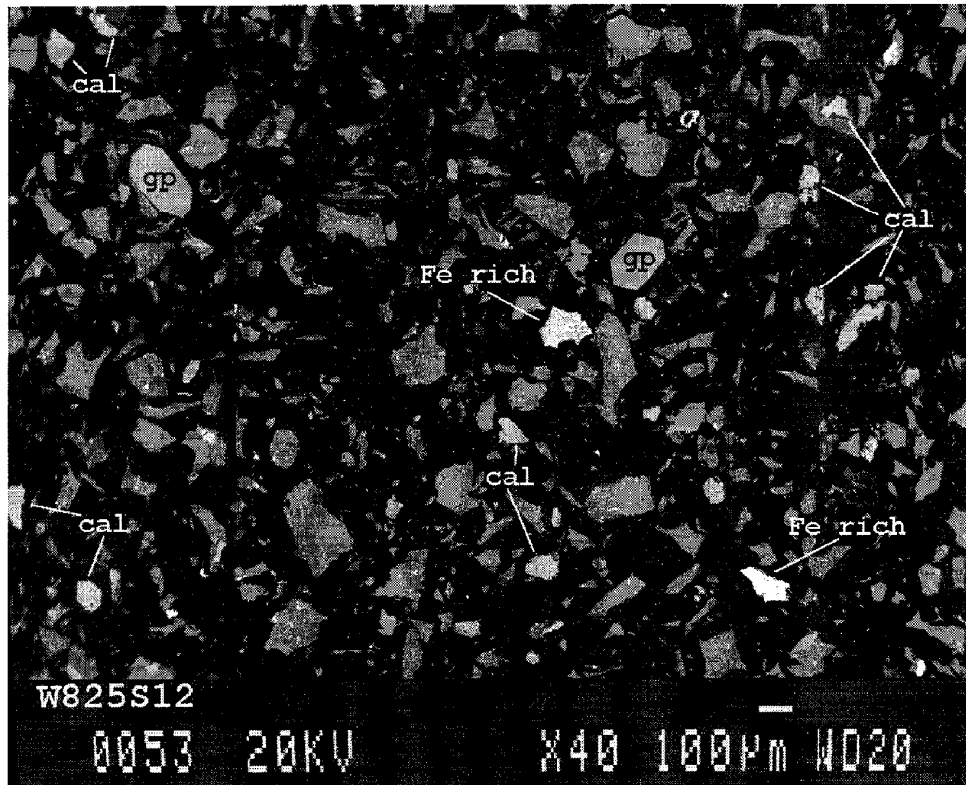
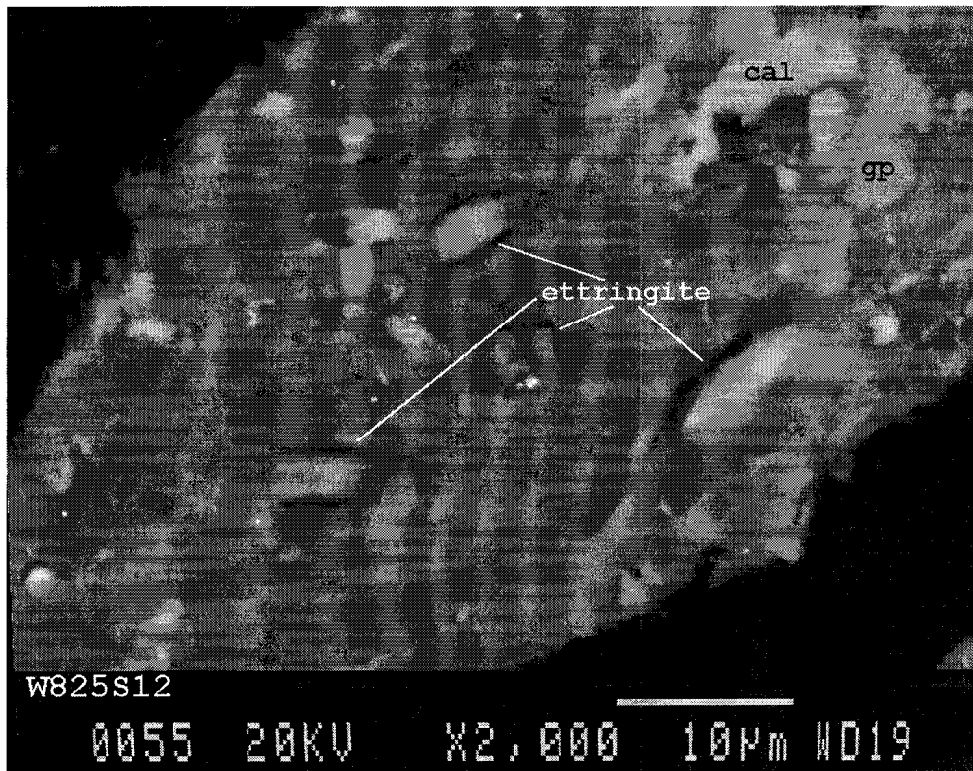
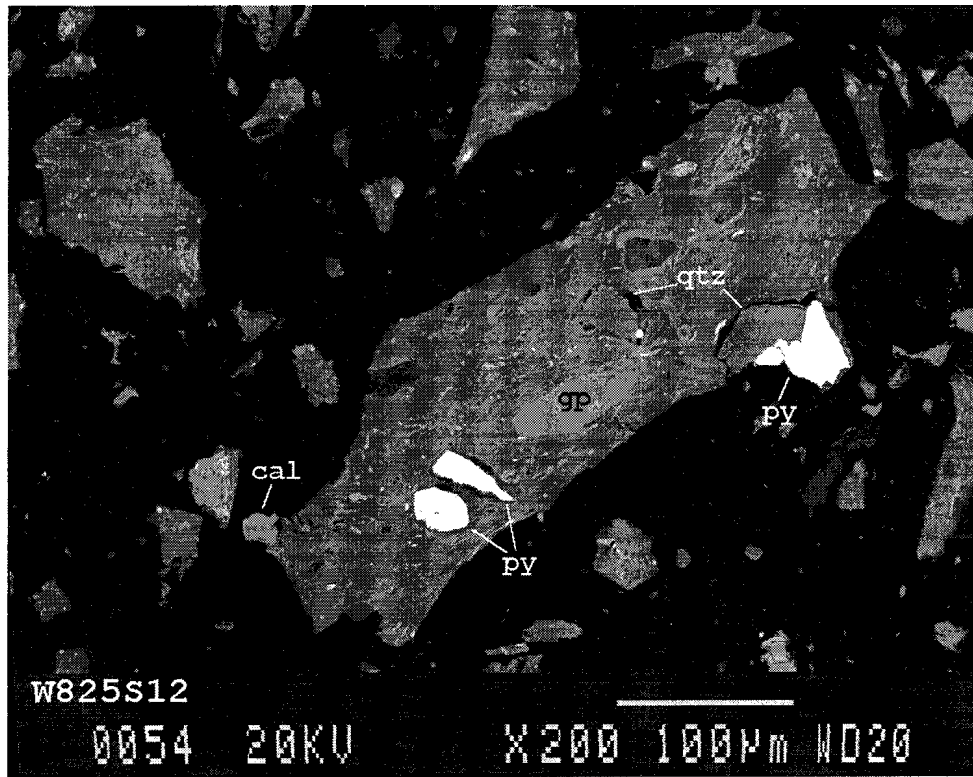


Fig. 17. X-ray diffractogram of sample W8-25S 1.





ID: HOGAN W8-25S-12, 21-OCT-97@13:30  
 File: Z04330.RAW Scan: 5-90/.05/ 1/#1701, Anode: CU

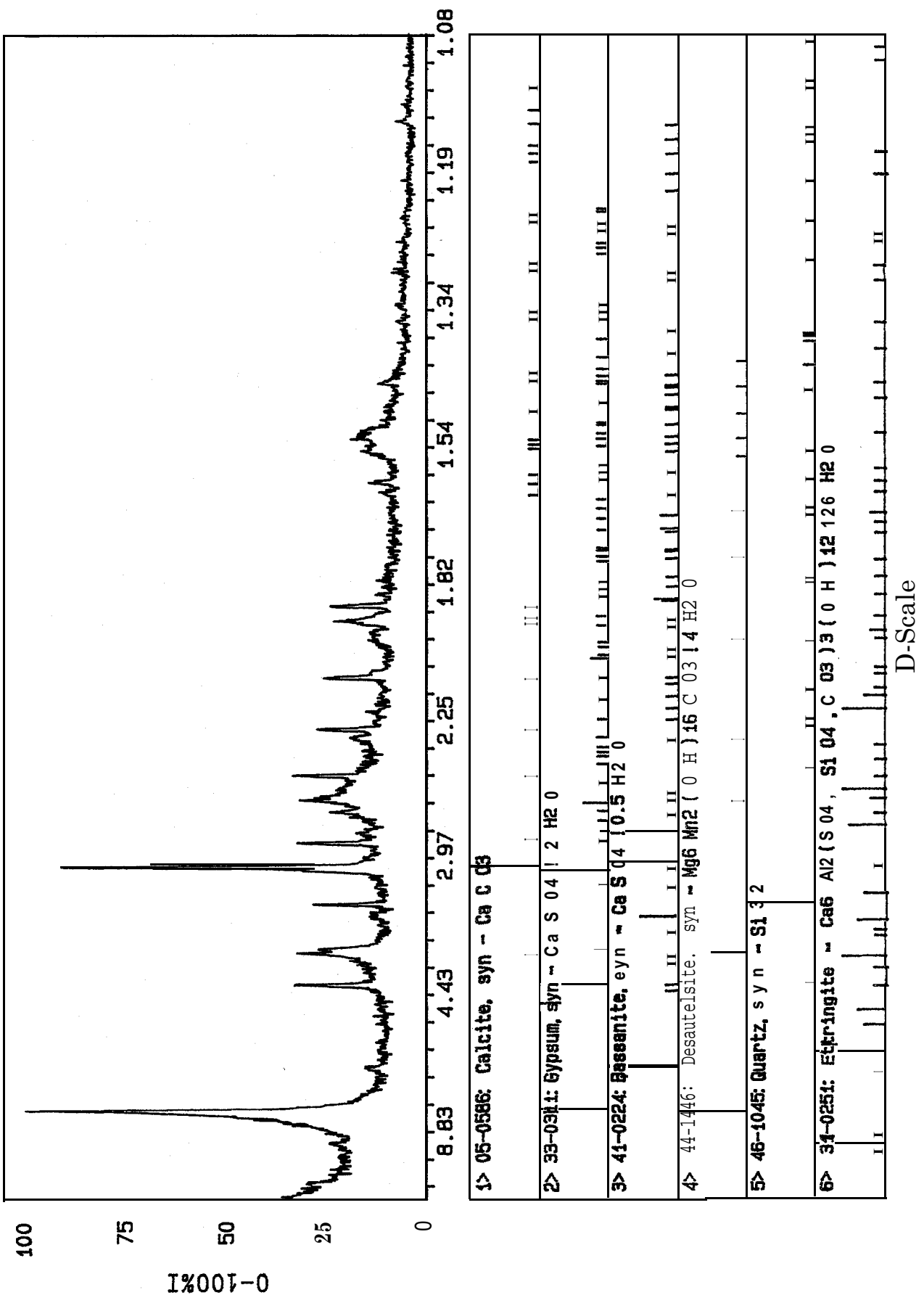
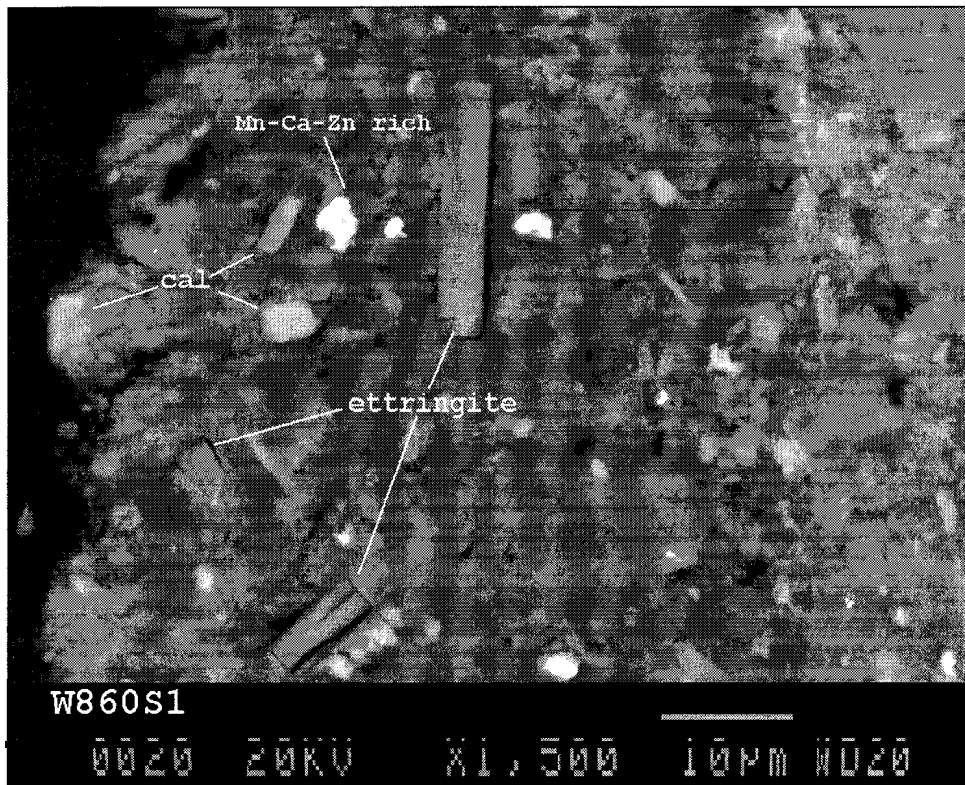
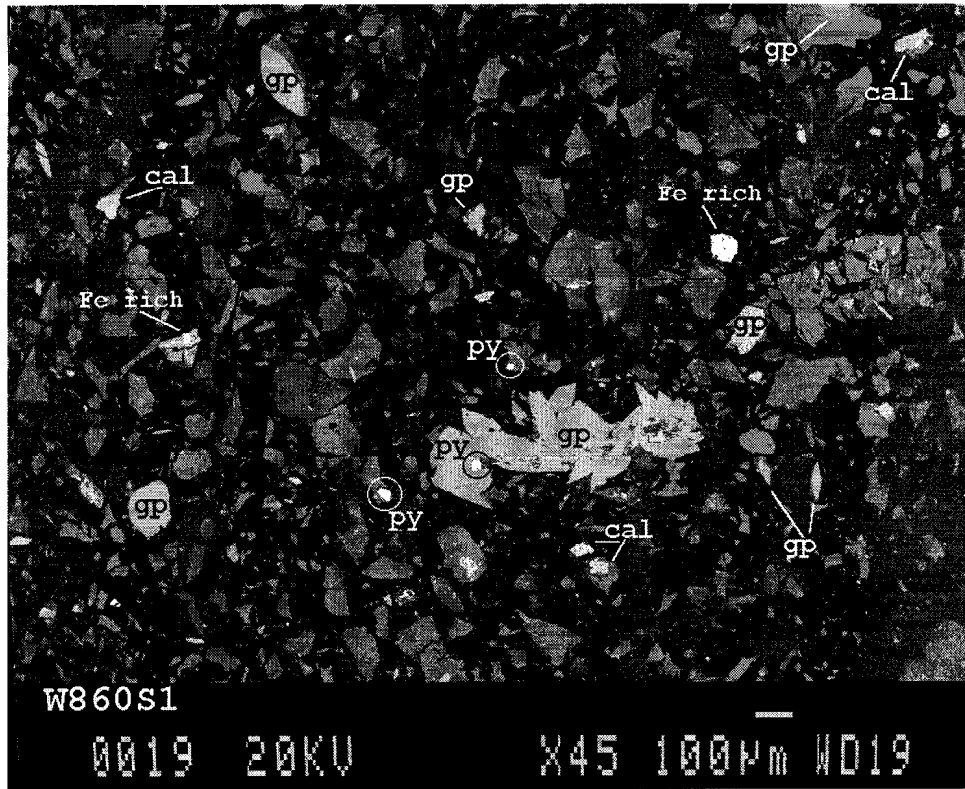


Fig. 18. X-ray diffractogram of sample W8-25S12.





ID: HOGAN W8-60S1, 21-OCT-97@10: 38  
 File: Z04323.RAW Scan: 5-90/.05/ 1/#1701, Anode: CU

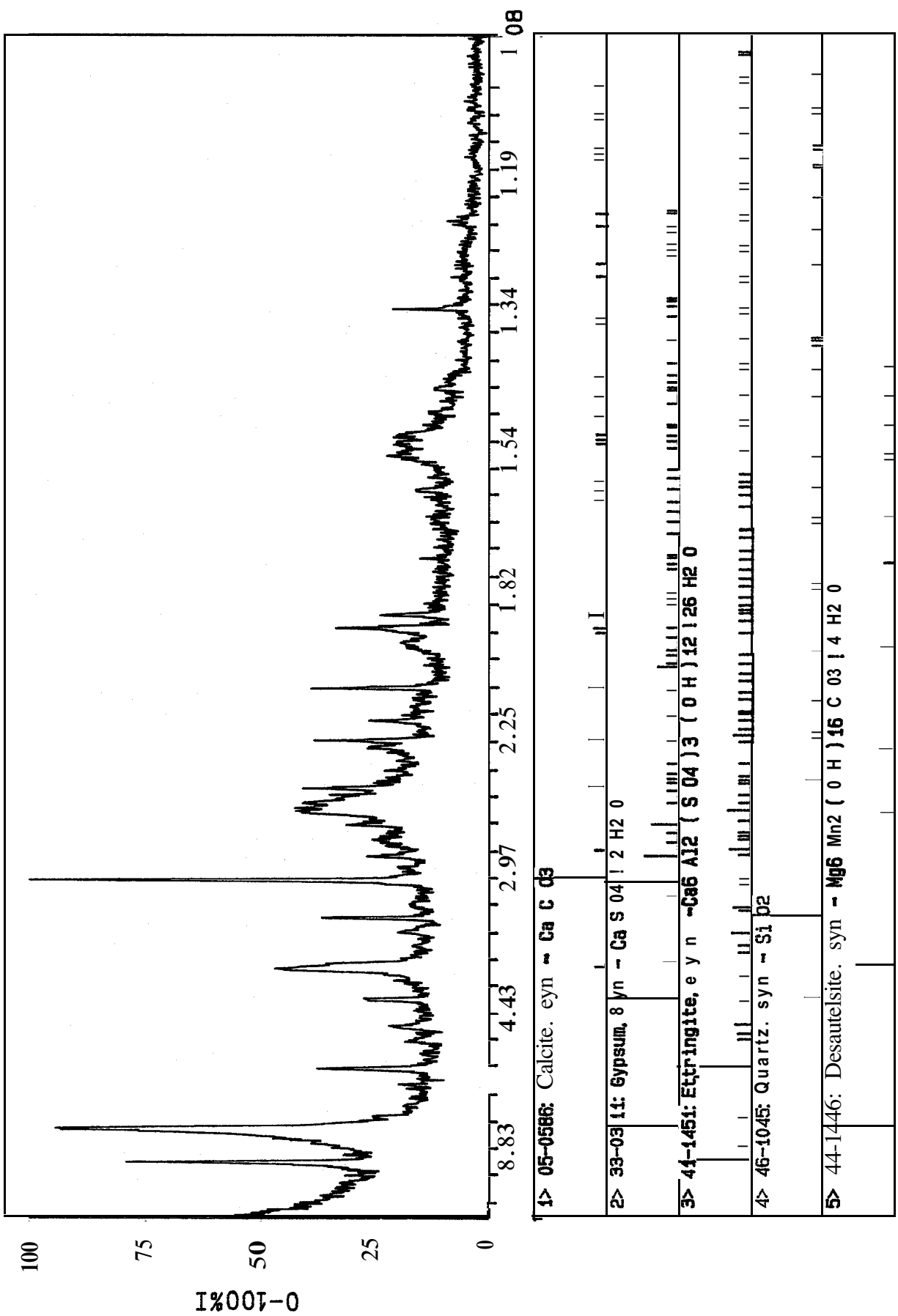
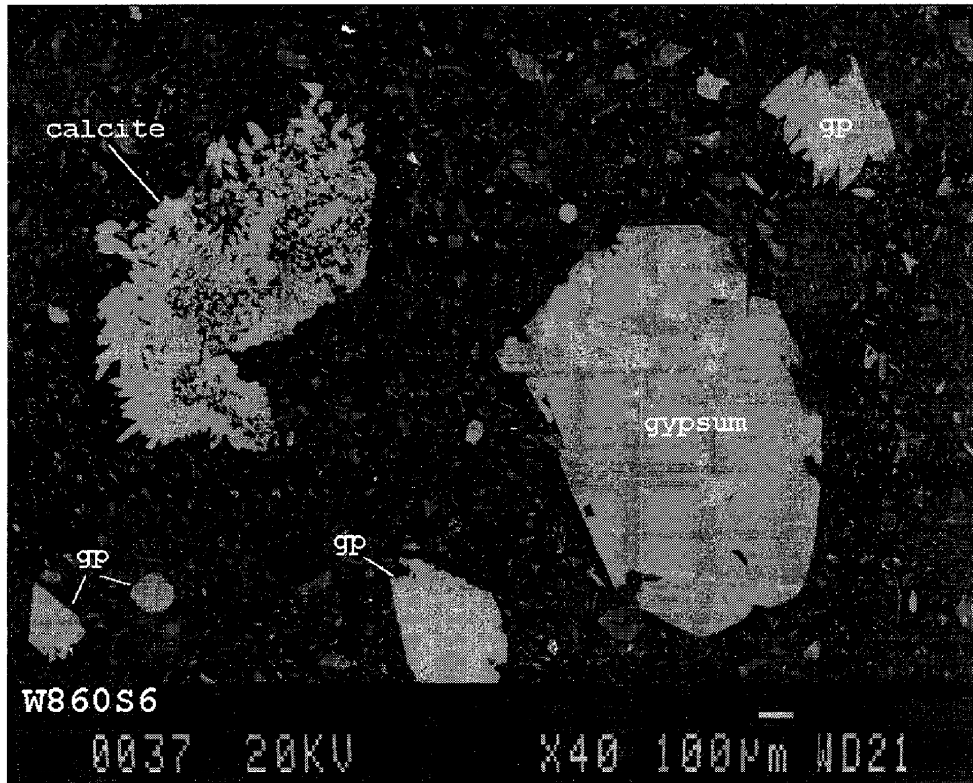
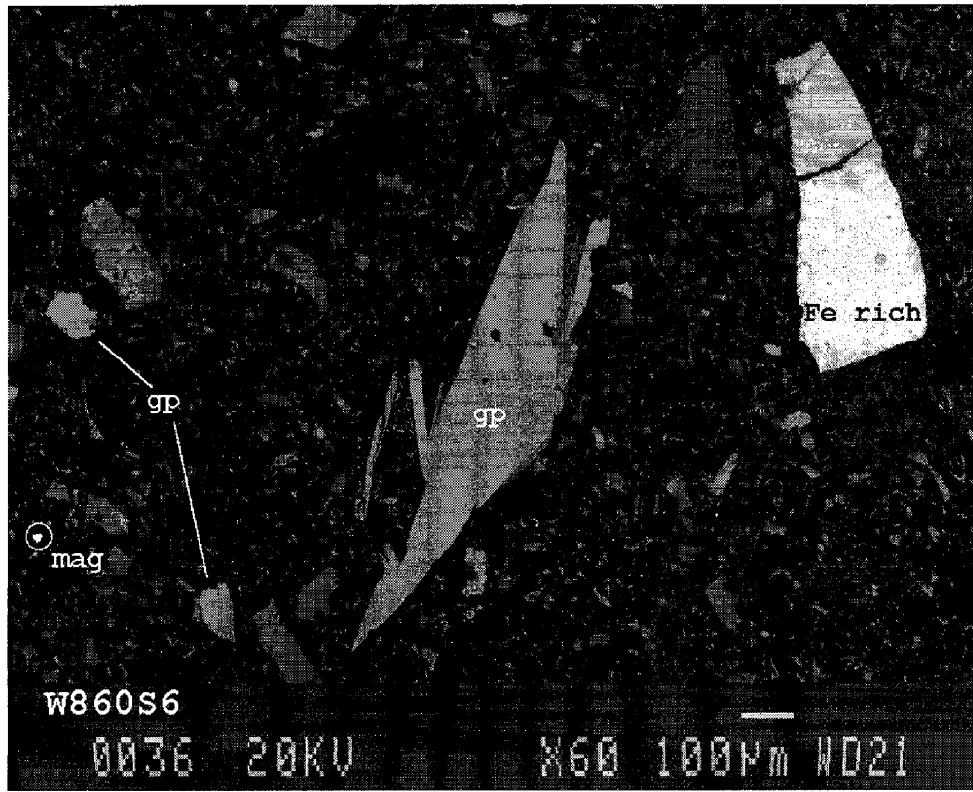
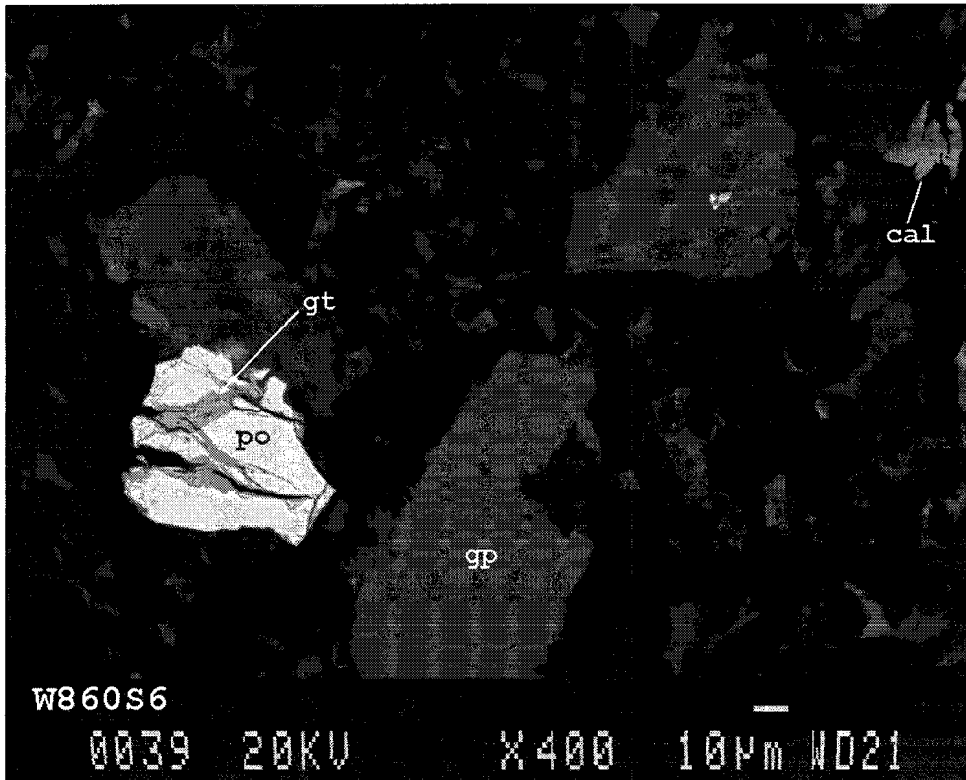
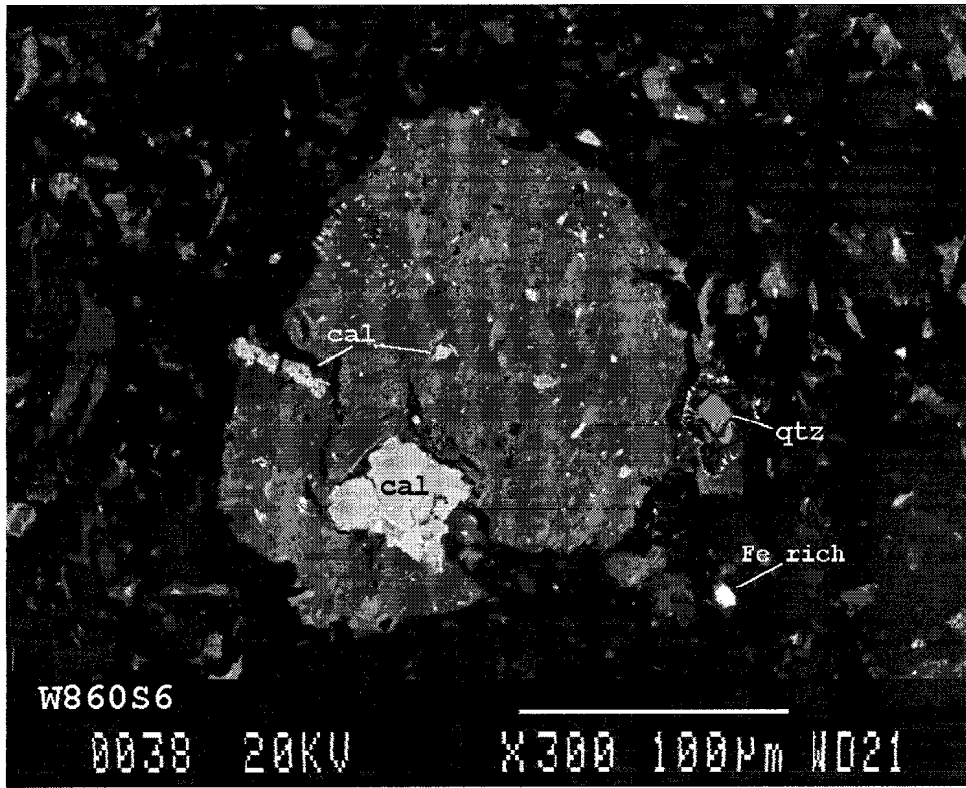


Fig. 19. X-ray diffractogram of sample W8-60S1





ID: GRIFFITH W8-60S6, 21-APP-97@13: 16  
 File: Z03880.RAW Scan: 5-90/.05/ 1/#1701, Anode: CU

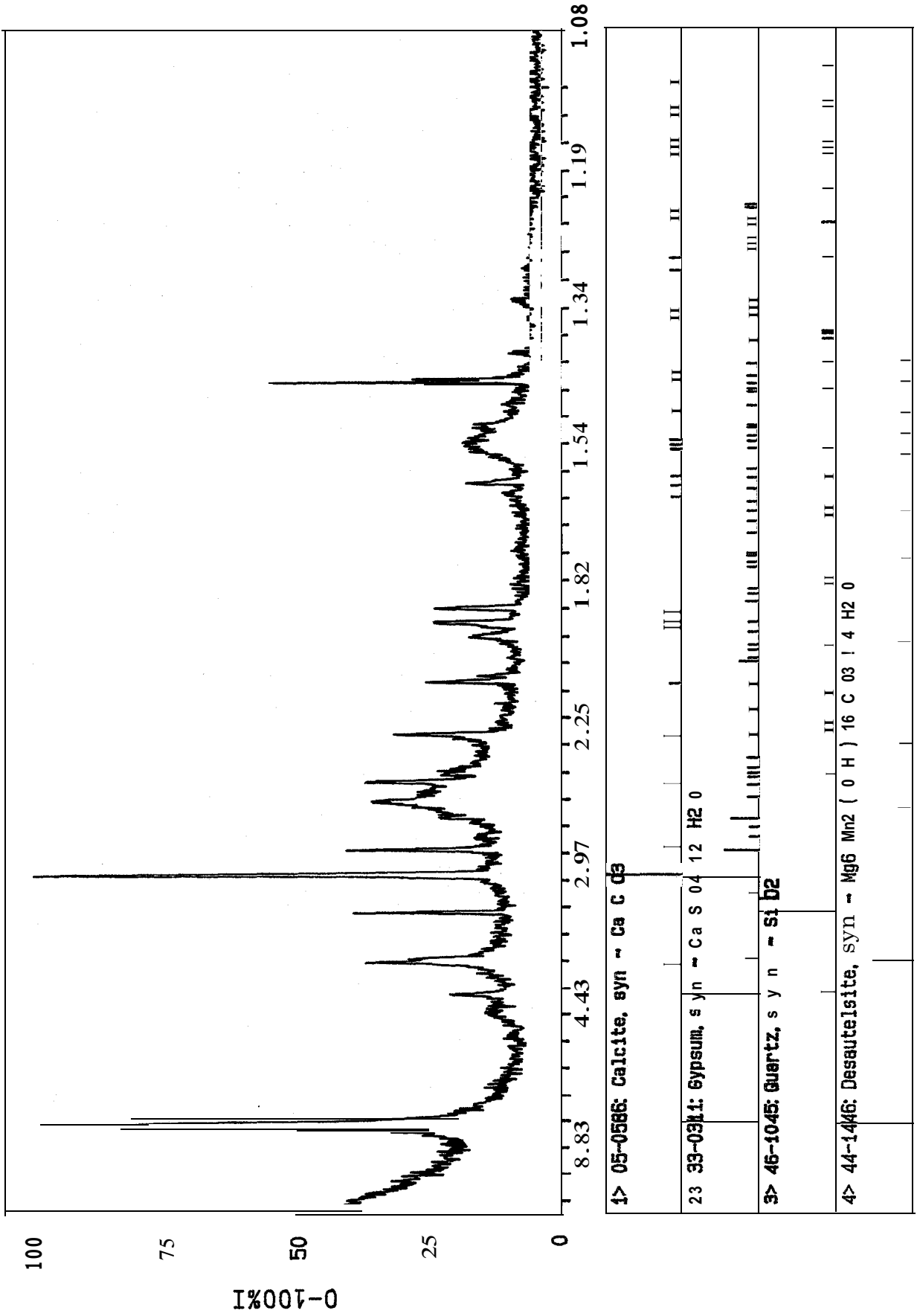
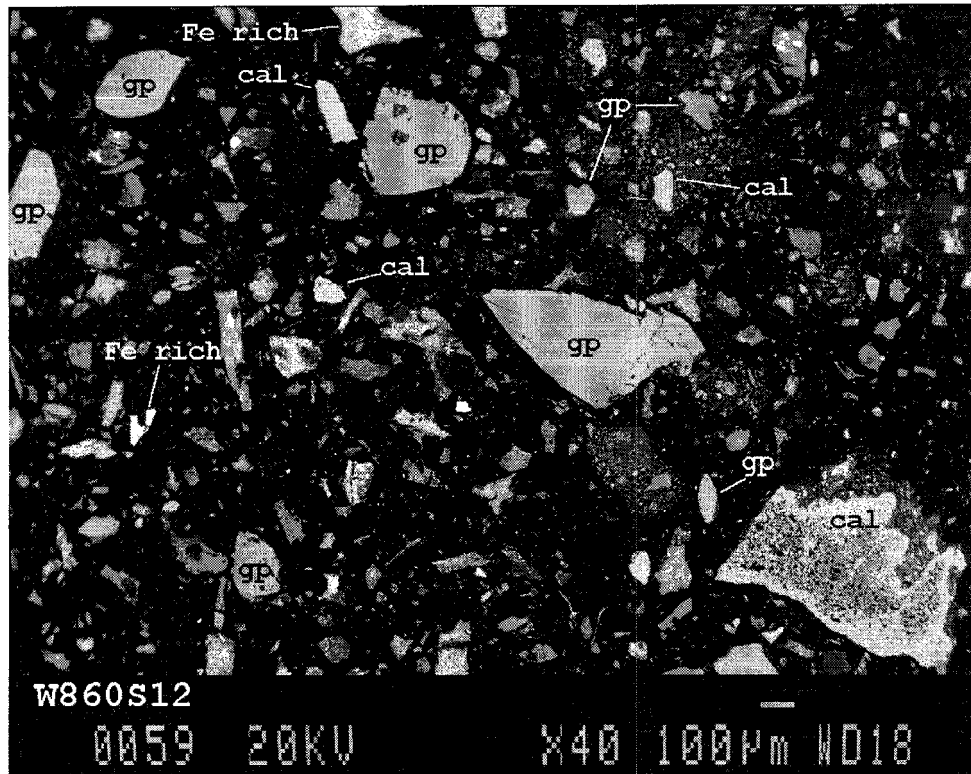
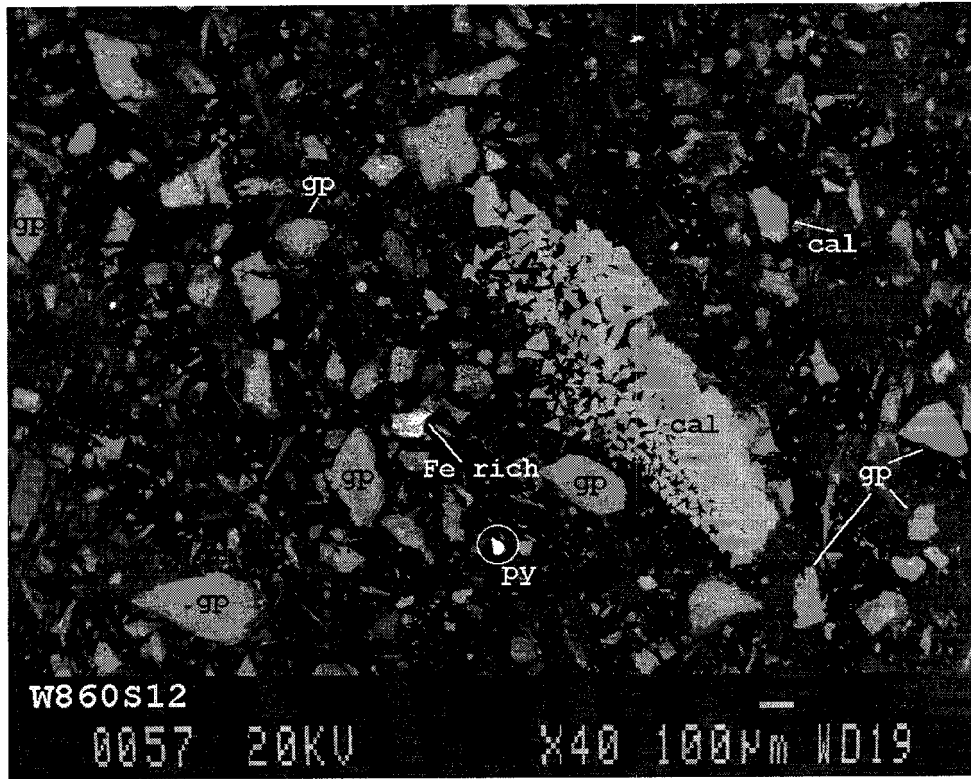
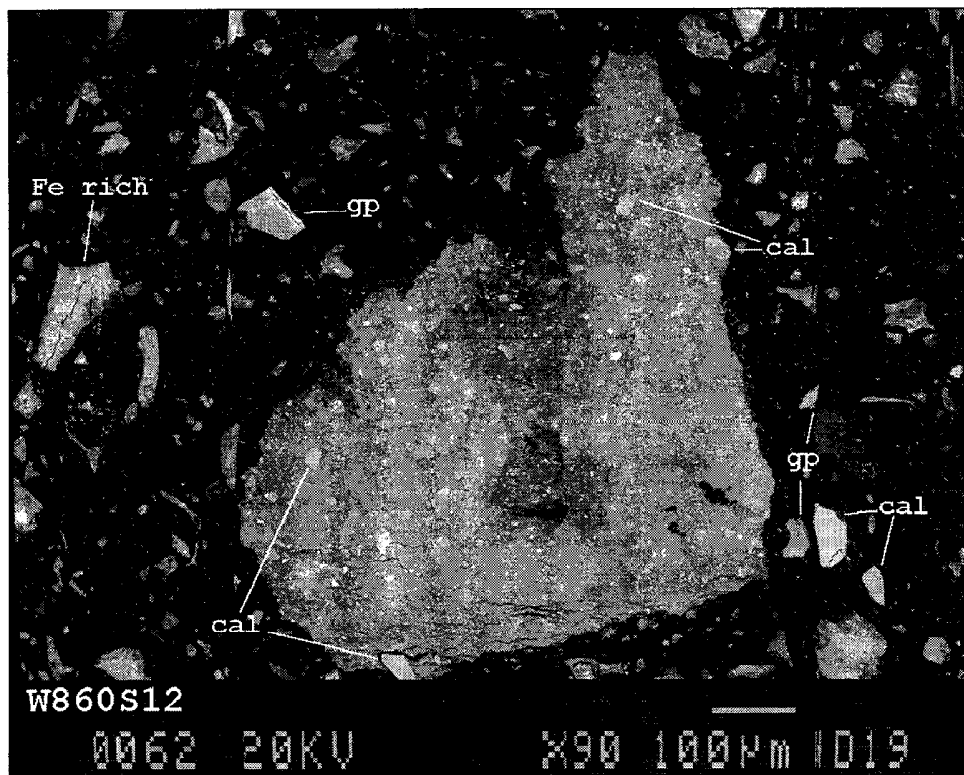
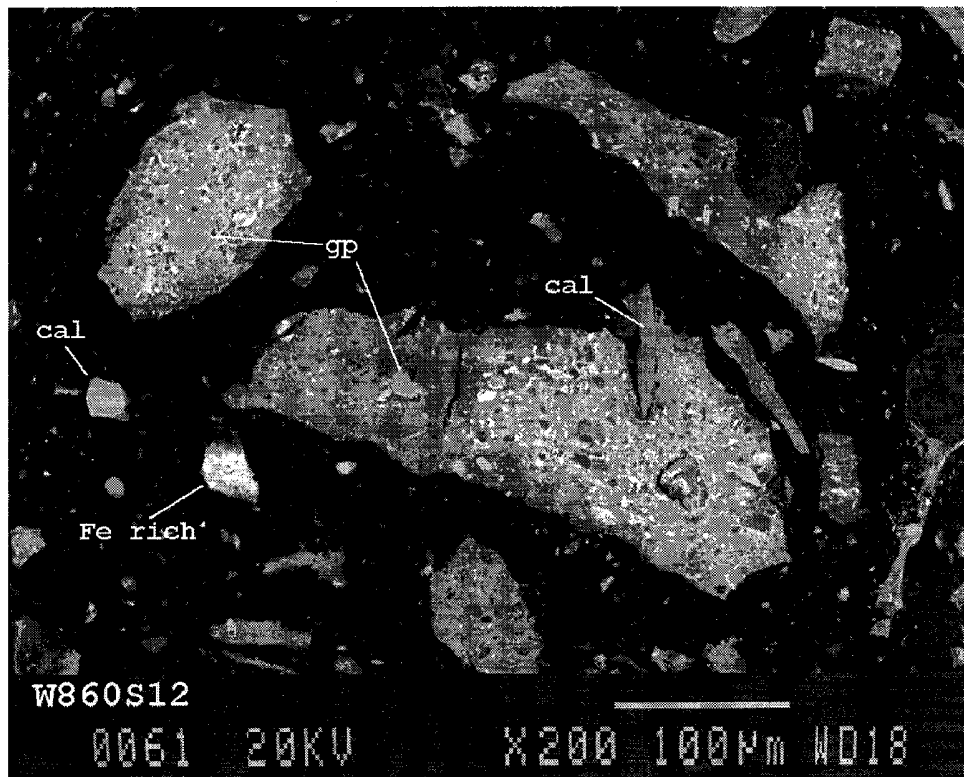
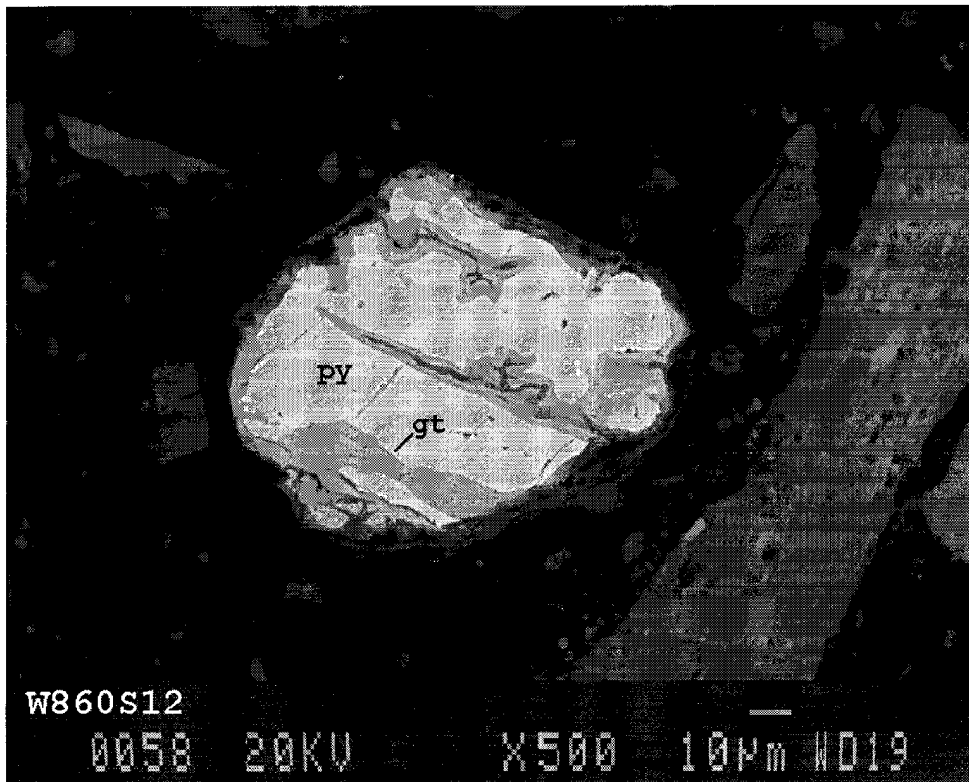
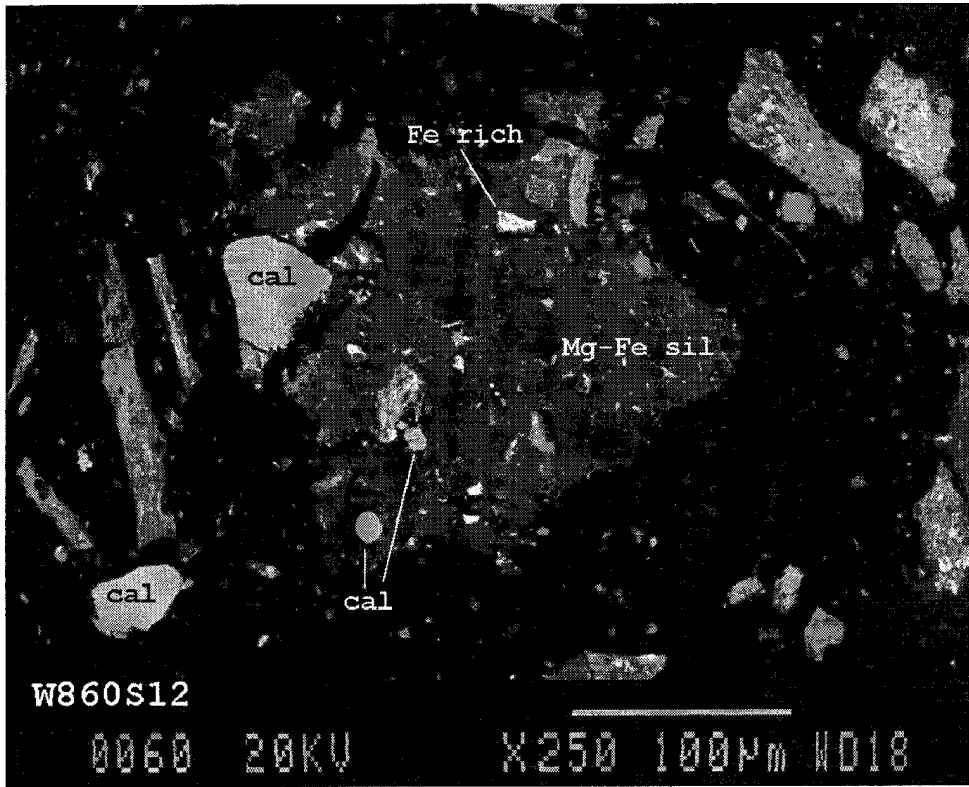


Fig. 20. X-ray diffractogram of sample W8-60S6.







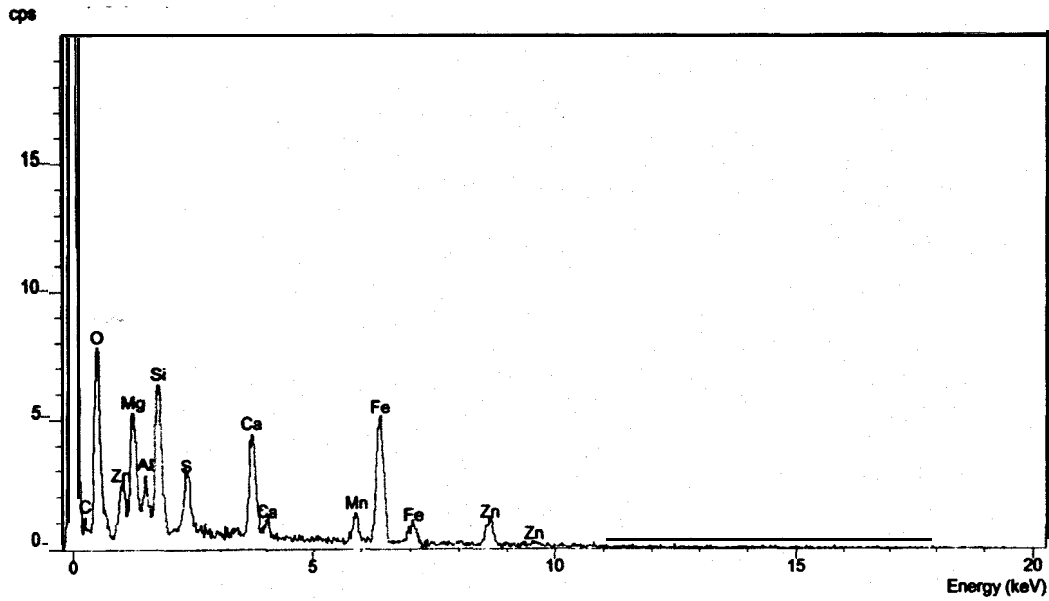


Fig. 21a. EDS of Si-rich "phase M"; area 1, W8-60S12.

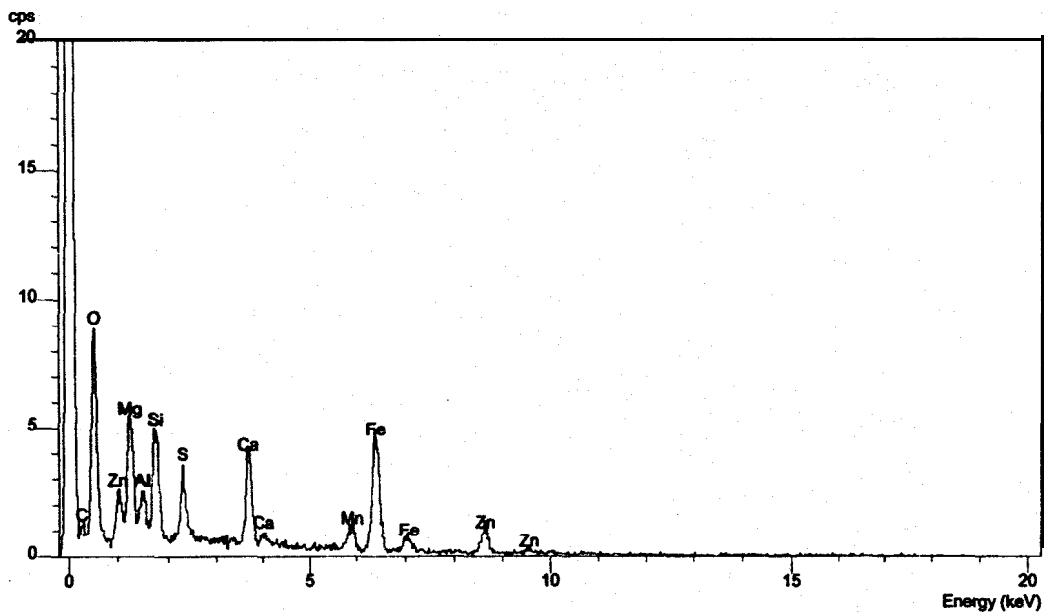


Fig. 21b. EDS of Si-rich "phase M"; area 2, W8-60S12.



ID: HOGAN W8-60S-12, 21-OCT-97@13:30  
 File: Z04332.RAW Scan: 5-90/.05/ 1/#1701, Anode: CU

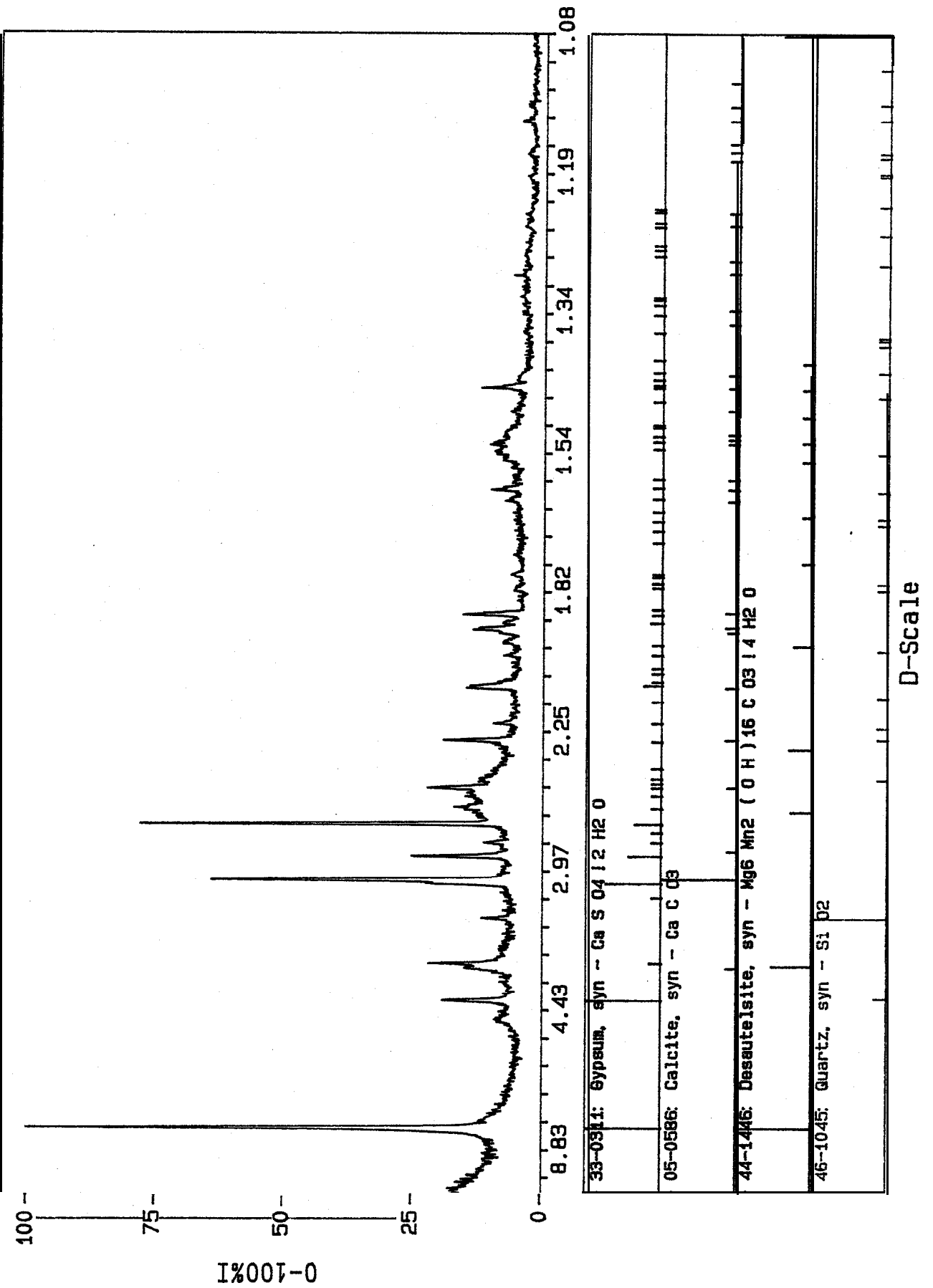


Fig. 22. X-ray diffractogram of sample W8-60S12.